

Regulation of Nanoparticle - Reactant Interaction Outplays Ligand Poisoning in Metal Nanoparticle Catalyzed Reactions

A Thesis

*Submitted Towards the Partial Fulfilment of the Requirements
for the Degree of*

Doctor of Philosophy

By

Soumendu Roy

ID: 20153383



**Indian Institute of Science Education and Research (IISER) Pune
Dr. Homi Bhabha Road, Pune-411008**

March 2020

Dedicated to
Maa, Baba and
Kaku
•Ranjan Chakraborty

Certificate

This is to certify that the work incorporated in the thesis entitled “*Regulation of Nanoparticle-Reactant Interaction Outplays Ligand Poisoning in Metal Nanoparticle Catalyzed Reactions*” submitted by Soumendu Roy has been carried out by the candidate at the Indian Institute of Science Education and Research (IISER), Pune, under my supervision. The work presented here or any part of it has not been included in any other thesis submitted previously for the award of any degree or diploma from any other University or Institution.

Date: 25.06.2020

Place: Pune



Dr. Pramod P. Pillai
(Research Supervisor)

Declaration

I, hereby declare that the thesis entitled “*Regulation of Nanoparticle-Reactant Interaction Outplays Ligand Poisoning in Metal Nanoparticle Catalyzed Reactions*” submitted for the degree of Doctor of Philosophy in Chemistry at Indian Institute of Science Education and Research (IISER), Pune has not been submitted by me to any other University or Institution. This work was carried out at the Department of Chemistry, Indian Institute of Science Education and Research (IISER), Pune, India under the supervision of Dr. Pramod P. Pillai.

Date: 25.06.2020

Place: Pune



Soumendu Roy

Acknowledgement

First and foremost, I wish to express my deepest gratitude to my thesis supervisor **Dr. Pramod P. Pillai** for his constant support and guidance throughout the journey of my PhD. He always encouraged me to be professional and do the right thing even when the road got tough. Each and every conversation (whether scientific or non-scientific), I had with him was stimulating and captivating. He was always there motivating and guiding me during the bad phases of my PhD. I feel fortunate to be a part of his esteemed research team and consider it as one of the finest experiences of my life. I sincerely thank you for being a true mentor. A special thanks to you for sponsoring the wonderful Kerala trip.

I would like to thank my Research Advisory Committee (RAC) members, **Dr. Nirmalya Ballav** and **Dr. Santhosh Babu Sukumaran** for managing their time to conduct my RAC meetings and giving valuable comments and suggestions on my research.

Research is always a collective and collaborative effort from multiple minds. I was fortunate, having a bunch of extremely talented and helpful people in the lab, who not only helped me in shaping my research but also maintained a feel good atmosphere inside the lab. I would like to acknowledge all my present (**Anish, Gayathri, Sumit, Indra, Kashyap, Pradyut, Vanshika, Shana and Sriram**) and past (**Sarah, Govind, Jewel, Yashika, Mahima, Preethi, Shalini, Ajesh, Swati, Rinku, Harshit, Avisikta and Saurabh**) lab members for their supports and contributions. A special credit goes to **Anish and Gayathri** for being there and helping me in a countless ways from the day one to the end of my PhD. The initial days of struggle (breaking RBs during QD synthesis, breaking cuvettes, vacating the whole Mendeleev block with thiols and so on) with you guys were amazing. It wouldn't have been possible without you guys.

I would like to acknowledge **Prof. K. George Thomas** for allowing me to work in his lab and get trained in the quantum dot synthesis. I would also like to thank **Sandeep K. Alangad**, for helping me with the synthesis.

I also thank **Prashant Kale** and **Prathamshetti Anil**, who trained me in the Sputter coating and Scanning electron microscopy instruments during my initial days of PhD.

I am grateful to **Prof. K. N. Ganesh** (former Chair Chemistry and Founder Director), **Prof. M. Jayakannan** (former Chair Chemistry) and **Prof. H. N. Gopi** (Chair Chemistry) for their support in various academic matters as well as ensuring a wonderful and healthy research environment in the Department.

I would like to thank all the faculty and staff members from the Department for their support in various academic matters. A special thanks to **Mayuresh Kulkarni, Sayalee Damble and Tushar Kurulkar** for helping me with the official matters.

I would also like to thank all my friends especially, **Debanjan, Rajarshi, Samraj, Rahul, Nasrina, Arunabha, Saptashwa, Sujoy, Samir and Krishna** for all the fun moments and sleepless nights I have spent with them, all those late night movies we have watched together and above all, for the enormous support I have gained from these guys during my ups and downs. A special thanks to my DADAGIRI team mates (**Chandra Da, Abhishek Da, Partha, Amit Da, Tarak Da, Subhajit, Sumanta, Prajjwal, Anweshi, Abdul, Abhirup, Ratheejit, Arnab and Prasun**) for all the exciting moments we have spent together on the cricket field.

I would like to take this opportunity to express my gratitude to all my teachers who have shaped my life in various ways. I would like to thank **Debabrata Rath, Pushpendu Panda, Subhamoy Mishra and Tarapada nandi** for teaching me valuable lessons during my school days.

Now, it's time to thank my family members. First of all, I would like to thank my maa and baba: **Mrs. Dipali Roy and Mr. Madan Mohan Roy** for their unconditional love, affection, blessings and everything. Whoever I am today, it's only because of their constant support and love. I would also like to thank my **Kakima, dada, dadabhai, boudi, piku, debda and golu** for their irresistible support and love. A special thanks to **Subha**, for being an integral part of my life, bearing all my frustrations, supporting me unconditionally and staying there during all the ups and downs.

Finally, I would like to express my gratitude to my kaku **Late Ranjan Chakraborty**, who was my first teacher and always motivated me to fulfil my dreams. His words inspire me in every moment and empower to climb up to new summits of life.

Thank You.

Soumendu Roy

Table of Content

1. Thesis Synopsis.....	i-iv
2. Chapter 1:.....	1-29
1.1. Introduction.....	1
1.2. Key parameters Dictating the Catalytic Properties of Metal NPs.....	1-13
1.2.1. High surface -to- volume ratio.....	1-4
1.2.2. Localized surface plasmon Resonance (LSPR).....	4
1.2.3. Plasmonic and Non-Plasmonic Metal NPs.....	5-6
1.2.4. Plasmon Excitation and Generation of Hot Carriers.....	7-8
1.2.5. Photocatalysis with Plasmonic Metal NPs.....	8-13
1.3. Ligand Poisoning.....	13-15
1.4. Strategies to Overcome Ligand Poisoning Effect.....	16-18
1.5. Ligand Directed Catalysis.....	18-19
1.6. Objective of the Thesis.....	20-21
1.7. References.....	21-29
3. Chapter 2:.....	30-66
2.1. Abstract.....	31
2.2. Introduction.....	31-36
2.3. Experimental Details.....	36-44
2.3.1. Materials and Reagents.....	36-37
2.3.2. Synthesis of AuNPs.....	37-38
2.3.3. Synthesis of Citrate Sabilized NPs.....	38-39
2.3.4. Transmission Electron Microscopy (TEM) Studies.....	39
2.3.5. Zeta Potential Studies.....	39
2.3.6. Thermo Gravimetric Analysis (TGA).....	40
2.3.7. ICP-MS Analysis.....	40
2.3.8. Catalytic Reduction.....	40
2.3.9. 4-Nitrophenol Reduction.....	40
2.3.10. 4-Nitroaniline Reduction.....	40
2.3.11. Potassium Ferricyanide Reduction.....	41
2.3.12. Product Characterization.....	41
2.3.13. Calculation of Screening Length.....	41-42
2.3.14. Calculation of Surface Potential.....	42-43
2.3.15. Determination of mol % of Au atoms in AuNP Catalyst.....	43
2.3.16. Estimation of Ligand Packing Density.....	44
2.4. Results and Discussion.....	45-58
2.4.1. Design and Characterization of AuNP Catalysts.....	45-46
2.4.2. Reduction of 4-Nitrophenol with Different AuNP Catalyst.....	46-48
2.4.3. Validation of Langmuir-Hinshelwood Mechanism.....	48-50
2.4.4. Effect of Surface Area.....	50-51
2.4.5. Effect of Dissolved Oxygen.....	52-53
2.4.6. Interaction Driven Catalysis.....	53-55
2.4.7. Temperature Dependent Catalytic Study.....	55-57
2.4.8. Generality of Hypothesis.....	57-58
2.5. Conclusion.....	59
2.6. References.....	59-63

2.7. Appendix.....	64-66
--------------------	-------

4. Chapter 3:.....67-114

3.1. Abstract.....	68
3.2. Introduction.....	68-73
3.3. Experimental Details.....	73-82
3.3.1. Materials and Reagents.....	73
3.3.2. Synthesis of NPs.....	73-74
3.3.3. Place Exchange of AuNPs.....	74-75
3.3.4. Microscopy Studies.....	75
3.3.5. Zeta Potential Studies.....	75
3.3.6. Photocatalytic Reduction.....	76
3.3.7. Kinetic Analysis.....	77-78
3.3.8. Quantum Yield Calculation.....	78-79
3.3.9. Theoretical Calculation for Ferricyanide Concentration Close to AuNP.....	79-82
3.3.10. Calculation of Free energy of activation (ΔG^\ddagger), Reorganization Energy (λ), and Electronic Coupling Term ($\Phi H_{ab} ^2$).....	82
3.4. Results and Discussion.....	82-99
3.4.1. Design and Characterization of AuNP Catalysts.....	82-83
3.4.2. Photocatalytic Reduction of Ferricyanide.....	84-86
3.4.3. Hot Electron vs Photothermal Heating.....	86-89
3.4.4. Effect of Hole Scavenger (Ethanol) on Photocatalysis.....	89-90
3.4.5. Interaction between AuNP Catalyst and Ferricyanide Ions.....	90-92
3.4.6. Interaction Driven Catalysis.....	92-93
3.4.7. Mechanism of Hot Electron Transfer.....	94-96
3.4.8. Experimental and Theoretical Estimation of Ferricyanide Ions Close to NP Surface.....	96-99
3.5. Recyclability Aspect.....	101-102
3.6. Conclusion.....	102-103
3.7. References.....	103-107
3.8. Appendix.....	108-114

5. Chapter 4:.....115-149

4.1. Abstract.....	116
4.2. Introduction.....	116-119
4.3. Experimental Details.....	120-126
4.3.1. Materials and Reagents.....	120
4.3.2. Synthesis of NPs.....	120-121
4.3.3. Place Exchange of AuNPs.....	121-122
4.3.4. Synthesis of Polyvinylpyrrolidone (PVP) AuNPs.....	122
4.3.5. Transmission Electron Microscopy (TEM) Study.....	122
4.3.6. Zeta Potential.....	122
4.3.7. Photocatalytic Reduction of Ferricyanide to Ferrocyanide.....	123
4.3.8. Photocatalytic Reduction of NAD ⁺ to NADH.....	123
4.3.9. Lipoamide Dehydrogenase (LDH) Assay.....	123-124
4.3.10. Calculation of Turnover Number (TON) and Turnover Frequency (TOF).....	124
4.3.11. Kinetic Analysis for the Photocatalytic Reduction of Ferricyanide.....	124-126
4.4. Results and Discussion.....	126-139
4.4.1. Design and Characterization of AuNP Catalysts.....	126-127

<i>4.4.2. Photocatalytic Reduction of Ferricyanide to Ferrocyanide</i>	127-129
<i>4.4.3. Photocatalytic Reduction of NAD⁺ to NADH</i>	129-132
<i>4.4.4. Role of Electrostatic Interaction</i>	132-133
<i>4.4.5. Determination of NAD⁺ to NADH Reduction Pathway</i>	133-134
<i>4.4.6. Intensity Dependent Study</i>	134-136
<i>4.4.7. Hot Electron vs Photothermal Heating</i>	136-137
<i>4.4.8. Wavelength Dependent study</i>	137-138
<i>4.4.9. Flexibility of the Strategy</i>	138-139
4.5. Conclusion	139-140
4.6. References	140-146
4.7. Appendix	146-155
List of Publications	156-157
Confernce Presentations	158
Permission and Copyrights	

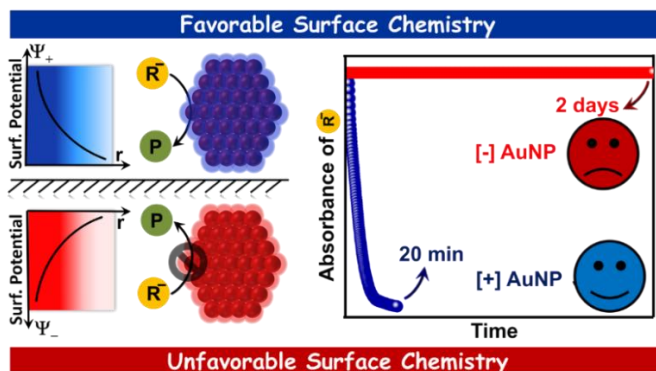
Thesis Synopsis

Surface ligands are ubiquitous in colloidal nanoscience. They provide the colloidal stability to nanoparticles (NPs) as well as dictate most of their physicochemical properties. However in the area of catalysis, the ligands have a *bad reputation* of poisoning the catalyst, either by hindering the surface accessibility (due to steric effect) or by creating an insulating barrier for the movement of electron and holes. So, how to overcome this challenge of “*ligand poisoning*”? Traditional strategies include the deposition of NPs onto a support or use ‘ligand free’ NPs for catalysis. However, the available surface area and stability of NPs are compromised during the course of catalysis. Thus, nanoparticles and ligands are two inseparable entities and strategies have to be developed to accomplish catalysis by retaining as well as utilizing the ligands on the NP surface. In this direction, the present thesis focuses on introducing a new strategy based on NP-reactant interaction (emanated from surface ligands) to address the so called “*ligand poisoning*” effect in the area of metal NP catalysis.

The thesis starts with a brief introduction on metal NP catalysis where, the intriguing role of surface-to-volume ratio and the localized surface plasmon property have been discussed in detail to highlight the potency of metal NPs as efficient catalysts. Despite of having a great potential, the broad application of metal NP catalysts, in general, are impeded by their poor catalytic efficiency. One of the primary reasons attributed to this is “*ligand poisoning*”. The present thesis is focused on addressing this challenge in metal NP catalysis. Therefore, the later section of Chapter -1 introduces the ligand poisoning effect in NP catalysis, and discusses about different existing strategies to overcome this challenge. Finally, the introduction Chapter ends by providing a brief outline about our interaction based strategy to circumvent this challenge.

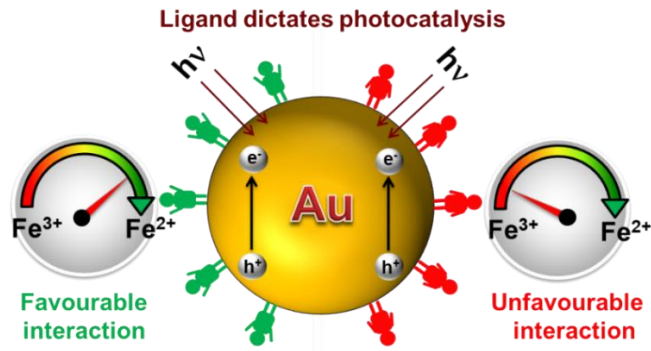
The second Chapter summarizes our efforts towards establishing the decisive role of surface ligands in improving as well as dictating the catalytic property of NPs in traditional gold nanoparticle (AuNP) catalysed reduction of nitro arenes to amines. The interactions between the reactant molecules and AuNP surface was made favourable (attractive) or unfavourable (repulsive) by fine tuning the NP surface potential, through judicious choice of ligands. An electrostatically assisted channelling of reactant molecules due to the attraction between oppositely charged reactants and AuNP catalysts was responsible for the dominance of [+] AuNP catalysts over other NP systems. The catalyst amount was brought down to a picomolar level through a favourable NP-

reactant interaction. No measurable catalysis was observed when unfavourable conditions for reactant binding were created using [-] AuNP as the catalyst (even up to ~ 1 mol %). At least an order of magnitude higher concentration of [-] AuNP was required to compete with the catalytic activity of [+] AuNP. Remarkably, the catalysis by [+] AuNP was superior to even citrate stabilized AuNP; the latter being often considered as a benchmark catalyst as it provides ~ 100 % of its surface for catalysis. Thus by tuning the NP-reactant interaction we were not only able to achieve efficient catalysis at low NP concentration, but also regulate the catalytic property between completely “on” and “off” states - rendering the same NP core as a catalyst and a non-catalyst.



Schematic representation of electrostatically dictated AuNP catalysed reduction of nitroarenes to amines.

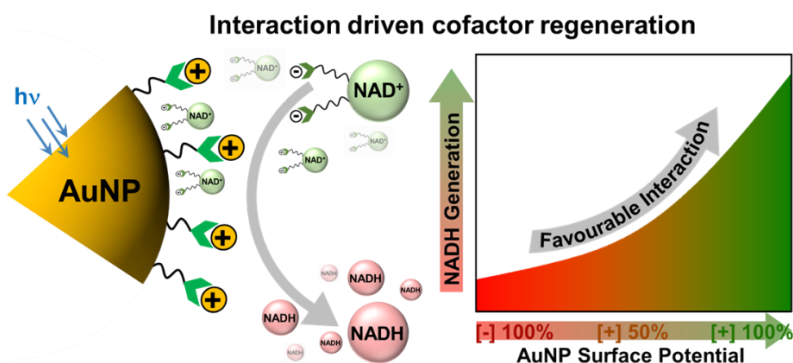
The third Chapter is focused on employing our *idea of interaction* to address the “*ligand poisoning*” effect in a more challenging photocatalytic reaction with plasmonic metal NPs. The photocatalytic activity of metal NPs predominantly depends on the rate of hot electron/hole transfer (within ~10-100 fs), which oftentimes is hindered by the insulating nature of the surface ligands resulting in a poor photocatalytic efficiency. In a model photocatalytic one electron reduction of ferricyanide to ferrocyanide, we have successfully demonstrated that a favourable NP-reactant interaction can indeed improve the rate of hot electron transfer, and hence the photocatalytic activity. For instance, the rate constant increased from $\sim 8 \times 10^{-4} \text{ min}^{-1}$ to $\sim 4 \times 10^{-3} \text{ min}^{-1}$ (~ 5 fold increment in reaction rate!), when the NP-reactant interaction was made favourable, along with an appreciable increase in the ferricyanide conversion yield (from ~ 10% for [-] AuNP to ~ 60% for [+] AuNP). A detailed mechanistic analysis based on Marcus theory revealed that a higher local concentration of reactant molecules close to the NP surface is the deciding factor for the enhanced rate of photocatalysis.



Schematic representation of surface ligand “gated” AuNP photocatalyzed reduction of ferricyanide to ferrocyanide.

The fourth Chapter of the thesis summarizes our efforts towards demonstrating the prodigious role of *precise NP-reactant interaction* in driving kinetically sluggish photocatalytic multielectron reaction, without the aid of any co-catalysts or electron mediators. Harvesting multiple electron-hole pairs in an efficient manner is one of the *holy grails* in the area of photocatalysis. The efficiency of a multielectron reaction relies on surplus generation and efficient transfer of multiple charge carriers from a photocatalyst to the reactant molecules. While the generation of multiple charge carriers depends on the intrinsic property of the photocatalyst, the transfer of these short lifetime multiple carriers relies on the interaction between the photocatalyst and the reactant molecules. A poor catalyst-reactant interaction oftentimes demands for the need of additional co-catalysts or charge mediators to facilitate the charge transfer process, and thereby increasing the complexity of the photocatalytic system. Thus, strategies to develop sole photocatalysts for multielectron reactions are highly desirable, but not yet widely accomplished. Here we introduce the idea of ‘*creating precise NP-reactant interaction*’ as a potent strategy to perform a challenging multielectron photocatalytic regeneration of the reduced form of Nicotinamide Adenine Dinucleotide (NADH) cofactor, by AuNP as a sole photocatalyst. Our studies reveal that the positive surface potential on AuNP regulates the channeling and local concentration of [-] NAD⁺ reactant molecule, and thereby facilitating the direct multielectron (2e⁻) transfer from [+] AuNP to [-] NAD⁺ molecules. This favorable interaction rendered an efficient generation of NADH cofactor (TON ~ 12 × 10³ / NP) with [+] AuNPs as the sole photocatalyst, without the aid of any co-catalysts or electron mediators. A ~10 times increase in the NADH formation, while switching from unfavorable to favorable interaction, proves the necessity of catalyst-reactant interaction in driving

challenging photocatalytic multielectron reactions. The most interesting feature of the present idea of interaction is its flexibility to be coupled with other existing strategies, to boost the overall catalytic performances. The photocatalytic parameters presented here are comparable or greater than most of the catalytic systems reported based on plasmonic NP, with the added advantage of being structurally less complex.



Schematic representation of electrostatically driven photocatalytic regeneration of NADH by AuNP.

In summary, the present thesis focuses on salvaging the *bad reputation* of surface ligands in metal NP catalysis, and introduces a promising strategy of “*ligand directed catalysis*” for addressing the long standing challenge of “*ligand poisoning*” in the area of NP catalysis.

Chapter 1

**Introduction on Metal Nanoparticle Catalysis and
Ligand Poisoning**

1.1. Introduction

Catalysis with nanoparticles (NPs) is undoubtedly one of the widely studied areas in the modern materials research.^{1,2} Nanocatalysts are often considered as a bridge between homogeneous and heterogeneous catalysts, encompassing the advantages from both the approaches.³⁻⁹ Nanoparticles can offer most of its surface active sites for catalysis (similar to the homogeneous catalysis) and at the same time remains insoluble (dispersed) in the solution providing the advantages of easy separation, product purification and reusability (similar to heterogeneous catalysis).³⁻⁹ Moreover a tunability in size, shape, composition and crystallinity, tuneable optical and chemical properties, make NPs a promising candidate for catalysis.^{6,9-13} Among several NP catalysts, the metal based nanocatalysts have gained special attention because of their high absorption cross section and the localized surface plasmon resonance (LSPR), and thus, have been explored both in the areas of nanocatalysis and photocatalysis.¹⁴⁻¹⁸ The present thesis is focused on the catalytic and photocatalytic properties of metal NPs. Especially, we have addressed a long standing challenge of ligand poisoning in the area of metal nanoparticle catalysis, by developing an interaction based strategy to circumvent this issue. In this direction, the first section of the introduction Chapter presents a brief overview of the metal NP based catalysis in the context of two aforementioned properties. The follow up sections introduces the concept of ligand poisoning and also discuss about the pros and cons of different existing strategies to address this issue. Finally, the introduction Chapter ends by giving a brief objective of the present thesis.

1.2. Key Parameters Dictating the Catalytic Properties of Metal NP

1.2.1. High Surface-to-Volume Ratio:

Surface-to-volume ratio is one of the key parameters that makes NPs, in general, a promising catalyst for various chemical transformations.¹⁴⁻¹⁹ Specifically, the surface-to-volume ratio represents the percentage of atoms on the surface of a NP, in a given volume. This ratio increases with decrease in the size of a NP, which essentially means that more number of active atoms are available for catalysis.¹⁴⁻¹⁹ Moreover, a reduction in size increases the surface free energy by introducing unsaturated co-ordination to the surface atoms which makes the metal sites more reactive towards interaction with the surroundings (**Figure 1.1 a**).¹⁴⁻¹⁹ Hence, the size of the particles play a crucial role in dictating the catalytic activity of metal NPs. Plethora of studies have been performed to explore the size dependent catalytic activity of metal NPs. **Figure 1.1 b** shows a compilation of a large number of reports on the size dependent CO oxidation activity of gold

nanoparticle (AuNP) on supported catalysts.¹⁸ As evident from the **Figure 1.1 b**, most of the reports reveal a dramatic increase in the catalytic activity below a size regime of ~ 5 nm. For instance the catalytic activity of 2 nm particles are almost 100 times higher compare to that of a 20 nm particle.¹⁸ Studies with other NP systems too have exhibited similar size dependent catalytic activity.

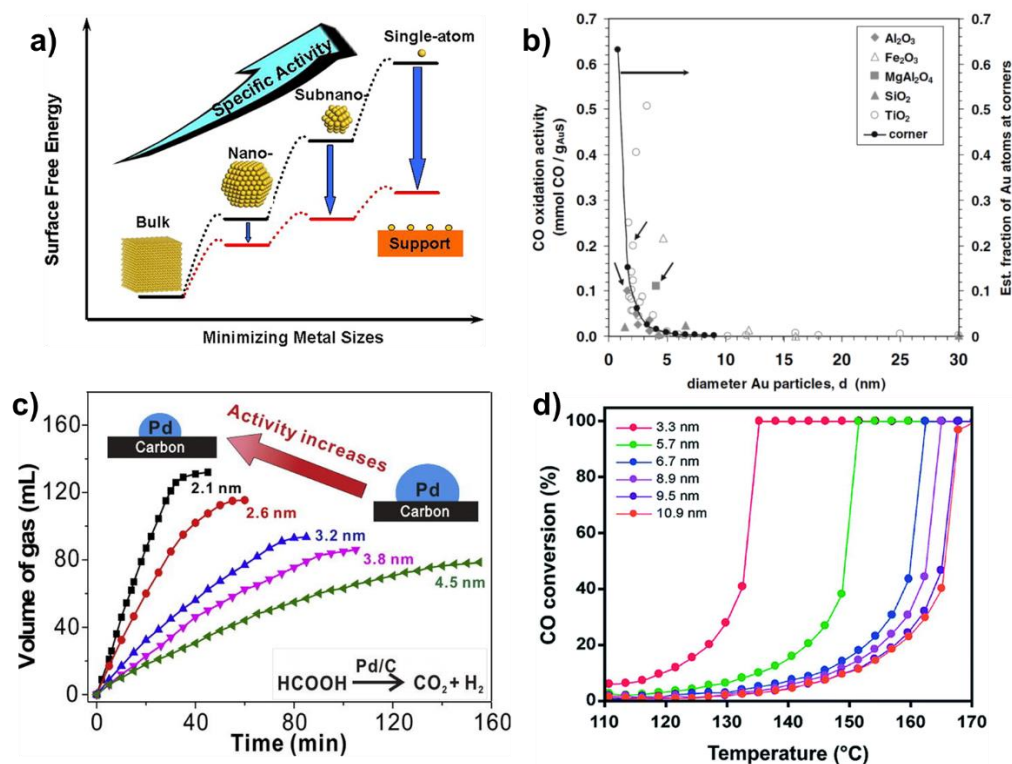


Figure 1.1. NP size effect on the catalytic activity of metal NPs. a) Schematic illustration of the change in surface free energy and specific activity per metal atom as a function of NP size. Adapted with permission from reference 14. Copyright 2013, American Chemical Society. b) Catalytic CO oxidation activity of different gold based catalysts as a function NP size. Adapted with permission from reference 18. Copyright 2007, Springer Nature. c) Rate of Catalytic reduction of HCOOH over Pd catalysts with varying sizes. Adapted with permission from reference 20. Copyright 2017, Elsevier. d) CO conversion yield for Rh NP as a function of varying sizes. Adapted with permission from reference 12. Copyright 2017, Chemical Society of Japan.

Lu and co-workers have studied the effect of NP size on the catalytic hydrogen generation from formic acid on a carbon supported Pd NP catalyst (**Figure 1.1 c**).²⁰ The studies show that the efficiency of hydrogen generation was boosted on going down to a size regime of 2-4 nm. The Turn-Over-Frequency (TOF) for 2 nm particle was 835/h which was among the highest values for monometallic Pd catalysts.²⁰ Detailed spectroscopic analysis revealed that a higher proportion of

both low and high co-ordination Pd atoms in smaller sized particles are responsible for the higher catalytic activity of these particles.²⁰ In another seminal work, Nagaoka and co-workers investigated the size dependent CO conversion activity of Rh NPs (**Figure 1.1 d**).¹² As per the study, the size of the NPs not only affect the catalytic activity but also have a prominent effect in controlling the temperature at which the reaction occurs. In consistent with other reports, the catalytic activity of the Rh NPs increased with decrease in the size of the particles, and the catalytic activity of the 3 nm particles was the highest (**Figure 1.1 d**).¹² Interestingly, a temperature dependent analysis showed that, apart from the catalytic activity, there was a steady decrease in the reaction temperature with decrease in the size of the particles. For instance, for a 3 nm particle, a 100 % conversion was achieved at a temperature of ~ 130 °C, whereas, > 160 °C temperature was required to achieve the same conversion efficiency with a 10 nm particle (**Figure 1.1 d**).¹² Thus, all the above reports demonstrate an increase in the catalytic activity with decrease in the size of the NPs. However, this is not true for all kind of reactions. The effect of NP size on the catalytic active strongly depends on the choice of reactions as well. Depending on the relation between the NP size and catalytic activity, the NP catalyzed reactions can be classified into three classes: (**Figure 1.2**)^{21,22}

i) *Positive size sensitive reactions*: The catalytic activity of NPs for these reactions increases with decrease in the size of the NPs.²¹ All the reactions discussed above fall under this category.

ii) *Negative size sensitive reactions*: The turn over frequency (TOF) for these kind of reactions decreases with decrease in the size of the NPs.²¹ Typical example of this category is the dissociation of CO₂, N₂, O₂ or NO which requires unique step-edge sites or co-ordination with multiple atoms on the surface of NPs. These kind of sites always do not exist in very small NPs. For instance, the dissociation of N₂ or NO require active B5 sites on the surface of NPs which oftentimes do not exist in very small NPs.²¹

iii) *Size insensitive reactions*: The TOF for these type of reactions are independent of size of the NPs. Hydrocarbon hydrogenation on transition metal catalyst is an example of this category.^{21,22}

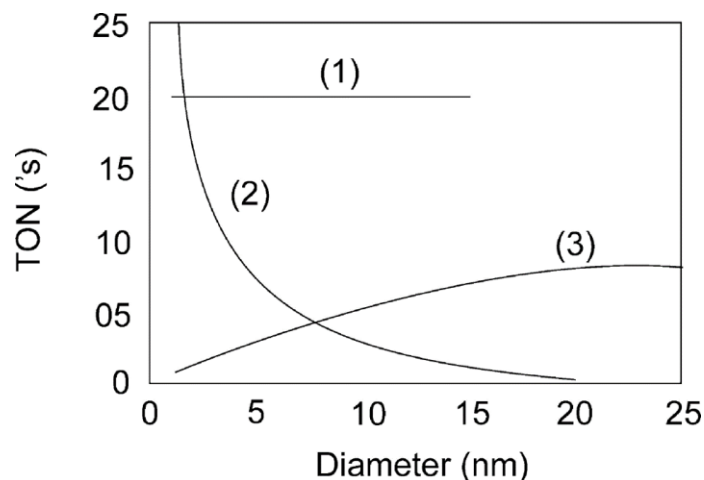


Figure 1.2. Variation in catalytic activity as a function of NP diameter for 1) size insensitive 2) negative size sensitive and 3) positive size sensitive reactions. Adapted with permission from reference 21. Copyright 2009, American Chemical Society.

1.2.2. Localized Surface Plasmon Resonance (LSPR):

Surface plasmon resonance is another important parameter which introduces light harvesting capability in metal NP catalysts.^{23–26} Strong interaction of plasmonic metal NPs with visible light induces a resonant and collective oscillation of free electrons on the surface of the NPs giving rise to the surface plasmon resonance (**Figure 1.3**). In case of a NP, the surface plasmon is confined in a nano regime of 1–100 nm, which is comparable or less than the wavelength of the incoming light and thus called localized surface plasmon resonance (LSPR). Because of this collective oscillation of sea of electrons, the optical cross section due to LSPR can extend up to ten times of the geometrical cross section of metal NPs.²⁷ Thus, plasmonic metal NPs, through LSPR can efficiently harvest the visible light energy and store in the form of hot charge carriers.^{23–26}

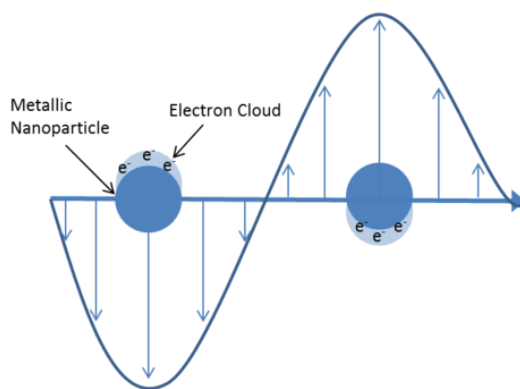


Figure 1.3. Schematic representation of the oscillation of surface electrons in metals under the influence of an electromagnetic radiation, leading to the generation of Surface Plasmon

Resonance. Adapted with permission from reference 30. Copyright 1999, American Chemical Society

1.2.3. Plasmonic and Non-Plasmonic Metal NPs:

Plasmon excitation involves a collective oscillation of sea of electrons on the surface of NPs and thus it offers a large optical extinction cross section at the resonant frequency.²⁸⁻³⁰ According to the Mie theory of dipole approximation, the extinction coefficient (k) for N number of spherical particles with volume V is given by the following equation³⁰⁻³²

$$k = \frac{18\pi N V \epsilon_m^{1.5}}{\lambda} \frac{\epsilon_2}{[\epsilon_1 + 2\epsilon_m]^2 + \epsilon_2^2}$$

Where, λ is the absorbing light wavelength, ϵ_m is the dielectric constant of the surrounding medium (frequency independent), ϵ_1 and ϵ_2 are the real and imaginary part of the material's dielectric constant³⁰⁻³²

$$\epsilon(\omega) = \epsilon_1(\omega) + i\epsilon_2(\omega)$$

where ω is the frequency of light. As per the above equation, the extinction coefficient for the plasmon excitation will be maximum when $\epsilon_1 = -2\epsilon_m$ and ϵ_2 is small, and weakly dependent on the frequency of light. ϵ_1 is the real part of the material dielectric function and is related to the polarizability of metals at different wavelengths.³⁰⁻³² As shown in **Figure 1.4 a**, a wide range of metals display a negative ϵ_1 value (throughout the visible wavelength) and therefore, satisfy the first (or primary) condition to exhibit surface plasmon property. However, ϵ_2 is the imaginary part of the dielectric function and its value depends on the probability of electronic excitation.³² Two types of electronic excitations are possible in metals: i) intraband s-s transition, where the electrons can be excited from the filled 's' state below the fermi level to the empty 's' state above the fermi level (**Figure 1.4 c,d**). The second type is the interband d-s transition where the excitation can happen from the filled 'd' state below the fermi level to the empty 's' state above the fermi level (**Figure 1.4 c,d**).³² The rate constant for the indirect intraband s-s transitions are typically small (10^{13} s^{-1})³³ due to its electronically forbidden nature and requirement of change in momentum for the charge carriers. Whereas the direct interband transitions are electronically allowed and have a higher rate constant of 10^{15} s^{-1} .³³ Thus, the ϵ_2 value is essentially dictated by

the probability of interband and intraband transitions in metals. Generally for noble metals (Au, Ag, and Cu), the filled 'd' band lies well

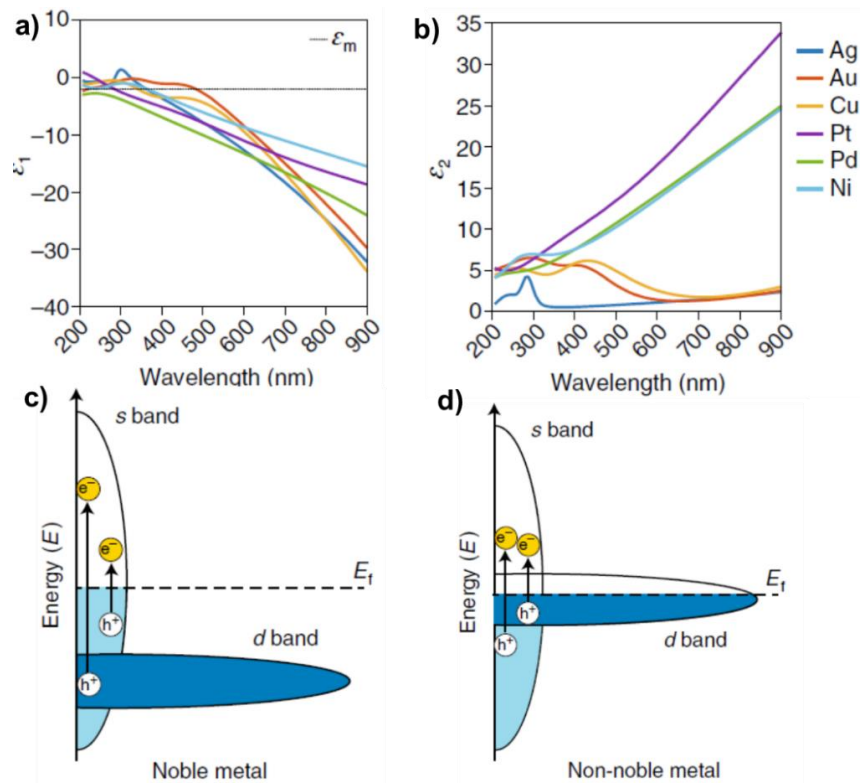


Figure 1.4. Variation in a) real and b) imaginary part of the dielectric function vs wavelength for noble and non-noble transition metals. c,d) Schematic representations of density of states for plasmonic noble metals and non-noble transition metals, respectively. Adapted with permission from reference 32. Copyright 2018, Springer Nature.

below the Fermi level and hence the probability of interband transitions in visible region is relatively lower (**Figure 1.4 c**).^{23,32} For instance, in Ag, the d-s transition is accessible only in the UV region.^{23,32} For Au and Cu, however, the energy of the 'd' band is higher in energy compared to Ag and the interband transition however, the energy of the 'd' band is higher in energy compared to Ag and the interband transition is accessible above a threshold frequency of light in the visible region (**Figure 1.4 c**).^{23,32} On the contrary, for non-noble metals (Pd, Pt, Ni) the 'd' band intersects the Fermi level and hence the interband transitions are accessible throughout the visible regions and dominate over the intraband transition (**Figure 1.4 d**).^{23,32} Because of a high probability of interband transition (with a higher rate constant) throughout the visible region, the ϵ_2 value for the non-noble metals are typically higher compared to the noble metals (**Figure 1.4 b**).^{25,30} Therefore,

the noble metals (Au, Ag, Cu) with a smaller value of ϵ_2 (**Figure 1.4 b**) in the visible region are usually considered as plasmonic metals.^{25,30}

1.2.4. Plasmon Excitation and Generation of Hot Carriers:

Visible light excitation of plasmonic metal NPs induces a collective and coherent oscillation of free electrons on the surface of NPs. Thus, the light energy is confined on the surface of NPs in the form an elevated electric field.²⁸⁻³⁰ The energy stored in this elevated LSPR then undergoes two decay pathways: i) radiative pathway through the re-emission of a photon (scattering), or ii) non-radiative pathway through the generation of hot carriers.^{26,34-37} The radiative photon emission is the dominant pathway for larger particle (> 50 nm for Ag), and have numerous applications in the area of Surface Enhanced Raman Spectroscopy, chemical sensing and so on; however they are not suitable for light harvesting.³⁸ Whereas the non-radiative pathway is dominant for smaller size particles and leads to the generation of hot electrons and holes.³⁹ As discussed earlier, electronic excitation in metals can happen either through interband or intraband pathway. The plasmon decay via d to s interband transition would be the prominent pathway whenever accessible.

Recently, Atwater and co-workers performed a first principle calculation to understand the effect of particle size on the non-radiative decay pathways for excited plasmon.³⁵ The authors concluded that, the interband decay pathways for plasmonic AuNPs dominate at energies where its energetically accessible, irrespective of the size of the NPs.³⁵ On the other hand, the contribution from the intraband decay pathway is size dependent and becomes prominent only when the interband transition is not energetically accessible (**Figure 1.5 a**).³⁵ However, in case of AgNP, the interband decay is not energetically accessible in the visible region and thus the decay of plasmon predominantly proceeds through the intraband electronic transition.³⁵ Further, the energy distribution of the hot carriers is primarily governed by the decay pathway of the surface plasmon. Intraband transition generates a hot electron in the 's' band above the fermi level and a hot hole in the same band below the fermi level.³⁵ Similar energies of the electrons and holes yields a flat charge carrier distribution function, which is usually seen for Al and Ag NPs, (**Figure 1.5 b**).³⁵ Whereas, in interband transition, the high energy hot holes in the 'd' band and low energy hot electrons in the 's' band creates an asymmetric charge carrier distribution near the fermi level, as seen in Au and Cu NPs (**Figure 1.5 b**).³⁵ After the creation of the hot carriers, either through interband or intraband plasmon decay, they undergo a relaxation pathway. These hot carriers first redistribute their energy via electron-electron scattering in a time scale of 10-100 fs leading to a

secondary excitation, followed by a hot fermi distribution of electrons and holes close to the fermi level.^{26,34–37} Subsequently, these hot carriers dissipate their energy via electron-phonon relaxation

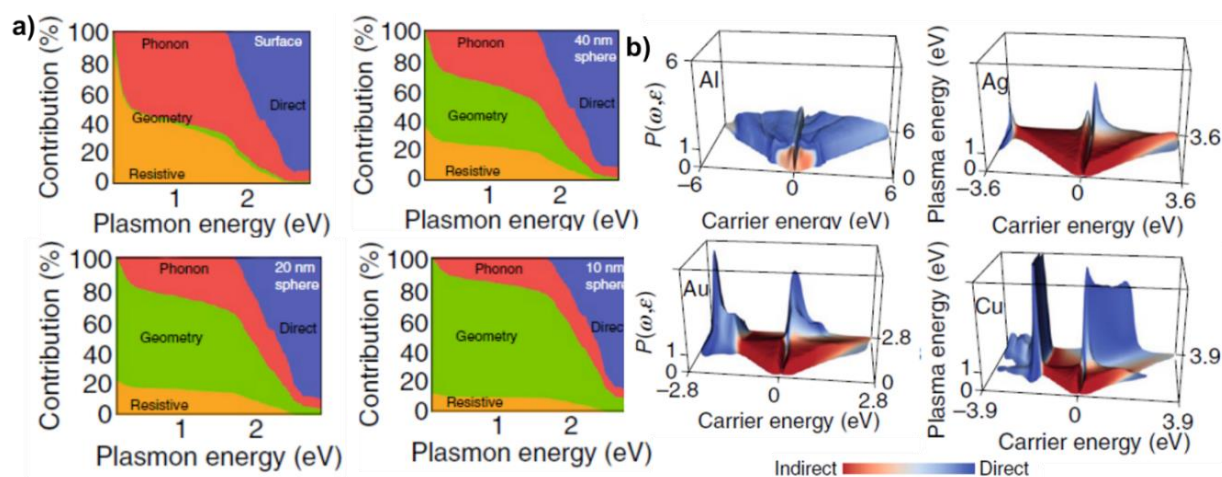


Figure 1.5. a) Contributions of geometry, phonon, resistive assisted, and direct excitations to absorption in a semi-infinite gold surface and spherical gold nanoparticles of various sizes as a function of plasmon energy. b) Energy distributions of initially excited hot carriers in Al, Ag, Au and Cu as a function of plasmon frequency and carrier energy. Adapted with permission from reference 35. Copyright 2016, American Chemical Society.

(~1 ps timescale) and releases heat to the NP lattice (plasmonic heating). Finally in a timescale of ~100 ps the NP lattice reaches a thermal equilibrium with the surroundings via phonon-phonon relaxation.^{26,34–37} Thus the hot electrons and holes generated through the plasmon decay can be used to trigger different oxidative or reductive transformations on the surface of NPs. This aspect has been discussed in the next section.

1.2.5. Photocatalysis with Plasmonic Metal Nanoparticles:

Efficient light absorption through LSPR and generation of hot charge carriers rendered the use of plasmonic metal NPs as an efficient photocatalyst.^{26,34–37,40–49} The initial photocatalytic studies were predominantly motivated by the use of metal NPs as a plasmonic antenna to improve the light absorption as well as charge separation efficiency of a metal/semiconductor hybrid photocatalytic systems.^{40–49} In this direction, one of the initial photocatalytic studies of metal@semiconductor composite materials were reported by Kamat and co-workers in Ag@TiO₂ core shell nanostructures (**Figure 1.6**).⁴³ The selective photoexcitation of TiO₂ shell with UV light resulted in the migration of electrons from semiconductor to the Ag metal core, which was accompanied by a shift in the surface plasmon band from 460 to 420 nm (**Figure 1.6 a,b**).⁴³ The stored electrons

were discharged using electron acceptors like O₂, thionine, or C₆₀ was introduced into the system (**Figure 1.6 c**).⁴¹ Charge equilibration with redox couple such as C₆₀/C₆₀^{•-} confirmed the

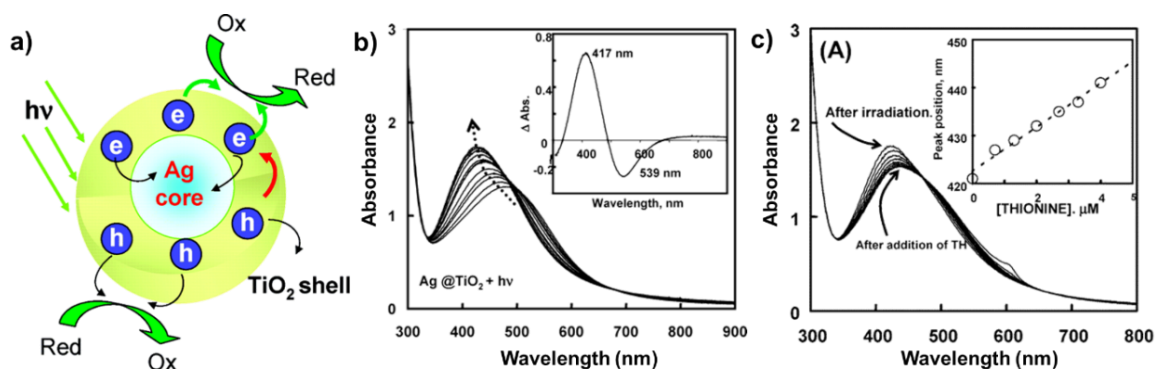


Figure 1.6. a) Schematic representation of electron-hole pair generation and migration of electrons from semiconductor to the metal. b) Spectral shift in the absorption of Ag@TiO₂ colloidal suspension in ethanol during UV-irradiation. The difference spectrum corresponding to the absorption changes is shown in the inset. c) Transfer of stored electrons from Ag@TiO₂ to a known amount of thionine dye. Inset shows the change in plasmon peak position as a function of concentration of thionine. Adapted with permission from reference 43. Copyright 2005, American Chemical Society.

ability of these structures to perform photocatalytic reduction reactions.⁴¹ The negative shift in the fermi level because of the charge equilibration between metal and semiconductor was found to be responsible for the higher photocatalytic activity of the hybrid system.⁴¹ Although, this was one of the very first experimental evidences for an efficient electron transfer between metal and semiconductor, the plasmon property of metal NPs was unexplored. The area of plasmon enhanced photocatalysis was largely invigorated by the seminal work from Tatsuma and co-workers, who for the first time investigated the effect of LSPR in improving the light absorption of semiconductor in an Au/TiO₂ nanohybrid system (**Figure 1.7 a,b**).⁴⁹ The photoexcitation of AuNP with visible light, resulted in an efficient injection of hot charge carriers from the NP to TiO₂ semiconductor (**Figure 1.7 a**).⁴⁷ The efficient electron transfer was accompanied by an increase in TiO₂ absorption at 600 nm. A 12 % Incident Photon to Current conversion efficiency (IPCE) was achieved by using Fe²⁺/Fe³⁺ as a redox mediator (**Figure 1.7 b**).⁴⁷ This was followed by numerous number of reports investigating the effect of LSPR in the photocatalytic activity of different semiconductor photocatalysts.⁴³⁻⁵² A series of investigations to understand the mechanism of enhanced charge separation have shown that a close contact between the metal and semiconductor creates a space charge region (i.e. Schottky junction) resulting in an upward or downward band

bending at the metal-semiconductor interface (depending on the n-type or p-type semiconductor, **Figure 1.7 c**).⁴⁷ This band bending at the interface induce a unidirectional movement to the electrons and holes reducing the rate of recombination (**Figure 1.7 c**).⁴⁷ Thus, the incorporation of plasmonic metals improve the light absorption capability as well as the charge separation efficiency in a metal/semiconductor hybrid photocatalytic system, which in turn improves the overall photocatalytic activity of the composite materials.

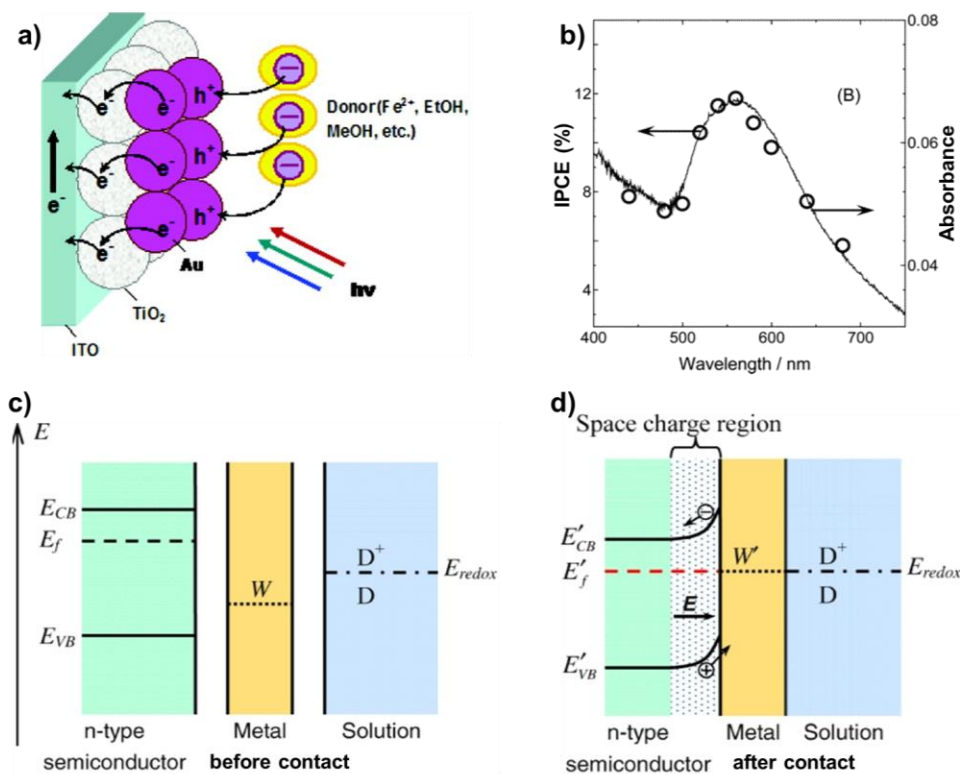


Figure 1.7. Plasmon enhanced photocatalysis in metal-semiconductor nanohybrid systems. a) Schematic illustration of the electron-hole pair generation and migration process from the metal to the semiconductor. The metal NP catalyst is usually regenerated by using a sacrificial electron donor. b) Action spectra for the changes in IPCE in Au/TiO₂ film. The IPCE values perfectly overlay with the absorption of the AuNPs. Adapted with permission from reference 49. Copyright 2005, American Chemical Society. c) Schematic illustration of the energy diagram of plasmonic metal-semiconductor nanohybrid systems before and after contact. Adapted with permission from reference 47. Copyright 2013, IOP Publishing.

Although, metal NPs have extensively been used as photosensitizers with semiconductor photocatalysts, their sole photocatalytic activity was only explored in recent years, where the hot carriers generated through the plasmon decay are being directly used to drive several reactions on

the surface of NPs.^{34,36,46,50–64} The hot electron chemistry was largely triggered by the seminal work from Linic and co-workers, who demonstrated the plasmonically driven epoxidation reaction with AgNPs. The oxidation of industrially relevant molecules like ethylene or propylene usually requires higher temperature and pressure. The plasmonic excitation of AgNPs under continuous wave (CW) visible light irradiation triggered the dissociation of the adsorbed O₂ molecule and lead to the oxidation of these molecules at room temperature and under ambient pressure. (**Figure 1.8 a,b,c**).⁶¹ A negligible rate of bond dissociation or oxidation in the absence of light, indicated that the plasmon excitation can trigger a chemical reaction on the surface of NPs.⁵⁹ In another study, Halas and co-workers demonstrated the H₂ dissociation reaction on plasmonic AuNPs (**Figure 1.9 a,b,c**).⁵⁵ Dissociation of H₂ is an extremely energy consuming reaction with a bond dissociation enthalpy of 435 kJ/mol.⁵³ The hot electrons generated through the plasmon decay were able to induce the dissociation of H₂ and D₂ molecule on the NP surface at room temperature.

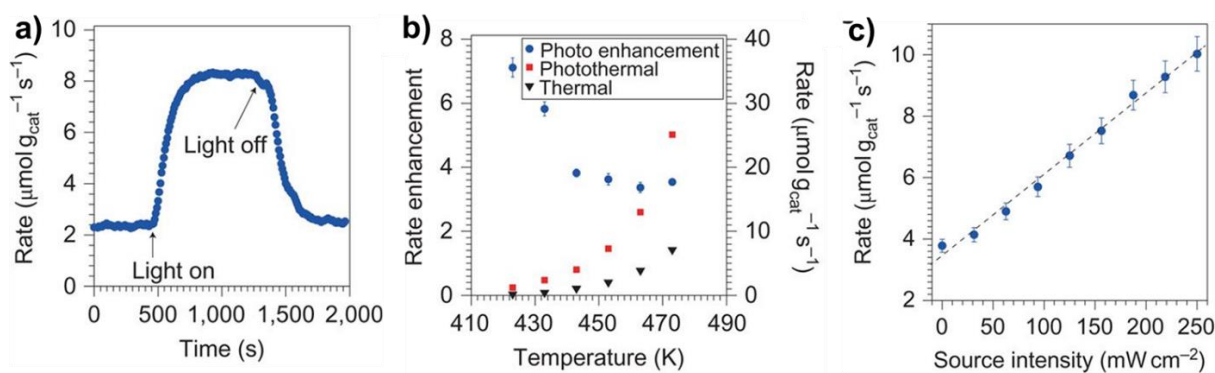


Figure 1.8. Plasmon driven photocatalytic ethylene epoxidation with AgNP as the catalyst. a) Ethylene epoxidation reaction at 450 K under dark and visible light irradiation. b) The enhancement in the photothermal rate (left axis) as a function of temperature. Rate enhancement factor was calculated by dividing the photothermal rate with that of thermal rate. The rate of the reaction (right axis) under photothermal and thermal condition as a function of temperature. c) Rate of ethylene epoxidation as a function of irradiation intensity. Adapted with permission from reference 61. Copyright 2011, Springer Nature.

A linear increase in the photocatalytic rate with the laser intensity confirmed the role of hot electrons in triggering the reaction (**Figure 1.9 c**).⁵³ A detailed first principle density functional theory calculation revealed that, the plasmonically excited NPs were able to deposit energy into the antibonding $1\sigma_u^*$ state of the adsorbed H₂ molecule, and thereby induced the dissociation of the molecule (**Figure 1.9 a**).⁵³ Recently, the multielectron transfer capability of plasmonic AuNP has been demonstrated by Jain and co-workers, where, plasmonic AuNPs photocatalyzed the

multielectron reduction of CO₂ to CH₄ and C₂H₆, under visible light irradiation

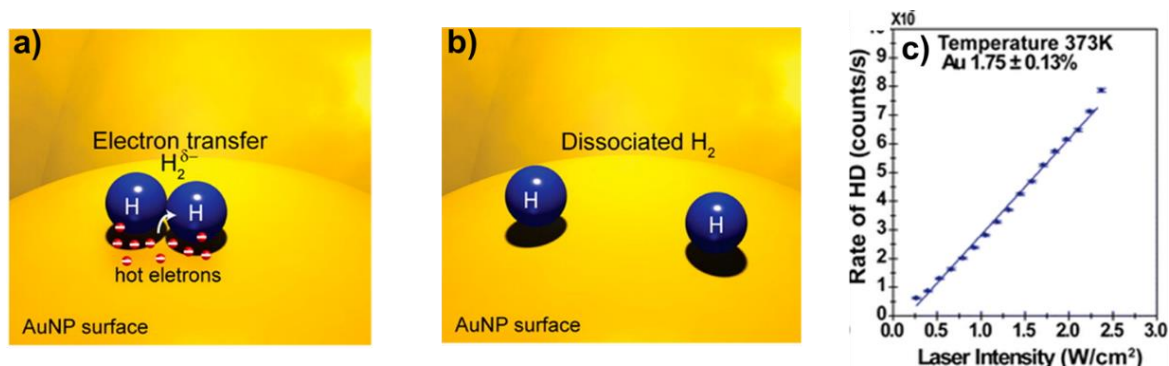


Figure 1.9. Photocatalytic H₂ dissociation on plasmonic AuNP. a,b) schematic illustration of the processes involved in photocatalytic H₂ dissociation on plasmonic AuNP surface. c) Rate of formation of HD on AuNP as a function irradiation intensity. Adapted with permission from reference 55. Copyright 2013, American Chemical Society.

(**Figure 1.10 a,b,c**).^{53,65} The reduction of CO₂ to CH₄ involves a 8e⁻-8H⁺ transfer whereas the production of C₂H₆ requires a 12e⁻-12H⁺ transfer step.^{53,65} A higher photon flux (to increase the rate of electron excitation) and the presence of a suitable hole scavenger (to suppress the rate of recombination) were found to be crucial for the accumulation and transfer of multiple charge carriers on the surface of NPs.^{53,65} Moreover, a control over the formation of CH₄ and C₂H₆ was achieved by tuning the intensity of the light irradiation, which in turn controls the generation of hot electrons and holes (**Figure 1.10 b,c**).⁵¹ In another study, Xiong and co-workers designed an Au/Ru plasmonic antenna reactor hybrid system for the photocatalytic reduction of N₂ to NH₃.⁵⁷ N₂ is an extremely stable and inert molecule with a high bond energy of 941 kJ/mole. Industrial production of NH₃ relies on the reduction of N₂ with Haber Bosch process, which requires a high temperature and pressure of 300⁰C and 100 atm, respectively.⁵⁷ The plasmonic properties of AuNP as well as the strong interaction between Ru and N₂ molecules were utilized for the photocatalytic reduction of N₂ to NH₃, in water under ambient condition.⁵⁷ Plethora of other studies have been performed to utilize the hot carriers in triggering different important chemical transformations like O₂ dissociation,^{61,62} water splitting,⁶⁴ NH₃ decomposition,⁵⁸ nitroaromatic reduction,^{59,60} metal ion reduction,⁵⁶ organic transformation⁵⁰ and so on.

Despite of being a great potential, the broad application of metal NP catalysts are in general impeded by their poor catalytic efficiency.⁶⁶⁻⁷³ One of the primary reasons attributed to the inertness of the metal NPs is the insulating surface ligands, which are essential to impart stability

to the NPs.^{66–73} Usually, the surface ligands inhibit the catalytic property of metal NPs and this is commonly known as “*ligand poisoning*” in the area of NP catalysis.^{66–73} The current theses is

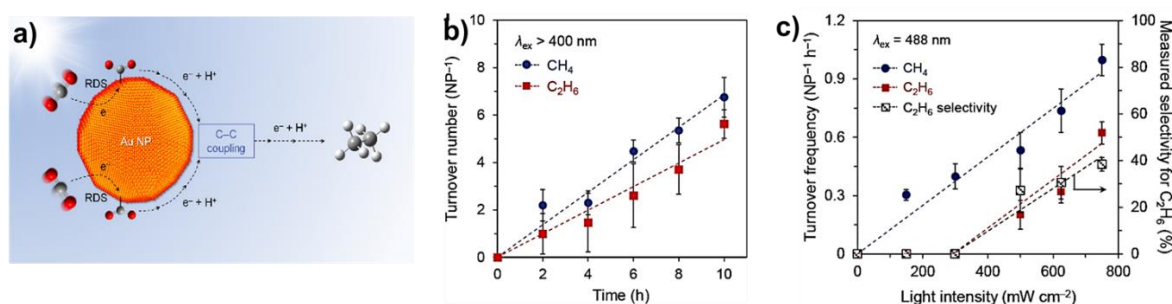


Figure 1.10. Photocatalytic CO₂ reduction on plasmonic AuNP. a) Schematic illustration for the photocatalytic multi-electron reduction of CO₂ on plasmonic AuNP. b) Time dependent CH₄ and C₂H₆ formation under the irradiation of CW visible light (> 400 nm). c) Intensity dependent CH₄ and C₂H₆ formation under CW 488nm laser irradiation. Adapted with permission from reference 53. Copyright 2018, American Chemical Society.

focused on developing an interaction based strategy to address this long standing fundamental challenge. The next section gives a brief description about the ligand poisoning effect, and provides a summary of different existing strategies to overcome this challenge.

1.3. Ligand Poisoning

In general, the metal NP catalysed reactions can be divided broadly into two categories. In certain reactions the metal NP helps to overcome the kinetic barrier for the reaction process by offering its surface for adsorption and mediating the transfer of electron between the reactant molecules. Here, the role of NPs is passive in nature.^{74–77} Reduction of nitro aromatics with borohydride¹⁶ and reduction of ferricyanide with borohydride¹⁶ are some of the classical examples of this category. On the contrary, in case of photocatalysis, the hot charge carriers generated through the photoexcitation of NPs are involved in the reaction process, and the NPs actively takes part in the reaction.³⁹ For both these types, a close proximity between NP catalyst and reactant molecules is required for the adsorption of reactant molecules on the NP surface.^{74–77} Oftentimes, during the process of adsorption, the reactant molecules have to encounter the insulating organic ligands on the surface of NPs which essentially hinders the diffusion of the molecules towards the NP surface. In general, surface ligands are ubiquitous in colloidal nanoscience. It stabilizes the NPs as well as dictates most of its physicochemical properties. However in catalysis, these surface ligands oftentimes play an inadvertent role by hindering the (i) accessibility of NP surface to the reactant

molecules (steric effect)^{67,70,72,78} and (ii) movement of hot carriers from the photoexcited NPs to the reactant molecules (due to insulating nature).^{66,73} This is commonly referred to as “*ligand poisoning*” in the area of NP catalysis.

Jain and co-workers, in their recent study have demonstrated the poisoning role of mercaptothiol ligands with different chain lengths in blocking the surface, and hence impeding the kinetics of galvanic exchange on individual AgNP (**Figure 1.11 a,b,c**).⁷⁰ Their study also proved that the ligand effect overpowered the role of NP size, shape and crystallinity on reaction kinetics. Longer chain mercaptothiols formed a thicker, and hence difficult to penetrate ligand shell resulting in poorer kinetics of galvanic exchange. Citrate capped AgNP, on the other hand, form loose ligand shells, and hence outperformed the mercaptothiol coated AgNP (**Figure 1.11 a,b,c**). In another study, Kitchens and co-workers investigated the effect of thiolated polyethylene glycol ligands (SH-PEG) on the catalytic reduction of 4-nitrophenol with AuNP as the catalyst (**Figure 1.11 d,e,f**).⁷⁸ The study revealed that the catalytic activity of the NPs are directly related to the ligand packing density as well as the chain length of the ligands. The low molecular weight ligands (1 kDa) with a higher surface coverage completely inhibited the reaction, whereas, there was a steady increase in the rate of the reaction with increase in the molecular weight of the polymer (**Figure 1.11 e,f**). Their study showed that low molecular weight PEG thiols, with a higher ligand packing density, were more prone towards poisoning the catalyst by blocking the surface accessibility; whereas the larger molecular weight PEG thiols were more suitable for catalytic reactions with colloidal AuNP. Recent work by Berlinguette and co-workers also demonstrated the poisoning effect of surface ligands on the adsorption and desorption equilibrium of H₂ molecule on Pd NP surface (**Figure 1.11 g,h,i**).⁶⁷ In situ X-ray monitoring experiments revealed a 10 times faster rate of H₂ adsorption and desorption process in pristine Pd NPs compare to that of ligated samples. The ligands were found to affect the phase transformation of the catalyst upon H₂ adsorption or desorption, and hence affecting the adsorption/desorption equilibrium. Thus, all these above representative studies show the inadvertent role played by the surface ligands to poison the catalytic activity of metal NPs. This ligand poisoning effect has been a long standing challenge in the area of NP catalysis, which needs to be addressed for further improvement of the catalytic property metal NPs.

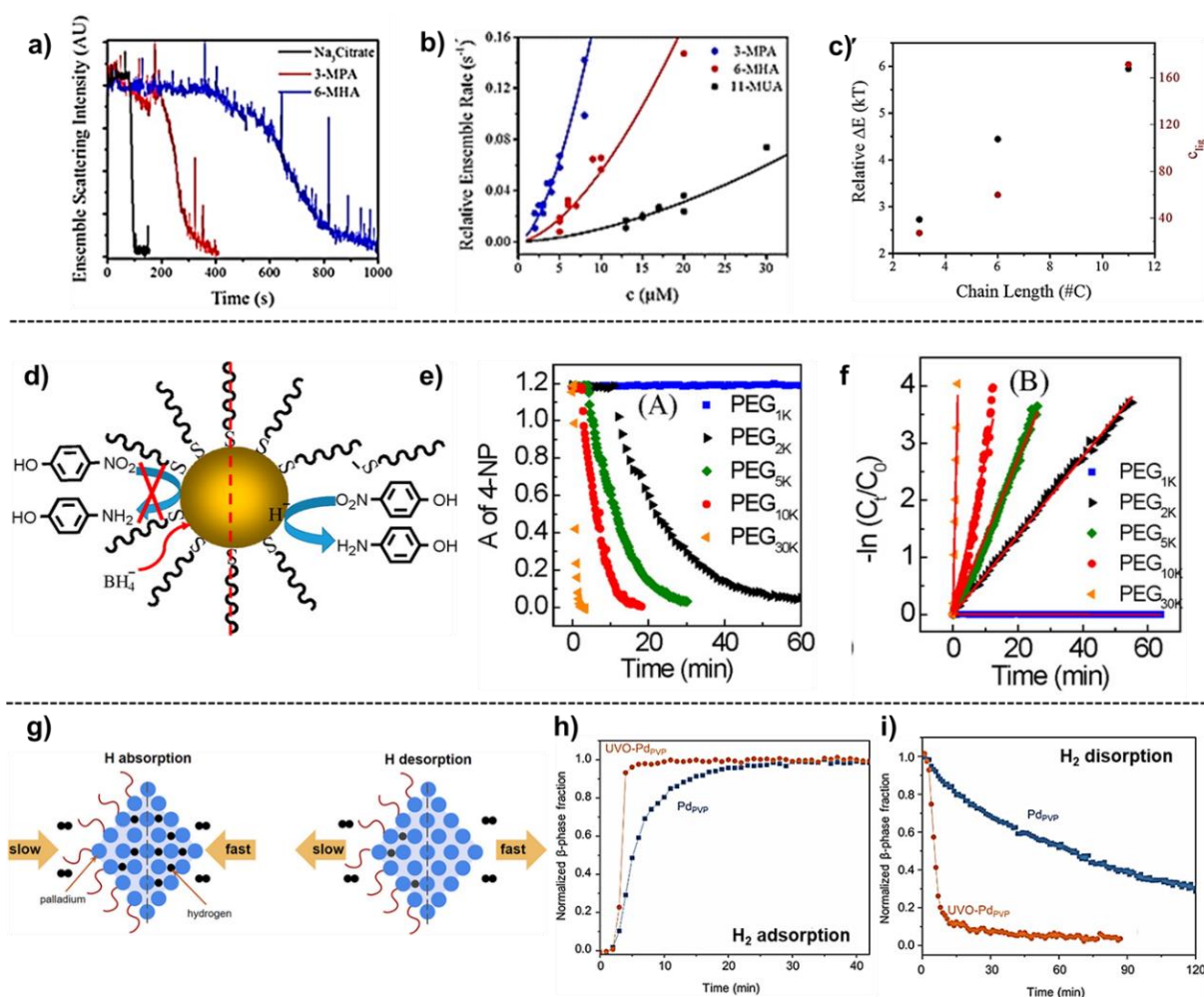


Figure 1.11. Ligand poisoning effect in metal NP catalysis. a) Kinetics of the galvanic exchange reaction. The ensemble trajectory generated through all single NP trajectories for three ligand coatings. The kinetics of the citrate capped NPs is faster compared to the thiolated NPs. b) The rate of the reaction as a function of chain length of ligands. The rate of galvanic exchange reaction decreased with increase in the chain length. c) Relative barrier height in terms of kT as a function of chain length. Adapted with permission from reference 70. Copyright 2016, American Chemical Society. d) Schematic illustration of ligand poisoning effect in the reduction of 4-nitro phenol with thiolated PEG capped AuNP. e) Progress of PNP reduction and f) corresponding linearized data for the first order analysis by tracking the absorption changes of PNP peak at 400 nm in the presence of AuNP capped with thiolated PEG ligands of varying molecular weights. The PEG ligands with highest molecular weight and lowest surface coverage value exhibited the highest rate of reaction. Adapted with permission from reference 78. Copyright 2016, American Chemical Society. g) Schematic representation of the ligand poisoning effect in H_2 adsorption and desorption reaction on the Pd NP surface. Comparison of h) H_2 adsorption kinetics and i) H_2 desorption kinetics on Pd NP surface with and without PVP ligands. Adapted with permission from reference 67. Copyright 2019, American Chemical Society

1.4. Strategies to Overcome Ligand Poisoning Effect

Two commonplace strategies to address the ligand poisoning effect are the (i) use of ligand free NPs^{66,73,79–81} or (ii) depositing NPs onto a solid support.⁸² The advantages and the limitations of these two strategies are discussed below.

Ligand Free NPs:

Synthesis of ligand free NPs is one of the attractive strategies to outweigh the poisoning effect of insulating organic ligands in catalytic and optoelectronic applications of colloidal NPs. Usually different small ions (instead of long chain organic molecules) like S^{2-} , BH_4^- , SH^- , NH_4^+ , Se^{2-} , HSe^- etc. are used to attain the colloidal stability of the NPs.^{66,73,79–81} These ligand free particles have already paved their way in numerous sensing, optoelectronic and device level applications with enhanced activity compared to that of ligated NPs.^{66,73,79–81} In catalysis too, these particles usually offer a higher surface area leading to a better catalytic activity.⁷⁹ However, there are two major limitations which restrict their use as a suitable alternate to outplay the ligand poisoning effect. Oftentimes, due to the absence of strongly bound surface ligands, the NPs get precipitated out of the solution during the first cycle of reaction, and thus the recyclability aspect of these particles are always questionable.⁷⁹ Secondly, a limited scope of surface chemistry forces their use to be solvent specific, which is not desirable for general catalysis. Thus, the ligand free NPs despite being a promising alternative in the area of optoelectronic devices, the catalytic property of these particles have not received much attention.

Heterogeneous Catalysis:

Another promising strategy to address the ligand poisoning effect is to stabilize the NPs by depositing them onto a solid support.⁸² This has been an attractive strategy to remove the surface ligands while keeping the activity of the particles intact. Several catalytic as well as photocatalytic reactions have been performed by depositing different metal NPs onto oxide based semiconductor supports (TiO_2 , ZnO , ZrO_2 etc.),^{46,55,83} carbon based solid supports,^{84,85} polymer supports^{86,87} and so on. Some of the major advantages of these heterogeneous catalysts are mentioned below.

(i) *High recyclability*: Because of the heterogeneous nature and stability, multiple cycles of reactions can be performed with the same catalyst particles, which is highly desirable for any catalytic applications.⁸²

(ii) *Comparable catalytic activity*: Successful deposition of the particles with the removal of surface ligands oftentimes improve the catalytic activity of these deposited metal NPs catalysts.⁸²

(iii) *Easy separation of catalysts*: Removal of catalyst particles from the reaction system is one of the major challenges in homogeneous catalysis. The heterogeneous nature of the deposited metal NPs allow an easy separation of the catalyst particles after the completion of the reaction.

Thus heterogeneous catalysts have evolved as a promising alternative in the area of metal NP catalysis.⁶⁰ However, from the fundamental point of view there are certain limitations associated with these catalytic systems.

(i) *Heterogeneity on the catalyst surface*: Synthesis of these heterogeneous catalysts commonly rely on the co-precipitation methods resulting in a heterogeneous and random distribution of metal NPs on the solid supports, which is not desirable for an in depth understanding of the mechanism of a particular reaction.⁸⁸

(ii) *Reduced surface area of NPs*: Oftentimes the NPs undergo aggregation during the synthesis of the catalyst resulting in the loss of active surface area. Moreover, because of deposition, a part of the active surface of the catalyst remains embedded into the solid support and the full potential of the catalyst remains unrealized.⁶¹

(iii) *Complexity of the system*: Involvement of more than one material oftentimes increase the complexity of the system and makes it difficult to unravel the individual contribution from each material, which is required to understand the full capability of the metal NP catalyst. Sometimes the semiconductor or the solid support can strongly interfere in the process of the reaction. Especially, in case of photocatalysis, several photophysical processes (charge separation, hot electron injection, nearfield enhancement, plasmon induced resonance energy transfer and so on) can take place at the interface,⁸⁹ which makes it extremely complex to understand the actual mechanism of the reaction. For instance, in case of plasmonic photocatalysis, the reaction on the surface of NPs can be triggered either by plasmon heating or by the hot electrons generated through the plasmon decay.⁹⁰ Oftentimes in heterogeneous plasmonic catalysts, the complex heat transport and inhomogeneous temperature distribution makes it difficult to disentangle the relative contribution and hence, leads to improper assumptions regarding the mechanism of the reaction.⁹⁰ Therefore, the colloidal photocatalytic systems with a constant heat flow from the NP surface to the bulk solution are usually considered to be the ideal system for addressing this fundamental question.⁹⁰ In short, the heterogeneous catalysis, although extremely relevant in terms of industrial applicability but not suitable for a fundamental in-depth understanding, and hence alternate design principles have to be developed. Specifically, systematic investigations with colloidal catalysis can

lead to new design principles, which will be beneficial for the advancement in heterogeneous catalysis. An ideal way will be to perform catalysis with dispersed NPs, for which the colloidal stability of the NPs is essential. Thus nanoparticles and ligands are two inseparable entities, and strategies have to be developed to perform efficient colloidal catalysis with ligands intact on the surface of the NPs. Moreover, an ideal strategy should be to use the surface ligands as a tool to improve as well as dictate the catalytic activity of metal NPs. Further, such strategies can be easily incorporated in heterogeneous catalysis, in order to realize the industrial prospects as well.

1.5. Ligand Directed Catalysis

A limited number of efforts have been invested so far to develop strategies for utilizing the surface ligands to improve the catalytic activity of NPs. In this direction, one of the very first reports were published by Medlin and co-workers who used the monolayer coating of n-alkenathiol ligands for the selective hydrogenation of 1-epoxy-3-butene (EpB) to 1-epoxybutane on Pd catalyst (**Figure 1.12 a,b**).⁹¹ Generally, the hydrogenation of EpB on Pd involves the formation of a series of undesirable by-products with a very poor selectivity towards the formation of 1-epoxybutane (**Figure 1.12 a**). The reaction proceeds through an epoxy ring opening step for the formation of an aldehyde intermediate, which further leads to the formation of undesired by-products. A strong interaction of EpB through the epoxy oxygen is responsible for this ring opening step. The authors observed a dramatic increase in the product selectivity from 11 % to 94 % upon coating the catalyst surface with a monolayer of n-alkane thiol ligands (**Figure 1.12 b**). A detailed investigation revealed that the poisoning effect of sulphur was responsible behind this improved selectivity. The co-ordination of sulphur on the Pd surface induce a change in the surface structure of Pd catalyst and some of the (111) crystal faces change their orientation into (100). The (100) face is less active compared to (111) crystal face, and thus the activity of Pd was reduced upon binding with sulphur. Because of this reduced activity the epoxy ring opening step was disfavoured and the reaction was stopped at the desired step. Thus, the catalyst poisoning effect of sulphur was cleverly utilized by the authors to induce selectivity into the Pd catalysed reaction. In another study, Zheng and co-workers demonstrated the ability of electron donating ethylenediamine (EDA) ligands to vary the electronic structure of ultrathin platinum nanowires, and studied their effects on the ability of hydrogenation of nitroaromatics (**Figure 1.12 c,d**).⁹² Commercial Pt catalyst efficiently reduces nitrobenzene to aniline or its derivatives. EDA coating on the platinum nanowires, due to its electron donating nature, made the nanowire surface electron rich resulting in the adsorption of

electron poor reactant, but not the electron rich N-hydroxylamine.

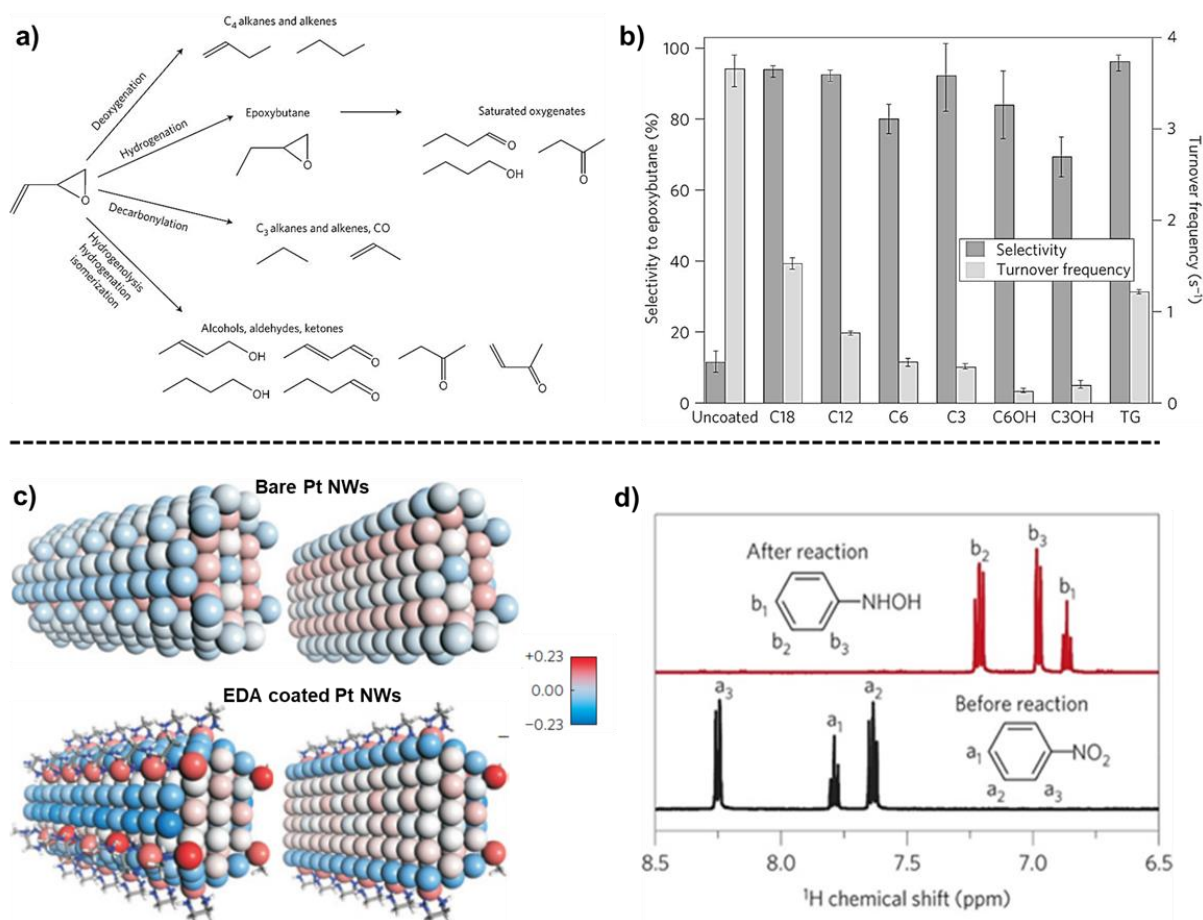


Figure 1.12. Ligand directed metal NP catalysis. a) Pathway for different product formation in the hydrogenation of epoxybutene on Pd NP catalyst. b) Bar diagram showing the selectivity (left axis) and the Turnover Number (TON) for the formation of epoxybutane after coating the catalyst surface with monolayer of n-alkane thiols of varying ligand chain length. Adapted with permission from reference 91. Copyright 2010, Springer Nature. c) Model of Pt nanowire with corresponding Bader Charge analysis in presence and absence of EDA ligands. d) 1H NMR spectrum of the product before and after the reaction. Adapted with permission from reference 92. Copyright 2016, Springer Nature.

This led to the turning-off of the reaction selectively at commercially valuable N-hydroxylamine (**Figure 1.12 c,d**). The knowledge gained was crucial in imparting selectivity to a commercially available Pt black catalyst for the production of N-hydroxylamine. Thus, the above two examples clearly demonstrate that the surface ligands, if utilized cleverly, can play a crucial role in not only improving the catalytic activity but also dictating the product selectivity.

1.6. Objective of the Thesis:

The present thesis focuses on circumventing the “*ligand poisoning*” effect by developing an interaction based strategy, where the surface ligands would be utilized to create a precise interaction between NP catalysts and reactant molecules to improve the catalytic property of NPs (**Figure 1.13**). We envision that, creating a precise interaction through judicious choice of surface ligands would help in channelling the reactant molecules towards the NP surface. This is expected to increase the local concentration of reactant molecules, which in turn will increase the probability of the reaction. Thus, the ligands on the surface of NPs, rather than blocking the surface accessibility would control the gating of the reactant molecules towards the NP surface. For a favourable surface chemistry, it would facilitate the diffusion of the reactant molecules towards the NP surface, which will improve the catalytic activity; whereas in case of unfavourable surface chemistry, the ligands would block the diffusion of the reactant molecules impeding the catalytic activity of NPs. Thus, a precise tuning of surface chemistry would not only improve the catalytic activity but also impart a control over the catalytic property of metal NPs. Furthermore, one of the major challenges in the area of hot electron catalysis is to improve the efficiency of the photocatalytic reaction, which most of the time rely on an efficient transfer of hot carriers from the NPs to the reactant molecules. We hypothesize that, creating a precise NP-reactant interaction would improve the efficiency of hot electron transfer, and hence the photocatalytic efficiency of metal NPs. Thus, a successful accomplishment of these objectives will introduce a new strategy of *ligand directed catalysis* for addressing a long standing challenge of “*ligand poisoning*” in the area of NP catalysis.

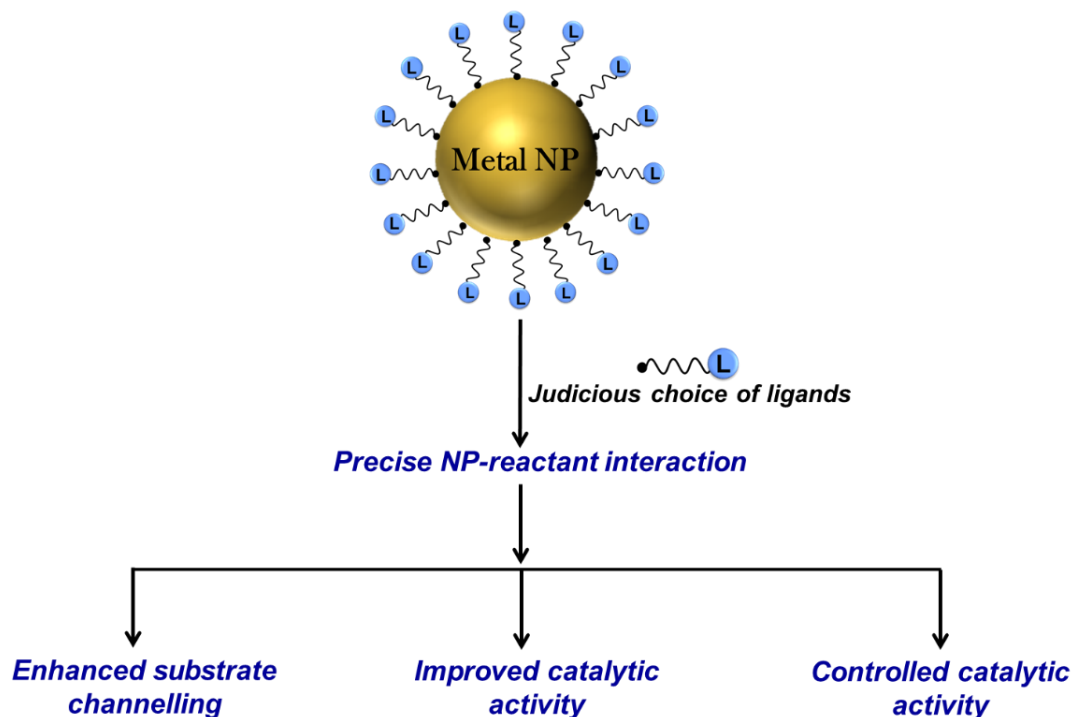


Figure 1.13: Schematic representation showing the main objective of the thesis.

1.7. References

- (1) Front Matter. In *Nanoparticles and Catalysis*; Astruc, D., Ed.; Wiley-VCH Verlag GmbH & Co. KGaA: Weinheim, Germany; pp I–XXIII.
- (2) Polshettiwar, V.; Varma, R. S. Green Chemistry by Nano-Catalysis. *Green Chem.* **2010**, *12*, 743.
- (3) Mohamed, R. M.; McKinney, D. L.; Sigmund, W. M. Enhanced Nanocatalysts. *Materials Science and Engineering: R: Reports* **2012**, *73*, 1–13.
- (4) Cole-Hamilton, D. J. Homogeneous Catalysis--New Approaches to Catalyst Separation, Recovery, and Recycling. *Science* **2003**, *299*, 1702–1706.
- (5) Astruc, D.; Lu, F.; Aranzaes, J. R. Nanoparticles as Recyclable Catalysts: The Frontier between Homogeneous and Heterogeneous Catalysis. *Angew. Chem. Int. Ed.* **2005**, *44*, 7852–7872.
- (6) Mahmoud, M. A.; O’Neil, D.; El-Sayed, M. A. Hollow and Solid Metallic Nanoparticles in Sensing and in Nanocatalysis. *Chem. Mater.* **2014**, *26*, 44–58.

- (7) Copéret, C.; Chabanas, M.; Petroff Saint-Arroman, R.; Basset, J.-M. Homogeneous and Heterogeneous Catalysis: Bridging the Gap through Surface Organometallic Chemistry. *Angew. Chem. Int. Ed.* **2003**, *42*, 156–181.
- (8) Corma, A. Heterogeneous Catalysis: Understanding for Designing, and Designing for Applications. *Angew. Chem. Int. Ed.* **2016**, *55*, 6112–6113.
- (9) Narayanan, R.; El-Sayed, M. A. Effect of Nanocatalysis in Colloidal Solution on the Tetrahedral and Cubic Nanoparticle SHAPE: Electron-Transfer Reaction Catalyzed by Platinum Nanoparticles. *J. Phys. Chem. B* **2004**, *108*, 5726–5733.
- (10) Mahmoud, M. A.; Narayanan, R.; El-Sayed, M. A. Enhancing Colloidal Metallic Nanocatalysis: Sharp Edges and Corners for Solid Nanoparticles and Cage Effect for Hollow Ones. *Acc. Chem. Res.* **2013**, *46*, 1795–1805.
- (11) Park, J.; Kwon, T.; Kim, J.; Jin, H.; Kim, H. Y.; Kim, B.; Joo, S. H.; Lee, K. Hollow Nanoparticles as Emerging Electrocatalysts for Renewable Energy Conversion Reactions. *Chem. Soc. Rev.* **2018**, *47*, 8173–8202.
- (12) Nishida, Y.; Sato, K.; Yamamoto, T.; Wu, D.; Kusada, K.; Kobayashi, H.; Matsumura, S.; Kitagawa, H.; Nagaoka, K. Facile Synthesis of Size-Controlled Rh Nanoparticles via Microwave-Assisted Alcohol Reduction and Their Catalysis of CO Oxidation. *Chem. Lett.* **2017**, *46*, 1254–1257.
- (13) Polshettiwar, V.; Luque, R.; Fihri, A.; Zhu, H.; Bouhrara, M.; Basset, J.-M. Magnetically Recoverable Nanocatalysts. *Chem. Rev.* **2011**, *111*, 3036–3075.
- (14) Yang, X.-F.; Wang, A.; Qiao, B.; Li, J.; Liu, J.; Zhang, T. Single-Atom Catalysts: A New Frontier in Heterogeneous Catalysis. *Acc. Chem. Res.* **2013**, *46*, 1740–1748.
- (15) Sonström, P.; Bäumer, M. Supported Colloidal Nanoparticles in Heterogeneous Gas Phase Catalysis: On the Way to Tailored Catalysts. *Phys. Chem. Chem. Phys.* **2011**, *13*, 19270.
- (16) Cao, S.; Tao, F. (Feng); Tang, Y.; Li, Y.; Yu, J. Size- and Shape-Dependent Catalytic Performances of Oxidation and Reduction Reactions on Nanocatalysts. *Chem. Soc. Rev.* **2016**, *45*, 4747–4765.
- (17) Rodrigues, T. S.; da Silva, A. G. M.; Camargo, P. H. C. Nanocatalysis by Noble Metal Nanoparticles: Controlled Synthesis for the Optimization and Understanding of Activities. *J. Mater. Chem. A* **2019**, *7*, 5857–5874.

- (18) Janssens, T. V. W.; Clausen, B. S.; Hvolbæk, B.; Falsig, H.; Christensen, C. H.; Bligaard, T.; Nørskov, J. K. Insights into the Reactivity of Supported Au Nanoparticles: Combining Theory and Experiments. *Top Catal* **2007**, *44*, 15–26.
- (19) Dong, C.; Lian, C.; Hu, S.; Deng, Z.; Gong, J.; Li, M.; Liu, H.; Xing, M.; Zhang, J. Size-Dependent Activity and Selectivity of Carbon Dioxide Photocatalytic Reduction over Platinum Nanoparticles. *Nat. Commun.* **2018**, *9*, 1252.
- (20) Li, J.; Chen, W.; Zhao, H.; Zheng, X.; Wu, L.; Pan, H.; Zhu, J.; Chen, Y.; Lu, J. Size-Dependent Catalytic Activity over Carbon-Supported Palladium Nanoparticles in Dehydrogenation of Formic Acid. *Journal of Catalysis* **2017**, *352*, 371–381.
- (21) Van Santen, R. A. Complementary Structure Sensitive and Insensitive Catalytic Relationships. *Acc. Chem. Res.* **2009**, *42*, 57–66.
- (22) Che, M.; Bennett, C. O. The Influence of Particle Size on the Catalytic Properties of Supported Metals. In *Advances in Catalysis*; Elsevier; Vol. 36, pp 55–172.
- (23) Hartland, G. V.; Besteiro, L. V.; Johns, P.; Govorov, A. O. What's so Hot about Electrons in Metal Nanoparticles? *ACS Energy Lett.* **2017**, *2*, 1641–1653.
- (24) Rao, V. G.; Aslam, U.; Linic, S. Chemical Requirement for Extracting Energetic Charge Carriers from Plasmonic Metal Nanoparticles to Perform Electron-Transfer Reactions. *J. Am. Chem. Soc.* **2019**, *141*, 643–647.
- (25) Linic, S.; Christopher, P.; Ingram, D. B. Plasmonic-Metal Nanostructures for Efficient Conversion of Solar to Chemical Energy. *Nat. Mater* **2011**, *10*, 911–921.
- (26) Brongersma, M. L.; Halas, N. J.; Nordlander, P. Plasmon-Induced Hot Carrier Science and Technology. *Nat. Nanotech.* **2015**, *10*, 25–34.
- (27) Langhammer, C.; Kasemo, B.; Zorić, I. Absorption and Scattering of Light by Pt, Pd, Ag, and Au Nanodisks: Absolute Cross Sections and Branching Ratios. *The Journal of Chemical Physics* **2007**, *126*, 194702.
- (28) El-Sayed, M. A. Some Interesting Properties of Metals Confined in Time and Nanometer Space of Different Shapes. *Acc. Chem. Res.* **2001**, *34*, 257–264.
- (29) Jain, P. K.; Huang, X.; El-Sayed, I. H.; El-Sayed, M. A. Noble Metals on the Nanoscale: Optical and Photothermal Properties and Some Applications in Imaging, Sensing, Biology, and Medicine. *Acc. Chem. Res.* **2008**, *41*, 1578–1586.

- (30) Link, S.; El-Sayed, M. A. Spectral Properties and Relaxation Dynamics of Surface Plasmon Electronic Oscillations in Gold and Silver Nanodots and Nanorods. *J. Phys. Chem. B* **1999**, *103*, 8410–8426.
- (31) Stiles, P. L.; Dieringer, J. A.; Shah, N. C.; Van Duyne, R. P. Surface-Enhanced Raman Spectroscopy. *Annual Rev. Anal. Chem.* **2008**, *1*, 601–626.
- (32) Aslam, U.; Rao, V. G.; Chavez, S.; Linic, S. Catalytic Conversion of Solar to Chemical Energy on Plasmonic Metal Nanostructures. *Nat. Catal.* **2018**, *1*, 656–665.
- (33) Khurgin, J. B. How to Deal with the Loss in Plasmonics and Metamaterials. *Nat. Nanotech.* **2015**, *10*, 2–6.
- (34) Yu, S.; Wilson, A. J.; Kumari, G.; Zhang, X.; Jain, P. K. Opportunities and Challenges of Solar-Energy-Driven Carbon Dioxide to Fuel Conversion with Plasmonic Catalysts. *ACS Energy Lett.* **2017**, *2*, 2058–2070.
- (35) Brown, A. M.; Sundararaman, R.; Narang, P.; Goddard, W. A.; Atwater, H. A. Nonradiative Plasmon Decay and Hot Carrier Dynamics: Effects of Phonons, Surfaces, and Geometry. *ACS Nano* **2016**, *10*, 957–966.
- (36) Kale, M. J.; Avanesian, T.; Christopher, P. Direct Photocatalysis by Plasmonic Nanostructures. *ACS Catal.* **2014**, *4*, 116–128.
- (37) Linic, S.; Aslam, U.; Boerigter, C.; Morabito, M. Photochemical Transformations on Plasmonic Metal Nanoparticles. *Nat. Mater.* **2015**, *14*, 567–576.
- (38) Jain, P. K.; Lee, K. S.; El-Sayed, I. H.; El-Sayed, M. A. Calculated Absorption and Scattering Properties of Gold Nanoparticles of Different Size, Shape, and Composition: Applications in Biological Imaging and Biomedicine. *J. Phys. Chem. B* **2006**, *110*, 7238–7248.
- (39) Evanoff, D. D.; Chumanov, G. Size-Controlled Synthesis of Nanoparticles. 2. Measurement of Extinction, Scattering, and Absorption Cross Sections. *J. Phys. Chem. B* **2004**, *108*, 13957–13962.
- (40) Hou, W.; Cronin, S. B. A Review of Surface Plasmon Resonance-Enhanced Photocatalysis. *Adv. Funct. Mater.* **2013**, *23*, 1612–1619.
- (41) Takai, A.; Kamat, P. V. Capture, Store, and Discharge. Shuttling Photogenerated Electrons across TiO₂–Silver Interface. *ACS Nano* **2011**, *5*, 7369–7376.

- (42) Zheng, Z.; Huang, B.; Qin, X.; Zhang, X.; Dai, Y.; Whangbo, M.-H. Facile in Situ Synthesis of Visible-Light Plasmonic Photocatalysts M@TiO₂ (M = Au, Pt, Ag) and Evaluation of Their Photocatalytic Oxidation of Benzene to Phenol. *J. Mater. Chem.* **2011**, *21*, 9079.
- (43) Hirakawa, T.; Kamat, P. V. Charge Separation and Catalytic Activity of Ag@TiO₂ Core–Shell Composite Clusters under UV–Irradiation. *J. Am. Chem. Soc.* **2005**, *127*, 3928–3934.
- (44) Subramanian, V.; Wolf, E. E.; Kamat, P. V. Catalysis with TiO₂/Gold Nanocomposites. Effect of Metal Particle Size on the Fermi Level Equilibration. *J. Am. Chem. Soc.* **2004**, *126*, 4943–4950.
- (45) Fu, Y.; Li, J.; Li, J. Metal/Semiconductor Nanocomposites for Photocatalysis: Fundamentals, Structures, Applications and Properties. *Nanomaterials* **2019**, *9*, 359.
- (46) Clavero, C. Plasmon-Induced Hot-Electron Generation at Nanoparticle/Metal-Oxide Interfaces for Photovoltaic and Photocatalytic Devices. *Nat. Photon* **2014**, *8*, 95–103.
- (47) Zhang, X.; Chen, Y. L.; Liu, R.-S.; Tsai, D. P. Plasmonic Photocatalysis. *Rep. Prog. Phys.* **2013**, *76*, 046401.
- (48) Zhang, N.; Han, C.; Fu, X.; Xu, Y.-J. Function-Oriented Engineering of Metal-Based Nanohybrids for Photoredox Catalysis: Exerting Plasmonic Effect and Beyond. *Chem* **2018**, *4*, 1832–1861.
- (49) Tian, Y.; Tatsuma, T. Mechanisms and Applications of Plasmon-Induced Charge Separation at TiO₂ Films Loaded with Gold Nanoparticles. *J. Am. Chem. Soc.* **2005**, *127*, 7632–7637.
- (50) Gellé, A.; Jin, T.; de la Garza, L.; Price, G. D.; Besteiro, L. V.; Moores, A. Applications of Plasmon-Enhanced Nanocatalysis to Organic Transformations. *Chem. Rev.* **2020**, *120*, 986–1041.
- (51) Dhiman, M.; Maity, A.; Das, A.; Belgamwar, R.; Chalke, B.; Lee, Y.; Sim, K.; Nam, J.-M.; Polshettiwar, V. Plasmonic Colloidosomes of Black Gold for Solar Energy Harvesting and Hotspots Directed Catalysis for CO₂ to Fuel Conversion. *Chem. Sci.* **2019**, *10*, 6594–6603.
- (52) Robotjazi, H.; Zhao, H.; Swearer, D. F.; Hogan, N. J.; Zhou, L.; Alabastri, A.; McClain, M. J.; Nordlander, P.; Halas, N. J. Plasmon-Induced Selective Carbon Dioxide Conversion on Earth-Abundant Aluminum-Cuprous Oxide Antenna-Reactor Nanoparticles. *Nat. Commun.* **2017**, *8*, 27.

- (53) Yu, S.; Wilson, A. J.; Heo, J.; Jain, P. K. Plasmonic Control of Multi-Electron Transfer and C–C Coupling in Visible-Light-Driven CO₂ Reduction on Au Nanoparticles. *Nano Lett.* **2018**, *18*, 2189–2194.
- (54) Zhang, X.; Li, X.; Zhang, D.; Su, N. Q.; Yang, W.; Everitt, H. O.; Liu, J. Product Selectivity in Plasmonic Photocatalysis for Carbon Dioxide Hydrogenation. *Nat. Commun.* **2017**, *8*, 14542.
- (55) Mukherjee, S.; Libisch, F.; Large, N.; Neumann, O.; Brown, L. V.; Cheng, J.; Lassiter, J. B.; Carter, E. A.; Nordlander, P.; Halas, N. J. Hot Electrons Do the Impossible: Plasmon-Induced Dissociation of H₂ on Au. *Nano Lett.* **2013**, *13*, 240–247.
- (56) Zhai, Y.; DuChene, J. S.; Wang, Y.-C.; Qiu, J.; Johnston-Peck, A. C.; You, B.; Guo, W.; DiCiaccio, B.; Qian, K.; Zhao, E. W.; et al. Polyvinylpyrrolidone-Induced Anisotropic Growth of Gold Nanoprisms in Plasmon-Driven Synthesis. *Nat. Mater.* **2016**, *15*, 889–895.
- (57) Hu, C.; Chen, X.; Jin, J.; Han, Y.; Chen, S.; Ju, H.; Cai, J.; Qiu, Y.; Gao, C.; Wang, C.; et al. Surface Plasmon Enabling Nitrogen Fixation in Pure Water through a Dissociative Mechanism under Mild Conditions. *J. Am. Chem. Soc.* **2019**, *141*, 7807–7814.
- (58) Zhou, L.; Swearer, D. F.; Zhang, C.; Robotjazi, H.; Zhao, H.; Henderson, L.; Dong, L.; Christopher, P.; Carter, E. A.; Nordlander, P.; et al. Quantifying Hot Carrier and Thermal Contributions in Plasmonic Photocatalysis. *Science* **2018**, *362*, 69–72.
- (59) Xie, W.; Schlücker, S. Hot Electron-Induced Reduction of Small Molecules on Photorecycling Metal Surfaces. *Nat. Commun.* **2015**, *6*, 7570.
- (60) Zhu, H.; Ke, X.; Yang, X.; Sarina, S.; Liu, H. Reduction of Nitroaromatic Compounds on Supported Gold Nanoparticles by Visible and Ultraviolet Light. *Angew. Chem. Int. Ed.* **2010**, *49*, 9657–9661.
- (61) Christopher, P.; Xin, H.; Linic, S. Visible-Light-Enhanced Catalytic Oxidation Reactions on Plasmonic Silver Nanostructures. *Nat. Chem.* **2011**, *3*, 467–472.
- (62) Christopher, P.; Xin, H.; Marimuthu, A.; Linic, S. Singular Characteristics and Unique Chemical Bond Activation Mechanisms of Photocatalytic Reactions on Plasmonic Nanostructures. *Nat. Mater.* **2012**, *11*, 1044–1050.
- (63) Zhang, Y.; He, S.; Guo, W.; Hu, Y.; Huang, J.; Mulcahy, J. R.; Wei, W. D. Surface-Plasmon-Driven Hot Electron Photochemistry. *Chem. Rev.* **2018**, *118*, 2927–2954.

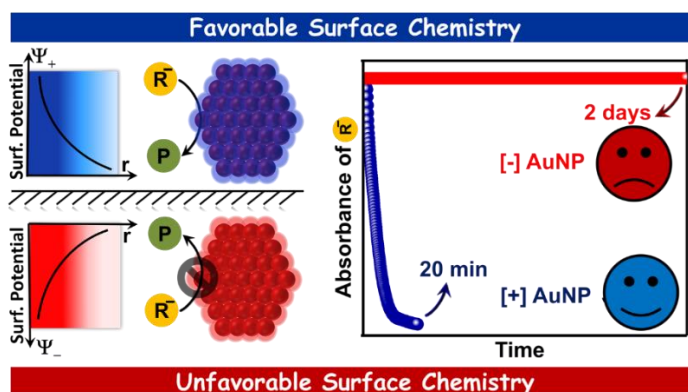
- (64) Mubeen, S.; Lee, J.; Singh, N.; Krämer, S.; Stucky, G. D.; Moskovits, M. An Autonomous Photosynthetic Device in Which All Charge Carriers Derive from Surface Plasmons. *Nat. Nanotech.* **2013**, *8*, 247–251.
- (65) Yu, S.; Jain, P. K. Plasmonic Photosynthesis of C1–C3 Hydrocarbons from Carbon Dioxide Assisted by an Ionic Liquid. *Nat. Commun.* **2019**, *10*, 2022.
- (66) Kovalenko, M. V.; Scheele, M.; Talapin, D. V. Colloidal Nanocrystals with Molecular Metal Chalcogenide Surface Ligands. *Science* **2009**, *324*, 1417–1420.
- (67) Johnson, N. J. J.; Lam, B.; Sherbo, R. S.; Fork, D. K.; Berlinguette, C. P. Ligands Affect Hydrogen Absorption and Desorption by Palladium Nanoparticles. *Chem. Mater.* **2019**, *31*, 8679–8684.
- (68) Gong, J. Structure and Surface Chemistry of Gold-Based Model Catalysts. *Chem. Rev.* **2012**, *112*, 2987–3054.
- (69) Li, D.; Wang, C.; Tripkovic, D.; Sun, S.; Markovic, N. M.; Stamenkovic, V. R. Surfactant Removal for Colloidal Nanoparticles from Solution Synthesis: The Effect on Catalytic Performance. *ACS Catal.* **2012**, *2*, 1358–1362.
- (70) Smith, J. G.; Jain, P. K. The Ligand Shell as an Energy Barrier in Surface Reactions on Transition Metal Nanoparticles. *J. Am. Chem. Soc.* **2016**, *138*, 6765–6773.
- (71) Kuhn, J. N.; Tsung, C.-K.; Huang, W.; Somorjai, G. A. Effect of Organic Capping Layers over Monodisperse Platinum Nanoparticles upon Activity for Ethylene Hydrogenation and Carbon Monoxide Oxidation. *Journal of Catalysis* **2009**, *265*, 209–215.
- (72) De Roo, J.; Van Driessche, I.; Martins, J. C.; Hens, Z. Colloidal Metal Oxide Nanocrystal Catalysis by Sustained Chemically Driven Ligand Displacement. *Nat. Mater.* **2016**, *15*, 517–521.
- (73) Lee, J.-S.; Kovalenko, M. V.; Huang, J.; Chung, D. S.; Talapin, D. V. Band-like Transport, High Electron Mobility and High Photoconductivity in All-Inorganic Nanocrystal Arrays. *Nat. Nanotech.* **2011**, *6*, 348–352.
- (74) Hervés, P.; Pérez-Lorenzo, M.; Liz-Marzán, L. M.; Dzubiella, J.; Lu, Y.; Ballauff, M. Catalysis by Metallic Nanoparticles in Aqueous Solution: Model Reactions. *Chem. Soc. Rev.* **2012**, *41*, 5577.
- (75) Pradhan, N.; Pal, A.; Pal, T. Catalytic Reduction of Aromatic Nitro Compounds by Coinage Metal Nanoparticles. *Langmuir* **2001**, *17*, 1800–1802.

- (76) Aditya, T.; Pal, A.; Pal, T. Nitroarene Reduction: A Trusted Model Reaction to Test Nanoparticle Catalysts. *Chem. Commun.* **2015**, *51*, 9410–9431.
- (77) Zhao, P.; Feng, X.; Huang, D.; Yang, G.; Astruc, D. Basic Concepts and Recent Advances in Nitrophenol Reduction by Gold- and Other Transition Metal Nanoparticles. *Coordination Chemistry Reviews* **2015**, *287*, 114–136.
- (78) Ansar, S. M.; Kitchens, C. L. Impact of Gold Nanoparticle Stabilizing Ligands on the Colloidal Catalytic Reduction of 4-Nitrophenol. *ACS Catal.* **2016**, *6*, 5553–5560.
- (79) Jagadeeswararao, M.; Dey, S.; Nag, A.; Rao, C. N. R. Visible Light-Induced Hydrogen Generation Using Colloidal (ZnS)_{0.4}(AgInS₂)_{0.6} Nanocrystals Capped by S²⁻ Ions. *J. Mater. Chem. A* **2015**, *3*, 8276–8279.
- (80) Kadlag, K. P.; Rao, M. J.; Nag, A. Ligand-Free, Colloidal, and Luminescent Metal Sulfide Nanocrystals. *J. Phys. Chem. Lett.* **2013**, *4*, 1676–1681.
- (81) Nag, A.; Kovalenko, M. V.; Lee, J.-S.; Liu, W.; Spokoyny, B.; Talapin, D. V. Metal-Free Inorganic Ligands for Colloidal Nanocrystals: S²⁻, HS⁻, Se²⁻, HSe⁻, Te²⁻, HTe⁻, TeS₃²⁻, OH⁻, and NH₂⁻ as Surface Ligands. *J. Am. Chem. Soc.* **2011**, *133*, 10612–10620.
- (82) Hu, H.; Xin, J. H.; Hu, H.; Wang, X.; Miao, D.; Liu, Y. Synthesis and Stabilization of Metal Nanocatalysts for Reduction Reactions – a Review. *J. Mater. Chem. A* **2015**, *3*, 11157–11182.
- (83) Lopez-Sanchez, J. A.; Dimitratos, N.; Hammond, C.; Brett, G. L.; Kesavan, L.; White, S.; Miedziak, P.; Tiruvalam, R.; Jenkins, R. L.; Carley, A. F.; et al. Facile Removal of Stabilizer-Ligands from Supported Gold Nanoparticles. *Nature Chem* **2011**, *3*, 551–556.
- (84) Liu, B.; Yao, H.; Song, W.; Jin, L.; Mosa, I. M.; Rusling, J. F.; Suib, S. L.; He, J. Ligand-Free Noble Metal Nanocluster Catalysts on Carbon Supports via “Soft” Nitriding. *J. Am. Chem. Soc.* **2016**, *138*, 4718–4721.
- (85) Lightcap, I. V.; Kosel, T. H.; Kamat, P. V. Anchoring Semiconductor and Metal Nanoparticles on a Two-Dimensional Catalyst Mat. Storing and Shuttling Electrons with Reduced Graphene Oxide. *Nano Lett.* **2010**, *10*, 577–583.
- (86) Wunder, S.; Lu, Y.; Albrecht, M.; Ballauff, M. Catalytic Activity of Faceted Gold Nanoparticles Studied by a Model Reaction: Evidence for Substrate-Induced Surface Restructuring. *ACS Catal.* **2011**, *1*, 908–916.

- (87) Esumi, K.; Isono, R.; Yoshimura, T. Preparation of PAMAM- and PPI-Metal (Silver, Platinum, and Palladium) Nanocomposites and Their Catalytic Activities for Reduction of 4-Nitrophenol. *Langmuir* **2004**, *20*, 237–243.
- (88) Munnik, P.; de Jongh, P. E.; de Jong, K. P. Recent Developments in the Synthesis of Supported Catalysts. *Chem. Rev.* **2015**, *115*, 6687–6718.
- (89) Zhao, H.; Zheng, X.; Feng, X.; Li, Y. CO₂ Reduction by Plasmonic Au Nanoparticle-Decorated TiO₂ Photocatalyst with an Ultrathin Al₂O₃ Interlayer. *J. Phys. Chem. C* **2018**, *122*, 18949–18956.
- (90) Jain, P. K. Taking the Heat Off of Plasmonic Chemistry. *J. Phys. Chem. C* **2019**, *123*, 24347–24351.
- (91) Marshall, S. T.; O'Brien, M.; Oetter, B.; Corpuz, A.; Richards, R. M.; Schwartz, D. K.; Medlin, J. W. Controlled Selectivity for Palladium Catalysts Using Self-Assembled Monolayers. *Nat. Mater.* **2010**, *9*, 853–858.
- (92) Chen, G.; Xu, C.; Huang, X.; Ye, J.; Gu, L.; Li, G.; Tang, Z.; Wu, B.; Yang, H.; Zhao, Z.; et al. Interfacial Electronic Effects Control the Reaction Selectivity of Platinum Catalysts. *Nat. Mater.* **2016**, *15*, 564–569.
- (93) Kim, Y.; Smith, J. G.; Jain, P. K. Harvesting Multiple Electron–Hole Pairs Generated through Plasmonic Excitation of Au Nanoparticles. *Nat. Chem.* **2018**, *10*, 763–769.

Chapter 2

Revealing the Role of Electrostatics in Gold Nanoparticle Catalyzed Reduction of Charged Molecules



This chapter is adapted with permission from the following paper. Copyright 2017, American Chemical Society.

Roy, S.; Rao, A.; Devatha, G.; Pillai, P. P.* Revealing the Role of Electrostatics in Gold-Nanoparticle-Catalyzed Reduction of Charged Substrates. *ACS Catal.* **2017**, *7*, 7141 - 7145.

2.1. Abstract

The present Chapter focuses on establishing the decisive role of electrostatic interaction, emanating from surface ligands, in AuNP catalyzed reduction. Regulation of interparticle forces is an important approach to explore various nanoparticle (NP) functionalities. Establishing the decisive role played by these forces in NP catalysis is one such fascinating phenomenon. In this regard, the current venture shows the potency of electrostatic effects ‘arising from NP surface’ in AuNP catalyzed reduction of charged molecules. The electrostatic potential around AuNP is controlled by varying the nature of ligands and ionic strength of the medium. The favorable interactions arising from the attraction between oppositely charged AuNP and reactant molecules results in the channeling of the reactants to the NP surface. This increases the local concentration of the substrates close to the NP surface, which in turn enhances the catalytic performance. The positively charged ([+]) AuNP outperformed other NP systems despite having comparable or even lower surface area for adsorption, proving the exclusivity of electrostatics in catalysis. At least an order of higher concentration of negatively charged ([-]) AuNP is required to compete with the catalytic activity of [+] AuNP. The long range electrostatic forces extending up to ~ 4 nm from the surface of NP helps in lowering the catalyst amount to picomolar level. The existence of electrostatic effects is successfully translated into the catalytic reduction of a Fe (III) complex, confirming the generality of our hypothesis. This interaction (emanated from surface ligands) driven control on the catalytic property of metal NPs can have far reaching impact in the emerging area of ‘ligand directed product formation’ in NP catalysis.

2.2. Introduction

The ‘high surface-to-volume ratio’ and ‘sea of electrons’ contained on the surface of metal NPs have been actively used for various catalytic processes.¹⁻¹⁰ In general, the metal NP catalysed reactions can be divided into two categories (**Figure 2.1**). In certain reactions the metal NPs help to overcome the kinetic barrier for the reaction process by offering its surface for adsorption and mediating transfer of electron between the reactant molecules.¹⁰ Here the role of NPs is passive in nature (**Figure 2.1 a**). Whereas, in the case of photocatalysis, the hot carriers generated through the photoexcitation of NPs are involved in the reaction, and the NPs actively take part in the reaction (**Figure 2.1 b**).⁷⁻⁹ The present Chapter deals with nanocatalysis (passive participation), and specifically focuses on investigating the potent role of interaction in controlling such kind of reactions on the surface of NPs.

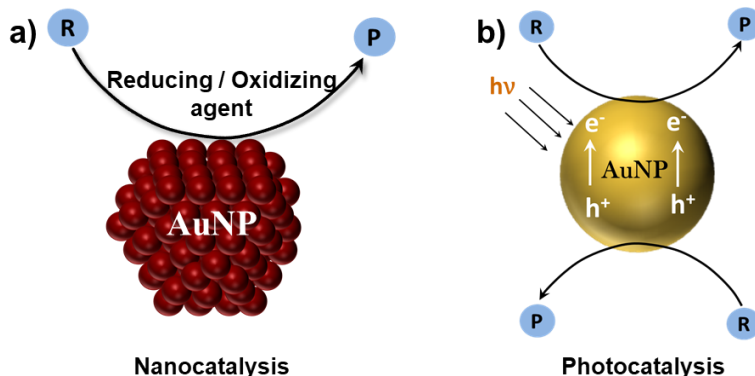


Figure 2.1. Schematic representation of a) passive participation (nanocatalysis) and b) active participation (photocatalysis) of AuNPs in two different classes of AuNP catalyzed reactions.

The metal NP catalysed reduction of nitro phenols to amino phenols by borohydride ions is a classic example in the area of nanocatalysis.¹⁰⁻¹² Some of characteristic features of this reaction includes single product formation without any side reactions, mild reaction condition, visible colour change upon reduction (yellow to colourless), and the possibility of temperature dependent kinetic analysis. This makes nitro to amine reduction an ideal reaction to assess the catalytic property of metal NPs as well as establishing different fundamental hypotheses regarding metal NP catalysis.¹⁰⁻¹² As per literature, the nitro to amine reduction on the surface of NPs proceed either through the Langmuir-Hinshelwood (LH) mechanism¹⁰⁻¹⁴ or through Eley-Rideal mechanism (ER)¹⁵ (**Figure 2.2**). In LH mechanism, the reaction proceeds through the adsorption of both the reactant molecules (nitrophenol and borohydride ions) on the surface of NPs, followed by hydride ion transfer mediated by the NPs (**Figure 2.2 a**).¹⁴ Whereas, in ER mechanism, the adsorption of the hydride ion on the surface of NPs is the rate determining step (**Figure 2.2 b**).^{15,16} Thus, the adsorption of reactant molecules on the NP catalyst surface is the key step for an efficient catalysis, in both the models. From a fundamental point, one of the challenges here is to identify and precisely control the factors influencing the diffusion of reactants to the NP surface. Factors such as NP crystallinity, ligand packing density, hydrophobicity and available NP surface area have all been well studied and documented in the literature.¹⁷⁻²⁴ Equally or even more important is the role of forces/and interactions between the NP surface and reactants on diffusion mediated catalysis, which is scarcely studied. In this direction, this chapter focuses on utilizing the ligands on the NP surface to tune the NP-reactant interaction and investigate how far it can control the adsorption of the reactant molecules and hence the catalytic properties of NPs. The negative charges on both the

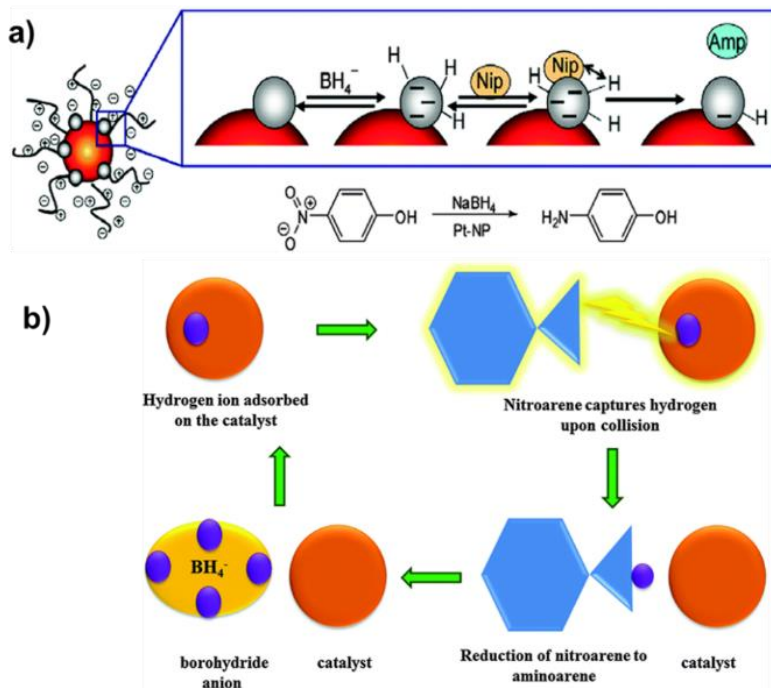


Figure 2.2. Schematic representation of a) LH mechanism and b) ER mechanism for the reduction of nitrophenol with borohydride on the surface of metal NPs. Adapted with permission from reference 11. Copyright 2015, The Royal Society of Chemistry.

reactant molecules (phenolate and borohydride ions) allowed us to use the electrostatic interactions as a tool to tune the interaction between NP catalysts and reactant molecules. The long range forces, mainly electrostatics, have already been proved to play a pivotal role in a wide range of NP applications like self-assembly,²⁵⁻²⁹ sensing,^{30,31} light harvesting,^{32,33} nanobiotechnology^{34,35} etc. In catalysis too the electrostatic forces, in principle, should be able to channelize the oppositely charged reactant molecules onto the NP surface, thereby improving the catalytic efficiency and selectivity. In this regard, a complete and conclusive evidence – in terms of both attractive (favourable) and repulsive (unfavourable) forces – is required to ascertain the existence of electrostatic effect in metal NP catalyzed reactions. The successful demonstration of such an effect will be a conceptual breakthrough that can be adapted to other NP catalyzed reactions as well.

Attempts have been made previously to study the effect of electrostatics on metal NP catalyzed reductions either in the presence of loosely bound charged surfactants or polymers.³⁶⁻⁴⁰ For instance, Pal and co-workers studied the effect of charged surfactants in the PdNP catalysed reduction of Rose Bengal dye (negatively charged) with borohydride ion (**Figure 2.3 a,b,c**).³⁶ An enhanced rate of reduction was observed in presence of positively charged CTAB surfactant

compare to that with negatively charged SDS surfactant. In another study, Xu and co-workers observed a higher rate of Methylene Blue (MB) reduction with polydopamine (PDA) supported AuNPs as the catalyst, compare to that with freely dispersed AuNPs (**Figure 2.3 d,e,f**). The electrostatic attraction between the positively charged MB and negatively charged PDA was reported to be the main reason behind the enhanced rate of MB reduction with PDA-AuNP as the catalyst. Interestingly, the PDA-Au NPs exhibited a lower catalytic activity for the negatively charged p-nitrophenol reduction because of an electrostatic repulsion.

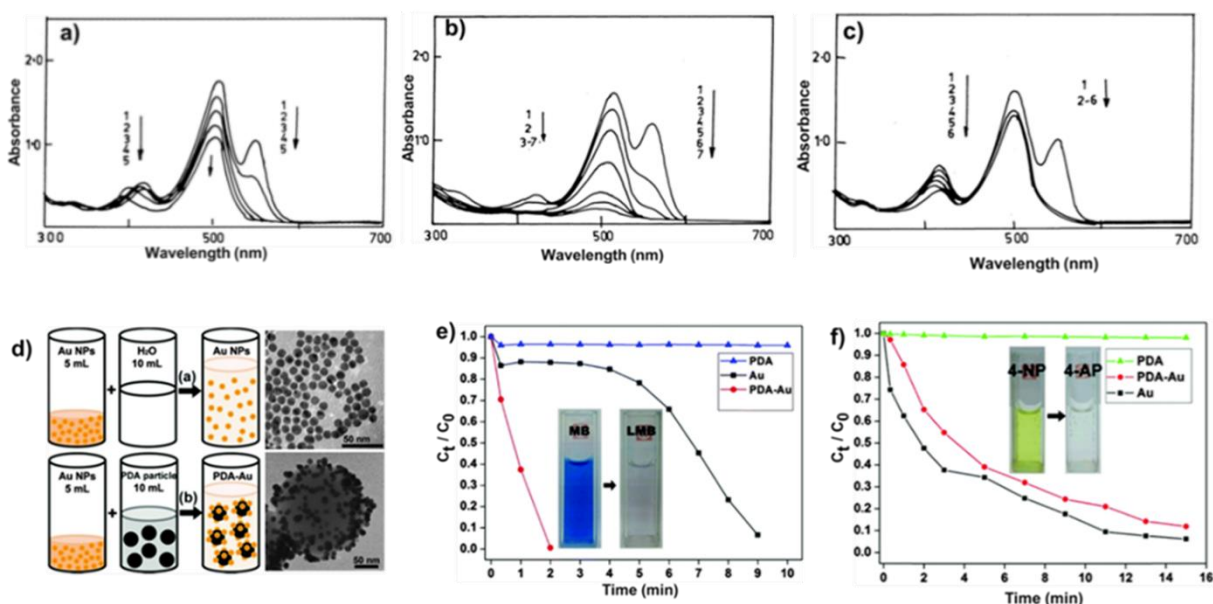


Figure 2.3. Progress of catalytic reduction of rose bengal dye with PdNPs in a) water b) presence of cationic CTAB surfactant and c) presence of anionic SDS surfactant. Adapted with permission from reference 36. Copyright 2000, American Chemical Society. d) Synthesis protocol and the corresponding TEM images of free and poludopamine (PDA) supported AuNP catalysts. e) Progress of methylene blue reduction by tracking the absorption change at 657 nm with free and PDA-AuNP catalysts. f) Progress of p-nitrophenol reduction by tracking the absorption change at 420 nm with free and PDA-AuNP catalysts. Adapted with permission from reference 39. Copyright 2015, The Royal Society of Chemistry.

Although the above representative examples reported about the effect of electrostatic interaction, the surface area available for the reactant adsorption was high in such NP systems, which will strongly assist the catalysis under both favorable and unfavorable conditions.¹⁸ Thus, the observed catalytic properties will be an outcome of the combined effects from surface area and electrostatics. A better approach to study the sole effect of electrostatics in AuNP catalysis will be to use charged small molecules that are tightly bound on the NP surface. Recently, we have employed AuNP

functionalized with charged thiolates to demonstrate the power of electrostatics in achieving an unprecedented phenomenon of controlled aggregation.³⁰ Similar sets of AuNP have been used in the present work to provide the much awaited conclusive proof for the existence of electrostatic effect in AuNP catalyzed reduction of charged substrates.

Specifically, we have studied the effect of electrostatics on catalysis via the control over surface potential (Ψ) and screening length (κ^{-1}) around the NPs by varying the ligands and ionic strengths, respectively (**Figure 2.4**). The range up to which the electrostatic field will be experienced by the reactant molecules (in terms of κ^{-1}) will vary as a function of ionic strength of the solution.⁴¹ We have estimated that the surface potential (both favourable and unfavourable) arising from charged AuNPs of both polarities can spread up to ~ 3 nm from the surface of ligands ($\kappa^{-1} \sim 3$ nm), in the presence of 10 mM BH_4^- ions. The magnitude of the surface potential around [+] and [-] AuNPs decays exponentially away from the surface as reported previously.⁴¹ Now, the concentration of negatively charged reactant molecules (here BH_4^- and phenolate anions) around the AuNP surface can be controlled by varying the surface potential, and this precisely forms the basis for our current work (**Figure 2.4**). The favourable electrostatic interaction between [+] AuNP and [-] reactant molecules helped in the channelling of the reactant molecules towards the NP surface (**Figure 2.4**). Consequently, the local concentration of the reactants increased around the ligand surface, which in turn enhances the reactant adsorption on NP surface. This resulted in the catalytic reduction of nitro arenes by [+] AuNP within 20 min, even when the catalyst concentration was as low as 0.1 mol % (~ 25 pM). Interestingly, no measurable catalysis was observed when unfavorable conditions for reactant binding were created using [-] AuNP as the catalyst (even up to ~ 1.2 mol %). At least an order of higher concentration of [-] AuNP was required to compete with the catalytic activity of [+] AuNP. Similarly, the [+] AuNP outperformed other NP systems despite having comparable or even lower surface area for adsorption, proving the exclusivity of electrostatics in AuNP catalysis. The effects of favourable and unfavourable interactions were successfully extended to the catalytic reduction of ferricyanides, ascertaining the scope of electrostatic effects beyond organic reactant molecules. The assistance of electrostatics helped in lowering the use of AuNP catalysts to picomolar level. Thus, we were successful to utilize the surface ligands as “gatekeepers” in controlling the diffusion of the reactant molecules towards the NP surface through electrostatic interaction.

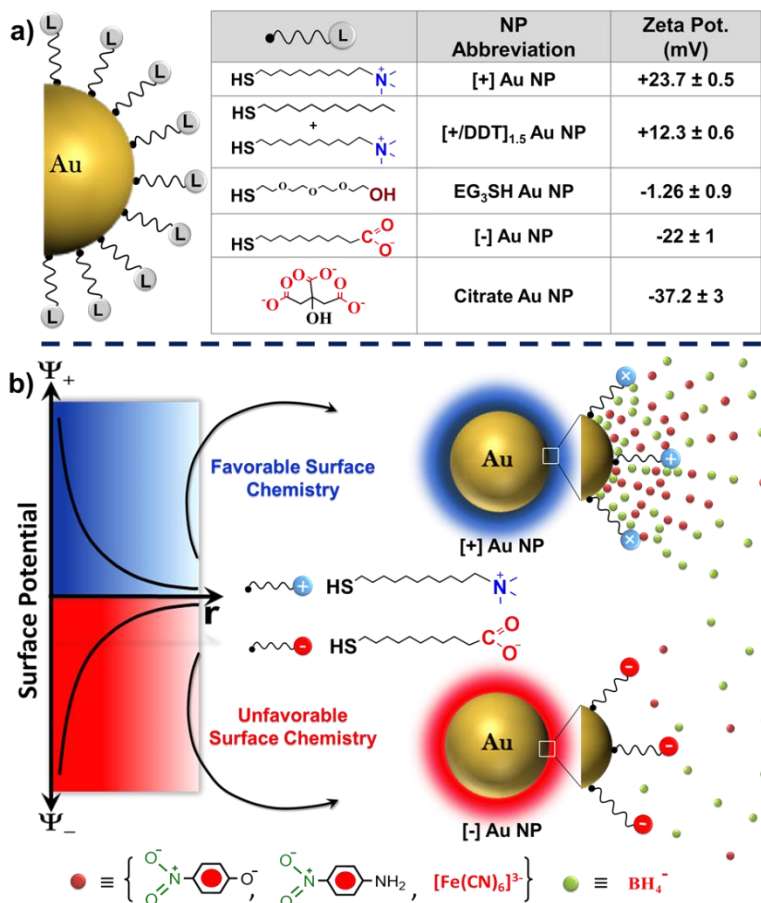


Figure 2.4. Electrostatically assisted channeling of reactants. a) Schematics of different AuNP systems under study with varying surface charges. b) The graph on the left shows the exponential decay of the surface potential around AuNPs of both polarities. Blue and red colors indicate positive and negative surface potentials arising from [+] and [-] AuNPs, respectively. The potentials of both polarities extend in the range of $\sim 3.0 - 0.5$ nm from the ligand surface, depending on the ionic strengths. The favorable interactions between [+] AuNP and [-] reactants assist in the channeling and adsorption of reactant molecules onto the NP surface (top right), which is responsible for the dominance of [+] AuNP over [-] AuNP (bottom right) in the catalytic reductions.

2.3. Experimental Details

2.3.1. Materials and Reagents:

Tetrachloroaurate trihydrate ($\text{HAuCl}_4 \cdot 3\text{H}_2\text{O}$), tetramethylammonium hydroxide (TMAOH) 25 wt. in water, 11-mercaptoundecanoic acid (MUA), hydrazine monohydrate ($\text{N}_2\text{H}_4 \cdot \text{H}_2\text{O}$ 50-60%), sodium citrate tribasic dihydrate, tetrabutylammonium borohydride (TBAB), 4-nitrophenol (PNP), 4-nitroaniline (PNA), sodium borohydride (NaBH_4), potassium ferricyanide, tannic acid, dodecane thiol (DDT) and 2-{2-[2-(2-mercaptoethoxy)ethoxy]ethoxy}ethanol (EG_3SH) were purchased from

Sigma-Aldrich. (Di-n-dodecyl) dimethyl ammonium bromide (DDAB) and dodecylamine (DDA), were purchased from Alfa Aesar. All the reagents were used as received without any further purification. The positively charged N,N,N-trimethyl(11- mercaptoundecyl) ammonium ion (TMA) was synthesized according to the reported procedure.⁴²

2.3.2. Synthesis of [+], [-], EG₃SH and [+/DDT]_{1.5} AuNPs (Place Exchange Reaction):

All the nanoparticles were synthesized following a place exchange reaction method. First, dodecylamine (DDA)-capped AuNPs in toluene were synthesized by following a modified reported procedure.^{30,43} HAuCl₄.3H₂O instead of AuCl₃ was used as the gold precursor. Hydrazine monohydrate (N₂H₄.H₂O) was used as the reducing agent. In a typical experiment, HAuCl₄.3H₂O (24 mg), DDA (222 mg), and DDAB (277 mg) were mixed together in toluene (7 mL) and sonicated for ~10 min for complete stabilization of Gold (III) ions. This was followed by a rapid injection of another toluene solution containing 58 mg of TBAB and 111 mg of DDAB. The resulting solution (seed solution) was left stirring overnight for ensuring the complete reduction of Gold (III). The seed particles were then grown to ~ 5 nm DDA-Au NPs. A growth solution was prepared by adding 1 g of DDAB, 2.6 g of DDA, 224 mg of HAuCl₄.3H₂O and 10 mL of seed solution in 60 mL toluene. The growth solution was further reduced with a dropwise addition of another toluene solution containing 300 μL of N₂H₄.H₂O and 2 g of DDAB. The solution was stirred overnight for complete growth of the particles yielding monodisperse 5.4 ± 0.7 nm of DDA-Au NPs. 20 mL of DDA-Au NPs were then purified by precipitating them in 50 mL methanol, yielding a black precipitate. The supernatant was carefully removed and the precipitate was then re-dispersed in 20 mL toluene. A ligand solution in 10 mL dichloromethane (DCM) was added. A ~ 40 fold molar excess of ligand was added during the place exchange (**Figure 2.5**). The solution was left overnight to ensure a complete ligand exchange. Next, the supernatant was decanted and the precipitate was washed with DCM (3 × 50 mL) and acetone (50 mL). The precipitate was then dried and redispersed in milliQ water. The [-] and EG₃SH AuNPs were synthesized by adding MUA and EG₃SH ligands during the place exchange reaction, respectively. A mixture of [+] and DDT ligands (in molar ratio 3:2) were used for synthesizing [+/DDT]_{1.5} AuNPs. All the AuNPs exhibited a surface plasmon band ~520 nm confirming the similarity in size. The similarity in size is necessary to compare the sole effect of surface chemistry in the catalytic property of metal NPs.

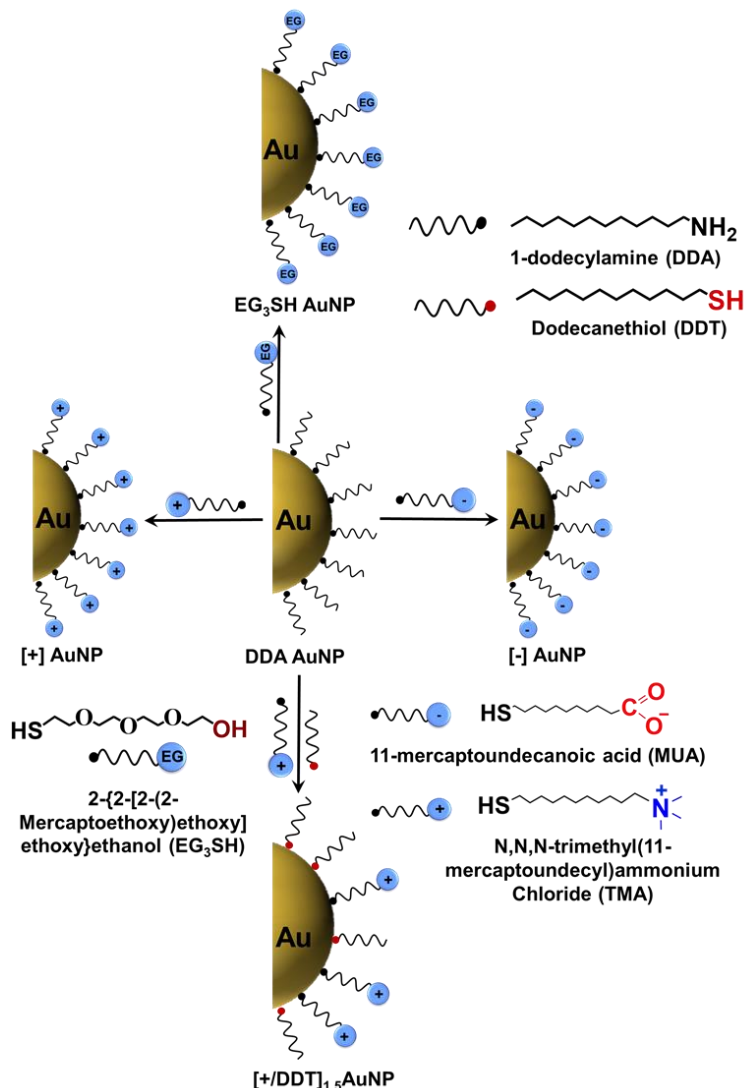


Figure 2.5. Schematic illustration of place exchange of DDA capped AuNPs. DDA capped AuNPs were place exchanged with [+], [-], EG₃SH and a mixture of [+] and DDT ligands to systematically vary the surface potential of AuNP catalysts.

2.3.3. Synthesis of Citrate Stabilized AuNPs:

Citrate stabilized AuNPs were synthesized following a reported procedure (Figure 2.6).⁴⁴ Briefly, 150 mL of freshly prepared sodium citrate solution (2.2 mM) was mixed with 0.1 mL of tannic acid solution (2.5 mM), and the pH of the solution was adjusted to ~ 10 by adding 1 mL of potassium carbonate (150 mM). The resulting solution was then heated to $\sim 70^\circ\text{C}$ with vigorous stirring. When the temperature reached at $\sim 70^\circ\text{C}$, a rapid injection of 1 mL $\text{HAuCl}_4 \cdot 3\text{H}_2\text{O}$ (25 mM) was performed. The color of the solution instantly transformed from black-gray to orange-red indicating the formation of seed particles. The solution was kept at $\sim 70^\circ\text{C}$ for 10 min to ensure

a complete reduction. The seed solution was then diluted by removing 55 mL of solution and the same amount of freshly prepared sodium citrate solution (2.2 mM) was added, followed by heating again at ~ 70 °C. Next, two subsequent additions of 0.5 mL of $\text{HAuCl}_4 \cdot 3\text{H}_2\text{O}$ (25 mM) were performed with a time interval of 10 min. This procedure was repeated until a surface plasmon band at ~ 520 nm was achieved.

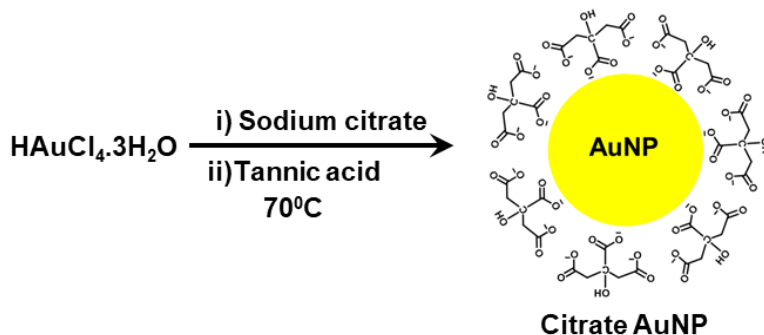


Figure 2.6. Schematic illustration for the synthesis of citrate stabilized AuNP.

2.3.4. Transmission Electron Microscopy (TEM) Studies:

A drop of AuNP solution was drop casted on 400 mesh carbon coated copper grid (Tedpella Inc.) and dried under vacuum. The High-Resolution Transmission Electron Microscopic (HRTEM) imaging was performed on TECNAI G2 20 TWIN at 200 kV.

2.3.5. Zeta Potential studies:

The zeta potential (ζ) of charged AuNPs were measured in milliQ water (pH ~ 7) on Nano ZS90 (Malvern) Zetasizer instrument. The optical density of the nanoparticle solution was maintained ~ 0.2 during all the measurements. The error was calculated from three different experiments. ζ was determined by measuring the electrophoretic mobility and using Henry's equation.

$$U_E = \frac{2\varepsilon\zeta f(k_a)}{3\eta}$$

U_E : Electrophoretic mobility

ζ : Zeta potential

ε : Dielectric constant

η : Viscosity

$f(Ka)$: Henry's Function

2.3.6. Thermo Gravimetric Analysis (TGA):

Thermogravimetry analysis was carried out on NETSZCH TGA-DSC system. The TGAs were done under N₂ gas flow (20 mL/min) (purge + protective), and samples were heated from RT to 600 °C at 2 K/min.

2.3.7. ICP-MS Analysis:

AuNP samples ([+] and [-]) were digested by adding 1 mL of aqua regia (3:1 v/v HCl: HNO₃) followed by gentle heating at ~ 45 °C. The amounts of Au and S in the digested samples were quantified using ICP-MS analysis performed on ELEMENT XR™ ICP-MS (Thermo Scientific) instrument.

2.3.8. Catalytic Reduction:

All the reduction kinetics was performed in a 3 mL quartz cell using SHIMADZU UV-3600 plus UV-Vis-NIR spectrophotometer. In a typical absorption experiment, AuNP solution, reactant, and NaBH₄ were mixed in a 3 mL quartz cell, and the absorption spectra were collected with a 2 min time interval. The time dependent kinetic experiments were performed by monitoring the absorbance of the reactant at its λ_{\max} with time. Temperature dependent kinetic measurements were performed with a temperature controller equipped with the UV-Vis-NIR spectrophotometer. All the catalysis experiments were performed under ambient conditions, unless specifically mentioned.

2.3.9. 4-Nitrophenol (PNP) Reduction:

Reduction of 4-nitrophenol (PNP) was performed by adding 60 μ L of PNP (5 mM), 300 μ L of NaBH₄ (0.1 M), 15 μ L of AuNP solution (10 nM) and 2.625 mL of milliQ water in a 3 mL quartz cell. Absorbance at 400 nm was monitored for the time dependent absorption measurements. All the AuNP concentrations are expressed in terms of nanoparticles by using $5.4 \times 10^7 \text{ M}^{-1}\text{cm}^{-1}$ as the extinction coefficient.⁴⁵ However, the mol % is expressed in terms of Au atoms.

2.3.10. 4-Nitroaniline (PNA) Reduction:

Reduction of 4-nitroaniline was performed by adding 60 μ L of PNA (5 mM), 300 μ L of NaBH₄ (0.1 M), 10 μ L of AuNP solution (10 nM) and 2.63 mL of milliQ water in a 3 mL quartz cell. Absorbance at 410 nm was monitored for time dependent absorption measurement. All the AuNP concentrations are expressed in terms of nanoparticles by using $5.4 \times 10^7 \text{ M}^{-1}\text{cm}^{-1}$ as the extinction coefficient.⁴⁵ However, the mol % is expressed in terms of Au atoms.

2.3.11. Potassium Ferricyanide $K_3[Fe(CN)_6]$ Reduction:

Reduction of ferricyanide was performed by adding 60 μL of $[Fe(CN)_6]^{3-}$ (5 mM), 30 μL of NaBH_4 (0.1 M), 15 μL of AuNP solution (10 nM) and 2.895 mL of milliQ water in a 3 mL quartz cell. The time dependent kinetic measurements were performed by monitoring the absorbance at 420 nm. The NaBH_4 concentration was 10 times higher than that of the substrate. The BH_4^- ions were able to partially reduce ferricyanides by itself; however a complete reduction was only observed in the presence of [+] AuNP catalyst. All the AuNP concentrations are expressed in terms of nanoparticles by using $5.4 \times 10^7 \text{ M}^{-1}\text{cm}^{-1}$ as the extinction coefficient.⁴⁵ However, the mol % is expressed in terms of Au atoms.

2.3.12. Product Characterization:

The products were thoroughly characterized by HRMS, GC-MS and ^1H NMR techniques. After a complete reduction, the reaction mixture was first passed through a celite column to separate AuNPs and excess NaBH_4 , followed by extraction with ethyl acetate. Finally, the product was dried with Na_2SO_4 and the solvent was evaporated yielding solid product. The NMR spectra were collected in deuterated DMSO (JEOL 400 MHz) and the GC-MS spectra were obtained using GC 2014, Shimadzu instrument.

2.3.13. Calculation of Screening Length:

Here, the concentrations of counter ions and residual base are considered to be negligible in comparison to the amount of NaBH_4 (10 mM) used in the reaction. The variation of electric potential (ψ) from the outer Helmholtz plane around a particle in such an environment is well approximated by the Poisson equation as given below.^{41,46}

$$\nabla^2\psi = -\frac{\rho}{\epsilon_0\epsilon} \quad (2.1)$$

where, ρ is the charge density outside the particle (in C/m^3), ϵ is the dielectric constant of the medium (80 for water) and ϵ_0 is the permittivity of the free space.

The charge density outside the particle, which follows Boltzmann distribution, is given as^{27,41}

$$\rho = \sum_i z_i e n_i^\infty \exp\left(-\frac{z_i e \psi}{k_b T}\right) \quad (1.2)$$

where, z_i is the valency of the i^{th} ion, e is the electron charge and n_i^∞ is the number of ions of type i per unit volume in the bulk solution. $z_i e \psi$ is the work done in bringing the i^{th} ion from infinity to the point where the potential is ψ . k_b is Boltzmann's constant and T is the temperature (in K).

Substituting (2.2) in (2.1), we get,

$$\nabla^2 \psi = -\frac{e}{\varepsilon_0 \varepsilon} \sum_i z_i e n_i^\infty \exp\left(-\frac{z_i e \psi}{k_b T}\right) \quad (2.3)$$

On simplification, (2.3) can be re-written as,^{27,44}

$$\nabla^2 \psi = \frac{N_a e^2}{\varepsilon_0 \varepsilon k_b T} \sum_i z_i^2 c_i^\infty \psi \quad (2.4)$$

Here, c_i^∞ is the concentration of ions of type i (in mol./m³), N_a is Avogadro's number.

The Debye-Hückel parameter (κ) is defined as^{46,47}

$$\kappa^2 = \frac{N_a e^2}{\varepsilon_0 \varepsilon k_b T} \sum_i z_i^2 c_i^\infty \quad (2.5)$$

The Debye-Hückel parameter has the units of m⁻¹ and can be used to get the value of Debye length (screening lengths, κ^{-1}) from the following equation^{27,41,46}

$$\kappa^{-1} = \left[\frac{N_a e^2}{\varepsilon_0 \varepsilon k_b T} \sum_i z_i^2 c_i^\infty \right]^{-1/2} \quad (2.2)$$

Using equation (2.6), the screening lengths for the reactions at different ionic strengths have been estimated and summarized in the table below.

Table 2.1. Variation of screening length with ionic strength of the reaction medium.

	Reaction in Water	Reaction in 1X PBS	Reaction in 2X PBS ^a
Screening length (κ^{-1})	3.04 nm	0.71 nm	0.51 nm ^a

^a The equation (6) which results from Debye-Hückel theory is not applicable at high ionic strengths (where Debye length becomes comparable to molecular dimensions); however it qualitatively shows that the Debye length (screening length) is vanishingly small.⁴⁵

2.3.14. Calculation of Surface Potential:

The surface charge density can be calculated from the zeta potential and the screening lengths using the following equation⁴⁸

$$\rho = \frac{\varepsilon_0 \varepsilon \zeta (1 + \kappa r)}{r} \quad (2.7)$$

Using the above equation, the surface charge density of nanoparticles with different surface chemistries in water was estimated and summarized in the table below

Table 2.2. Variation of surface charge density with zeta potential.

	Zeta potential (mV)	Surface charge density (C/m ²)
[+] AuNP	23.7	0.0117
[+]/DDT _{1.5} AuNP	12.3	0.00609
Neutral EG ₃ SH AuNP	-1.26	-0.000624
[-] AuNP	-22	-0.0109
Citrate AuNP	-37	-0.0183

2.3.15. Determination of mol % of Au atoms in AuNP Catalyst:

The average no. of gold atoms in each nanoparticle sphere can be calculated as per previously reported equation⁴⁷

$$N = 30.89602 \times D^3$$

where 'N' is the average number of gold atoms per nanoparticle and 'D' is the average diameter of the particles.

The average diameter of the particles is 5.4 ± 0.7 nm as calculated from TEM analysis. So the average number of gold atoms per nanoparticle is estimated to be

$$\begin{aligned} N &= 30.89602 \times (5.4)^3 \\ &= 4865 \end{aligned}$$

The concentration of AuNP used in the catalytic experiment is 50 pM (in terms of gold nanoparticle). So the concentration in terms of gold atoms will be

$$50 \times 4865 = 243250 \text{ pM (in terms of gold atoms)}$$

Thus, the mol % of Au atoms for 50 pM AuNP will be 0.2.

2.3.16. Estimation of Ligand Packing Density or Surface Coverage on [+] and [-] AuNPs:

AuNPs:

Thermo Gravimetric Analysis (TGA):

The packing density was calculated using the following formula as reported previously¹⁸

$$SC_{nm2} = m_{NP} \times w_1 \times N_{AV} / w_{NP} \times MW_1 \times SA_{NP}$$

Where 'm_{NP}' is the mass of each nanoparticle (1.59×10⁻¹⁸, as the average size of the particles is 5.4 nm). 'w₁' is the weight fraction of the [+] and [-] ligands, which is ~ 12 % and ~ 9 % respectively, as calculated from the TGA experiment. 'w_{NP}' is the weight fraction of nanoparticle which is ~ 88 % and ~ 91 % for [+] and [-] AuNPs, respectively. The surface area (SA_{NP}) of individual nanoparticle is 91.60 nm² by assuming each nanoparticle as a solid sphere with radius (r = 2.7 nm). Thus, the nominal packing density estimated was 5.05 and 4.73 molecule/nm² for [+] and [-] ligands on nanoparticle surface, respectively.

ICP-MS:

The amount of Au and S measured from ICP-MS analysis is mentioned below.

Sample	Au (ppm)	S (ppm)
[+] Au NP	240.4	4.1
[-] Au NP	510.7	8.4

The surface coverage (ligand/nm²) for individual nanoparticle was calculated by the following formula.

$$SC_{nm2} = \text{total no. of ligands per nanoparticle} / \text{surface area of each nanoparticle}$$

Total number of ligands per nanoparticle calculated from the ICP-MS data is 518 and 497 for [+] and [-] AuNPs, respectively. The surface area (SA_{NP}) of individual nanoparticle is 91.60 nm² by assuming each nanoparticle as a solid sphere with radius (r = 2.7 nm). So the surface coverage for individual nanoparticle will be 5.6 and 5.4 molecule/nm² for [+] and [-] AuNPs, respectively.

2.4. Results and Discussion

2.4.1. Design and Characterization of AuNP Catalysts:

AuNPs with varying surface charges were used as catalysts for the reduction of PNP by BH_4^- , to demonstrate the role of electrostatics in NP catalysis. Accordingly, N,N,N-trimethyl(11-mercaptoundecyl)ammonium chloride (TMA, [+]) and 11-mercaptoundecanoic acid (MUA, [-]) ligands were functionalized to render positive and negative surface potentials around AuNPs, respectively (**Figure 2.7 a,b**). Details on the synthesis are provided in the **Experimental Section 2.3.2**.^{30,42} Further fine tuning in the surface potential was achieved by diluting the [+] surface potential with dodecanethiol (DDT) ligands or decorating the surface with a neutral 2-{2-[2-(2-mercaptoethoxy)ethoxy]ethoxy}ethanol (EG_3SH) ligand (**Figure 2.7 a,b**). A decrease in the positive zeta potential from $+24.2 \pm 1$ mV to $+12 \pm 1.2$ mV was observed upon dilution of [+] ligands with $\sim 40\%$ of DDT ligands, which further decreased to -2.0 ± 0.5 mV with the functionalization of neutral EG_3SH ligands (**Figure 2.7 a,b**). To compare the effect of surface area, citrate functionalized AuNPs were also synthesized. Spectroscopic (UV-Vis absorption) and Microscopy (Transmission Electron Microscopy, TEM) studies confirm negligible changes in the stability and average size of AuNP upon various surface functionalization (**Figure 2.7 c-e**). Thus, similar sized AuNPs (5.4 ± 0.7 nm from TEM) with varying surface potentials were successfully prepared, which is crucial for comparing their catalytic performances.

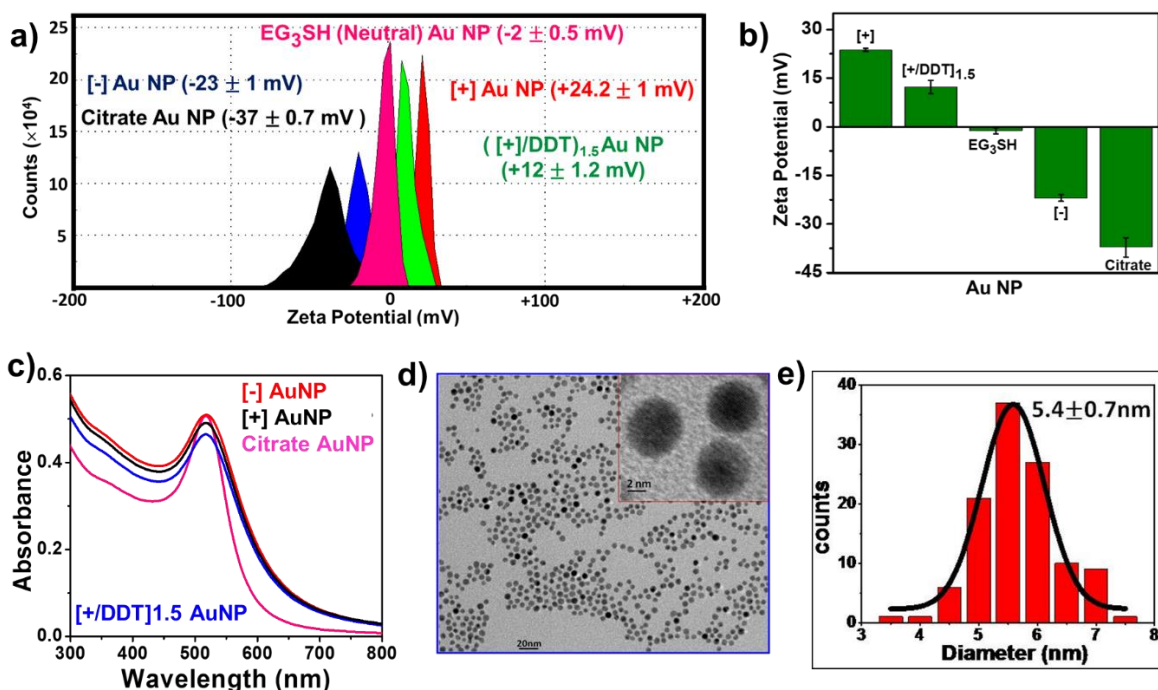


Figure 2.7. Spectroscopic, microscopic and surface characterization of AuNPs. a) Typical zeta potential plots for different sets of AuNPs with varying ligands. b) A bar diagram showing the variation of zeta potential as a function of ligands on the surface of AuNPs. The error bars correspond to standard deviations based on three different sets of experiment. c) UV-Vis absorption showing negligible changes in the stability and average size of AuNPs upon various surface functionalization. e) A representative TEM image of [+] AuNPs with e) their size distribution histogram (from ~ 300 NPs).

2.4.2. Reduction of Nitrophenol (PNP) to Aminophenol with Different AuNP Catalysts:

The reduction of PNP with BH_4^- was selected as a model reaction to establish the decisive role of electrostatics in AuNP catalysis. No noticeable reduction of PNP (100 μM) by BH_4^- (10 mM) in the absence of catalyst (**Figure 2.8 a**) confirms the necessity of NPs in driving the reaction. AuNPs provide its surface for the adsorption of both the reactant molecules, and thus overcoming the kinetic barrier of the reaction. A rapid reduction of PNP by BH_4^- was observed within ~ 20 min when 0.2 mol% of [+] AuNP (50 pM) was used as the catalyst (**Figure 2.8 a**). The reduction process was accompanied by a decrease in the absorption of 4-nitrophenolate ion with a concomitant formation of a new band around ~ 300 nm (**Figure 2.8 b**). The presence of two isosbestic points around ~ 320 and ~ 280 nm confirm the formation of only one product, namely 4-amino phenol,¹⁰ which was well characterized using various analytical techniques (**Figures 2.18, 2.19 in the Appendix**). The absence of a plasmon band around ~ 20 nm signifies the low amount of AuNP in catalytic reduction, which will boost its role in industrial applications. Interestingly, no appreciable catalytic reduction by BH_4^- was observed up to 2 days in the presence of 0.2 mol % of [-] AuNP (**Figures 2.8 a**). The initial results clearly indicated that the favourable and unfavourable interactions arising from the electrostatics between the reactant molecules and catalysts were crucial, which demands for a detailed investigation. Accordingly, time-dependent absorption experiments were performed to study the progress of PNP reduction. An induction time of 0.7 - 1.5 min with a rate constant of 0.27 min^{-1} was observed for the PNP reduction in the presence 0.2 mol% [+] AuNPs, which improved upon increasing the mol % of [+] AuNP catalyst (**Figure 2.8 c,d**). For instance, the induction time was lowered from 1.3 min to 0.4 min, and the rate constant increased from 0.27 min^{-1} to 0.71 min^{-1} as the [+] AuNP concentration was increased from 0.2 mol % to 1 mol%, respectively (**Figure 2.8 c,d**). On the other hand, even 1 mol % of

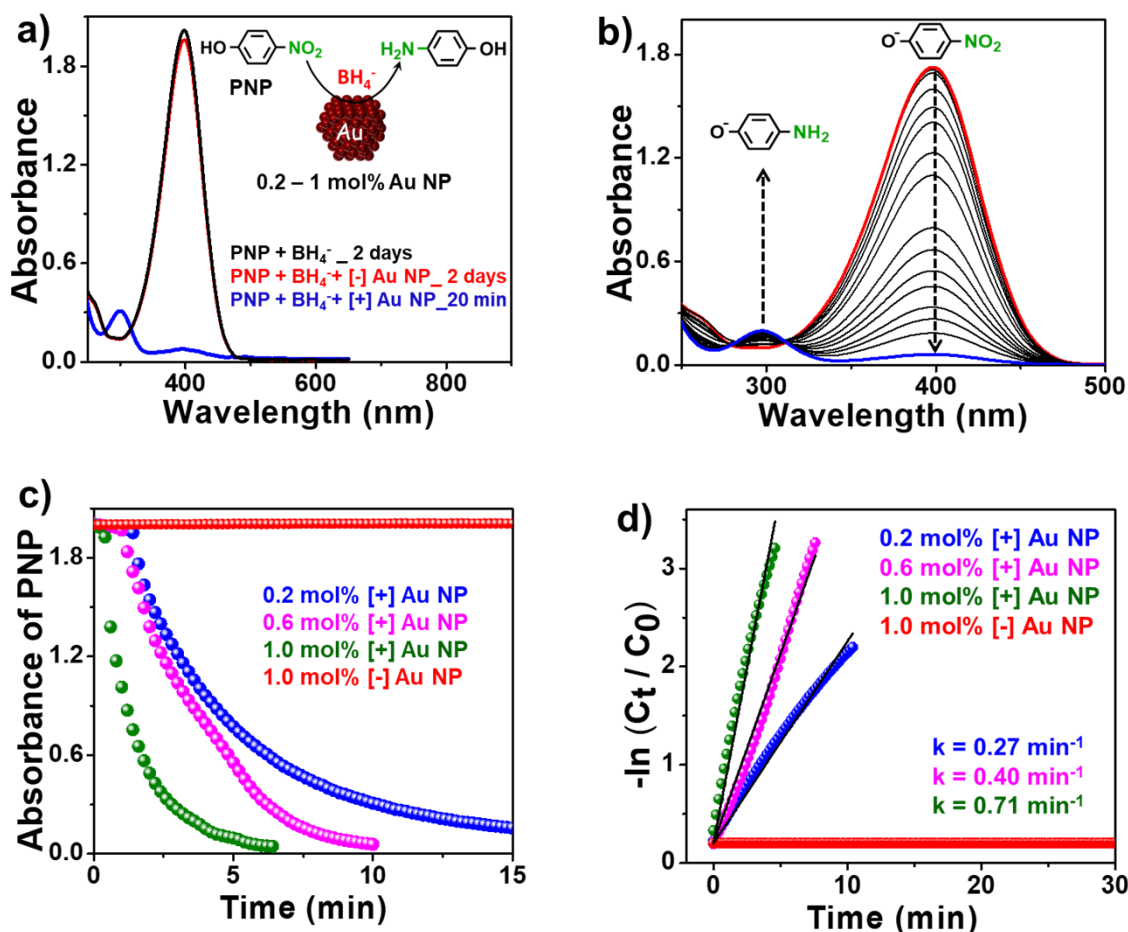


Figure 2.8. AuNP catalyzed PNP reduction. a) A complete dampening of PNP absorption peak at ~ 400 nm was observed in the presence of 10 mM BH_4^- and 0.2 mol% [+] AuNP. No appreciable spectral changes were observed up to ~ 2 days in the presence of BH_4^- alone or BH_4^- and 0.2 mol% [-] AuNP. b) A gradual decrease in the 4-nitrophenolate absorption with a concomitant formation of a new band ~ 300 nm was observed in the presence of 0.2 mol% [+] AuNP. c) Progress of PNP reduction, and d) corresponding linearized data for the first order analysis by tracking the absorption changes of PNP peak at ~ 400 nm in the presence of varying concentrations of AuNPs.

[-] AuNP failed to catalyze the PNP reduction for up to 8 h (**Figure 2.9 a**). Appreciable catalysis with [-] AuNP was observed only when the concentration was increased to 1.2 mol% (with an induction time ~ 30 min and rate constant = 0.1 min^{-1} ; **Figure 2.9 b,c**). At least an order of magnitude higher concentration of [-] AuNP was required to compete with catalytic performance of [+] AuNP. For e.g., an induction time of ~ 4 min was observed in the presence of 12 mol% of [-] AuNP (3 nM), whereas the reaction was spontaneous even with 1.2 mol% of [+] AuNP (300 pM; **Figure 2.9 b-d**).

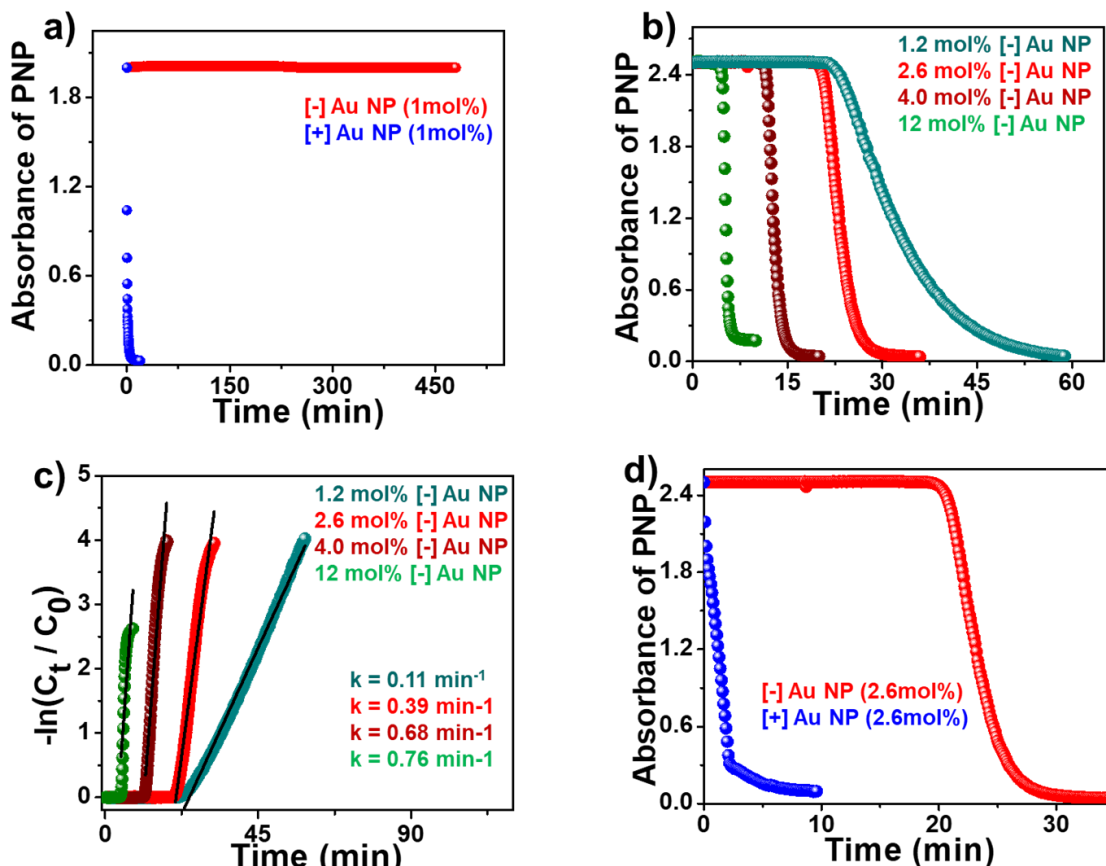


Figure 2.9. Catalytic reduction of PNP with varying concentrations of [-] AuNPs. a) Progress of PNP reduction by tracking the absorption changes of PNP peak at 400 nm with time in the presence of 1 mol % (250 pM) of [+] and [-] AuNPs. b) Progress of PNP reduction, and c) corresponding linearized data for first order analysis by tracking the absorption changes of PNP peak at 400 nm with time in the presence of varying concentration of [-] AuNPs. d) The comparison of catalytic performance between [+] and [-] AuNPs at 2.6 mol % (650 pM) of AuNPs.

2.4.3. Validation of Langmuir-Hinshelwood Mechanism:

Motivated with the result, our next objective was to understand the mechanism of the reaction. As mentioned in the introduction section, the reduction of p-nitrophenol with borohydride can proceed either through the Langmuir-Hinshelwood (LH) mechanism¹⁰⁻¹⁴ or through the Eley-Rideal (ER) mechanism.¹⁵ According to the Langmuir-Hinshelwood mechanism, nitrophenol and the hydride ion derived from the borohydride adsorbed on the surface of NPs. This step is rapid, reversible and can be described in terms of Langmuir Isotherm.¹³ Next, the reduction of PNP to 4-amino phenol takes place on the surface of NP through the transfer of electrons between the surface adsorbed hydride ions and PNP. This is followed by desorption of 4-amino phenol, which generates a vacant active site on the NP surface and the next cycle of reduction will start. Ballauff and co-workers

have demonstrated that a conclusive proof of Langmuir-Hinshelwood mechanism can be obtained by performing catalytic reductions as a function of PNP concentration.¹³ There should be a decrease in the catalytic activity with increase in the concentration of PNP. This is because, as per the Langmuir-Hinshelwood mechanism both the reactants have to be adsorbed on the surface of NPs. At a higher PNP concentration most of the active sites on the NP surface will be occupied by PNP, since it has a higher adsorption constant than BH_4^- . As a result, the reaction between NP and BH_4^- will slow down, which will ultimately lower the catalytic activity. These reactant dependent catalytic studies have been well accepted as the model experiments to prove that the reaction kinetic for AuNP catalyzed reduction of PNP follows the Langmuir-Hinshelwood mechanism.¹⁰⁻¹⁴ We too followed similar experiments as reported by Ballauff and co-workers to elucidate the Langmuir-Hinshelwood mechanism in our system. In our experiments too, a decrease in the catalytic activity of [+] AuNP (with lower rate constant and higher induction time) was observed with an increase in the PNP concentration (Figure 2.10 a,b). Furthermore, a nonlinear correlation of rate constants as a function of PNP concentration as depicted from the Langmuir-Hinshelwood model, again confirms that, the PNP reduction by AuNPs follows the Langmuir-Hinshelwood mechanism (Figure 2.10 c).

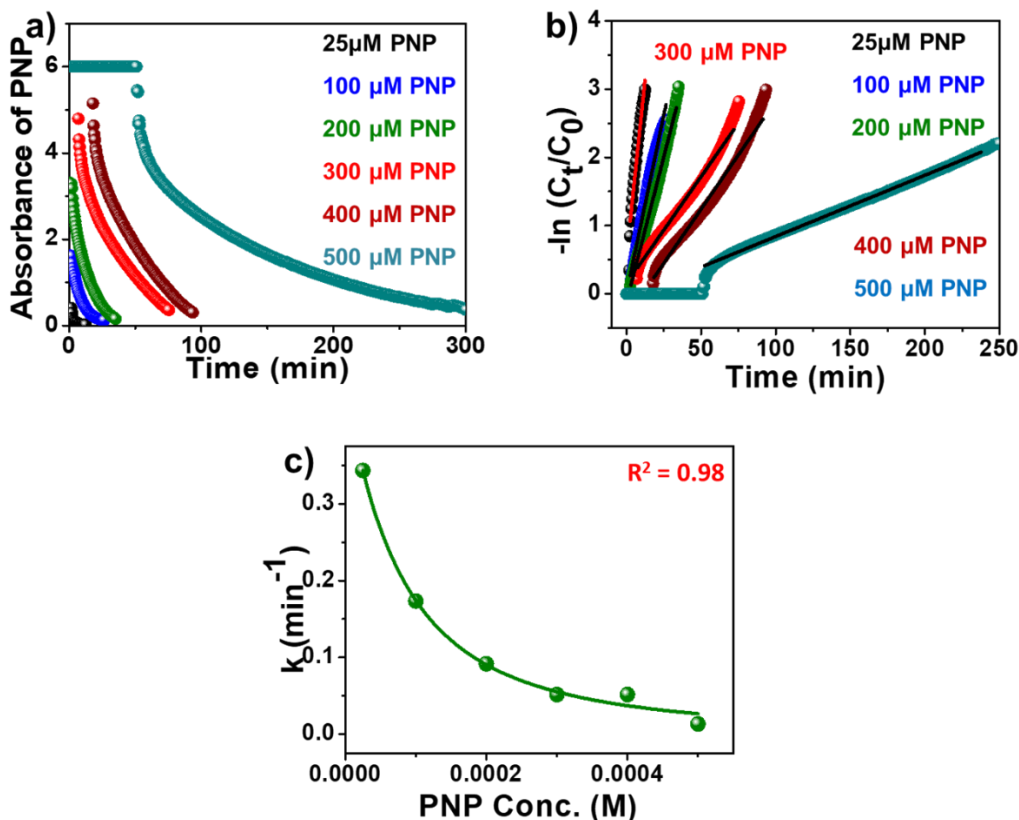


Figure 2.10. Validation of Langmuir-Hinshelwood mechanism for the reaction kinetics of PNP reduction with [+] AuNP. a) Variation in the kinetic traces for the PNP reduction by 10 mM BH_4^- in the presence of 0.2 mol% of [+] AuNP as a function of PNP concentration. b) The corresponding linearized data for the first order analysis assuming that the reduction follows a Langmuir–Hinshelwood mechanism. A decrease in the rate constant was obtained upon increasing the PNP concentration. c) Correlation of rate constant as a function of PNP concentration.

The plot of rate constant vs PNP concentration was fitted with the following Langmuir–Hinshelwood model.¹³ A perfect fit again confirms that the AuNP catalysed reduction of PNP is following the Langmuir–Hinshelwood mechanism.

$$k_{app} = \frac{k \cdot S \cdot K_{PNP}^n \cdot c_{PNP}^{n-1} \cdot (K_{\text{BH}_4^-} \cdot c_{\text{BH}_4^-})^m}{(1 + (K_{PNP} \cdot c_{PNP})^n + (K_{\text{BH}_4^-} \cdot c_{\text{BH}_4^-})^m)^2}$$

where k is molar rate constant per sq. meter. S is surface area. $K_{\text{BH}_4^-}$ and K_{PNP} are the adsorption coefficient of borohydride and p-nitrophenol, respectively. $c_{\text{BH}_4^-}$ and c_{PNP} are the concentration of borohydride and p-nitrophenol, respectively. n and m are the Freundlich constants.

2.4.4. Effect of Surface Area:

Our next idea was to overrule the effect of surface area. Since the reduction of nitrophenol predominantly depends on the adsorption of the reactant molecules on the surface of NPs, the surface area can be a prudent factor behind the dominance of [+] AuNP. To overrule the effect of surface area, we first estimated the ligand packing density for both the NP systems based on two independent techniques, namely Thermo Gravimetric Analysis (TGA; **Figure 2.11 a,b**) and Inductively Coupled Plasma - Mass Spectrometry (ICP-MS). As shown in **Figure 2.11 c**, both these experiments confirmed similar ligand packing density on [+] and [-] AuNPs (Detailed calculation for ligand packing density is provided in **Experimental Section 2.3.16**). Next we compared the catalytic activity of [+] AuNPs to that of citrate stabilized AuNPs of similar size. Remarkably, the catalysis by [+] AuNP was superior to even citrate stabilized Au NP (**Figure 2.12 a,b**). The latter being often considered as a benchmark catalyst as it provides ~100 % of its surface for catalysis.¹⁸ Thus, the [+] AuNP exhibited the highest catalytic activity among other NP systems despite having comparable or even lower surface area available for adsorption, confirming the exclusivity of electrostatics in the present studies.

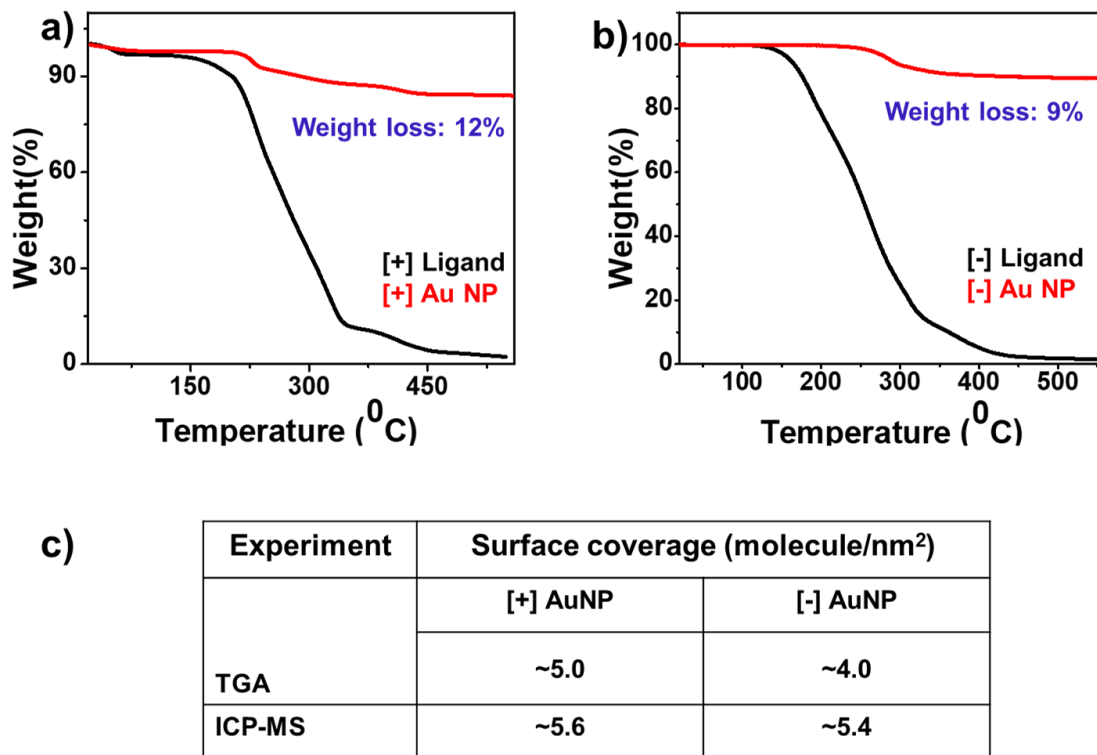


Figure 2.11. TGA curves of a) positively and b) negatively charged ligands and AuNPs. c) Table summarizing the estimation of surface coverage for both [+] and [-] AuNPs using two independent experiments.

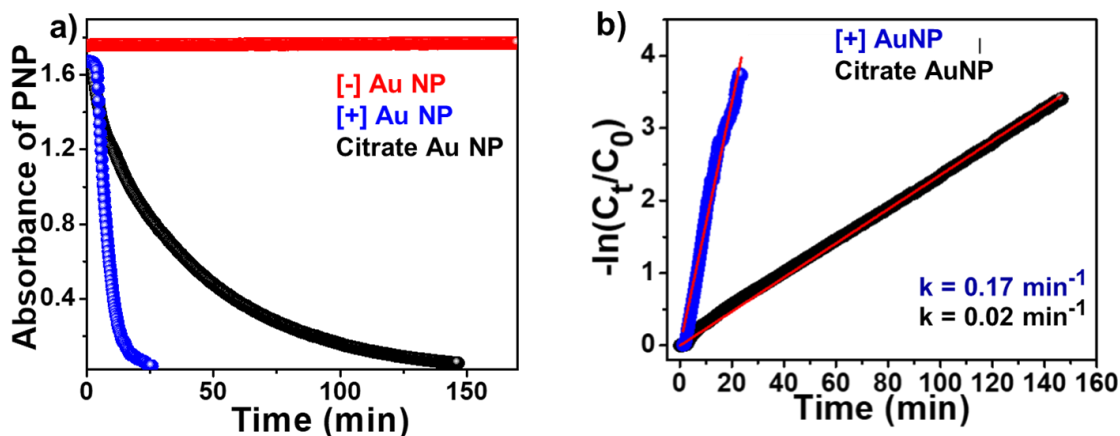


Figure 2.12. Comparison of catalytic activity of [+] and citrate stabilized AuNPs. a) The progress of PNP reduction by tracking the absorption changes of PNP peak at 400 nm with time in water by BH_4^- in the presence of 0.2 mol % [+], [-] and citrate stabilized AuNPs. b) The corresponding linearized data for the first order analysis assuming that the reduction follows a Langmuir–Hinshelwood mechanism.

2.4.5. Effect of Dissolved Oxygen:

The reduction of nitrophenol with borohydride in presence of metal NP is always associated with a typical time delay which is commonly known as induction time. Various hypotheses have been suggested to explain the reason behind the appearance of an induction time. Recently, Neretina and co-workers have demonstrated that the dissolved oxygen play a crucial role in the appearance of the induction time.⁴⁹ As per the study, the dissolved oxygen in the solution can initiate the oxidation of aminophenol back to nitrophenol and can inhibit the forward reaction (appearance of induction time). Thus the effect of dissolved oxygen should be taken into account before confirming the effect of electrostatics in dictating the catalytic property of AuNPs. Accordingly, detailed catalytic studies were performed by removing oxygen from the reaction medium to validate the effect of electrostatics under different experimental conditions. This was achieved by purging the reactant solution and NP catalysts separately with argon, followed by monitoring the reduction under argon atmosphere as reported previously.⁴⁹ The catalysis with 50 pM [+] AuNPs proceeded without any induction time under inert condition (**Figure 2.13 a,b**),

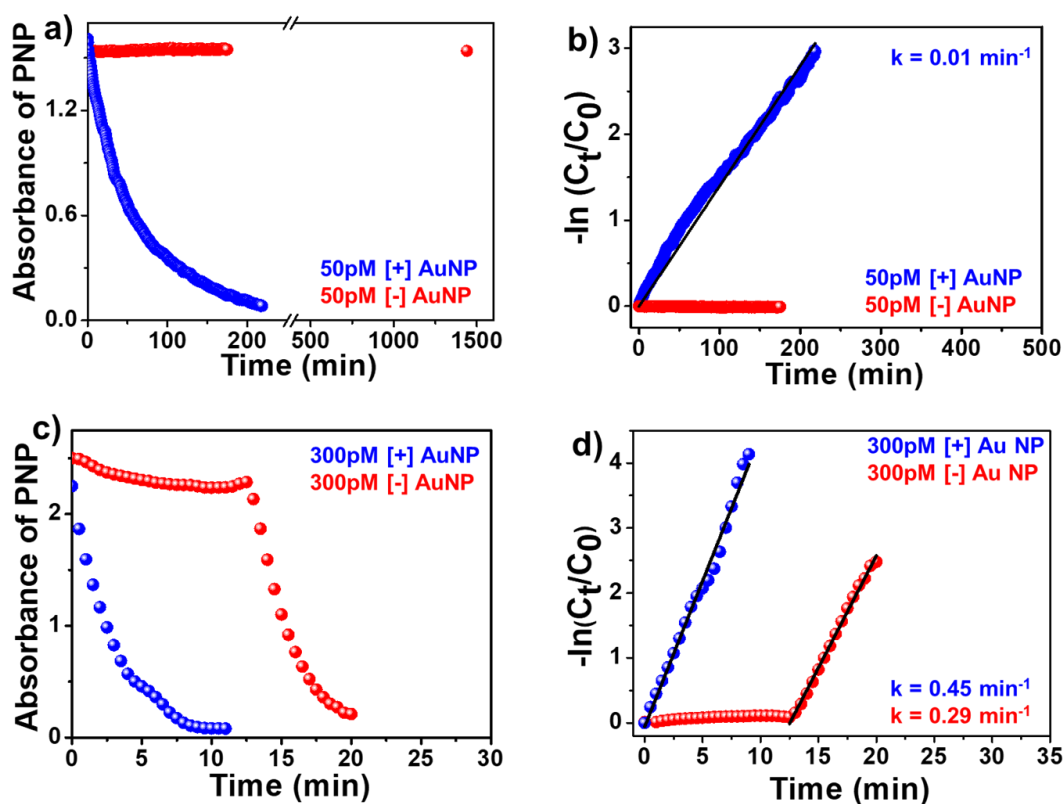


Figure 2.13. AuNP catalyzed reduction of PNP in the absence of oxygen (by purging the reactant solution and NP catalysts separately with argon for 15 min, and then monitoring the catalysis under argon atmosphere). Kinetic traces for the reduction of 100 μM PNP by 10 mM BH_4^- in the presence

of a) 0.2 mol % and c) 1.2 mol % of AuNPs of both polarities. The corresponding linearized data for the first order analysis assuming that the reduction follows a Langmuir–Hinshelwood mechanism is shown in b) and d).

as reported for BH_4^- stabilized AuNPs. Interestingly, no noticeable reduction of PNP was observed for even up to ~1 day when 50 pM [-] AuNP was used as the catalyst, under the same conditions (**Figure 2.13 a,b**). A clear dominance of [+] AuNP over [-] AuNP was even observed for higher catalyst concentrations (300 pM, 1.2 mol%), where NPs of both polarities are capable of catalyzing the PNP reduction (**Figure 2.13 c,d**). Thus, the effect of electrostatics on AuNP catalyzed reduction of PNP is consistently observed both in the presence and absence of dissolved oxygen. Consequently, all the further experiments were performed under ambient conditions that are most likely to be followed for practical applications.

2.4.6. Interaction Driven Catalysis:

The presence of charges on AuNP as well as on the reactant molecules (phenolate ion and BH_4^-) point towards the involvement of electrostatic forces in dictating the NP-reactant interactions, and hence their catalytic performances. To ascertain this, a series of catalytic experiments were performed by systematically varying the electrostatic potential around AuNPs through precise ligand functionalization. Our hypothesis is based on the favourable interactions arising from the electrostatic attraction between [+] AuNP and [-] reactant molecules. A reduction in this favourable interaction, in principle, should lower the catalytic efficiency of [+] AuNPs. Accordingly, the favourable interactions were lowered by diluting the [+] charges on AuNPs with neutral ligands (**Figures 2.14 and 2.7 a,b**). In one instance, the dilution was achieved by introducing dodecanethiol (DDT) onto the NP surface. This resulted in the formation of $[\text{+}/\text{DDT}]_{1.5}$ AuNP having ~ 70 % TMA and ~ 30 % DDT ligands on AuNPs (as calculated from previous NMR studies).^{30,50} The decrease in the zeta potential of $[\text{+}/\text{DDT}]_{1.5}$ AuNP to $+12.3 \pm 1.2$ mV confirmed the reduction in the magnitude of surface potential (**Figure 2.7 a,b**). The induction time was increased to ~ 4 min and the rate constant was lowered to 0.16 min^{-1} , when $[\text{DDT}/\text{+}]_{1.5}$ AuNP was used as the catalyst (**Figure 2.14 a,b**). Similarly, the use of neutral EG_3SH functionalized AuNP as the catalyst further decreased the favourable interactions ($\zeta = -2 \text{ mV} \pm 0.5 \text{ mV}$; **Figure 2.7 a,b**). This was evident from the increase in the induction time to ~18 min and lowering of rate constant to 0.10 min^{-1} (**Figure 2.14 a,b**). Secondly, we decreased the favourable interactions through screening of the charges on [+] AuNP surface by performing the reaction in high ionic

concentrations (like Phosphate Buffered Saline, PBS). An increase of induction time from ~ 0.7 min to ~ 3 min, and lowering of rate constants from 0.25 min^{-1} to 0.14 min^{-1} was observed when the reaction medium was changed from water to 1X PBS (Figure 2.14 c,d). The favourable interactions declined further when the salt concentration was increased by changing the reaction medium to 2X PBS, and no noticeable catalysis was observed for ~ 2 days (Figure 2.14 c,d).

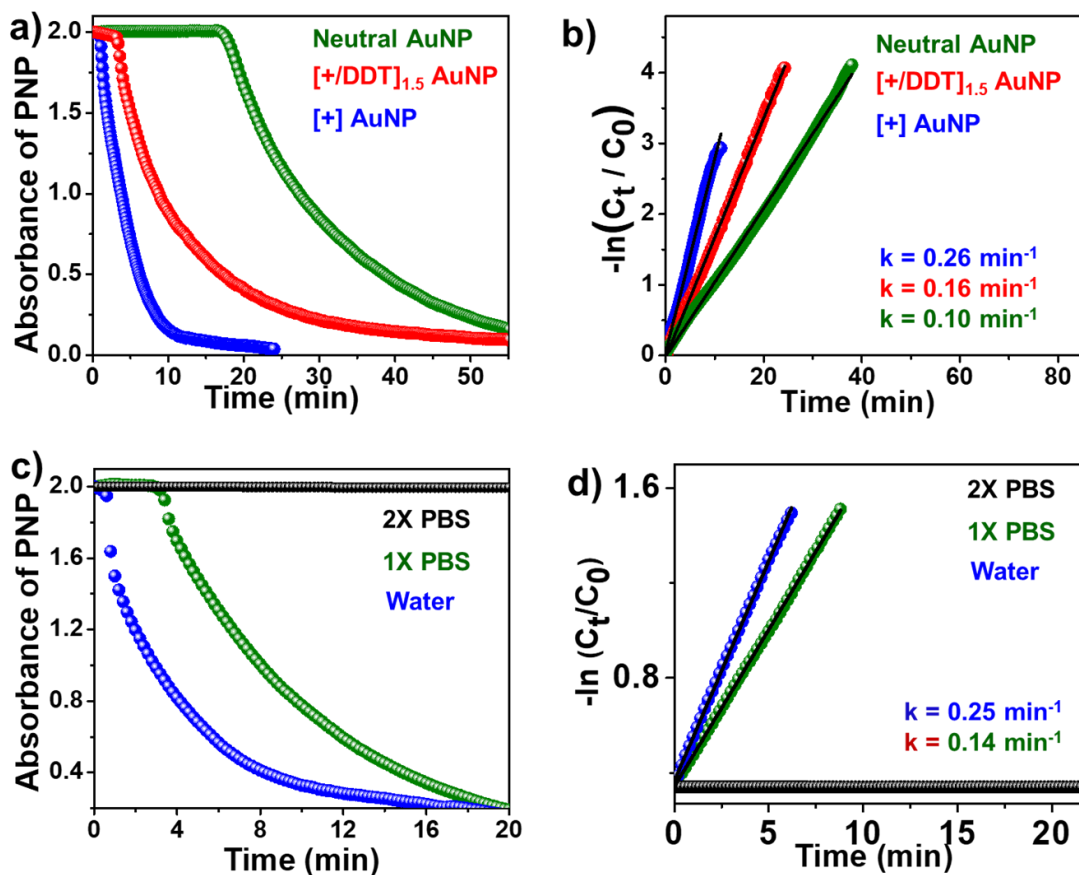


Figure 2.14. Proof for electrostatic effects in AuNP catalyzed PNP reduction. a) Progress of PNP reduction by 10 mM BH_4^- in presence of $0.2 \text{ mol } \%$ [+]/ (blue), [+]/DDT_{1.5} (red) and neutral EG₃SH (green) AuNPs in water. b) The corresponding linearized data for the first order analysis assuming that the reduction follows the Langmuir–Hinshelwood mechanism. c) Kinetic traces for PNP reduction by 10 mM BH_4^- in presence of $0.2 \text{ mol } \%$ of [+]/ AuNP in a) water (blue), 1X PBS (green) and 2X PBS (black) reaction medium. d) The corresponding linearized data for the first order analysis assuming that the reduction follows the Langmuir–Hinshelwood mechanism.

The effect of ions on the screening of charges was supported by screening length calculations. The screening length decreased from $\sim 3.0 \text{ nm}$ to $\sim 0.7 \text{ nm}$, and further to $\sim 0.5 \text{ nm}$ as the medium was

changed from water to 1X PBS to 2X PBS (correlation of ionic strength and screening length with reaction kinetics is given in **Table 2.3**). The ionic strength of solution is expected to change the outcome of the reaction due to its strong influence on the electrostatic potential arising from the NP surface (both favourable and unfavourable). For instance, an increase in the ionic strength lowers the magnitude as well as the extent of the electrostatic field arising from charged NP surfaces. This reduced charge density affects the reaction kinetics as summarized in **Table 2.3** (Detailed calculation for screening length and surface potential is provided in **Experimental Section 2.3.13 and 2.3.14 respectively**). Specifically, the catalytic activity of [+] AuNP for PNP reduction decreased as the ionic strength of the medium was increased.

Catalyst (0.2 mol%)	Zeta potential (mV)	Reaction medium	Ionic strength (mM) ^a	Range of electrostatic field ^b	Rate constant (min ⁻¹)	Induction time (min)
[+] Au NP	+ 24.2± 0.1	DI H ₂ O	10	3.04 nm	~ 0.27	0.7-1.5
		1X PBS	181.5	0.71 nm	~ 0.14	~ 3.0
		2X PBS	353	0.51 nm	No catalysis	No catalysis

Table 2.3: Correlation between surface potential and ionic strengths with reaction kinetics for the reduction of 100 μM PNP by 10 mM BH₄⁻ in the presence of 0.2 mol % of [+] AuNP, under ambient conditions.

$$I = \frac{1}{2} \sum_{i=1}^n m_i z_i^2$$

^a Estimated using the equation

^b Calculated from equation (2.6).

2.4.7. Temperature Dependent Catalytic Study:

Next, we performed a detailed temperature dependent catalytic study to further prove the exclusivity of the electrostatics in dictating the catalytic property AuNPs. Temperature dependent catalytic studies too proved the dominance of [+] AuNP over [+/DDT]_{1.5} and [-] AuNPs in the PNP reduction (**Figure 2.15 a-d**). Interestingly, 0.2 mol % of [-] AuNP was unable to catalyze the reduction even at 45 °C. The raw spectra for the temperature dependent analysis are provided in the Appendix of this Chapter. Further, we investigated the effect of electrostatics in the activation energy of the reaction. For this, 300 pM (1.2 mol %) of AuNPs were used, since [-] AuNP failed to catalyze the reaction for ~ 8 h below this concentration. The distinction in the rate

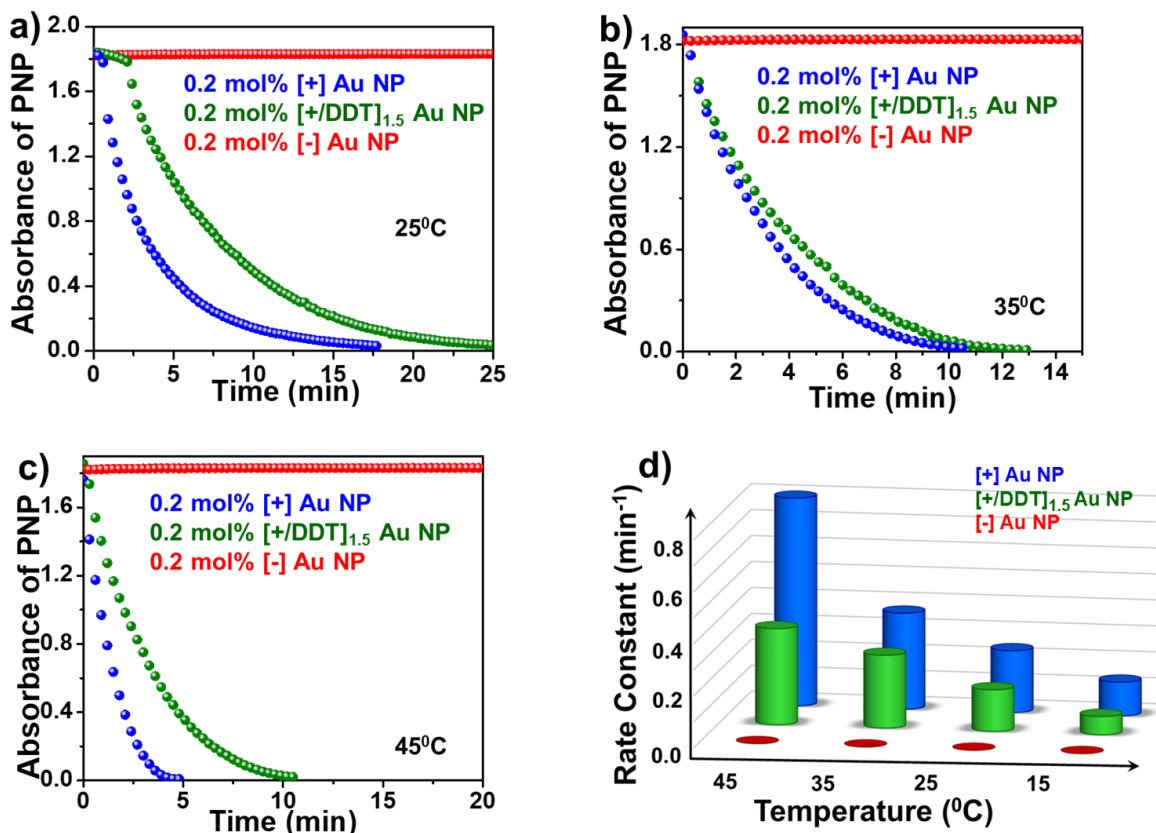


Figure 2.15. Temperature dependent catalytic reduction of PNP by different sets of AuNPs. The progress of PNP reduction by tracking the absorption changes of PNP peak at 400 nm in the presence of 0.2 mol % of [+], [-], and [+]/DDT]_{1.5} AuNPs at a) 25 °C, b) 35 °C, c) 45 °C. d) Plot showing the variation in the rate constant of PNP reduction by 10 mM BH₄⁻ in the presence of different AuNP catalysts at different temperatures.

constant and induction time was maintained between [+]₁ and [-]₁ AuNPs even at 1.2 mol % and at higher temperatures (**Figure 2.16 a-c**). The apparent activation energy for PNP reduction was lower in the presence of [+]₁ AuNP compared to [-]₁ AuNP ($E_{a[+]AuNP} \sim 30$ kJ/mol and $E_{a[-]AuNP} \sim 45$ kJ/mol). The raw spectra for the activation energy calculation are provided in the Appendix of this Chapter.

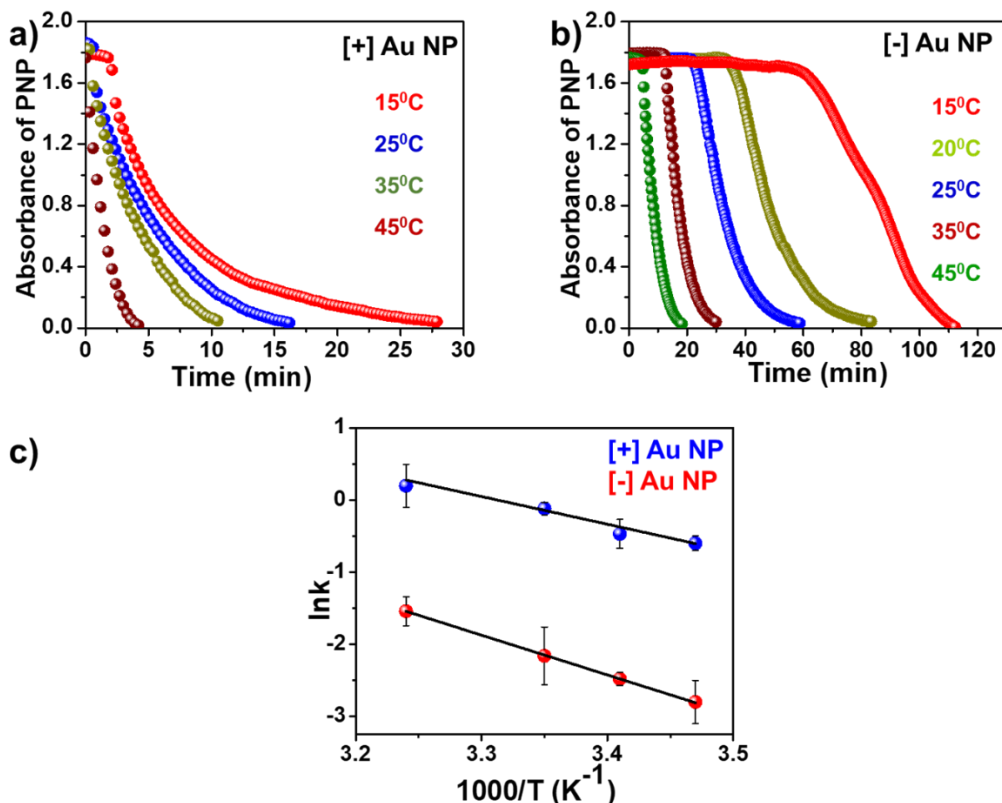


Figure 2.16. Temperature dependent catalytic reduction of PNP by 1.2 mol % of [+] and [-] AuNPs. The progress of PNP reduction by tracking the absorption changes of PNP peak at 400 nm in the presence of 1.2 mol % of a) [+] and b) [-] AuNPs. c) Plot of $\ln k$ vs $1/T$ for the PNP reduction by 10 mM BH_4^- in the presence of 1.2 mol % of [+] and [-] AuNPs.

2.4.8. Generality of Hypothesis:

Next we discuss about the generality of our hypothesis in other molecular systems. The catalytic dominance of [+] AuNP over [-] AuNP was clearly observed in the reduction of 4-nitro aniline (PNA) by BH_4^- . The PNA reduction was completed within ~ 20 min in the presence of ~ 0.1 mol% [+] AuNP, with an induction time of ~ 4 min and rate constant of 0.25 min^{-1} (Figure 2.17 a,b). On the other hand, [-] AuNP failed to catalyze the PNA reduction even up to ~ 2 days. A similar trend was observed in the reduction of ferricyanides by BH_4^- in the presence of AuNPs (Figure 2.17 c,d). Here too, the effect of favorable interaction between [+] AuNP and [-] reactants ($[\text{Fe}(\text{CN})_6]^{3-}$ complex and BH_4^-) was evident. A complete reduction of ferricyanide absorption at ~ 420 nm was observed in presence of 0.2 mol % AuNP within 5 min, confirming the reduction of Fe(III) to Fe(II) complex⁴⁶ (rate constant of 0.59 min^{-1}). However, the reduction of Fe(III) was not complete

by BH_4^- even up to ~ 12 h using 0.2 mol% of [-] AuNP (Figure 2.17 d). Thus, the last example expands the scope of electrostatics in the catalytic reduction of inorganic complexes as well.

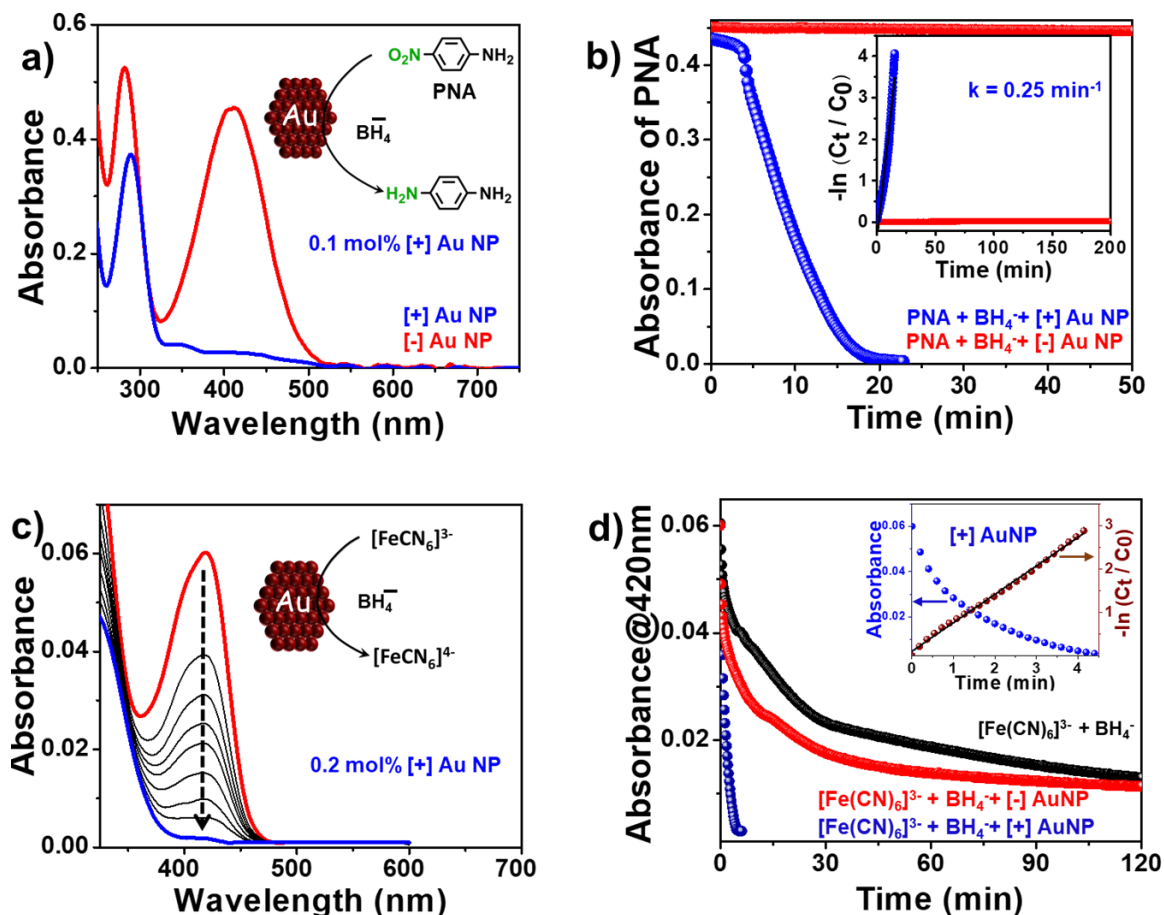


Figure 2.17. Role of electrostatics in AuNP catalyzed reduction of PNA and ferricyanides. a) A complete reduction of PNA absorption peak at ~ 420 nm was observed in the presence of 10 mM BH_4^- and 0.1 mol% [+] AuNP. No appreciable spectral changes were observed up to 2 days when 0.1 mol% [-] AuNP was used as the catalyst. b) Kinetic traces for PNA reduction in presence of 0.1 mol% [+] and [-] AuNPs. Inset show the corresponding linearized data for the first order analysis. c) Spectral changes confirming the reduction of ferricyanides by 10 mM BH_4^- in presence of 0.2 mol % [+] AuNP. d) Kinetic traces of absorbance at 420 nm during the reduction of ferricyanide using 0.2 mol% [+] and [-] AuNPs. The inset shows the linearized data for the first order analysis for ferricyanide reduction by [+] AuNPs.

2.5. Conclusion

In summary, the effects of electrostatics in terms of both attractive (favorable) and repulsive (unfavorable) interactions on AuNP catalyzed reduction of charged reactants was successfully demonstrated. The interactions between the reactants and AuNP surface was made favorable or unfavorable by fine tuning the NP surface potential. An electrostatically assisted channeling of substrates due to the attraction between oppositely charged substrates and AuNP surface was responsible for the dominance of [+] AuNP over other NP systems. A series of experiments with AuNPs having varying surface charges confirmed the exclusivity of electrostatics in catalytic reductions. The potency of electrostatics was established in [+] AuNP despite having a lower or comparable surface area for catalysis. The assistance of electrostatics helped in lowering the use of AuNP catalyst to picomolar level, which can boost its use in industrial applications. The concept of electrostatic effects was extended towards the catalytic reduction of ferricyanides, validating our hypothesis beyond organic substrates.

A plausible future direction could be to extend this *idea of interaction* in the area of plasmonic photocatalysis. The photocatalytic activity of metal NPs predominantly depends on the rate of hot electron/hole transfer (within ~10-100 fs), which oftentimes is hindered by the insulating nature of the surface ligands. The idea of precise NP-reactant interaction, through judicious surface chemistry, could be an effective strategy to circumvent the “*ligand poisoning*” effect in metal NP photocatalysis. The next Chapter focuses on this particular aspect and investigates the role of precise NP-reactant interaction in dictating the photocatalytic activity of metal NPs.

2.6. References

1. Narayanan, R.; El-Sayed, M. A. Catalysis with Transition Metal Nanoparticles in Colloidal Solution: Nanoparticle Shape Dependence and Stability *J. Phys. Chem. B* **2005**, *109*, 12663-12676.
2. Astruc, D.; Lu, F.; Aranzaes, J. R. Nanoparticles as Recyclable Catalysts: The Frontier between Homogeneous and Heterogeneous Catalysis. *Angew. Chem. Int. Ed.* **2005**, *44*, 7852-7872.
3. Linic, S.; Christopher, P.; Xin, H.; Marimuthu, A. Catalytic and Photocatalytic Transformations on Metal Nanoparticles with Targeted Geometric and Plasmonic Properties *Acc. Chem. Res.* **2013**, *46*, 1890-1899.

4. Pradhan, N.; Pal, A.; Pal, T. Silver Nanoparticle Catalyzed Reduction of Aromatic Nitro Compounds *Colloid Surf. A* **2002**, *196*, 247-257.
5. Tao, F.; Schneider, W. F.; Kamat, P. V. *Heterogeneous Catalysis at Nanoscale for Energy Application*; John Wiley & Sons, Inc.: Hoboken, NJ, 2015.
6. Zhou, D.; Li, Y. C.; Xu, P.; McCool, N. S.; Li, L.; Wang, W.; Mallouk, T. E. Visible-light Controlled Catalytic Cu₂O–Au Micromotors. *Nanoscale* **2017**, *9*, 75-78.
7. Kale, M. J.; Avanesian, T. & Christopher, P. Direct photocatalysis by plasmonic nanostructures. *ACS Catal.* **2014**, *4*, 116-128.
8. Kim, Y.; Torres, D. D.; Jain, P. K. Activation Energies of Plasmonic Catalysts. *Nano Lett.* **2016**, *16*, 3399-3407.
9. Christopher, P.; Xin, H.; Linic, S. Visible-Light-Enhanced Catalytic Oxidation Reactions on Plasmonic Silver Nanostructures. *Nat. Chem.* **2011**, *3*, 467–472.
10. Herve, P.; Perez-Lorenzo, M.; Liz-Marzan, L. M.; Dzubilla, J.; Lu, Y.; Ballauff, M. Catalysis by metallic nanoparticles in aqueous solution: model reactions *Chem. Soc. Rev.* **2012**, *41*, 5577-5587.
11. Aditya, T.; Pal, A.; Pal, T. Nitroarene Reduction: A Trusted Model Reaction to Test Nanoparticle Catalysts. *Chem. Commun.* **2015**, *51*, 9410-9431.
12. Zhao, P.; Feng, X.; Huang, D.; Yang, G.; Astruc, D. Basic Concepts and Recent Advances in Nitrophenol Reduction by Gold and Other Transition Metal Nanoparticles. *Coordin. Chem. Rev.* **2015**, *287*, 114-136.
13. Wunder, S.; Polzer, F.; Lu, Y.; Mei, Y.; Ballauff, M. Kinetic Analysis of Catalytic Reduction of 4-Nitrophenol by Metallic Nanoparticles Immobilized in Spherical Polyelectrolyte Brushes *J. Phys. Chem. C* **2010**, *114*, 8814-8820.
14. Wunder, S.; Lu, Y.; Albrecht, M.; Ballauff, M. Catalytic Activity of Faceted Gold Nanoparticles Studied by a Model Reaction: Evidence for Substrate-Induced Surface Restructuring. *ACS Catal.* **2011**, *1*, 908-916.
15. Khalavka, Y.; Becker, J.; Sonnichsen, C. Synthesis of Rod-Shaped Gold Nanorattles with Improved Plasmon Sensitivity and Catalytic Activity. *J. Am. Chem. Soc.* **2009**, *131*, 1871–1875.
16. Eley, D. D. Rideal, E. K. Parahydrogen Conversion on Tungsten. *Nature*, **1940**, *146*, 401.

17. Pradhan, N.; Pal, A.; Pal, T. Catalytic Reduction of Aromatic Nitro Compounds by Coinage Metal Nanoparticles. *Langmuir* **2001**, *17*, 1800-1802.
18. Ansar, S. M.; Kitchens, C. L. Impact of Gold Nanoparticle Stabilizing Ligands on the Colloidal Catalytic Reduction of 4-Nitrophenol *ACS Catal.* **2016**, *6*, 5553-5560.
19. Ciganda, R.; Li, N.; Deraedt, C.; Gatard, S.; Zhao, P.; Salmon, L.; Hernandez, R.; Ruiza, J.; Astruc, D. Gold Nanoparticles as Electron Reservoir Redox Catalysts for 4-Nitrophenol Reduction: a Strong Stereoelectronic Ligand Influence. *Chem. Commun.* **2014**, *50*, 10126-10129.
20. Wei, J.; Wang, H.; Deng, Y.; Sun, Z.; Shi, L.; Tu, B.; Luqman, M.; Zhao, D. Solvent Evaporation Induced Aggregating Assembly Approach to Three-Dimensional Ordered Mesoporous Silica with Ultralarge Accessible Mesopores *J. Am. Chem. Soc.* **2011**, *133*, 20369-20377.
21. Zhou, X.; Xu, W.; Liu, G.; Panda, D.; Chen, P. Size-Dependent Catalytic Activity and Dynamics of Gold Nanoparticles at the Single-Molecule Level. *J. Am. Chem. Soc.* **2010**, *132*, 138-146.
22. Mahmoud, M. A.; Saira, F.; El-Sayed, M. A. Experimental Evidence for The Nanocage Effect In Catalysis With Hollow Nanoparticles. *Nano Lett.* **2010**, *10*, 3764-3769.
23. Zeng, J.; Zhang, Q.; Chen, J.; Xia, Y. A Comparison Study of the Catalytic Properties of Au-Based Nanocages, Nanoboxes, and Nanoparticles. *Nano Lett.* **2010**, *10*, 30-35.
24. Ghosh, S. K.; Kundu, S.; Mandal, M.; Pal, T. Silver and Gold Nanocluster Catalyzed Reduction of Methylene Blue by Arsine in a Micellar Medium. *Langmuir* **2002**, *18*, 8756-8760.
25. Pillai, P. P.; Kowalczyk, B.; Grzybowski, B. A. Self-Assembly of Like-Charged Nanoparticles into Microscopic Crystals. *Nanoscale* **2016**, *8*, 157-161.
26. Kundu, P. K.; Samanta, D.; Leizrowice, R.; Margulis, B.; Zhao, H.; Börner, M.; Udayabhaskararao, T.; Manna, D.; Klajn, R. Light-controlled self-assembly of non-photoresponsive nanoparticles *Nat. Chem.* **2015**, *7*, 646-652.
27. Bishop, K. J. M.; Wilmer, C. E.; Soh, S.; Grzybowski, B. A. Nanoscale Forces and Their Uses in Self-Assembly. *Small* **2009**, *5*, 1600-1630.

28. Xu, L.; Ma, W.; Wang, L.; Xu, C.; Kuang, Hua.; Kotov N. A. Nanoparticle Assemblies: Dimensional Transformation of Nanomaterials and Scalability. *Chem. Soc. Rev.* **2013**, *42*, 3114-3126.
29. Taniguchi, Y.; Takishita, T.; Kawai, T.; Nakashima T. End-to-End Self-Assembly of Semiconductor Nanorods in Water by Using an Amphiphilic Surface Design. *Angew. Chem. Int. Ed.* **2016**, *55*, 2083-2086.
30. Rao, A.; Roy, S.; Unnikrishnan, M.; Bhosale, S. S.; Devatha, G.; Pillai, P. P. regulation of Interparticle Forces Reveals Controlled Aggregation in Charged nanoparticles. *Chem. Mater.* **2016**, *28*, 2348-2355.
31. Jimenez- de- Aberasturi, D.; Montenegro, J. M.; Ruiz- de- Lar-ramendi, I.; Rojo, T.; Klar, T. A.; Alvarez-Puebla, R.; Liz-Marzan, L. M.; Parak, W. J. Optical Sensing of Small Ions with Colloidal Nanoparticles W. J. *Chem. Mater.* **2012**, *24*, 738-745.
32. Devatha, G.; Roy, S.; Rao, A.; Mallick, A.; Basu, S.; Pillai, P. P. Electrostatically Driven Resonance Energy Transfer in Cationic Bio-Compatible InP Quantum Dots. *Chem. Sci.* **2017**, *8*, 3879-3884.
33. Hoffman, J. B.; Alam, R.; Kamat, P. V. Why Surface Chemistry Matters for QD-QD Resonance Energy Transfer. *ACS Energy Lett.* **2017**, *2*, 391-396.
34. Mout, R.; Moyano, D. F.; Rana, S.; Rotello, V. M. Surface functionalization of nanoparticles for nanomedicine *Chem. Soc. Rev.* 2012, *41*, 2539-2544.
35. Pillai, P. P.; Kowalczyk, B.; Kandere-Grzybowska, K.; Borkowska, M.; Grzybowski B. A. Engineering Gram Selectivity of Mixed-Charge Gold Nanoparticles by Tuning the Balance of Surface Charges. *Angew.Chem. Int. Ed.* **2016**, *55*, 8610-8614.
36. Jana, N. R.; Wang, Z. L.; Pal, T. Redox Catalytic Properties of Palladium Nanoparticles: Surfactant and Electron Donor-Acceptor Effects. *Langmuir* **2000**, *16*, 2457-2463.
37. Park, D. K.; Lee, S. J.; Lee, J. H.; Choi, M. Y.; Han, S. W. A Comprehensive Review on the Synthesis, Characterization, and Biomedical Application of Platinum Nanoparticles. *Chem. Phys. Lett.* **2010**, *484*, 254-257.
38. Choi, S.; Jeong, Y.; Yu, J. Tuning the Hydride Reductions Catalyzed on Metal Nanoparticle Surfaces. *RSC Adv.* **2016**, *6*, 73805-73809.

39. Ma, A.; Xie, Y.; Xu, J.; Zeng, H.; Xu, H. The Significant Impact of Polydopamine on the Catalytic Performance of the Carried Au Nanoparticles. *Chem. Commun.* **2015**, *51*, 1469-1471.
40. Kim, Y.; Wilson, A. J.; Jain, P. K. The Nature of Plasmonically Assisted Hot-Electron Transfer in a Donor-Bridge-Acceptor Complex. *ACS Catal.* **2017**, *7*, 4360-4365.
41. Walker, D. A.; Wilmer, C. E.; Kowalczyk, B.; Bishop, K. J. M.; Grzybowski, B. A. Precision Assembly of Oppositely and Like-Charged Nanoobjects Mediated by Charge-Induced Dipole Interaction. *Nano Lett.* **2010**, *10*, 2275-2280.
42. Tien, J.; Terfort, A.; Whitesides, G. M. Microfabrication Through Electrostatic Self-Assembly. *Langmuir* **1997**, *13*, 5349-5355.
43. Jana, N. R.; Peng, X. Single-Phase and Gram-Scale Routes toward Nearly Monodisperse Au and Other Noble Metal Nanocrystals. *J. Am. Chem. Soc.* **2003**, *125*, 14280-14281
44. Piella, J.; Bastús, N. G.; Puntès, V. Size-Controlled Synthesis of Sub-10-nanometer Citrate-Stabilized Gold Nanoparticles and Related Optical Properties *Chem. Mater.* **2016**, *28*, 1066-1075.
45. Liu, X.; Atwater, M.; Wang, J.; Huo, Q. Extinction Coefficient of Gold Nanoparticles with Different Sizes and Different Capping Ligands. *Colloid Surface B.* **2007**, *58*, 3
46. Ghosh, P. *Colloid and Interface Science* Ch.10 (PHI Learning Private limited, New Delhi, 2009)
47. Smith, A. M.; Lee, A. A.; Perkin, S. The Electrostatic Screening Length in Concentrated Electrolytes Increases with Concentration *J. Phys. Chem. Lett.* **2016**, *7*, 2157-2163.
48. Nag, A.; Chung, D. S.; Dolzhnikov, D. S.; Dimitrijevic, N. M.; Chattopadhyay, S.; Shibata, T.; Talapin, D. V. Effect of Metal Ions on Photoluminescence, Charge Transport, Magnetic and Catalytic Properties of All-Inorganic Colloidal Nanocrystals and Nanocrystal Solids *J. Am. Chem. Soc.* **2012**, *134*, 13604-13615.
49. Menumerov, E.; Hughes, R. A.; Neretina, S. Catalytic Reduction of 4-Nitrophenol: A Quantitative Assessment of the Role of Dissolved Oxygen in Determining the Induction Time. *Nano Lett.* **2016**, *16*, 7791-7797.
50. Pillai, P. P.; Kowalczyk, B.; Pudlo, W. J.; Grzybowski, B. A. Electrostatic Titrations Reveal Surface Compositions of Mixed, On Nanoparticle Monolayers Comprising Positively and Negatively Charged Ligands. *J. Phys. Chem. C* **2016**, *120*, 4139-4144.

2.7. Appendix

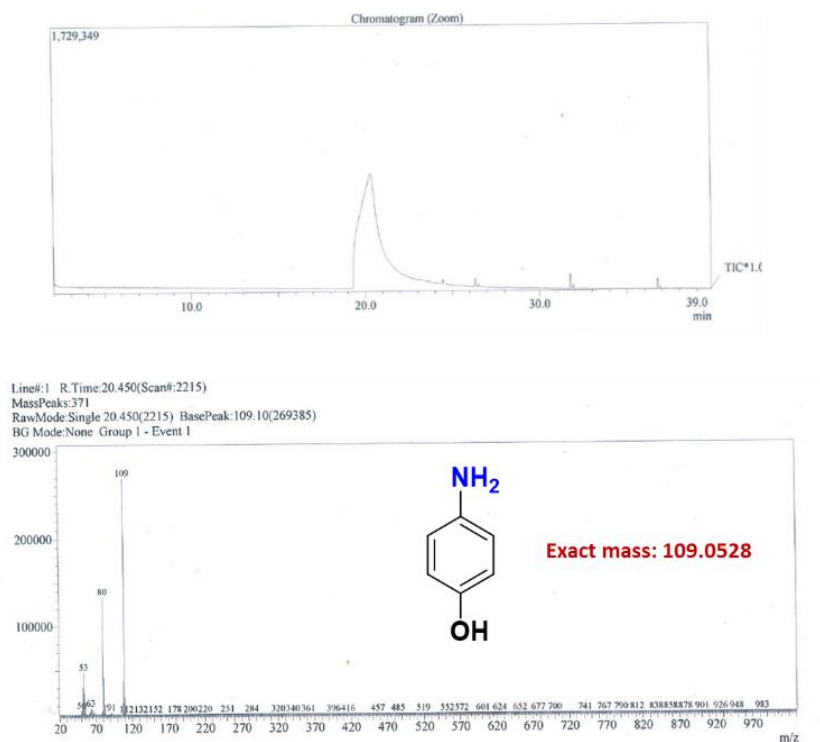


Figure 2.18. GC-MS spectra of p-aminophenol that was produced by the catalytic reduction of PNP by 0.2 mol % [+] AuNPs.

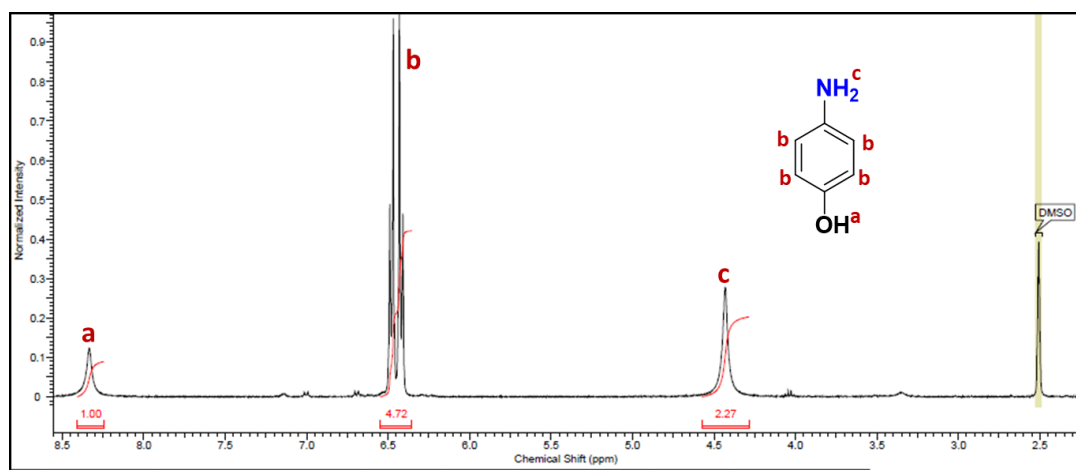


Figure 2.19. ^1H NMR spectra of p-aminophenol that was produced by the catalytic reduction of PNP by 0.2 mol % [+] AuNPs.

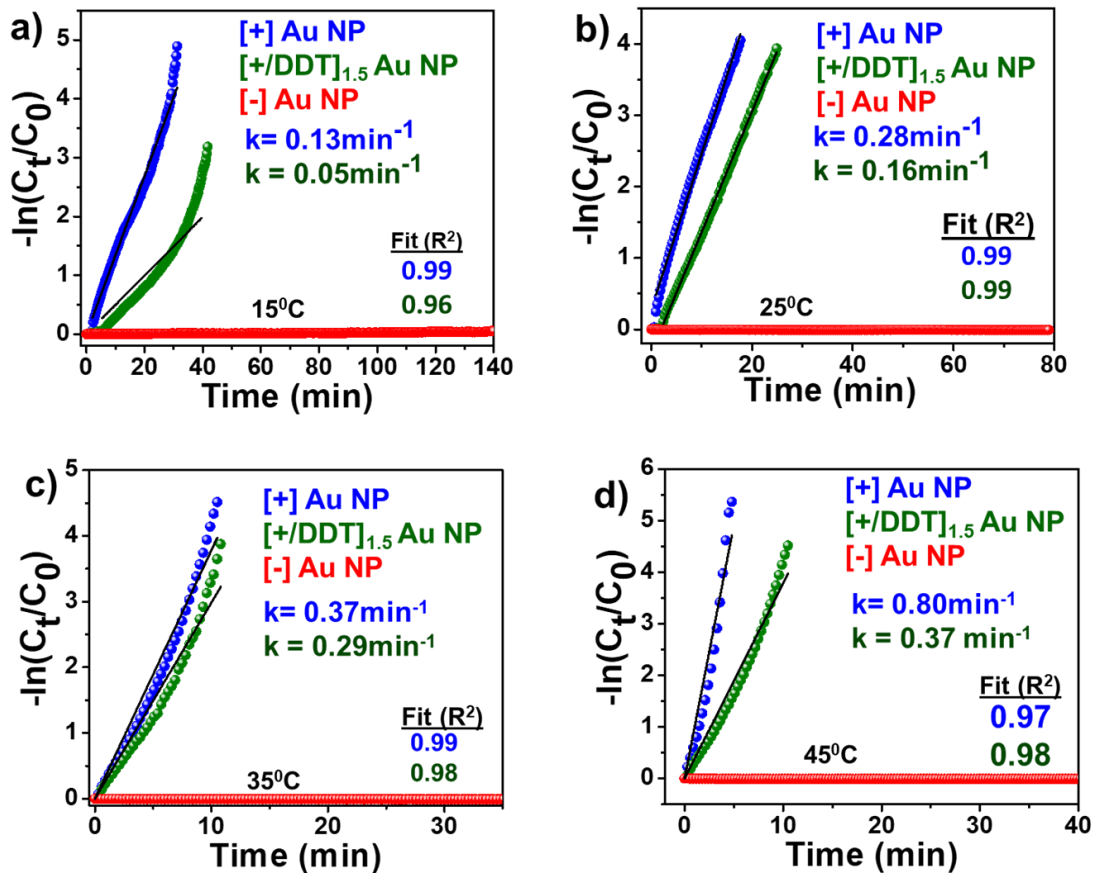


Figure 2.20. Temperature dependent catalytic reduction of PNP by different sets of AuNPs. Linearized data for first order analysis obtained by tracking the absorption changes of PNP peak at 400 nm with time in the presence of 0.2 mol % of [+], [-], and [+]/DDT]1.5 Au NPs at a) 15 °C, b) 25 °C, (c) 35 °C, and d) 45 °C.

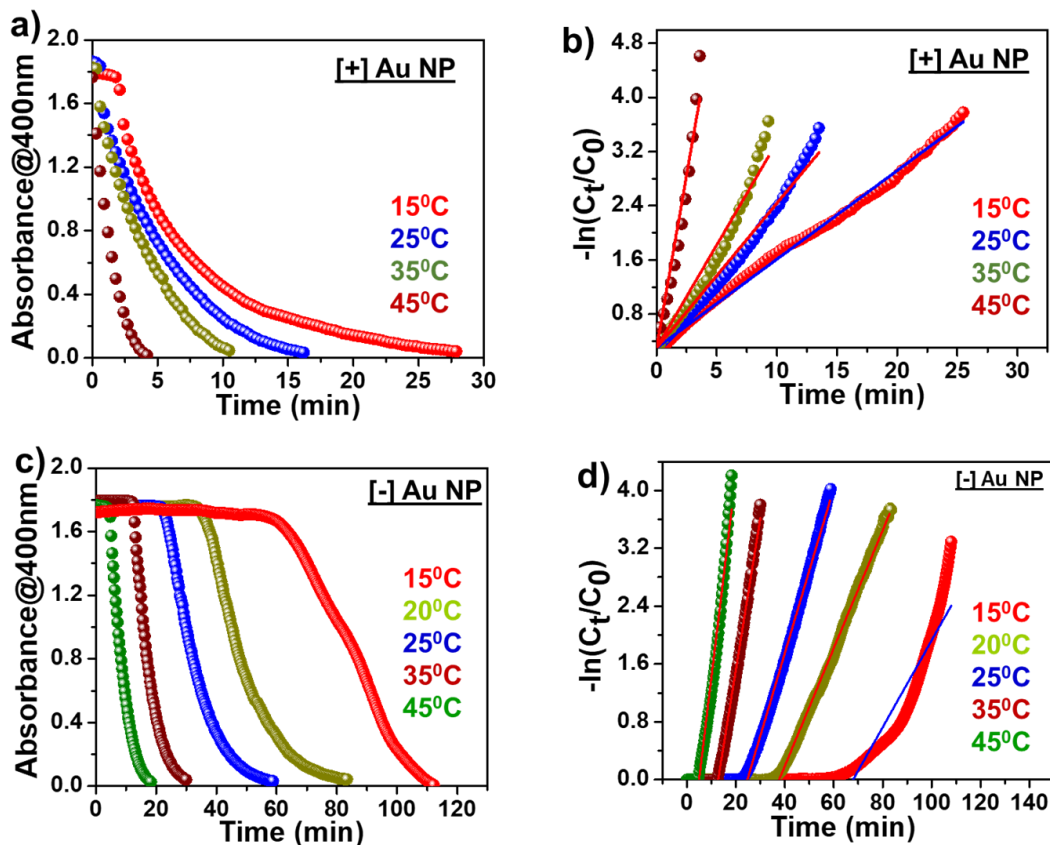
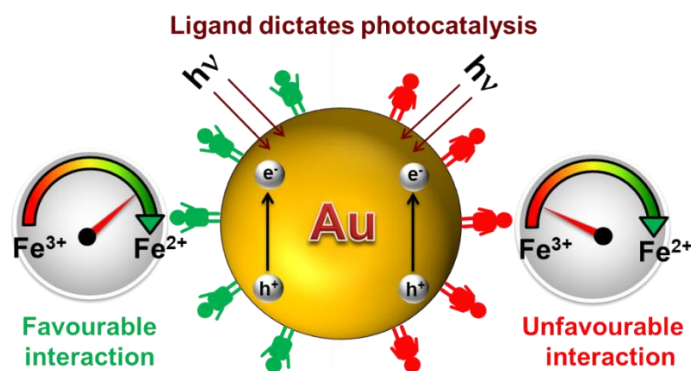


Figure 2.21. Temperature dependent catalytic reduction of PNP by 1.2 mol % of [+] and [-] AuNPs. a,c) The progress of PNP reduction and b, d) corresponding linearized data for first order analysis obtained by tracking the absorption changes of PNP peak at 400 nm with time in the presence of 1.2 mol % of a,b) [+] and c,d) [-] AuNPs at different temperatures. The rate constants from this plot were used for the calculation of apparent activation energies shown in **Figure 2.14**.

Chapter 3

Precise Nanoparticle-Reactant Interaction Outplays Ligand Poisoning in Visible-Light Photocatalysis



This Chapter is adapted with permission from the following paper. Copyright 2018, American Chemical Society.

Roy, S.; Roy, S.; Rao, A.; Devatha, G.; Pillai, P. P.* Precise Nanoparticle-Reactant Interaction Outplays Ligand Poisoning in Visible Light Photocatalysis. *Chem. Mater.* **2018**, *30*, 8415 - 8419

3.1. Abstract

Metal nanoparticles (NPs) and ligands are two inseparable entities. However, ligands present on the NP surface can ‘poison’ a photocatalyst by hindering the NP accessibility to the reactants and movement of charge carriers. In this Chapter, we present an elegant strategy to accomplish efficient photocatalysis by taking the advantage of ligands on the NP surface. Our approach of introducing favourable interactions between NP catalyst and substrate is tested in the model photocatalytic reduction of ferricyanide by plasmonic gold-nanoparticles (AuNP). Favourable interaction arising from the precise tuning of electrostatic potential results in the localization of reactant molecules around the AuNP catalyst. Close proximity between AuNP and ferricyanide improves the NP accessibility and electron transfer rate, thereby suppressing the ligand poisoning effect. Catalytic activities presented here are four-five folds better than the best reported values. Such interaction driven enhancement in photocatalytic performances can be prominent in the emerging area of ‘ligand directed product formation’ in NP catalysis.

3.2. Introduction

The ability to move electrons under the influence of light in an efficient manner is one of the most fundamental challenges in photocatalysis.¹⁻³ A diverse pool of systems ranging from molecular to organic to inorganic materials have been explored for harvesting photons to drive different chemical reactions.³⁻⁷ Among them, plasmonic metal nanoparticles (Au, Ag, Cu NPs) have gained special attention because of their high absorption cross-section in the visible region and the generation of hot charge carriers (electron/hole) through plasmon decay.⁷⁻¹² In general, after visible light excitation of Localized Surface Plasmon Resonance (LSPR), the excited plasmon undergoes two decay pathways: i) radiative pathway through the re-emission of a photon (scattering)¹⁰⁻¹² or ii) non-radiative pathway through electron-electron or electron-phonon coupling (Landau Damping).^{10,11} The radiative photon emission is the dominant pathway for larger particle size (> 50 nm for Ag)¹³ and have numerous applications in the area of Surface Enhanced Raman Spectroscopy; however not suitable for light harvesting. Whereas the non-radiative pathway is dominant for smaller sized particles and leads to the generation of hot electrons and holes, which are useful in driving different chemical transformations on the surface of NPs.¹⁰⁻¹² Typically, in non-radiative decay pathways, the excited plasmon first redistribute their energy via electron-electron scattering (10-100 fs timescale) leading to the electronic excitation either through intraband (s to sp) or through interband (d to sp) transition. These hot carriers subsequently

dissipate their energy via electron-phonon relaxation (~ 1 ps timescale) and releases heat to the NP lattice (plasmonic heating). Finally in a timescale of 100 ps the NP lattice reaches a thermal equilibrium with the surroundings via phonon-phonon relaxation (**Figure 3.1**).^{10,12,14}

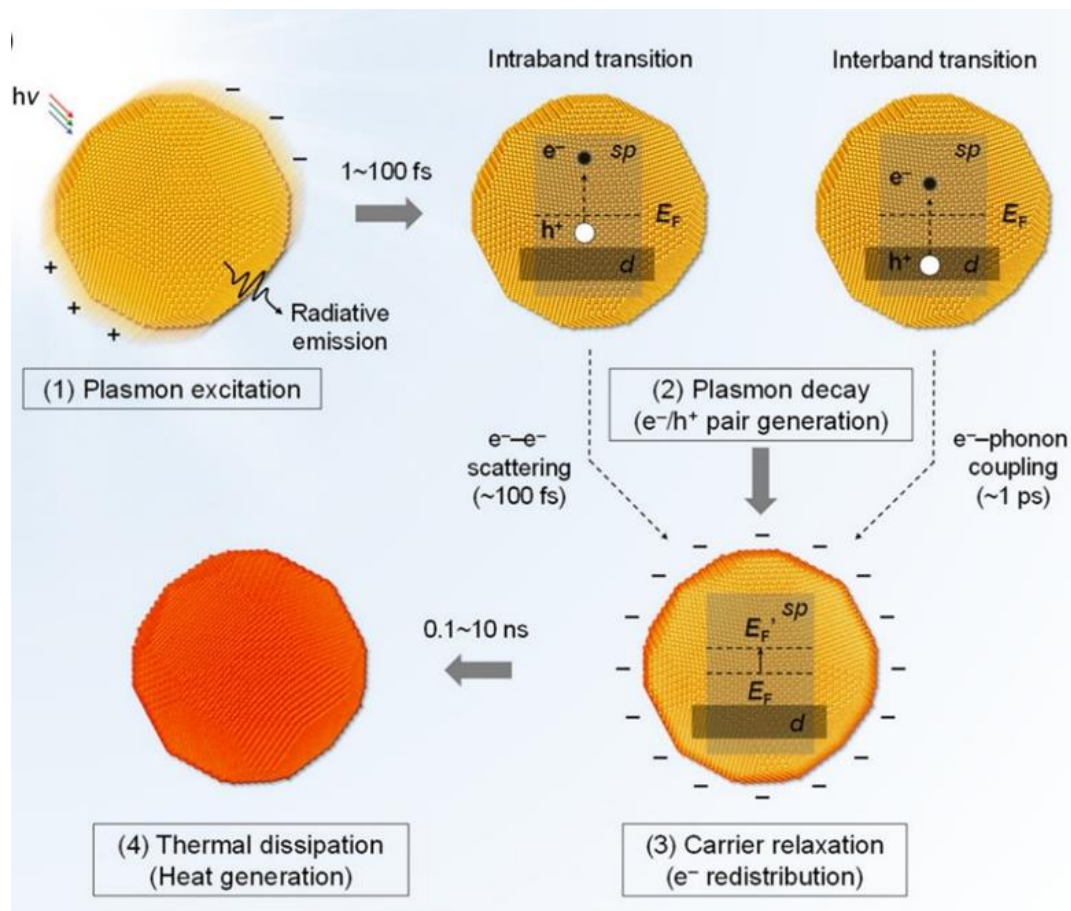


Figure 3.1. Plasmon decay process and generation of hot carriers in photoexcited plasmonic metal NPs. 1) Plasmon excitation of metal NPs. 2) The decay of plasmon, followed by the generation of hot electrons and hot holes through interband and intraband electronic transition. 3) Relaxation of hot carriers via electron-electron scattering. 4) Dissipation of heat to the NP lattice through electron-phonon coupling. Adapted with permission from reference 14. Copyright 2017, American Chemical Society.

Thus the hot electrons and holes generated through the plasmon decay can be used to trigger different oxidative or reductive transformation on the surface of NPs. The area of hot electron driven chemistry was largely triggered by the seminal work from Linic and co-workers who demonstrated that the plasmonic excitation of AgNP under continuous wave (CW) visible light irradiation can trigger the dissociation of the adsorbed O_2 molecule and lead to the oxidation of

industrially relevant molecules like ethylene or propylene, which otherwise happens at higher temperature and pressure (**Figure 3.2**).¹⁵

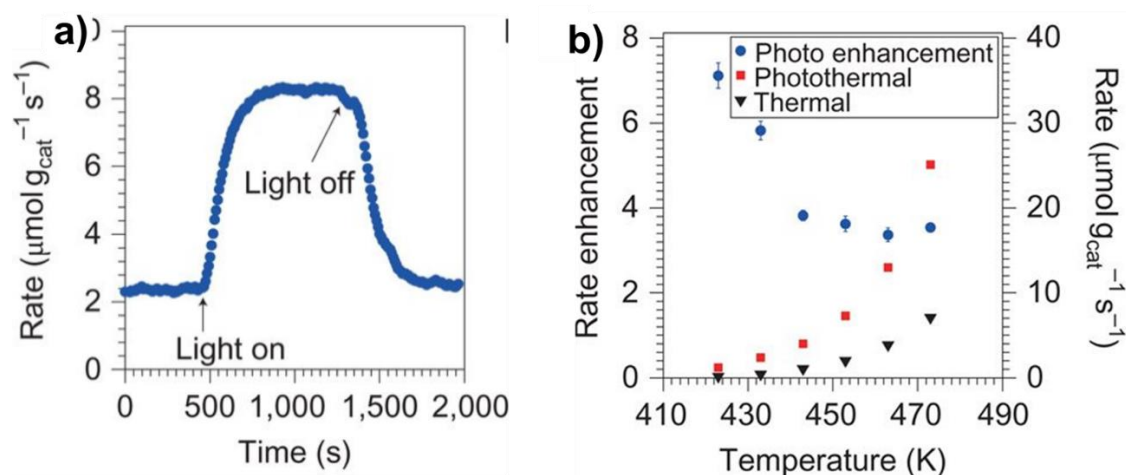


Figure 3.2. Plasmon driven photocatalytic ethylene epoxidation with AgNP as the catalyst. a) Ethylene epoxidation reaction at 450 K under dark and visible light irradiation. b) The enhancement in the photothermal rate (left axis) as a function of temperature. Rate enhancement factor was calculated by dividing the photothermal rate with that of thermal rate. The rate of the reaction (right axis) under photothermal and thermal condition as a function of temperature. Adapted with permission from reference 15. Copyright 2011, Springer Nature.

A negligible rate of bond dissociation or oxidation in absence of light indicated that the plasmon excitation can enhance the rate of a chemical reaction (**Figure 3.2**). Thereafter, a plethora of studies have been performed to utilize the hot carriers in triggering different important chemical transformations like propylene epoxidation,¹⁶ O_2 dissociation,¹⁷ water splitting,¹⁸ H_2 dissociation,¹⁹ NH_3 decomposition,²⁰ CO_2 reduction,^{21,22} nitroaromatic reduction,²³ metal ion reduction,²⁴ and so on. Despite a great advancement in this area, some of the major challenges are centered on poor efficiency and selectivity in the product formation.⁸ The efficiency of a photocatalytic reaction largely relies on an efficient transfer of hot carriers (within their very short lifetime of 10-100 fs) from the NPs to the reactant molecules. During this process of charge transfer, the electrons and holes, oftentimes, have to encounter the ‘insulating’ organic ligands capped on the NPs, which restricts the efficient transfer of hot carriers.^{26,27} This is a long standing challenge in the area of nanoparticle photocatalysis and commonly attributed as “*ligand poisoning*”. Generally, the surface ligand plays a crucial role in stabilizing the NP as well as dictating its physicochemical properties. Judicious choice of ligands and fine tuning of surface chemistry has often rendered numerous exciting applications of NPs in sensing,²⁸ light

harvesting,²⁹ bio-targeting,³⁰ and so on. However, for applications in photocatalysis - where the stability as well as the surface accessibility of NPs is desirable - the role of surface ligands is conflicting. In principle, the surface ligands can 'poison' the photocatalysts by hindering the (i) movement of electrons/holes (due to its insulating nature)²⁶ and (ii) accessibility of the NP surface to the reactant molecules (due to steric effect).^{27,31} The alternative is to deposit NPs onto a substrate or use 'ligand free' NPs (like stabilized with borohydride)^{32,33} for catalysis. However, the available surface area (for deposited NPs) and long term stability of plasmonic property (for 'ligand free' NPs) are compromised during the course of catalysis.³³ Thus, metal NPs and surface ligands are two inseparable entities, and strategies have to be developed to accomplish photocatalysis by retaining and taking advantage of the stabilizing ligands on the NP surface. The present Chapter deals with this challenge by creating precise NP- reactant interaction through judicious choice of surface ligands. We envisage that a precise NP-reactant interaction (through precise surface chemistry) would help us in two ways. i) improve the rate of hot electron transfer by facilitating the adsorption of the reactant molecules on the surface of NPs and ii) induce selectivity through direct charge transfer mechanism, which depends on the hybridization of adsorbate state with the metal electronic state through strong metal-adsorbate interaction (**Figure 3.3**).^{8,34} As shown in **Figure 3.3**, the hot electron transfer from the NPs to the reactant molecules can follow two pathways. In the indirect pathway, hot carrier transfer happens after the decay of plasmon through the creation of a hot Fermi-Dirac distribution of electrons and holes close to the fermi level of the metal. Whereas, in direct charge transfer, a strong adsorption of the reactant molecules on the metal surface leads to the generation of ground metal-adsorbate hybridized state. Upon LSPR excitation, there can be a direct transfer of electrons to some of these unoccupied hybridized states. Thus, in direct mechanism, modulation of plasmonic property or fine-tuning of catalyst-reactant interaction can lead to the rate enhancement of targeted electronic excitation and therefore the rate of chemical processes which proceeds through only those electronic excitations. Therefore, we envisage that, a precise NP-reactant interaction can induce selectivity to the reaction via direct charge transfer pathway. Moreover, to the best of our knowledge, the hypothesis of studying the influence of NP catalyst-reactant interactions on photocatalytic activities of metal NPs is scarcely discussed in literature.

Our hypothesis was tested in the model photocatalytic reaction of ferricyanide reduction by plasmonic AuNPs. Photocatalytic one electron reduction of ferricyanide to ferrocyanide is often

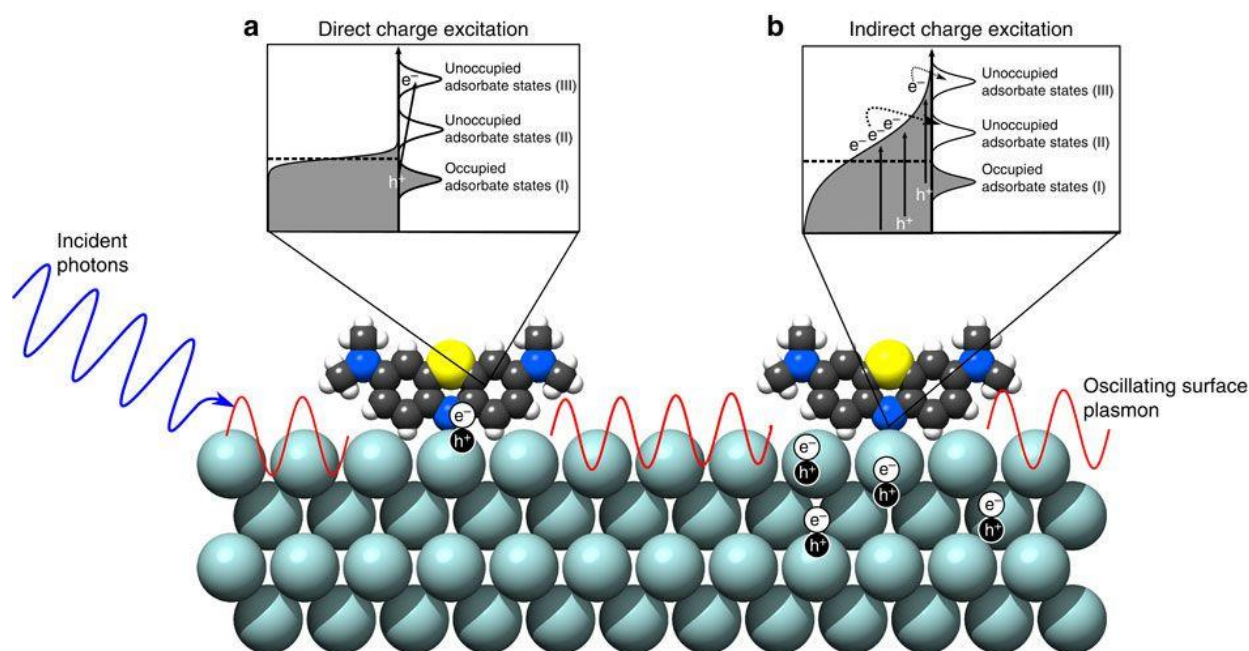


Figure 3.3. Schematic illustration of hot carrier transfer mechanism in plasmonic photocatalysis. a) Direct charge transfer: direct transfer of hot electrons to the unoccupied hybridized metal-adsorbate states. b) Indirect charge transfer: generation of a hot Fermi-Dirac distribution of electrons and holes close to the Fermi level followed by transfer of electrons to the unoccupied state of the adsorbates. Adapted from the reference 34 (open access).

considered as a model reaction to establish different fundamental hypotheses regarding plasmonic photocatalysis. The photostability of ferricyanide as well as its negligible absorption at LSPR of AuNPs (~ 520 nm) makes it an ideal reaction to test the photocatalytic activity of AuNPs. Furthermore, the negative charge on the ferricyanide ions allowed us to tune the electrostatic interaction between the AuNPs and the reactant molecules through precise surface engineering.

A favourable interaction between NP catalyst and ferricyanide was created through precise surface engineering, which resulted in the enhancement of photocatalytic activities (both in terms of hot electron transfer rate constant and conversion yield). Cationic ([+]) and anionic ([−]) organic ligands were functionalized on AuNP surface to generate favourable and unfavourable interactions with [−] ferricyanide, respectively. Our studies show that the favourable interaction, arising from the strong electrostatic attraction, increases the local concentration of [−] ferricyanide around the [+] AuNP catalyst. Consequently, the NP accessibility and probability of hot electron injection from [+] AuNP to [−] ferricyanide was enhanced. On the other hand, the local concentration of the reactant molecules and catalytic activities were lower when standard [−] AuNP was used as the catalyst. For instance, the rate constant increased from $\sim 8 \times 10^{-4} \text{ min}^{-1}$ to $\sim 4 \times 10^{-3} \text{ min}^{-1}$ (~ 5 fold

increment in reaction rate!) when the NP-reactant interaction was made favourable, along with an appreciable increase in the ferricyanide conversion yield (from ~ 10 % for [-] AuNP to ~ 60 % for [+] AuNP). Further, the dependence of catalytic activities on the NP surface potential ascertained the potency of electrostatics in enhancing the photocatalytic activity. The thermodynamic analysis based on Marcus model of outer sphere electron transfer revealed a higher pre-exponential factor (Φ) for [+] AuNP catalyst, a parameter directly related to the local concentration of reactants. Thus, the introduction of favourable interaction between the NP and reactants helped in outplaying the ‘poisoning’ effect of the ‘insulating’ organic ligands, by increasing the NP accessibility to the reactants and the probability of hot electron transfer.

3.3. Experimental Details

3.3.1. Materials and Reagents:

Tetrachloroaurate trihydrate ($\text{HAuCl}_4 \cdot 3\text{H}_2\text{O}$), tetramethylammonium hydroxide (TMAOH) 25 % wt. in water, 11-mercaptoundecanoic acid (MUA), hydrazine monohydrate ($\text{N}_2\text{H}_4 \cdot \text{H}_2\text{O}$ 50-60%), tetrabutylammonium borohydride (TBAB) and potassium ferricyanide were purchased from Sigma-Aldrich. (Di-n-dodecyl) dimethyl ammonium bromide (DDAB) and dodecylamine (DDA) were purchased from Alfa Aesar. All the reagents were used as received without any further purification. The positively charged N,N,N-trimethyl(11-mercaptoundecyl) ammonium ion (TMA) was synthesized according to the reported procedure.³⁵

3.3.2. Synthesis of AuNPs:

All the nanoparticles were synthesized following a modified literature procedure.²⁸ Hydrazine monohydrate ($\text{N}_2\text{H}_4 \cdot \text{H}_2\text{O}$) was used as the reducing agent. In a typical experiment, $\text{HAuCl}_4 \cdot 3\text{H}_2\text{O}$ (6 mg), DDA (70 mg), and DDAB (70 mg) were mixed together in toluene (2 mL) and sonicated for ~10 min for complete stabilization of Gold (III) ions. This was followed by a rapid injection of another toluene solution containing 15 mg of TBAB and 28 mg of DDAB. The resulting solution was left stirring overnight to ensure the complete reduction of Gold (III). The seed particles were then grown to 5.5 ± 0.7 nm DDA-Au NPs. A growth solution was prepared by adding 280 mg of DDAB, 700 mg of DDA, 60 mg of $\text{HAuCl}_4 \cdot 3\text{H}_2\text{O}$ and seed solution in 15 mL toluene. The growth solution was further reduced with a dropwise addition of another toluene solution containing 80 μL of $\text{N}_2\text{H}_4 \cdot \text{H}_2\text{O}$ and 280 mg of DDAB. The solution was stirred overnight for complete growth of the particles yielding monodisperse 5.5 ± 0.7 nm of DDA-Au NPs. The particles were further grown to

~ 11 nm DDA-Au NPs. A growth solution was prepared by adding 4 g of DDAB, 6.5 g of DDA, 595 mg of $\text{HAuCl}_4 \cdot 3\text{H}_2\text{O}$ and seed solution in 100 mL toluene. The growth solution was further reduced with a dropwise addition of another toluene solution containing 650 μL of $\text{N}_2\text{H}_4 \cdot \text{H}_2\text{O}$ and 4.4 g of DDAB. The solution was stirred overnight for complete growth of the particles yielding monodisperse 11 ± 1.3 nm of DDA-AuNPs as confirmed through TEM analysis. The detail procedure for the place exchange of DDA-AuNP with different charged ligands (**Figure 3.4**) is described below.

3.3.3. Place Exchange of AuNPs:

In a typical synthesis of $[+]$ AuNPs, DDA-Au NPs (20 mL) were first precipitated by adding 50 mL of methanol which yielded a black precipitate. The supernatant was carefully removed and the precipitate was then re-dispersed in 20 mL toluene. $[+]$ TMA ligand (equal to the moles of Au(III) in solution) dissolved in 10 mL dichloromethane (DCM) was added. The solution was left overnight to ensure a complete ligand exchange. Next, the supernatant was decanted and the precipitate was washed with DCM (3×50 mL) and acetone (50 mL). The precipitate was then dried and redispersed in miliQ water for further studies. A similar place exchange protocol was adopted for the preparation of $[-]$ AuNPs, where, only MUA ligands were fed during the place exchange reaction. The $[-]$ AuNPs were finally redispersed in miliQ water by adding ~ 20 μL of TMAOH (25 % wt. in water) base to deprotonate the carboxylic acid group. $[+/-]_4$ and $[+/-]_9$ AuNPs were synthesized by adding TMA and MUA ligands in a molar ratio of 1:4 and 1:9, respectively.

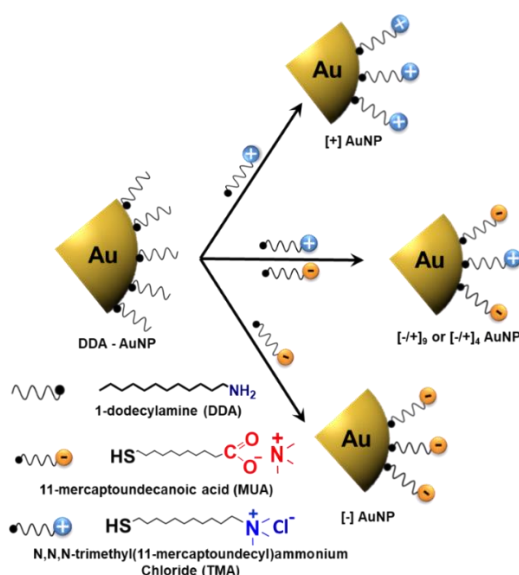


Figure 3.4. Schematic illustration of place exchange of DDA capped AuNPs. DDA capped AuNPs were place exchanged with either [+], [-] or a mixture of [+] and [-] to synthesize positively, negatively or heterogeneously charged AuNPs, respectively.

3.3.4. Microscopy Studies:

Microscopy studies were performed to characterize the AuNPs as well as to understand the interaction between AuNP and reactant (ferricyanide ions). The TEM sample for the individual nanoparticles was prepared by drop casting AuNP solution on a 400 mesh carbon coated copper grid (Tedpella Inc.), and dried under vacuum. The AFM sample for [+] and [-] AuNP with ferricyanide solution was prepared carefully to minimize the drying effect. ~ 20 μL of [+] and [-] AuNP – ferricyanide solution was drop casted on a mica substrate and subsequently the drop was removed with a tissue paper after 10 min (to minimize the drying effect), and allowed the particles to sediment. The sample was then dried at room temperature. The High-Resolution Transmission Electron Microscopic (HRTEM) imaging was performed on FEI Tecnai G2 F20 (200 kV) HR-TEM. The AFM imaging was performed on Key Sight 5500 instrument (Agilent Technology) under tapping mode with silicon nitride tip.

3.3.5. Zeta Potential Studies:

The zeta potential (ζ) of charged AuNPs were measured in Nano ZS90 (Malvern) Zetasizer instrument. The optical density of the nanoparticle solution was maintained ~0.2 during all the measurements. The error bar was calculated from three different experiments. ζ was determined by measuring the electrophoretic mobility and using Henry's equation.

$$U_E = \frac{2\varepsilon\zeta f(k_a)}{3\eta}$$

U_E : Electrophoretic mobility

ζ : Zeta potential

ε : Dielectric constant

η : Viscosity

$f(K_a)$: Henry's Function

3.3.6. Photocatalytic Reduction:

All the photocatalytic reduction experiments were performed in a 3 mL quartz cuvette under the irradiation with two Blue LEDs (3W each, light intensity measured at the cuvette wall is ~ 65 mW/cm²). All the kinetic measurements were performed using Shimadzu UV-3600 plus spectrophotometer. Temperature of the reaction mixture was maintained with a temperature controller equipped with the spectrophotometer. The difference between the actual temperature at the reaction mixture and set temperature was ~ 2 °C under experimental conditions. In a typical experiment, AuNP (absorbance was set to ~ 1 for all the NP systems), 880 μ L of 5M EtOH and 500 μ M potassium ferricyanide were mixed in a 3 mL quartz cuvette and purged with Ar for 15 min. The cuvette was then sealed with Teflon and kept at a particular temperature for 15 min for temperature equilibration, prior to the irradiation. Photoreduction of ferricyanide was monitored by measuring the absorbance of the solution at a fast scan mode, at 15 min interval for 2 h. Photograph of the entire experimental set-up is shown below (**Figure 3.5**). Light intensity dependent experiments were performed by varying the power of the LED. The intensity of the incident irradiation was measured by using an optical power meter from Newport (Model 842.PE).

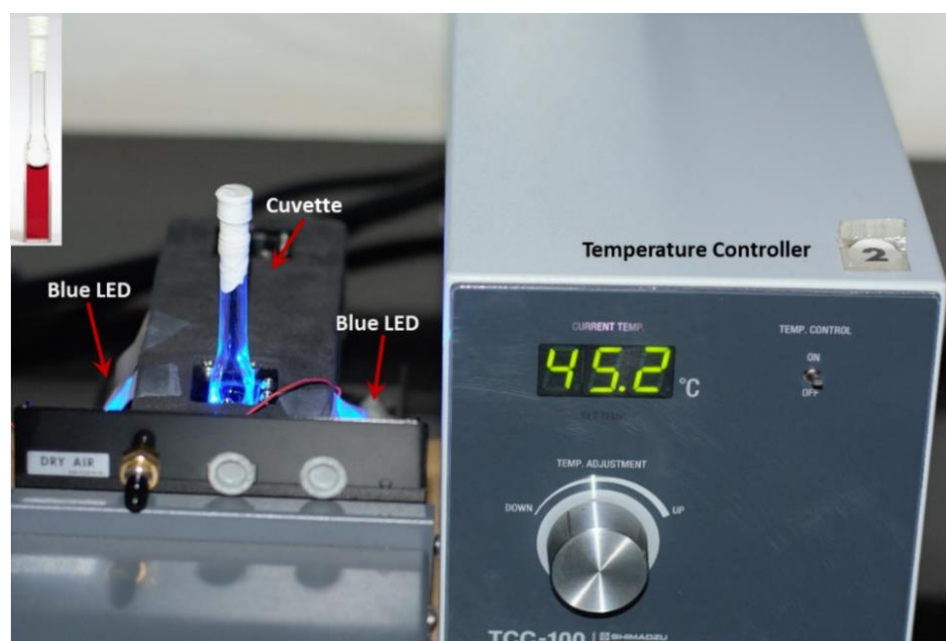


Figure 3.5. Photograph of the experimental set-up used for the photocatalytic reduction of ferricyanide by AuNPs. Inset shows the cuvette with the reaction mixture, at the start of the reaction.

3.3.7. Kinetic Analysis:

Construction of Corrected Spectra:

The corrected spectra have been constructed by following a reported procedure to subtract the effect of AuNP in rate constant calculation.^{36,37}

$$\text{Spectrum}_{\text{corrected}} = \text{spectrum}_{\text{sample}} - (\text{peak absorbance}_{\text{sample}} / \text{peak absorbance}_{\text{AuNP}}) \times \text{spectrum}_{\text{AuNP}}$$

Peak absorbance *sample* is the difference between the absorbance at $\lambda_{\text{max AuNP}}$ and at 800 nm for reaction mixture. Peak absorbance *AuNP* is the difference between the absorbance at $\lambda_{\text{max AuNP}}$ and at 800 nm for only AuNP (without ferricyanide) with the same NP concentration as in the reaction mixture.

Determination of Rate Constant:

The rate constant for the photoreduction reaction was calculated in two different approaches. The photocatalytic reduction of ferricyanide was monitored by following the decrease in the absorbance peak at ~ 420 nm.

Approach #1:

In the first approach, we calculated the photoconversion of ferricyanide (in units of M) from the corrected spectra, as a function of time. The photoconversion was calculated following a recently reported procedure as described below.^{36,37}

$$\text{Conversion (t)} = - (A_{420\text{nm}}(t) - A_{420\text{nm}}(t=0)) / 1050$$

$$\text{Conversion (t)} = (A_{240\text{nm}}(t) - A_{240\text{nm}}(t=0)) / 6250$$

The extinction coefficient of ferricyanide and ferrocyanide are $1050 \text{ M}^{-1} \text{ cm}^{-1}$ and $6250 \text{ M}^{-1} \text{ cm}^{-1}$ respectively.³⁷ The photoconversion vs time spectra was plotted by taking an average of the two aforementioned conversion and then fitted with a first order rate equation of the type

$$c = c_0(1 - e^{-kt})$$

Where C_0 is the initial concentration of ferricyanide and k is the first order rate constant.

The rate at $t = 0$ is given as

$$k' = C_0 \times k$$

$$k = k' / 0.0005$$

[The initial concentration of ferricyanide was $500 \mu\text{M}$]

The conversion vs time plot for [+] AuNP at two different temperatures is shown below (**Figure 3.6 a**).

Approach #2:

The second approach involved the calculation of rate constant from first order rate equation ($-\ln C_t/C_0$ vs time) as reported previously.³⁸ Here the decrease in absorbance at ~ 420 nm was plotted against time to calculate the rate constant (**Figure 3.6 b**). The rate constant values calculated from both the approaches were comparable. We have followed approach #2 to calculate the rate constants in our further studies, since both the approaches were giving similar results (**Figure 3.6 b**).

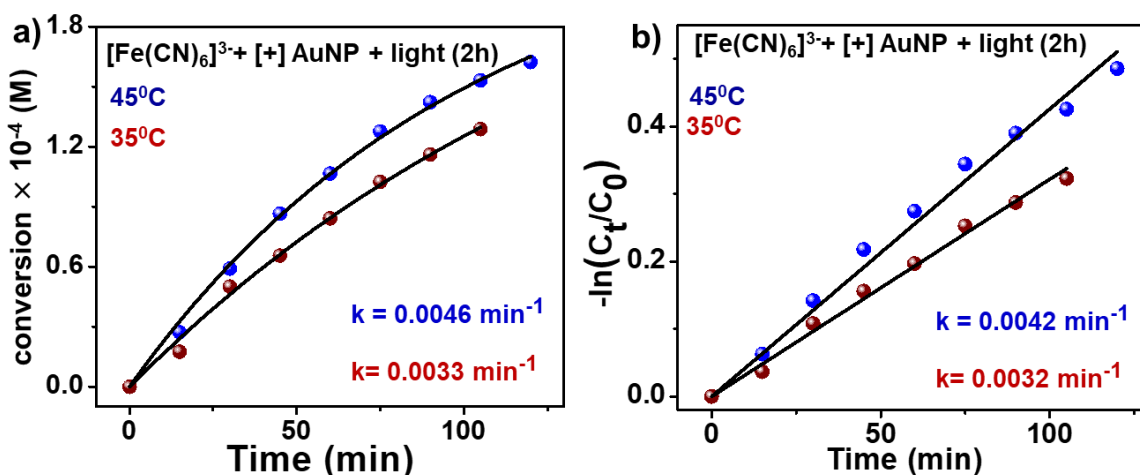


Figure 3.6. Determination of rate constant. a) Plot of photoconversion vs time with [+] AuNP, 880 μL of 5 M EtOH and 500 μM of ferricyanide at two different temperatures. The rate constant value was calculated by fitting the plot with first order exponential equation of the type $C = C_0 \times (1 - e^{-kt})$ (approach #1). b) Linearized fit for the first order analysis by tracking the absorption changes of $[\text{Fe}(\text{CN})_6]^{3-}$ at 420 nm, and calculating the rate constants from the slope (approach #2).

Calculation of Conversion Yield (%):

Conversion yield was calculated by monitoring the percentage of decrease in the ferricyanide absorption at ~ 420 nm (from corrected spectra) after ~ 2 h of irradiation.

3.3.8. Quantum Yield (QY) Calculation:

The quantum yield was calculated by using the following equation:³⁶

$$\text{QY} = \frac{6.023 \times 10^{23} \times \text{total conversion (in moles after 120 min)}}{\text{No. of photons incident per second (photon flux)} \times (1 - 10^{-A}) \times 60 \times 120}$$

Where, A is the absorbance of the nanoparticle solution, which was maintained at ~ 1 for all the experiments.

The photon flux or the number of photons incident per second was calculated using the following equation:

$$\text{Photon flux} = \frac{\text{Excitation energy}}{\text{Energy per photon}}$$

The incident power on the cuvette is 65 mW/cm² and the area of the cuvette is 4 cm². So the excitation energy is

$$\begin{aligned} \text{Excitation Energy} &= \text{Incident Power} \times \text{Area of the Cuvette} \\ &= 65 \text{ mW/cm}^2 \times 4 \text{ cm}^2 = 260 \text{ mW} \end{aligned}$$

Upon substituting the value of excitation energy,

$$\text{Photon flux} = \frac{0.26 \text{ J/s}}{4.4 \times 10^{-19} \text{ J}} = 5.90 \times 10^{17} \text{ photons/s}$$

3.3.9. Theoretical Calculation for the Concentration of Ferricyanide Ion Close to the AuNP Surface:

The concentrations of [Fe(CN)₆]³⁻ and K⁺ in the diffused layer, follows the Boltzmann distribution, and is given by the following equation^{39,40}

$$c_{\pm} = c_0 \exp\left(\mp \frac{ze\phi}{k_b T}\right) \quad (3.1)$$

Here,

c_+ and c_- are the concentrations of K⁺ and [Fe(CN)₆]³⁻ respectively,

c_0 is the concentration of salt K₃[Fe(CN)₆] in the bulk, ~ 0.5 mM,

z is the valency of the ions,

ϕ is the surface potential at a given point,

$k_b T$ is the thermal energy

In order to get the variation in c_+ and c_- , we need the variation in ϕ as a function of distance (in the present case, from the Stern layer, as shown in **Figure 3.7**).

The variation in ϕ as a function of distance (x) in the diffused layer is given by the Poisson Boltzmann equation^{39,40}

$$\nabla^2 \phi = -\frac{\rho}{\epsilon} \quad (3.2)$$

Here,

ρ is the charge density, and

ϵ is the dielectric constant of the medium

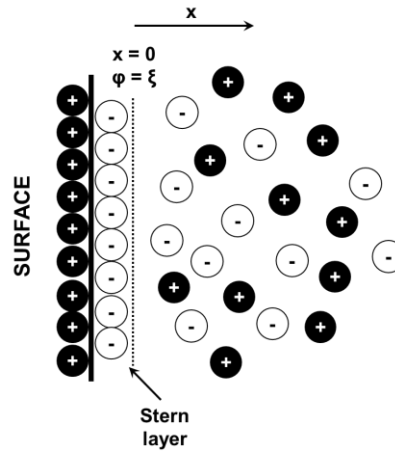


Figure 3.7. Schematic illustration of distribution of ions from a positively charged surface.

Considering a surface infinitely long in y and z direction, the variation of ϕ in x direction can be expressed as^{39,40}

$$\frac{d^2\phi}{dx^2} = -\frac{\rho}{\epsilon} = -\frac{zF(c_+ - c_-)}{\epsilon} \quad (3.3)$$

Here,

F = Faraday Constant

Substituting the value of c_+ and c_- from (3.1) in (3.3)-

$$\begin{aligned} \frac{d^2\phi}{dx^2} &= \frac{c_0 zF}{\epsilon} \left[\exp\left(\frac{ze\phi}{k_b T}\right) - \exp\left(-\frac{ze\phi}{k_b T}\right) \right] \\ &= \frac{2c_0 zF}{\epsilon} \sinh\left(\frac{ze\phi}{k_b T}\right) \end{aligned} \quad (3.4)$$

Applying the necessary boundary condition,^{18,19}

$$\phi(x=0) = \zeta, \text{ and } \phi(x=\infty) = 0$$

Here,

ζ is the zeta potential (~30.0 mV in our case)

We know for dilute solutions (Debye-Huckel approximation), $\frac{ze\phi}{k_b T} \ll 1$, equation (3.4) becomes

$$\begin{aligned} \frac{d^2\phi}{dx^2} &= \frac{c_0 zF}{\epsilon} \left[\left(1 + \frac{ze\phi}{k_b T}\right) - \left(1 - \frac{ze\phi}{k_b T}\right) \right] \\ &= \frac{c_0 zF}{\epsilon} \left[\frac{2ze\phi}{k_b T} \right] \end{aligned}$$

$$= \frac{2(ze)^2 N_a c_0 \varphi}{\epsilon k_b T}$$

$$\frac{d^2 \varphi}{dx^2} = \frac{\varphi}{\kappa^2} \quad (3.5)$$

Here,

$$\kappa = \sqrt{\frac{\epsilon k_b T}{2(ze)^2 N_a c_0}}$$

κ is the Debye length.

N_a is Avogadro's number

e is the charge on an electron

Solving equation (5) for φ , we get³⁹

$$\varphi = \zeta \exp\left(-\frac{x}{\kappa}\right) \quad (3.6)$$

Using (3.1) and (3.6), we can get the concentrations of $[\text{Fe}(\text{CN})_6]^{3-}$ and K^+ as a function of distance. The computed graphs are shown below:

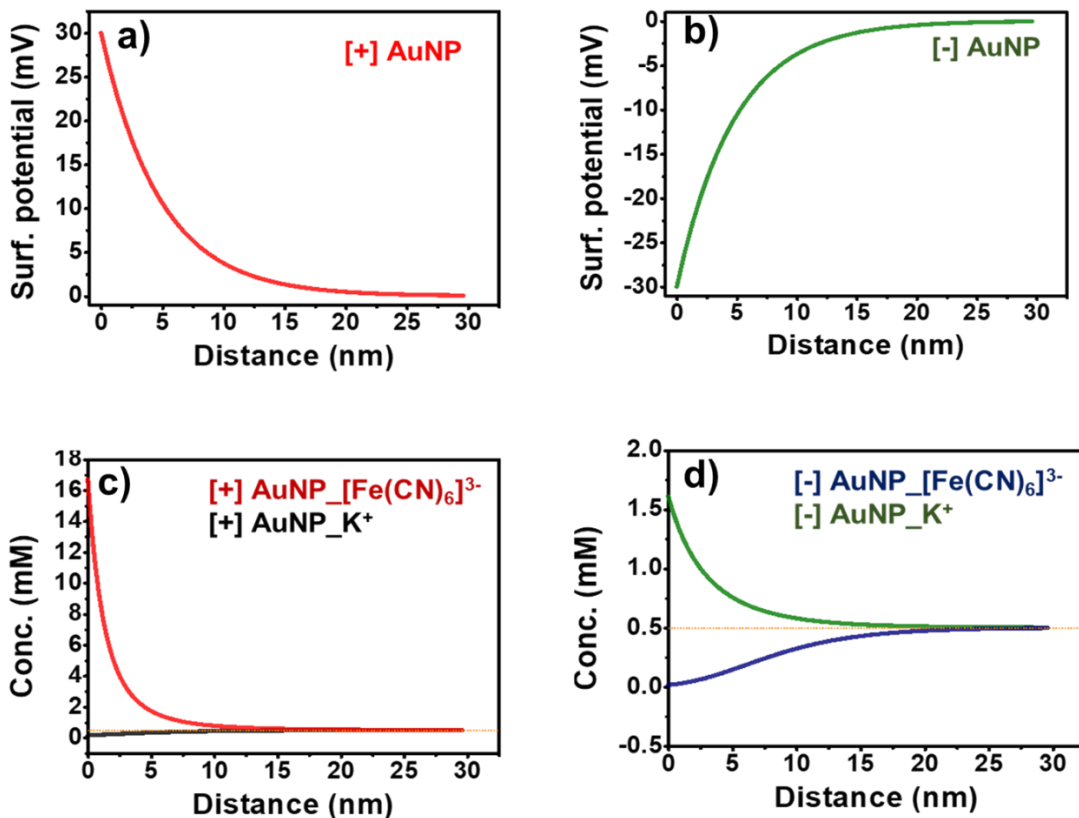


Figure 3.8. Variation in the surface potential as a function of distance from the surface of a) [+] AuNP and b) [-] AuNP. Variation in the concentrations of $[\text{Fe}(\text{CN})_6]^{3-}$ and K^+ as a function of distance from the surface of c) [+] AuNP and d) [-] AuNP.

3.3.10. Calculation of Free Energy of Activation (ΔG^\ddagger), Reorganization Energy (λ) and Electronic Coupling Term ($\Phi|H_{ab}|^2$):

The rate constant of hot electron transfer was estimated by following a Marcus theory for outer sphere electron transfer, which can be written as⁴¹

$$k = \Phi \sqrt{\frac{\pi}{\hbar^2 \lambda k_B T}} |H_{ab}|^2 e^{-\Delta G^\ddagger / k_B T}$$

Taking log on both side

$$\ln k\sqrt{T} = \ln \left(\Phi \sqrt{\frac{\pi}{\hbar^2 \lambda k_B T}} |H_{ab}|^2 \right) - \frac{\Delta G^\ddagger}{k_B T}$$

Plot of $\ln k\sqrt{T}$ vs $1/T$ can be fitted to a linear function with slope $-\frac{\Delta G^\ddagger}{k_B}$ and intercept

$\ln \left(\Phi \sqrt{\frac{\pi}{\hbar^2 \lambda k_B T}} |H_{ab}|^2 \right)$. The free energy of activation can be calculated as $\Delta G^\ddagger = -(\text{slope}/1000 \times R)$ in kJ/mol, where the value of $R = 8.314 \text{ J K}^{-1} \text{ mol}^{-1}$. The reorganization energy (λ) was calculated by solving the following quadratic equation.

$$\Delta G^\ddagger = \frac{(\Delta G^0 + \lambda)^2}{4\lambda}$$

The ΔG^0 value was taken as -77.5 kJ/mol as per previous report for ferricyanide to ferrocyanide reduction.⁴¹ Solving the quadratic equation will provide two roots. The root with $\lambda < \Delta G^0$ (normal Marcus region) was considered as per previous report.⁴¹ The $(\Phi|H_{ab}|^2)$ value was calculated from the intercept of the $\ln k\sqrt{T}$ vs $1/T$ plot as follow

$$\Phi|H_{ab}|^2 = e^{\text{intercept}} \cdot \sqrt{\hbar^2 \lambda k_B / \pi}$$

3.4. Results and Discussion

3.4.1. Design and Characterization of Plasmonic AuNP Catalysts:

The hypothesis of the present work was to investigate the role of interaction between AuNP catalyst and ferricyanide ion on the NP accessibility and efficiency of hot electron transfer. The presence of negative charge on ferricyanide allowed the use of electrostatic forces as a handle to tune the catalyst-reactant interactions. The electrostatic field experienced by [-] ferricyanide ion can be controlled by precise tuning of the surface ligands on AuNPs. Accordingly, N,N,N-

trimethyl (11-mercaptoundecyl)ammonium chloride (TMA, [+]) and 11-mercaptoundecanoic acid (MUA, [-]) ligands were functionalized to render positive and negative surface potential around AuNPs, respectively (**Figure 3.9 a,b**).^{28,30} Further fine tuning in the surface potential was achieved by functionalizing a mixture of [+] and [-] ligands on the AuNP surface through a place exchange reaction (**Figure 3.9 a,b**). Details on the synthesis are provided in the **Experimental Section 3.3.2**.^{22,37} A decrease in the negative zeta potential from -30.0 ± 1.4 mV to -24.0 ± 2.0 mV was observed upon dilution of [-] ligands with $\sim 10\%$ of [+] ligands, which further decreased to -16.0 ± 2.0 mV with $\sim 20\%$ of [+] ligands (**Figure 3.9 a,b**). Spectroscopic (UV-Vis absorption and Dynamic Light Scattering, DLS) and Microscopy (Transmission Electron Microscopy, TEM) studies confirm negligible changes in the stability and average size of AuNPs upon various surface functionalizations (**Figure 3.9 c-e**). Thus, similar sized AuNPs (15.0 ± 0.5 nm from DLS and 11.0 ± 1.3 nm from TEM) with varying surface potentials were successfully prepared, which is crucial for comparing their photocatalytic performances.

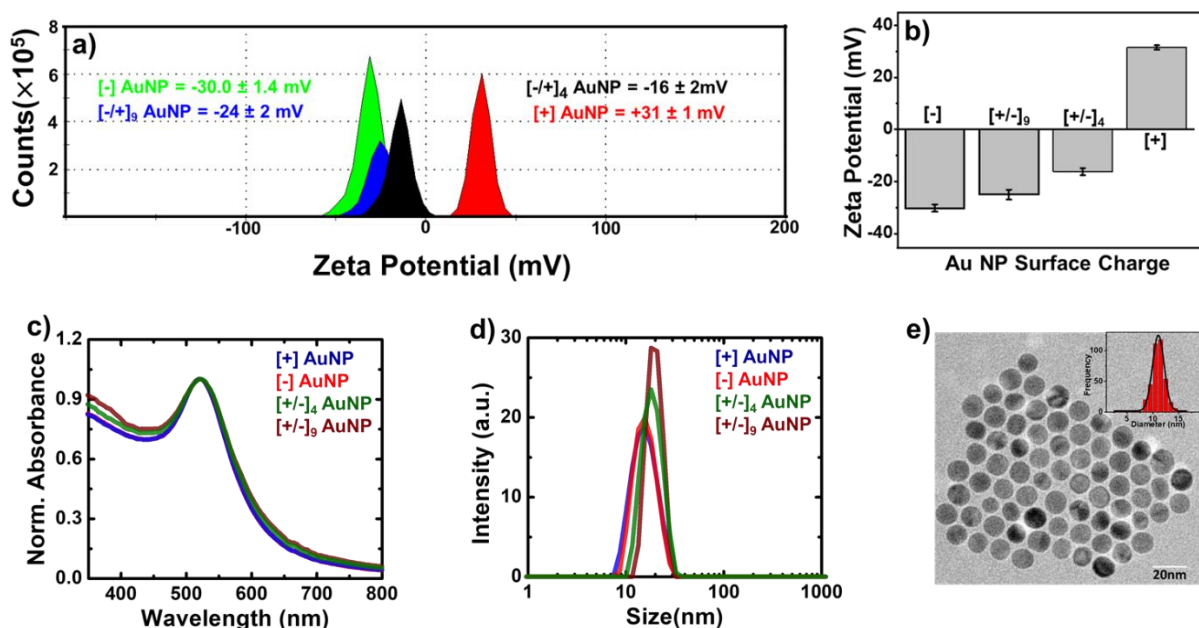


Figure 3.9. Spectroscopic, microscopic and surface characterization of AuNPs. a) Typical zeta potential plots for different sets of AuNPs with varying ligands. b) A bar diagram showing the variation of zeta potential as a function of ligands on the surface of AuNPs. The error bars correspond to standard deviations based on three different sets of experiment. c) UV-Vis absorption and d) DLS data of AuNP catalysts, showing negligible changes in the stability and average size of AuNPs upon various surface functionalization. e) A representative TEM image of [+] AuNPs with their size distribution histogram (from ~ 300 NPs) shown in the inset.

3.4.2. Photocatalytic Reduction of Ferricyanide to Ferrocyanide:

The photocatalytic one electron reduction of ferricyanide to ferrocyanide was selected as the model reaction due to its negligible interference with the AuNP plasmon band and high photostability under visible light.^{36-38,41} The first step in the catalytic reduction is the photoexcitation of AuNPs resulting in the generation of hot charge carriers (hole and electron). This is followed by the transfer of hot electrons to ferricyanide ions causing the reduction, which can be visualized through a decrease in the ferricyanide absorption at ~ 420 nm.³⁶ Finally, the holes generated in AuNP photocatalysts are scavenged by the hole scavenger (ethanol) used in the reaction. The photocatalytic reduction of ferricyanide was performed as per standard protocol in ethanol under inert condition at ~ 45 °C (see **experimental section 3.3.6 for detailed procedure**).³⁶ The absorbance of AuNP catalyst was maintained at ~ 1 (~ 20 nM in term of AuNPs) and two 3W blue light emitting diodes (LEDs) were used as the irradiation source (**Figure 3.5**). The progress of photocatalytic reduction was followed by monitoring the changes in the absorption of ferricyanide at ~ 420 nm. No noticeable decrease in ferricyanide absorption was observed in the absence of AuNPs under continuous irradiation for ~ 2 h, which confirms the photostability of ferricyanide ion (**Figure 3.10 a**). No change in the AuNP absorption under continuous irradiation also confirms the stability of the catalyst under the experimental condition (**Figure 3.10 b**).

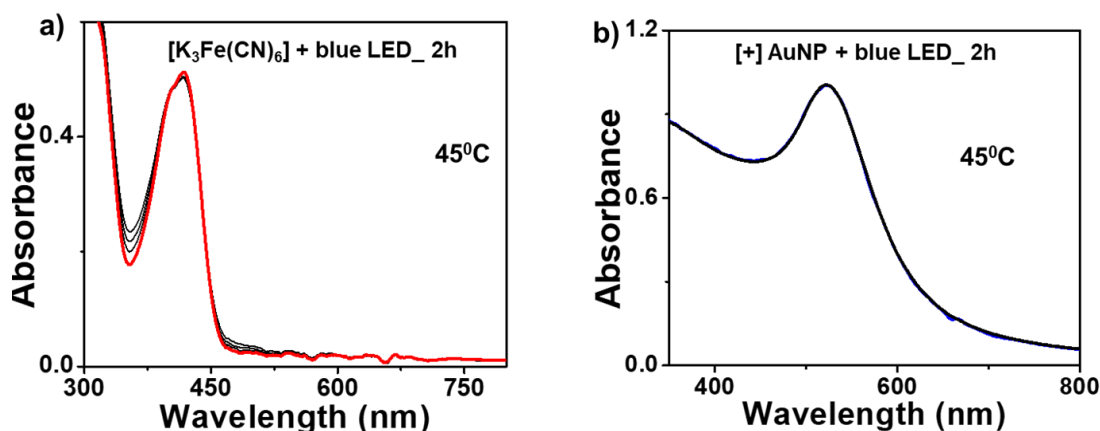


Figure 3.10. Control reactions with [+] AuNP and ferricyanide. Absorbance of a) Ferricyanide and b) [+] AuNP under continuous light irradiation with blue LEDs at 45 °C. Negligible changes in absorbance of both AuNP and ferricyanide confirm their photostability under the experimental condition.

A slight decrease (~ 10 %) in the ferricyanide absorption was observed in the presence of commonly used [-] AuNP catalyst, which is in accordance with the literature reports

(Figure 3.11 a).⁴¹ The marginal reduction of ferricyanide by [-] AuNP can be attributed to the poisoning of the NP catalyst by the insulating MUA ligand by hindering the NP surface accessibility to [-] ferricyanide,⁴¹ and thereby lowering the rate of electron transfer. As mentioned in previous sections, we decided to use catalyst – reactant interaction as a tool to outplay the poisoning effect of ligands. First signs of encouraging results were obtained when the photocatalysis of ferricyanide reduction was performed in the presence of [+] AuNP (Figure 3.11 b).

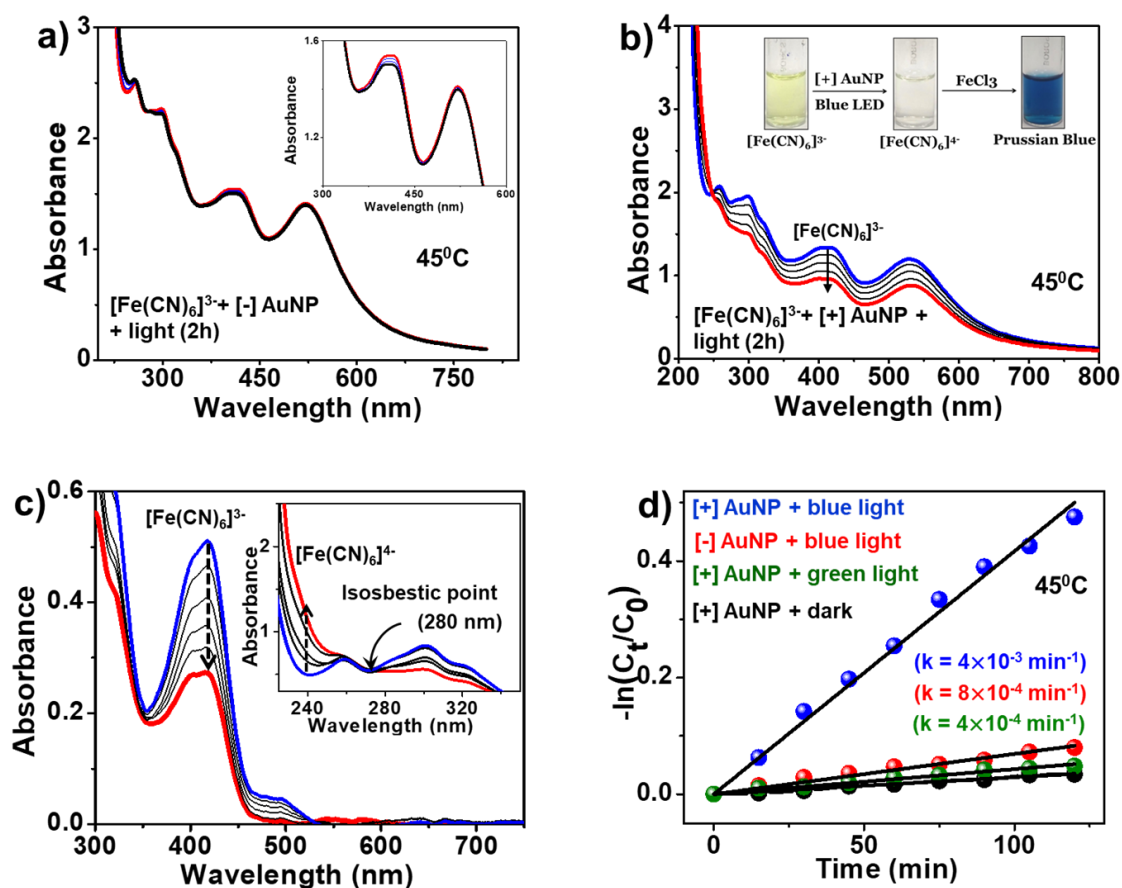


Figure 3.11. Photocatalytic reduction of ferricyanide with [+] and [-] AuNPs. Progress of photocatalytic reduction of ferricyanide in the presence of a) [+] AuNP and b) [-] AuNP at 45 °C by tracking the absorption changes at 15 min interval. Inset of a) shows the absorbance decrease in ferricyanide peak with [-] AuNP catalyst. Inset of b) shows the photographs of vials corresponding to different stages of reduction in the presence of [+] AuNP catalyst. c) Time-dependent spectral changes in the ferricyanide absorption in the presence of ~ 20 nM [+] AuNPs, under irradiation with 3W blue LED at ~ 45 °C. Inset of c) shows the isosbestic point as well as the increase in the ferricyanide absorption with time. d) The linearized first order fits following the spectral changes at 420 nm band for the photocatalytic reduction of ferricyanide by various AuNP systems at ~ 45 °C.

A considerable decrease in the ferricyanide absorption ($\sim 60\%$) was observed in the presence of [+] AuNP catalyst, indicating the reduction of ferricyanide to ferrocyanide. Having obtained a drastic difference in the activities of [-] and [+] AuNPs, systematic time-dependent UV-Vis studies were performed. **Figure 3.11 c** is the corrected spectra (to remove the contribution from AuNP plasmon band³⁶) showing the progress of ferricyanide reduction by [+] AuNP over a period of ~ 2 h. A gradual decrease in the absorption at ~ 420 nm (corresponding to ferricyanide) was observed as a function of time, with a concomitant increase in the peak at ~ 240 nm (corresponding to ferrocyanide) through a clear isosbestic point at ~ 280 nm. The first order kinetic analysis performed on the spectral changes at 420 nm revealed a rate constant of $\sim 4 \times 10^{-3} \text{ min}^{-1}$, which is at least five folds greater than the rate constant obtained with standard [-] AuNP as the photocatalyst ($\sim 8 \times 10^{-4} \text{ min}^{-1}$, **Figure 3.11 d. Experimental section 3.3.7**). Both linearized and exponential fits of first order decay curve gave similar values for rate of electron transfer. The formation of Prussian blue colour upon the addition of FeCl_3 to the reduced solution confirms the formation of the product ferrocyanide (**inset of Figure 3.11 b**). Control experiments performed by incubating ferricyanide with [+] AuNPs under dark resulted in a negligible reduction, which ensures the necessity of light irradiation (**Figure 3.11 d**).

3.4.3. Hot Electron vs Photothermal Heating:

Motivated with our desired result, the next task was to ascertain the role of hot electrons in driving the photocatalytic reduction of ferricyanide. Photochemical transformations on metal nanoparticles can be induced either through the hot electrons or holes (created through non-radiative decay of energetic charge carriers) or through the photothermal heating (due to electron-phonon coupling).^{7,10,42} The elevated temperature on the NP surface can play a crucial role in catalysing the reaction on the NP surface. One of the important aspects in metal nanoparticle driven photocatalysis is to assess the contribution from hot charge carriers and photothermal heating towards the observed photocatalytic rate.

The involvement of hot charge carriers in driving chemical transformation can be understood experimentally by investigating the catalytic rate dependence on illumination intensity.^{7,11,12,15,36} Usually a linear relationship indicates the participation of hot charge carriers in driving the reaction and it implies that, each reaction is induced by a single photon absorption event followed by the interaction between the charge carriers and the reactants.^{7,11,12,15,36} Whereas if the reaction is

induced via photothermal heating then the rate of the reaction should increase exponentially as per the following equation.^{7,15}

$$\Delta T_{\text{plasmon}} = c \times I \quad \dots\dots(3.7)$$

$$\text{Rate} = A \times e^{-E_a/RT} \quad \dots\dots(3.8)$$

$$\text{Rate}(I) = A \times e^{-E_a/R(T+cl)} \quad \dots\dots(3.9)$$

Where $\Delta T_{\text{plasmon}}$ is the temperature increase due to the plasmon damping. As per previous report, the temperature increase due to plasmon damping has a linear relationship with the intensity of irradiation (I).⁴³ Now, when a reaction is catalysed purely through photothermal heating then in principle it should follow the Arrhenius rate law and there should be an exponential increase in the rate of the reaction with increase in the intensity of irradiation.

A detailed intensity dependent analysis was performed to understand the involvement of hot electrons in driving the photocatalytic reduction of ferricyanide. A linear relationship between the observed catalytic rates with illumination intensity (**Figure 3.12**) confirms the participation of hot electrons in driving the photocatalytic reduction of ferricyanide ions under our experimental condition.

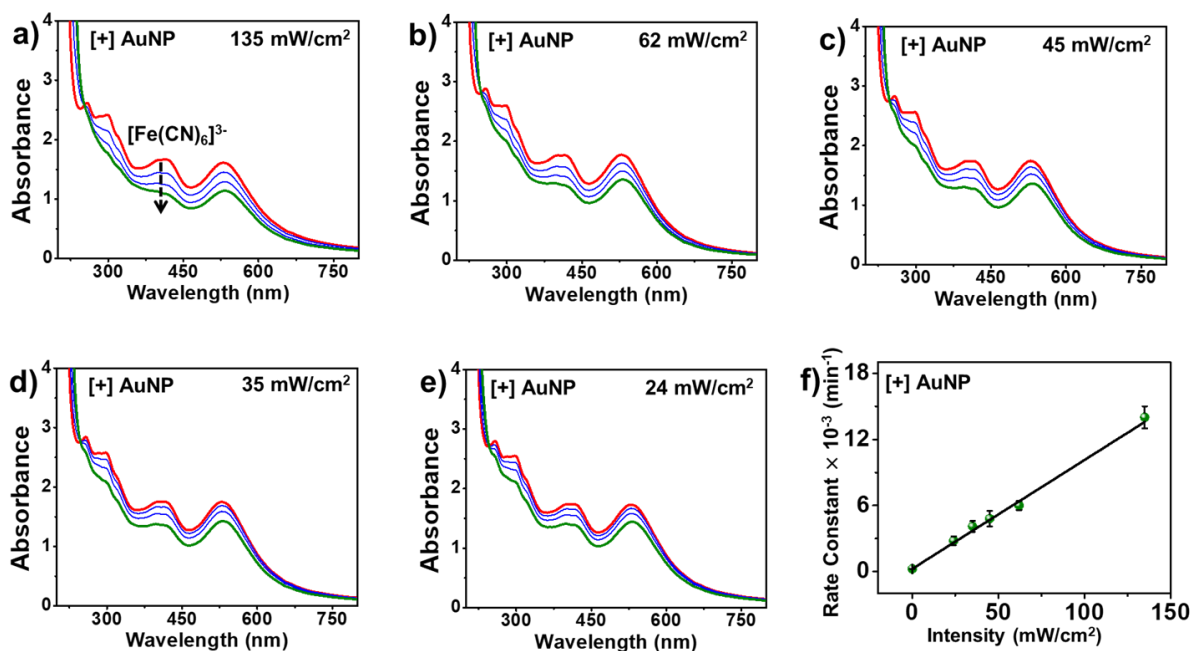


Figure 3.12. Intensity dependent photocatalytic reduction of ferricyanide with [+] AuNP and under irradiation from blue LED. Progress of photocatalytic reduction of ferricyanide by tracking the absorption changes at 15 min interval at an irradiation intensity of a) 135 mW/cm², b) 62

mW/cm², c) 45 mW/cm², d) 35 mW/cm², e) 24 mW/cm², and f) Plot of observed photocatalytic rate constant with [+] AuNP catalyst as a function of illumination intensity.

Next, to further confirm the contribution of the hot electrons we performed a control experiment under dark at an elevated temperature of 50 °C, which was measured to be the bulk temperature during the irradiation process (**Figure 3.13 a**). Considering the higher thermal conductivity of water and our present experimental condition which consists of well dispersed colloidal NP catalyst and a CW light irradiation, the difference between bulk temperature and that on the surface of NP (ΔT) will be negligible and can be expressed as^{22,42}

$$\Delta T = T_s - T_{bulk} = \frac{\sigma I}{4\pi k r}$$

Where, 'r' is the radius of the AuNP which is ~6 nm in the present study, ' σ ' is the absorption cross section at the maxima of LSPR and reported to be 50 nm² for ~12 nm AuNPs,²² 'I' is the intensity of light and 'k' is the thermal conductivity of water (0.6 w m⁻¹ K⁻¹). With all these values, the temperature difference at an intensity as high as 1 kW/cm² would be in the order of 10⁻² K. So under our experimental condition the bulk temperature (50 °C) can be considered as a proxy for the surface temperature of AuNPs.

A negligible reduction under dark condition at 50 °C (**Figure 3.13 a,b**) further confirms the involvement of hot electrons in the reduction process. Finally a wavelength dependent study revealed a lower photocatalytic rate constant at 530 nm irradiation compared to that of 465 nm (**Figure 3.13 c,d**). This can be explained in terms of intraband vs interband transition.^{22,36,37} The higher energy 465 nm excitation generates hot carriers predominantly through interband 'd' – 'sp' transition. Whereas, the 530 nm excitation generates hot carriers through intraband 's' to 's' or 's' to 'p' transition.^{36,37} The 'd' band hole created through interband transition is typically 1.9 eV more energetic than a 'sp' band hole created through intraband transition.⁴⁴ The more oxidizing power of the 'd' band hole is beneficial to complete the oxidation half cycle in a photoredox reaction. Moreover the lifetime of the hot carriers generated through the interband transition is higher compared to that in intraband transition, leading to a higher photocatalytic efficiency. All these above experiments clearly confirms the prodigious contribution of the hot electrons in the photocatalytic reduction of ferricyanide to ferrocyanide. However, the effect of photothermal heating cannot be completely ruled out it requires separate elaborate study to disentangle the relative effect of hot electrons and the photothermal heating.

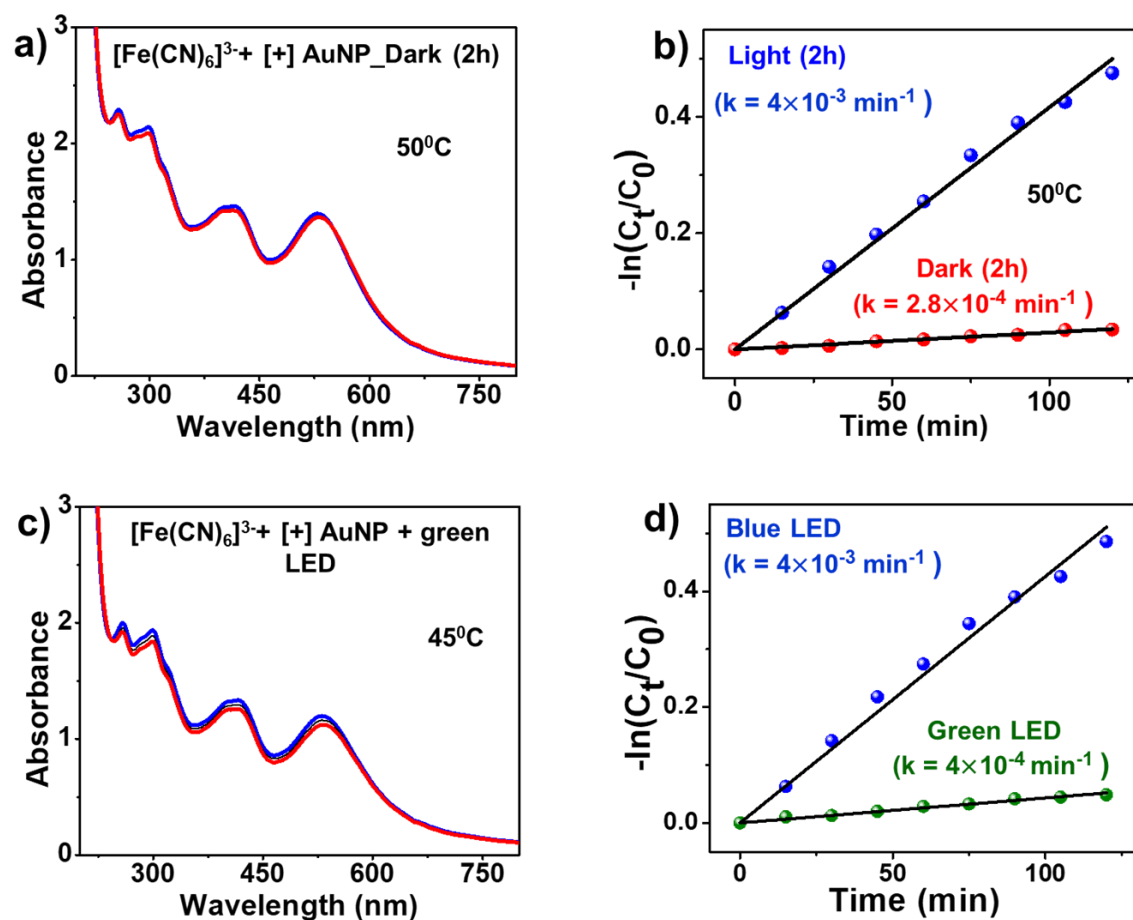


Figure 3.13. a) Progress of photocatalytic reduction of ferricyanide in the presence of [+] AuNP at 50 °C under dark. b) Linearized fit for the first order analysis by tracking the absorbance at 420 nm under light irradiation and dark. c) Progress of photocatalytic reduction of ferricyanide in the presence of [+] AuNP under green light ($\lambda_{\text{irr}} = 530\text{nm}$) irradiation. d) Linearized fit for the first order analysis by tracking the absorbance at 420 nm under blue light ($\lambda_{\text{irr}} = 465\text{nm}$) and green light ($\lambda_{\text{irr}} = 530\text{nm}$) irradiations.

3.4.4. Effect of Hole Scavenger (Ethanol) on Photocatalysis:

Another indirect way to assess the contribution of hot carriers is to investigate the role of hole scavenger in the photocatalytic reaction. In general, the efficiency of a photoredox reaction on the NP surface relies on the higher lifetime or low recombination rate of hot carriers generated through the photoexcitation of the NPs. It is already known in literature that the high $e^- - h^+$ recombination rate often adversely affect the quantum yield of AuNP catalyzed photo-redox reactions.⁴⁴ To address this, a common practice is to use an additional hole scavenger or sacrificial electron donor (typically alcohols and amines) to suppress the $e^- - h^+$ recombination rate, and complete the full redox cycle through the oxidation of hole scavenger.^{36,44} In our present study, we have used 1 M

ethanol as the sacrificial electron donor. Our next idea was to understand the role of hole scavenger in facilitating the reduction of ferricyanide. In the absence of ethanol, water assumes the role of a sacrificial electron donor.³⁶ The oxidation of water is a slow process due to the large potential required for water oxidation ($E_{\text{SHE}} = 1.23 \text{ eV}$)³⁶ and the charge recombination process predominates over the one electron reduction, resulting in a poor reaction quantum yield. For instance, the quantum yield (QY) of ferricyanide reduction by [+] AuNP photocatalysts in water was estimated to be 1.90×10^{-5} (corresponding to $\sim 40 \mu\text{M}$ of conversion, see **Figure 3.14 b and** experimental **Section 3.3.8** for the QY calculation), which is in agreement with the value reported by Jain and Coworkers.³⁶ Ethanol, unlike water, can be readily oxidized to acetaldehyde ($E_{\text{SHE}} = 0.22 \text{ eV}$)⁵ and can serve as an effective hole scavenger. Therefore the addition of ethanol increases the quantum yield (1.10×10^{-4}) as well as the ferricyanide conversion by a factor of ~ 6 ($230 \mu\text{M}$ of conversion), as shown in **Figure 3.14 a,c**. The complete redox cycle in the presence of ethanol can therefore be summarized into the following two half reactions.³⁶

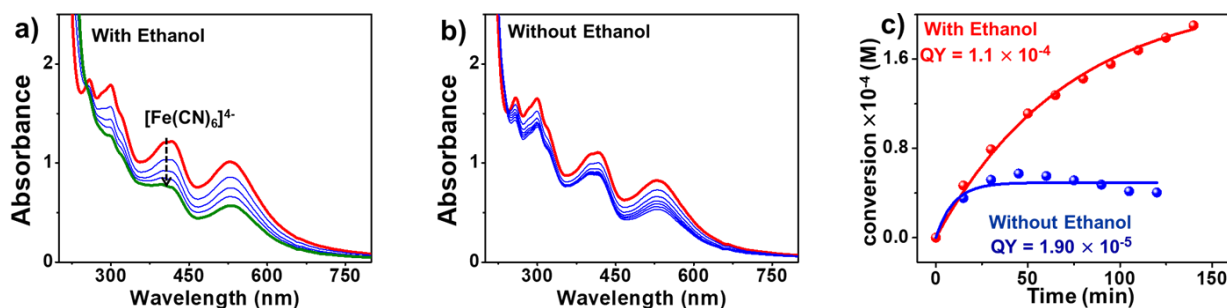


Figure 3.14. Progress of photocatalytic reduction of ferricyanide with [+] AuNP a) in presence of hole scavenger ethanol, and b) in absence of hole scavenger ethanol. c) Plot of photoconversion of ferricyanide as a function of time with [+] AuNPs at 45°C in the presence (red points) and absence (blue points) of the hole scavenger ethanol.

3.4.5. Interaction between AuNP Catalyst and Ferricyanide Ions:

After ascertaining the role of hot charge carriers in driving the reduction, our next idea was to understand the interaction between the charged NPs and the ferricyanide ions. The dominance of [+] AuNP over [-] AuNP clearly shows the potency of favourable NP-reactant interaction and

motivated us to investigate the interactions in detail. The surface plasmon band is highly sensitive to the local environment of NPs and thus, monitoring the variation in the plasmon band position/intensity is an effective strategy to study the interaction of AuNPs with ferricyanide ions.²⁸ The addition of ferricyanide resulted in a spontaneous bathochromic shift (~ 8 nm) in the plasmon band of [+] AuNP, which further shifted to longer wavelengths during the course of photocatalytic reduction (~ 14 nm shift; the λ_{max} shifted from ~ 522 nm to ~ 536 nm by the end of the reaction, **Figure 3.15 a**). The bathochromic shift can be attributed to the strong and favourable interaction between oppositely charged [+] AuNP and [-] ferricyanide, resulting in the screening of positive charges^{28,46} on NPs and triggering the NP aggregation. The interaction and process of NP aggregation was followed by Dynamic Light Scattering (DLS) and Atomic Force Microscopic (AFM) studies (**Figures 3.15 c,e and 3.23 in the Appendix**). The gradual increase in the size of NPs from ~ 15 nm to ~ 380 nm during the course of photocatalytic reduction of ferricyanide confirms the process of aggregation in [+] AuNP. On the other hand, the addition of ferricyanide to [-] AuNP failed to generate noticeable changes in the plasmon band and NP aggregation, confirming the negligible interaction between [-] AuNP and [-] ferricyanide ions (**Figures 3 b,d,f and 3.24 in the Appendix**).

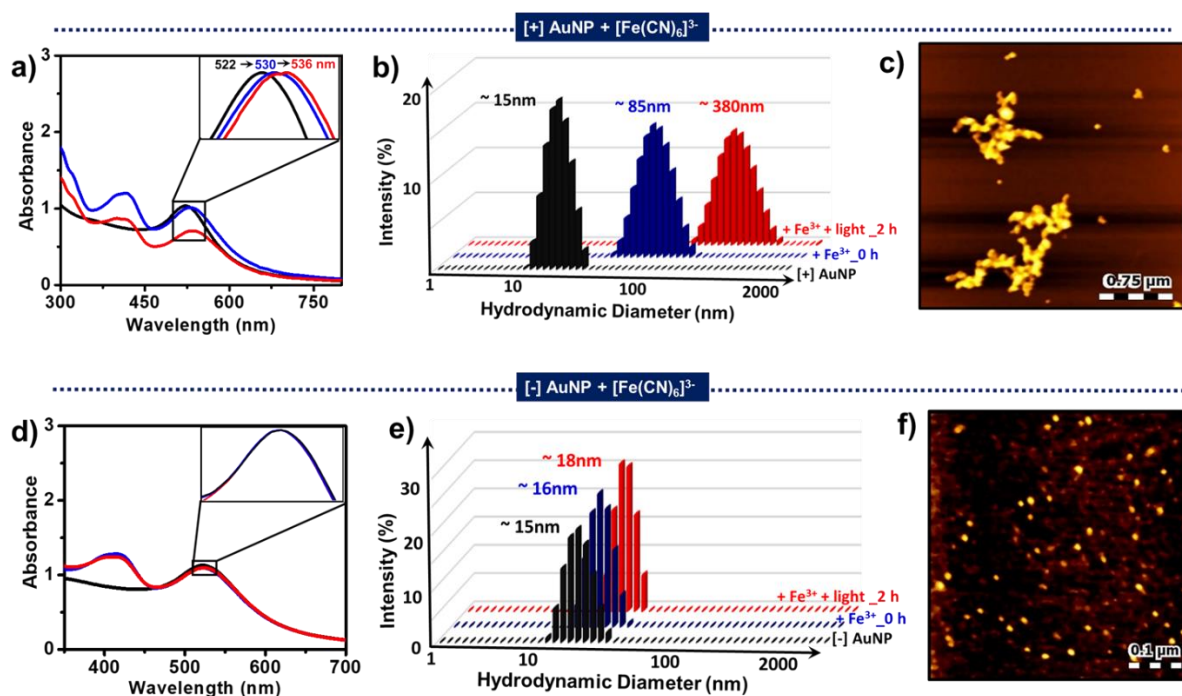


Figure 3.15. Investigation of favourable and unfavourable AuNP catalyst–ferricyanide interactions. Monitoring the surface plasmon band of a) [+] AuNP and b) [-] AuNP during the

progress of photocatalytic reduction of ferricyanide. The corresponding DLS and AFM images are shown in c,d), and e,f), respectively. A bathochromic shift in the surface plasmon band of [+] AuNPs, along with an increase in the size, confirms the aggregation of [+] AuNP during the progress of photocatalysis. However, no noticeable changes were observed for [-] AuNP confirming a weak interaction between [-] AuNP and ferricyanide.

3.4.6. Interaction Driven Photocatalysis:

The presence of charges on AuNP as well as ferricyanide points towards the involvement of electrostatic forces in dictating the NP-reactant interactions, and hence their catalytic performances. To ascertain this, a series of photocatalytic experiments were performed by systematically varying the electrostatic potential around AuNPs through precise ligand functionalization (**Figure 3.16**). The lower activity of [-] AuNP is attributed to the strong electrostatic repulsion between the catalyst and ferricyanide ions. Thus, a lowering of the negative surface potential around [-] AuNPs can, in principle, improve the photocatalytic performances. Accordingly, the [-] MUA ligands on AuNPs was diluted with ~ 10 % and ~ 20 % of [+] TMA ligands to yield heterogeneously charged [-/+]₉ and [-/+]₄ AuNPs, respectively. The on-NP ratio of [+] TMA ligands was estimated from NMR studies, as reported previously, to be ~ 12% and ~ 3 % in [-/+]₉ and [-/+]₄ AuNPs, respectively.^{28,46} Time-dependent UV-Vis studies were performed to investigate the effect of NP surface potential on the photocatalytic reduction of ferricyanide. **Figure 3.16 a,b,c** summarize the linearized fits for the first order kinetic analysis performed on the spectral changes recorded at 420 nm, upon addition of AuNP catalysts of varying surface potentials (all the raw spectra are provided in the Appendix). Both the rate constant and conversion yields increased as the negative surface potential (unfavourable interaction) around AuNPs was lowered. For instance, the rate constant increased from $\sim 8 \times 10^{-4} \text{ min}^{-1}$ (~ 10% conversion) to $\sim 1.5 \times 10^{-3} \text{ min}^{-1}$ (~ 25 % conversion) and further to $\sim 3 \times 10^{-3} \text{ min}^{-1}$ (~ 40% conversion) as [-] AuNP was replaced with [-/+]₉ and [-/+]₄ AuNPs, respectively. The highest photocatalytic performance was achieved when [+] AuNPs was used as the catalyst and the trend was retained at different temperatures as well (**Figure 3.16 d**). A steady increase in the rate constant and conversion yield on moving from [-] to [+] surface potential, at all the four temperatures, shows the power of electrostatic forces in dictating the interaction and efficiency of hot electron transfer between AuNP and ferricyanide. The favourable interaction arising from the strong electrostatic attraction between NP catalyst and ferricyanide ion is hypothesized to increase the local concentration of the reactants around the AuNPs. Thus, the accessibility of the NP surface to the

ferricyanide ions as well as the probability of electron transfer is increased (thereby lowering the “*ligand poisoning*” effect), which is responsible for the enhancement in the photocatalytic performances.

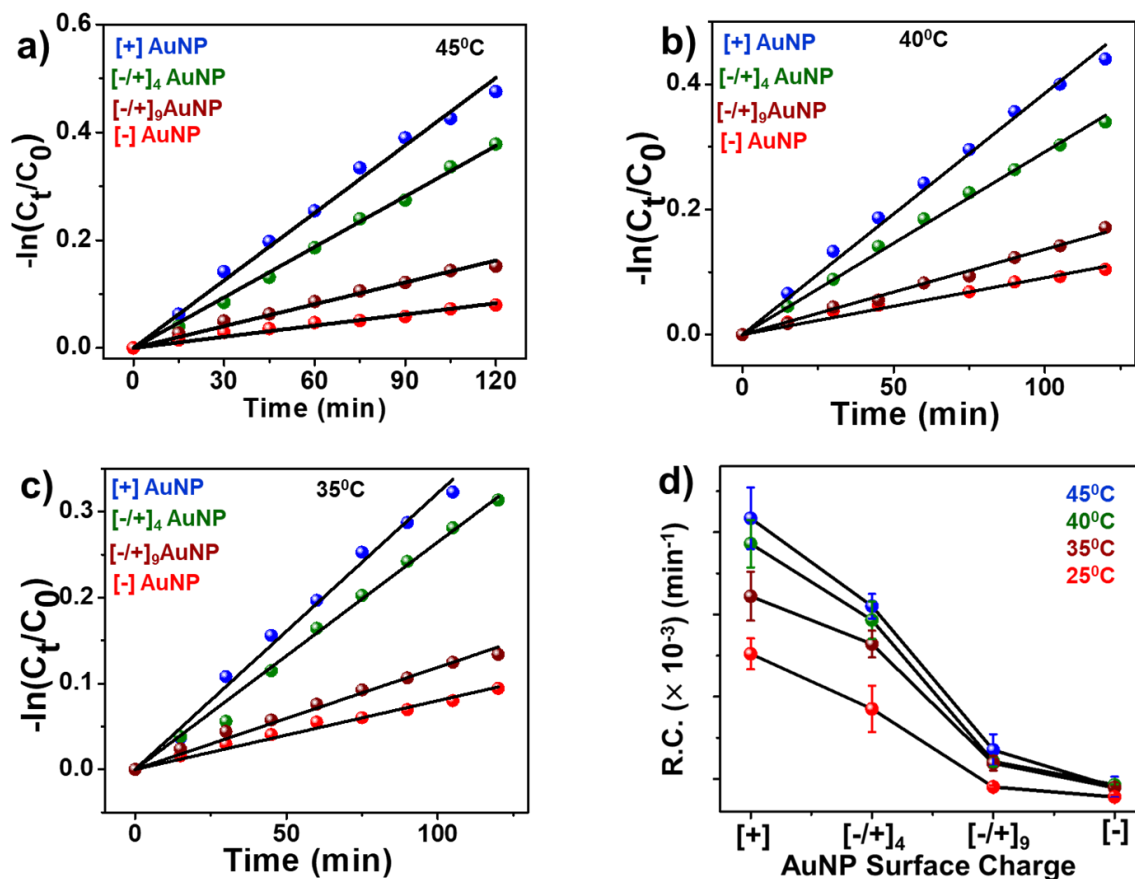


Fig. 3.16. Linearized first order fits following the spectral changes at 420 nm band for the photocatalytic reduction of ferricyanide by AuNP of varying surface potentials, under irradiation with 3W blue LED at a) 45 °C. b) 40 °C. c) 35 °C. All the raw spectra have been provided in the appendix. d) Variation in the hot electron rate constant as a function of NP surface potential and temperature.

3.4.7. Mechanism of Hot Electron Transfer:

The next target was to understand the underlying mechanism of the photocatalytic reduction of ferricyanide by AuNPs. Recent studies by Jain and co-workers have reported that the transfer of hot electrons from [-] AuNP to ferricyanide follows a Marcus model for outer-sphere electron transfer mechanism.⁴¹ The dependence of rate constant on the donor-acceptor distance proved that the hot electrons reach the ferricyanide ions through a multiple incoherent hopping mechanism. Our NP catalytic systems are close to the above reported ones, and similar distance dependent

photocatalytic studies were performed by varying the chain length of [+] ligands. The electron transfer rate constant at $\sim 40\text{ }^{\circ}\text{C}$ increased from $\sim 2.9 \times 10^{-3}\text{ min}^{-1}$ to $\sim 3.7 \times 10^{-3}\text{ min}^{-1}$ as the ligand chain length was reduced from $\sim 19\text{ \AA}$ (C_{11} [+]) to $\sim 14\text{ \AA}$ (C_8 [+], **Figure 3.17**). The variation of rate constant as a function of spacer length (here, C_{11} -TMA and C_8 -TMA) allowed us to model the photocatalytic reduction of ferricyanide by [+] AuNP using the Marcus theory for outer-sphere electron transfer.

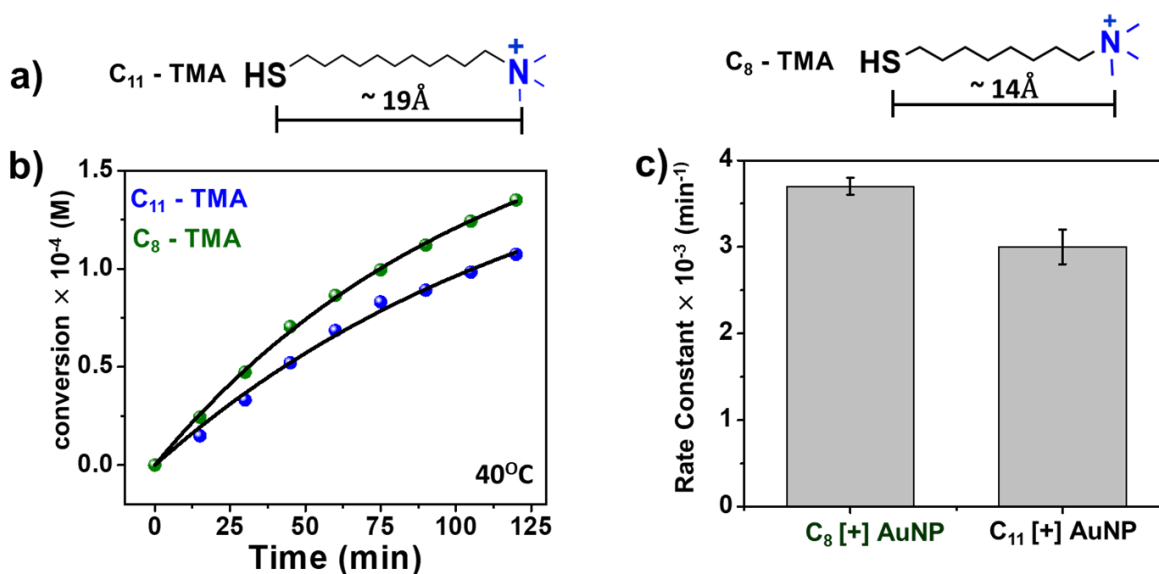


Figure 3.17. Distance dependent variation in rate constant for the catalytic reduction of ferricyanide with [+] AuNP of variable chain lengths of TMA ligands. a) Schemes of TMA ligands with C_8 and C_{11} chain lengths. b) Plots of photoconversion vs time using [+] AuNP catalyst of C_8 and C_{11} chain lengths at $40\text{ }^{\circ}\text{C}$. The rate constants were calculated by fitting the plot with first order exponential equation of the type $C = C_0 \times (1 - e^{-kt})$. c) Comparison of rate constants using [+] AuNP catalysts of C_8 and C_{11} chain lengths

According to the Marcus model, the rate of electron transfer is depicted by the following equation:^{41,47}

$$k = \Phi \sqrt{\frac{\pi}{\hbar^2 \lambda k_B T}} |H_{ab}|^2 e^{-\Delta G^\ddagger / k_B T}$$

Where k_B is the Boltzmann constant, λ is the reorganization energy, ΔG^\ddagger is the free energy of activation, $|H_{ab}|$ is the electronic coupling term between the donor and the acceptor, and Φ is the pre-exponential factor. In the present system, the free energy of activation and $\Phi |H_{ab}|^2$ term are the two key parameters that will dictate the rate of hot electron transfer from AuNP catalyst to

ferricyanide ion. The free energy of activation, as a function of NP surface potential, was calculated from the slope of the plot of $\ln(kT^{1/2})$ vs $1/T$ as shown in **Figure 3.18 a**. (See experimental section 3.3.10 for detailed calculation). The free energy of activation for [+] and [-] AuNP was estimated to be ~ 23 kJ/mol and ~ 20 kJ/mol respectively, which is in close agreement with the reported values for [-] AuNP (**Figure 3.18 a**).⁴¹ Even though there was an appreciable difference in the rate constant values at all the different temperatures, surprisingly, the free energy of activation for all the AuNP catalysts was comparable. This led us to focus on the second important factor, $\Phi|H_{ab}|^2$ term, which was calculated from the intercept of the $\ln(kT^{1/2})$ vs $1/T$ plot. Interestingly, the $\Phi|H_{ab}|^2$ value for [+] AuNP was ~ 30 times higher than that of [-] AuNPs (**Figure 3.18 b,c**). A steady increase in $\Phi|H_{ab}|^2$ value was observed as the NP surface potential was varied from [-] to [+] (**Figure 3.18 b**).

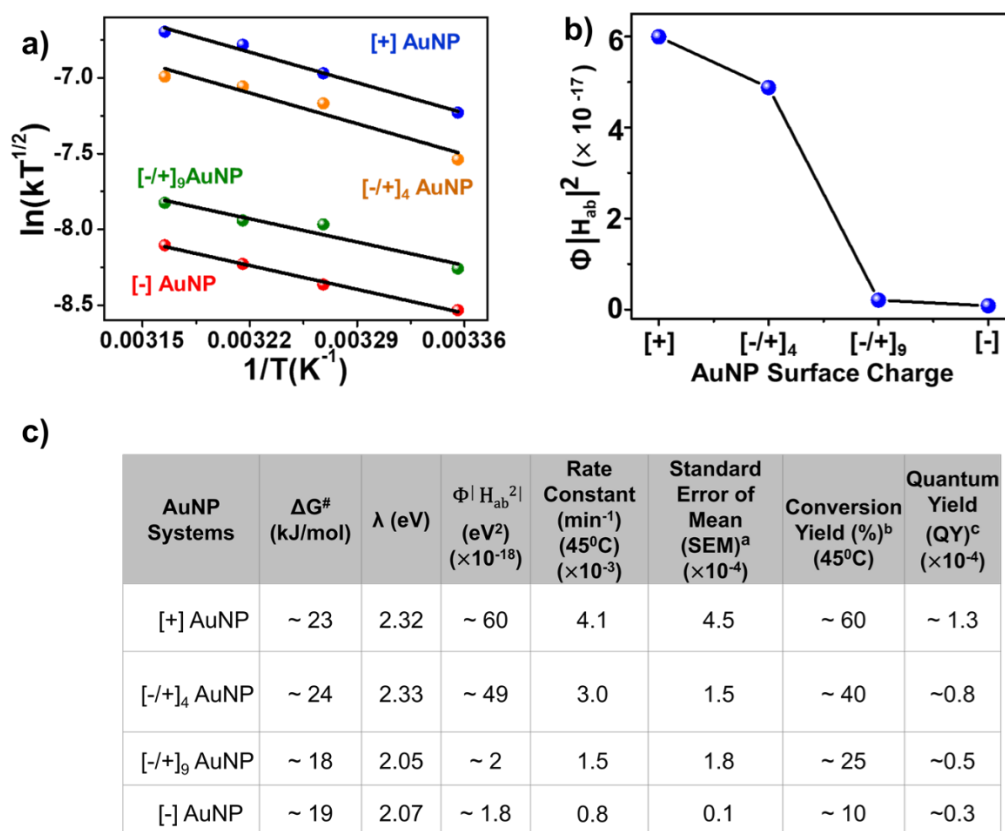


Figure 3.18. a) Variation in the plot of $\ln(kT^{1/2})$ vs $1/T$ as a function of varying surface potential of AuNP catalysts. b) Variation of $\Phi|H_{ab}|^2$ as a function of varying surface potential of AuNP catalysts. c) Table summarizing various thermodynamic parameters for the photocatalytic reduction of ferricyanide by AuNP of varying surface potentials, based on Marcus model of outer-sphere electron transfer. ^aThe standard error of mean (SEM) was calculated from three independent

experiments. ^bThe conversion yield was calculated by monitoring the percentage of decrease in the ferricyanide absorption at 420 nm (from corrected spectra) after ~ 2 h of irradiation. ^cDetails on the quantum yield calculation are given in experimental section.

H_{ab} is the electronic matrix element which dictates the electronic coupling between the donor and acceptor electronic states, and often decreases exponentially with increasing the donor-acceptor distance.⁴¹ In the present study, the $|H_{ab}|^2$ values for [+] and [-] AuNP catalytic systems are comparable as the length of [+] and [-] ligands on AuNPs are similar. Thus, the pre-exponential term (Φ) will be the predominant factor responsible for the observed difference in the $\Phi|H_{ab}|^2$ values for [+] and [-] AuNP systems. It has been reported that the pre-exponential factor is directly dependent on the number of reactant molecules close to the catalyst surface.⁴¹ So, a higher concentration of ferricyanide ions around [+] AuNP surface will increase the pre-exponential factor, thereby justifying the corresponding increase in the $\Phi|H_{ab}|^2$ value. Thus, the detailed analysis with Marcus model indicates that a higher local concentration of ferricyanide ion close to the [+] AuNP surface (through electrostatic attraction) can be the limiting factor to dictate the rate of hot electron transfer as well as the photocatalytic activity of the AuNP systems.

3.4.8. Experimental and Theoretical Estimation of Ferricyanide Ions Close to NP Surface:

The Detailed thermodynamic analysis using Marcus model for outer-sphere electron transfer revealed that the local concentration of ferricyanide close to the NP surface can be the limiting factor. Our next task was to estimate or compare the concentration of ferricyanide ion close to both [+] and [-] AuNPs for further validation of this hypothesis. The direct measurement of concentration of counter-ions and co-ions surrounding charged nanoparticles, to the best of our knowledge, is highly nontrivial.⁴⁸ Researchers, therefore, heavily rely on theoretical models that have been developed to understand electrostatic interactions in charged nanoparticle systems.⁴⁸ The mean field Poisson- Boltzmann theory is one of such models which has been extensively used in the literature to understand how the presence of dissolved ions influence the electrostatic potential surrounding the charged nanoparticles.⁴⁸ A similar model has been used in the present study (for detailed calculations, see **Section 3.3.9 in experimental section**) to calculate the concentration of the ferricyanide ions surrounding [+] and [-] charged AuNPs. **Figures 3.19 and 3.7** show the variation in the concentration of ferricyanide ions as a function of distance from the

surface of [+] and [-] AuNPs. A higher concentration of ferricyanide ion was estimated close to [+] AuNP as compared to [-] AuNP, which then exponentially decays to its bulk concentration moving away from the NP surface. For instance, the concentration of ferricyanide was estimated to be ~ 5 mM and ~ 0.05 mM at a distance of ~ 2 nm from the surface of [+] and [-] AuNPs, respectively. A close proximity of the ferricyanide ion on [+] AuNP helps in improving the NP accessibility and probability of electron transfer, thereby suppressing the ligand poisoning effect.

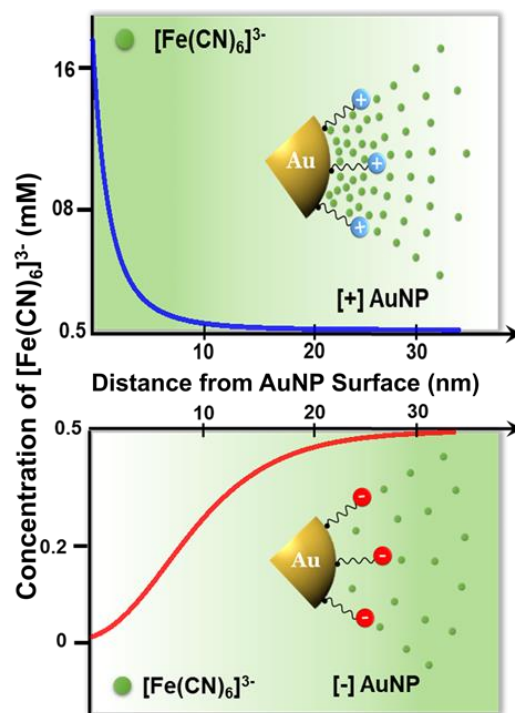


Figure 3.19. Variation in the concentration of ferricyanide, estimated theoretically, as a function of distance from the surface of [+] and [-] AuNPs.

Although a direct estimation of the ferricyanide ions at the surface of [+] and the [-] AuNP systems is nontrivial, we have used three independent experimental techniques (UV-Vis absorption, ICP-MS and cyclic voltammetry) for an indirect estimation. These techniques were used to estimate the amount of ferricyanide adsorbed to the charged AuNPs to prove the role of electrostatics in dictating the distribution of ferricyanide ions.

UV-Vis absorption and ICP-MS method:

In a typical experiment, equal concentrations (~ 20 nM) of [+] and [-] AuNPs were mixed with ~ 500 μ M of ferricyanide in 1M ethanol/water mixture and kept under dark for ~ 2 h for equilibration. In order to separate the adsorbed ferricyanide on AuNP from un-adsorbed ferricyanide, the

solution was centrifuged at 12,000 rpm for 10 min using a 100 kDa molecular weight cut off (MWCO) filter. The AuNP did not pass through the filter, and the filtrate was analyzed with UV-Vis absorption to find out the concentration of un-adsorbed ferricyanide. From this, the adsorbed ferricyanide concentration was then calculated using the following equation, with the help of Beer-Lambert's law.

$$[\text{Ferricyanide}]_{\text{adsorbed}} = [\text{Ferricyanide}]_{\text{initial}} - [\text{Ferricyanide}]_{\text{filtrate}}$$

Here,

$[\text{Ferricyanide}]_{\text{initial}}$ = concentration of ferricyanide estimated from its absorbance value at 420 nm and Beer-Lambert's law (Molar extinction coefficient of Ferricyanide at 420 nm = $1050 \text{ M}^{-1} \text{ cm}^{-1}$). The concentration of adsorbed ferricyanide ions on [+] and [-] AuNPs was estimated to be $\sim 45 \mu\text{M}$ and $\sim 10 \mu\text{M}$, respectively (**Table 3.1**). This higher amount (~ 4.5 times) of ferricyanide on the surface of [+] AuNP is attributed to the favorable electrostatic attraction between [+] AuNP and ferricyanide.

In order to directly estimate the concentration of ferricyanide adsorbed on the surface of charged AuNPs, we digested the residue in the filter (AuNPs with adsorbed ferricyanide ions) with aqua regia, and estimated the concentrations of Au and Fe using Inductively Coupled Plasma-Mass Spectrometry (**Table 3.1**). Similar to the UV-Vis absorption studies, ~ 4 times higher concentration of ferricyanide was estimated for [+] AuNP when compared to [-] AuNP. We would like to emphasize here that the step of centrifuging the solution will disturb the equilibrium distribution of ferricyanide ions around the charged AuNP, and can lead to the physical adsorption as well. Nevertheless, a significantly higher amount of ferricyanide (4 - 4.5 times higher) is observed around [+] AuNP, emphasizing the role of electrostatics in dictating the local concentration of negatively charged ferricyanide around the NP catalyst.

Experiments	Ferricyanide Concentration on [+] AuNP	Ferricyanide Concentration on [-] AuNP	$\frac{[\text{Fe}^{3+}]_{\text{[+] AuNP}}}{[\text{Fe}^{3+}]_{\text{[-] AuNP}}}$
UV-Vis	$\sim 45 \text{ mM}$	$\sim 10 \text{ mM}$	~ 4.5
ICP-MS (Fe/Au)	$\sim 0.13 \text{ ppm}$	$\sim 0.03 \text{ ppm}$	~ 4.3

Table 3.1. Table summarizing the estimation of ferricyanide concentration around the surface of [+] and [-] AuNPs using two independent experiments.

Cyclic Voltammetry method:

The redox behavior of ferricyanide can be used as a tool to estimate its concentration on the surface of [+] and [-] AuNPs using electrochemistry. Accordingly, Cyclic Voltammetry (CV) experiments were performed to study the redox behavior of ferricyanide/ferrocyanide couple in the presence of [+] and [-] AuNPs, adsorbed on the glassy carbon electrode (GCE). Specifically, we estimated the concentrations of ferricyanide adsorbed to the charged AuNPs from the peak current densities in the cyclic voltammogram.

In a typical experiment, equal concentrations of [+] and [-] AuNPs (~ 20 nM) were drop casted on the active area of the GC electrode and then dried overnight under vacuum. Prior to drop casting, the GC electrode was first polished with alumina polishing powder and then cleaned electrochemically. The cyclic voltammetry experiments of 5 mM ferricyanide in 100 mM KCl (supporting electrolyte) were then performed with AuNP coated GC electrode as the working electrode, Pt mesh as the counter electrode and Ag/AgCl(s)/(satd. KCl) as the reference electrode. The electrochemically active surface area was measured by the scan rate dependent cyclic voltammetry of AuNP coated GC electrode in 100 mM KCl. The double layer capacitance (Cdl) was extracted from the plot of capacitance current as a function of scan rate. The obtained Cdl was divided by the theoretically expected value of capacitance for a flat electrode to get the electrochemically active surface area.⁴⁹ A Nernstian behavior with a peak to peak separation (ΔE_p) of ~ 70 mV (which is close to the theoretical value of 59 mV for the one electron transfer⁴⁹) is observed for [+] AuNP. Whereas a clear blocking effect with increased peak to peak separation (~ 343 mV) and suppressed peak currents were observed for [-] AuNP (**Figure 3.20**). This is due to a strong electrostatic repulsion between the [-] AuNP and negatively charged ferricyanide ions in the solution.

We estimated the concentration of ferricyanide by integrating the area under the reduction peak. Detailed calculations are shown below:

$$Q_{red.} = \frac{\text{Integrated area under reduction peak (mA.V)}}{\text{Scan rate (Vs}^{-1}\text{)}}$$

Where, $Q_{red.}$ = Total charge related to the reduction peak current.

The number of moles of ferricyanide was then estimated using the following equation:

$$\text{No. of moles of ferricyanide} = \frac{Q_{red.}}{nF}$$

Where, n = no. of electrons involved in the reduction

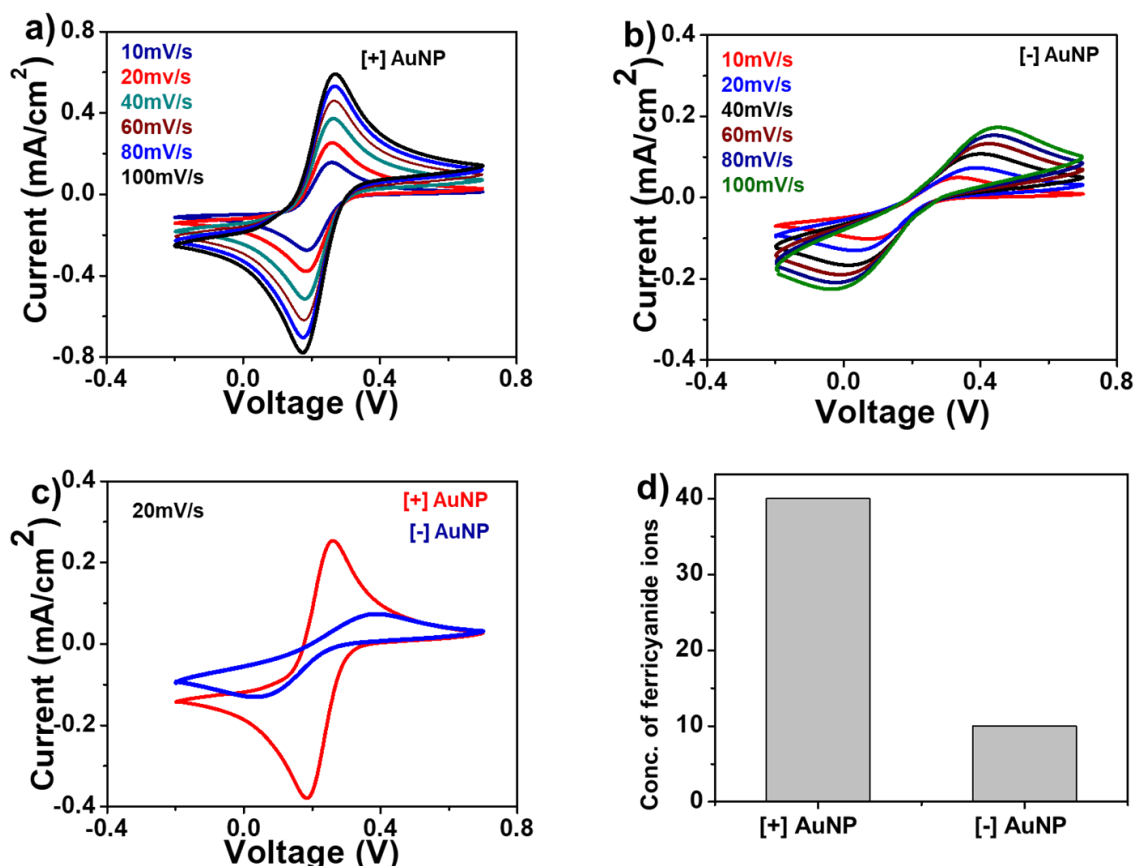


Figure 3.20. Cyclic voltammograms of 5 mM ferricyanide (0.1M KCl as supporting electrolyte) with a) [+] AuNP and b) [-] AuNP coated GC electrodes at different scan rates. Currents are normalized to the geometric surface area. c) Comparative Cyclic voltammograms with [+] AuNP and [-] AuNP coated GC electrodes at a scan rate of 20 mV/s. The current is normalized with respect to the electrochemically active surface area of the electrodes. d) Bar diagram showing the difference in concentration of ferricyanide for [+] and [-] AuNP coated GC electrodes.

F = Faraday constant, 96485 C mol^{-1}

Using the above calculations, the number of moles of ferricyanide was estimated to be $\sim 40 \text{ nmol}$ and $\sim 10 \text{ nmol}$ for the GC electrode coated with [+] and [-] AuNPs, respectively. This observation of ~ 4 times higher concentration of ferricyanide on the surface of [+] AuNP corroborates the presence of favorable electrostatic interactions between AuNP and ferricyanide. Thus, both the theoretical as well as the experimental data clearly confirms the higher concentration of ferricyanide ions close to the [+] AuNP surface compared to that of [-] AuNP, and this in turn is dictated by a precise electrostatic interaction between the charged AuNP and the ferricyanide ions.

3.5. Recyclability aspect

The recyclability aspect of the [+] AuNPs was tested for the photocatalytic reduction of ferricyanide ions. In a typical experiment, after the completion of first cycle of ferricyanide reduction, a fresh ferricyanide solution (500 μM) was added to the [+] AuNP aggregates and further irradiated with visible light to carry out the 2nd cycle of reduction. As shown In **Figure 3.21**, only $\sim 25\%$ catalytic activity of [+] AuNP was retained in the 2nd cycle (conversion yields of [+] AuNP in 1st and 2nd cycles were estimated to be $\sim 58\%$ and $\sim 15\%$, respectively). The lower catalytic activity of the AuNP aggregates can be attributed to the reorganization of the ligand shell (thus affecting the electrostatics), destabilization of the NP system and the reduction in the active surface area available for catalysis: commonly observed factors in homogeneous catalysis with AuNPs.³³ Thus, the process of aggregation can be considered as a poisoning as it reduces the catalytic performance.

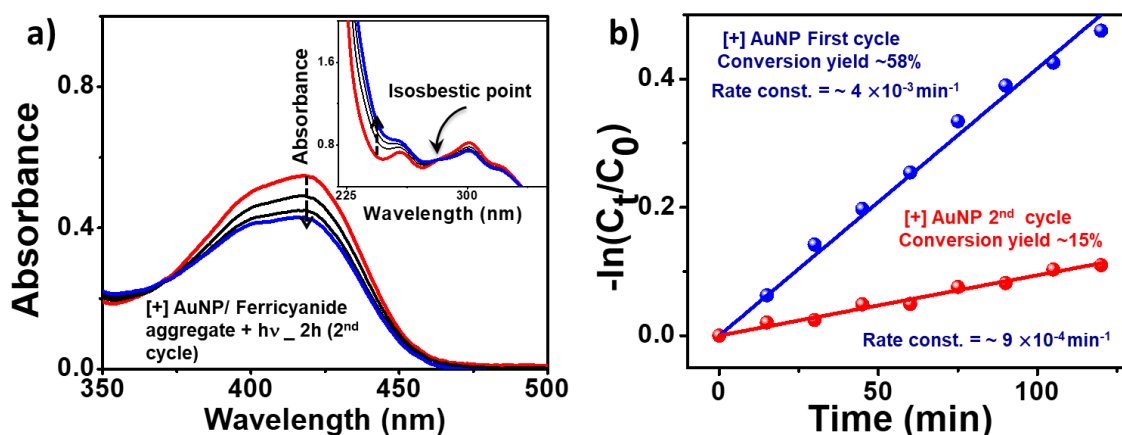


Figure 3.21. a) Time-dependent spectral changes in the ferricyanide absorption in the presence of aggregated [+] AuNPs, under irradiation with 3W blue LED at $\sim 45^{\circ}\text{C}$ (All the spectra were corrected to remove the NP absorption). The aggregated [+] AuNPs obtained after the 1st cycle of photoreduction was used as the catalyst. The inset shows the increase in the ferrocyanide absorption along with an isosbestic point at ~ 280 nm. b) The linearized first order fits following the spectral changes at 420 nm band for the 1st (blue points) and 2nd (red points) cycles of ferricyanide reduction by [+] AuNPs.

Having said that, the present catalyst design has the flexibility of reducing the extent of NP aggregation by fine tuning the electrostatic interactions. For instance, significantly lower aggregation was observed for $[+/-]_4$ AuNP (λ_{max} shift = ~ 5 nm) in the presence of ferricyanide as

compared to $[+]$ AuNP (λ_{\max} shift = ~ 14 nm). As a result, $\sim 60\%$ of the catalytic activity was retained by $[+/-]_4$ AuNP in the 2nd cycle of reduction (conversion yields of $[+/-]_4$ AuNP in 1st and 2nd cycles were estimated to be $\sim 40\%$ and $\sim 25\%$, respectively. **Figure 3.22**). Thus, the present catalyst design has the flexibility to achieve either high catalytic efficiency or high catalytic recyclability, as per the demand.

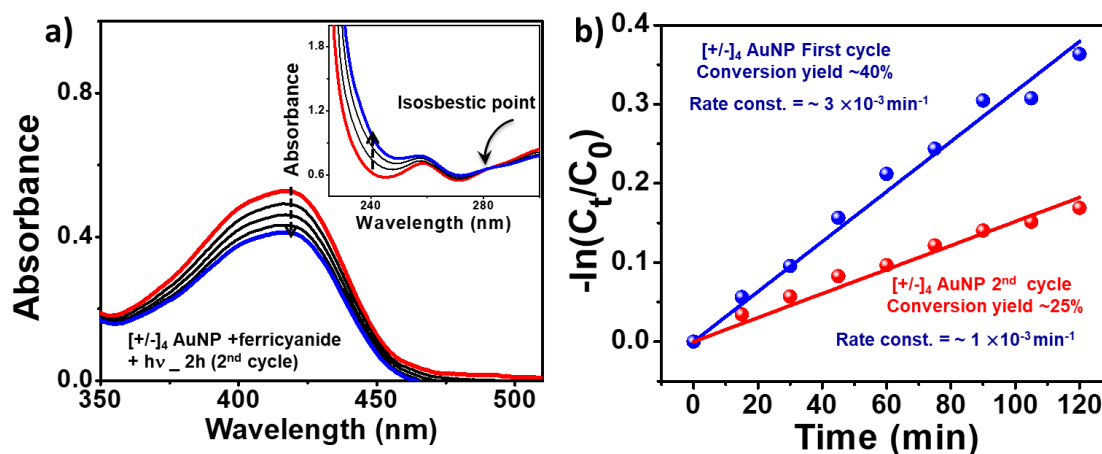


Figure 3.22. a) Time-dependent spectral changes during the 2nd cycle of ferricyanide reduction by $[+/-]_4$ AuNPs (All the spectra were corrected to remove the NP absorption). The inset shows the increase in the ferrocyanide absorption along with an isosbestic point at ~ 280 nm. b) The linearized first order fits following the spectral changes at 420 nm band for the 1st (blue points) and 2nd (red points) cycles of ferricyanide reduction by $[+/-]_4$ AuNPs.

3.6. Conclusion

In conclusion, the potency of favourable interaction between NP catalyst and reactant molecules in suppressing the ligand poisoning effect is demonstrated in the model photocatalytic reaction of ferricyanide reduction. The dependence of catalytic activities on the AuNP surface potential revealed the role of electrostatics in enhancing the photocatalytic performances. The favourable interaction arising from electrostatic forces was tuned by varying the surface potential around AuNP catalysts through precise ligand functionalization. The strong electrostatic attraction between $[+]$ AuNP and $[-]$ ferricyanide resulted in an increase in the local concentration of ferricyanide around the NP surface. A close proximity of ferricyanide ions on $[+]$ AuNPs improves the accessibility of NP to substrates, and the probability of hot electron transfer. The catalytic performance of $[+]$ AuNP catalyst was four-five folds better than the commonly used $[-]$ AuNP

catalyst. The thermodynamic analysis based on Marcus model of outer-sphere electron transfer proved that the dominance of [+] AuNP is due to the higher pre-exponential factor (Φ), which is directly related to the local concentration of reactants. Thus, the introduction of favourable interactions through precise surface functionalization helped in achieving an efficient photocatalysis with plasmonic AuNP capped with insulating ligands.

Such strategies of tuning the catalytic activities through favourable – unfavourable interactions can be conveniently adapted to a broader class of reactions, especially in case of multielectron conversions, where a strong NP-reactant interaction is crucial for the transfer of multiple charge carriers within a very short lifetime. The next Chapter focuses on this particular aspect and investigates the role of NP-reactant interaction in more challenging photocatalytic multielectron reactions.

3.7. References

1. Tao, F.; Schneider, W. F.; Kamat, P. V. *Heterogeneous Catalysis at Nanoscale for Energy Application*; John Wiley & Sons, Inc.: Hoboken, NJ, 2015.
2. Kamat, P. V. Meeting the Clean Energy Demand: Nanostructure Architectures for Solar Energy. *J. Phys. Chem. C* **2007**, *111*, 2834–2860.
3. Kim, D.; Sakimoto, K. K.; Hong, D.; Yang, P. Artificial Photosynthesis for Sustainable Fuel and Chemical Production. *Angew. Chem., Int. Ed.* **2015**, *54*, 3259–3266.
4. Shaw, M. H.; Twilton, J.; MacMillan, D. W. C. Photoredox Catalysis in Organic Chemistry. *J. Org. Chem.* **2016**, *81*, 6898–6926.
5. Wang, L.; Zhang, Y.; Chen, L.; Xu, H.; Xiong, Y. 2D Polymers as Emerging Materials for Photocatalytic Overall Water Splitting. *Adv. Mater.* **2018**, *30*, 1801955.
6. Prieto, G.; Tüysüz, H.; Duyckaerts, N.; Knossalla, J.; Wang, G. H.; Schüth, F. Hollow Nano- and Microstructures as Catalysts. *Chem. Rev.* **2016**, *116*, 14056–14119.
7. Kale, M. J.; Avanesian, T. & Christopher, P. Direct Photocatalysis by Plasmonic Nanostructures. *ACS Catal.* **2014**, *4*, 116–128.
8. Aslam, U.; Rao, V. G.; Chavez, S.; Linic, S. Catalytic Conversion of Solar to Chemical Energy on Plasmonic Metal Nanostructures. *Nat. Catal.* **2018**, *1*, 656–665.
9. Zhang, Y.; He, S.; Guo, W.; Hu, Y.; Huang, J.; Mulcahy, J. R. & Wei, W. D. Surface-plasmon-driven hot electron photochemistry. *Chem. Rev.* **2018**, *118*, 2927–2954.

10. Brongersma, M. L.; Halas, N. J.; Nordlander, P. Plasmon-induced Hot Carrier Science and Technology. *Nat. Nanotechnol.* **2015**, *10*, 25-34.
11. Linic, S.; Aslam, U.; Boerigter, C. & Morabito, M. Photochemical transformations on plasmonic metal nanoparticles. *Nat. Mater.* **2015**, *14*, 567-576.
12. Kale, M. J.; Avanesian, T. & Christopher, P. Direct photocatalysis by plasmonic nanostructures. *ACS Catal.* **2014**, *4*, 116-128.
13. Evanoff, D. D.; Chumanov, G. Size-controlled synthesis of nanoparticles. 2. Measurement of extinction, scattering, and absorption cross sections. *J. Phys. Chem. B* **2004**, *108*, 13957–13962.
14. Yu, S.; Wilson, A. J.; Kumari, G.; Zhang, X.; Jain, P. K. Opportunities and Challenges of Solar-Energy-Driven Carbon Dioxide to Fuel Conversion with Plasmonic Catalysts. *ACS Energy Lett.* **2017**, *2*, 2058–2070.
15. Christopher, P.; Xin, H.; Linic, S. Visible-Light-Enhanced Catalytic Oxidation Reactions on Plasmonic Silver Nanostructures. *Nat. Chem.* **2011**, *3*, 467–472.
16. Marimuthu, A.; Zhang, J.; Linic, S. Tuning Selectivity in Propylene Epoxidation by Plasmon Mediated Photo-Switching of Cu Oxidation State. *Science* **2015**, *339*, 1590-1593.
17. Christopher, P.; Xin, H.; Marimuthu, A.; Linic, S. Singular Characteristics and Unique Chemical Bond Activation Mechanisms of Photocatalytic Reactions on Plasmonic Nanostructures. *Nat. Mater.* **2012**, *11*, 1044-1050.
18. Mubeen, S.; Lee, J.; Singh, N.; Kramer, S.; Stucky, G. D.; Moskovits, M. An Autonomous Photosynthetic Device in which All Charge Carriers Derive from Surface Plasmons. *Nat. Nanotechnol.* **2013**, *8*, 247-251.
19. Mukherjee, S.; Libisch, F.; Large, N.; Neumann, O.; Brown, L. V.; Cheng, J.; Lassiter, J. B.; Carter, E. A.; Nordlander, P.; Halas, N. J. Hot Electrons Do the Impossible: Plasmon-Induced Dissociation of H₂ on Au. *Nano Lett.* **2013**, *13*, 240-247.
20. Zhou, L.; Swearer, D. F.; Zhang, C.; Robotjazi, H.; Zhao, H.; Henderson, L.; Dong, L.; Christopher, P.; Carter, E. A.; Nordlander, P.; Halas, N. J. Quantifying Hot Carrier and Thermal Contributions in Plasmonic Photocatalysis. *Science* **2018**, *362*, 69-72.
21. Robotjazi, H.; Zhao, H.; Swearer, D. F.; Hogan, N. J.; Zhou, L.; Alabastri, A.; McClain, M. J.; Nordlander, P.; Halas, N. J. Plasmon-Induced Selective Carbon Dioxide Conversion

- on Earth-Abundant Aluminum-Cuprous Oxide Antenna-Reactor Nanoparticles. *Nat. Commun.* **2017**, *8*, 1-10.
22. Yu, S.; Wilson, A. J.; Heo, J.; Jain, P. K. Plasmonic Control of Multi-Electron Transfer and C–C Coupling in Visible-Light-Driven CO₂ Reduction on Au Nanoparticles. *Nano Lett.* **2018**, *18*, 2189–2194.
23. Zhu, H.; Ke, X.; Yang, X.; Sarina, S. & Liu, H. Reduction of Nitroaromatic Compounds on Supported Gold Nanoparticles by Visible and Ultraviolet Light. *Angew. Chem. Int. Ed.* **2010**, *49*, 9657-9661.
24. Zhai, Y.; DuChene, J. S.; Wang, Y. C.; Qiu, J.; Johnston-Peck, A. C.; You, B.; Guo, W.; DiCiaccio, B.; Qian, K.; Zhao, E. W.; et al. Polyvinylpyrrolidone-Induced Anisotropic Growth of Gold Nanoprisms in Plasmon-Driven Synthesis. *Nat. Mater.* **2016**, *15*, 889–895.
25. Hu, C.; Chen, X.; Jin, J.; Han, Y.; Chen, S.; Ju, H.; Cai, J.; Qiu, Y.; Gao, C.; Wang, C.; et al. Surface Plasmon Enabling Nitrogen Fixation in Pure Water through a Dissociative Mechanism under Mild Conditions. *J. Am. Chem. Soc.* **2019**, *141*, 7807.
26. Dolzhenkov, D. S.; Zhang, H.; Jang, J.; Son, J. S.; Panthani, M. G.; Shibata, T.; Chattopadhyay, S.; Talapin, D. V. Composition-Matched Molecular “Solders” for Semiconductors. *Science* **2015**, *347*, 425-428.
27. Smith, J. G.; Jain, P. K. The Ligand Shell as an Energy Barrier in Surface Reactions on Transition Metal Nanoparticles. *J. Am. Chem. Soc.* **2016**, *138*, 6765-6773.
28. Rao, A.; Roy, S.; Unnikrishnan, M.; Bhosale, S. S.; Devatha, G.; Pillai, P. P. Regulation of Interparticle Forces Reveals Controlled Aggregation in Charged Nanoparticles. *Chem. Mater.* **2016**, *28*, 2348-2355.
29. Devatha, G.; Roy, S.; Rao, A.; Mallick, A.; Basu, S.; Pillai, P. P. Electrostatically Driven Resonance Energy Transfer in “Cationic” Biocompatible Indium Phosphide Quantum Dots. *Chem. Sci.* **2017**, *8*, 3879-3884.
30. Pillai, P. P.; Kowalczyk, B.; Kandere-Grzybowska, K.; Borkowska, M.; Grzybowski B. A. Engineering Gram Selectivity of Mixed-Charge Gold Nanoparticles by Tuning the Balance of Surface Charges. *Angew. Chem. Int. Ed.* **2016**, *55*, 8610-8614.
31. Ansar, S. M.; Kitchens, C. L. Impact of Gold Nanoparticle Stabilizing Ligands on the Colloidal Catalytic Reduction of 4-Nitrophenol. *ACS Catal.* **2016**, *6*, 5553-5560.

32. Lopez-Sanchez, J. A.; Dimitratos, N.; Hammond, C.; Brett, G. L.; Kesavan, L.; White, S.; Miedziak, P.; Tiruvalam, R.; Jenkins, R. L.; Carley, A. F.; Knight, D.; Kiely, C. J.; Hutchings, G. J. Facile Removal of Stabilizer-Ligands from Supported Gold Nanoparticles. *Nat. Chem.* **2011**, *3*, 551-556.
33. Menumerov, E.; Hughes, R. A.; Neretina, S. Catalytic Reduction of 4-Nitrophenol: A Quantitative Assessment of the Role of Dissolved Oxygen in Determining the Induction Time. *Nano Lett.* **2016**, *16*, 7791-7797.
34. Boerigter, C.; Campana, R.; Morabito, M. & Linic, S. Evidence and Implications of Direct Charge Excitation as the Dominant Mechanism in Plasmon-Mediated Photocatalysis. *Nat. Commun.* **2016**, *7*, 10545.
35. Tien, J.; Terfort, A.; Whitesides, G. M. Microfabrication Through Electrostatic Self-Assembly. *Langmuir* 1997, *13*, 5349-5355.
36. Kim, Y.; Smith, J. G.; Jain, P. K. Harvesting Multiple Electron-Hole Pairs Generated Through Plasmonic Excitation of Au Nanoparticles. *Nat. Chem.* **2018**, *10*, 763-769.
37. Kim, Y.; Torres, D. D.; Jain, P. K. Activation Energies of Plasmonic Catalysts. *Nano Lett.* **2016**, *16*, 3399-3407.
38. Yen, C. W.; El-Sayed, M. A. Plasmonic Field Effect on the Hexacyanoferrate (III)-Thiosulfate Electron Transfer Catalytic Reaction on Gold Nanoparticles: Electromagnetic or Thermal? *J. Phys. Chem. C* **2009**, *113*, 19585-19590.
39. Israelachvili, J. N. *Intermolecular and Surface Forces (Third Edition)*. Academic Press, Amsterdam, 2011.
40. Tabeling, P. *Introduction to Microfluidics*. Oxford University Press, Oxford, 2005
41. Kim, Y.; Wilson, A. J.; Jain, P. K. The Nature of Plasmonically Assisted Hot-Electron Transfer in a Donor-Bridge-Acceptor Complex. *ACS Catal.* **2017**, *7*, 4360-4365.
42. Jain, P. K. Taking the Heat Off of Plasmonic Chemistry. *J. Phys. Chem. C* **2019**, *123*, 24347-24351.
43. Govorov, A. O.; Richardson, H. H. Generating heat with Metal nanoparticles. *Nano Today*, **2007**, *2*, 30-38.
44. Yu, S.; Mohan, V.; Jain, P. K. Using Plasmonically Generated Carriers as Redox Equivalents. *MRS Bulletin*, **2020**, *45*, 43-48.

45. Rao, V. G.; Aslam, U.; Linic, S. Chemical Requirement for Extracting Energetic Charge Carriers from Plasmonic Metal Nanoparticles to Perform Electron-Transfer Reactions. *J. Am. Chem. Soc.* **2019**, *141*, 643–647.
46. Pillai, P. P.; Kowalczyk, B.; Pudlo, W. J.; Grzybowski, B. A. Electrostatic Titrations Reveal Surface Compositions of Mixed, On Nanoparticle Monolayers Comprising Positively and Negatively Charged Ligands. *J. Phys. Chem. C* **2016**, *120*, 4139-4144.
47. Siddarth, P.; Marcus, R. A. Calculation of Electron-Transfer Matrix Elements of Bridged Systems using a Molecular Fragment Approach *J. Phys. Chem.* **1992**, *96*, 3213-3217.
48. Walker, D. A.; Kowalczyk, B.; De la Cruz, M. O.; Grzybowski, B. A. Electrostatics at the Nanoscale. *Nanoscale*, **2011**, *3*, 1316–1344.
49. Łukaszewski, M.; Soszko, M.; Czerwiński, A. Electrochemical Methods of Real Surface Area Determination of Noble Metal Electrodes – an Overview. *Int. J. Electrochem. Sci.*, **2016**, *11*, 4442-4469.

3.8. Appendix

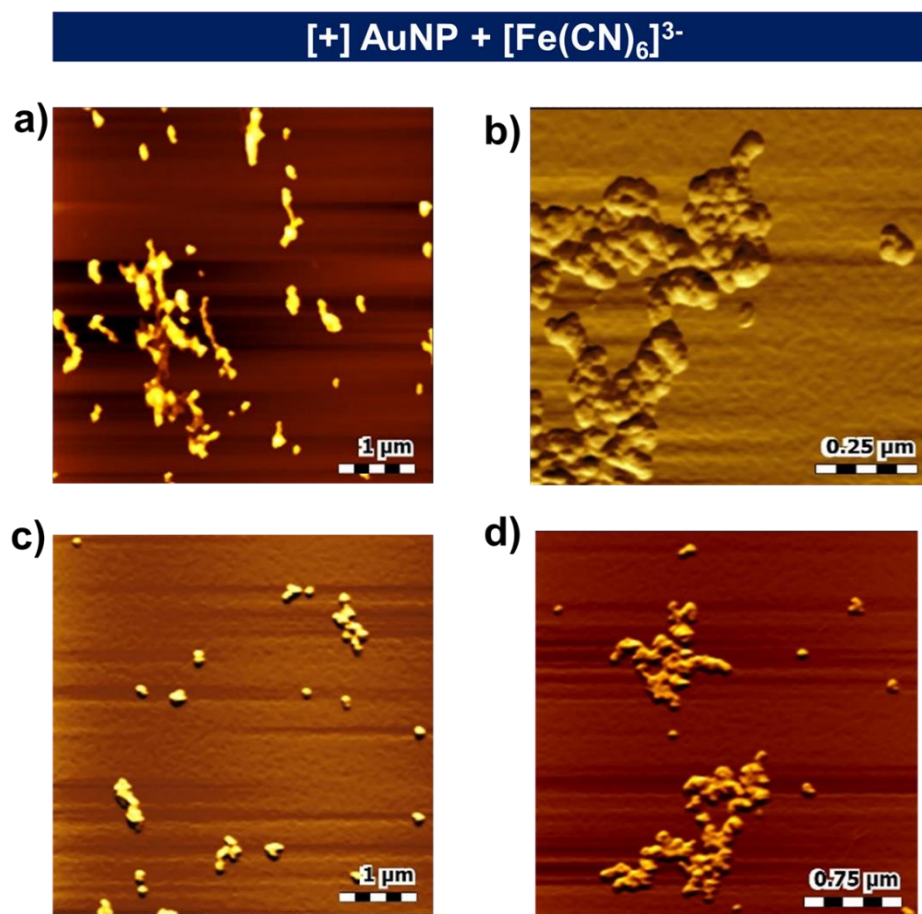


Figure 3.23. Tapping mode AFM images of [+] AuNP catalyst with ferricyanide ion. a-d) 2D and e) 3D AFM height images of [+] AuNP after the completion of photocatalysis. A clear aggregation of [+] AuNP was observed, which confirms a strong electrostatic attraction (favorable interaction) between [+] AuNP catalyst and [-] ferricyanide ion.

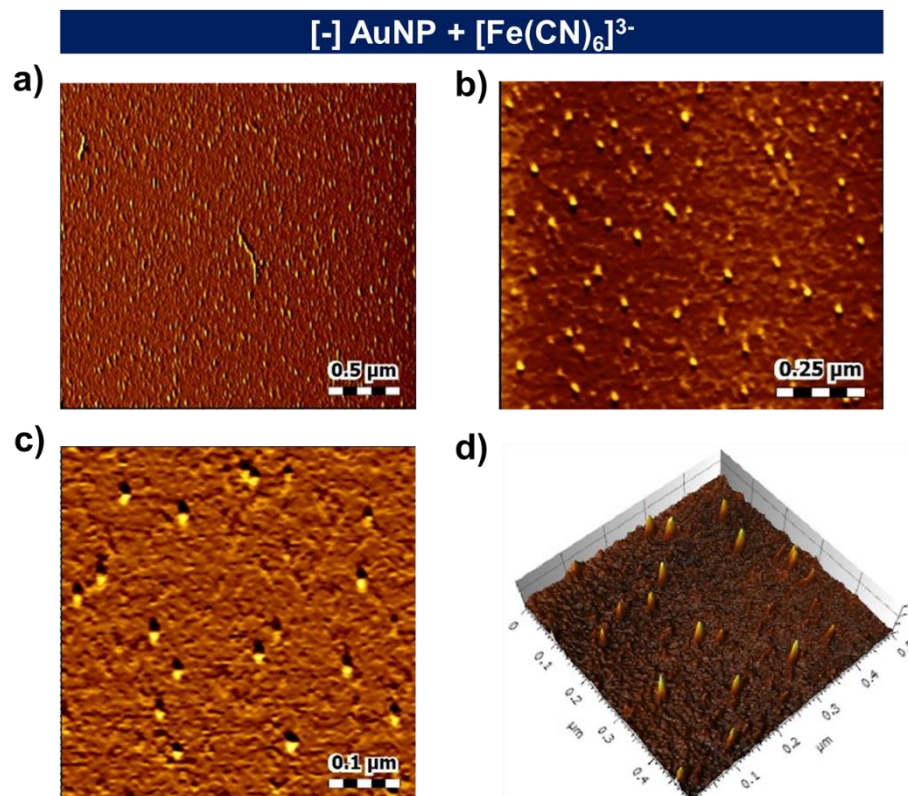


Figure 3.24. Tapping mode AFM images of [-] AuNP catalyst with ferricyanide ion. a-c) 2D and d) 3D AFM height images of [-] AuNPs after the completion of photocatalysis. Negligible changes in the size and morphology of [-] AuNPs were observed. This confirms a strong electrostatic repulsion (unfavorable interaction) between [-] AuNP catalyst and [-] ferricyanide ion.

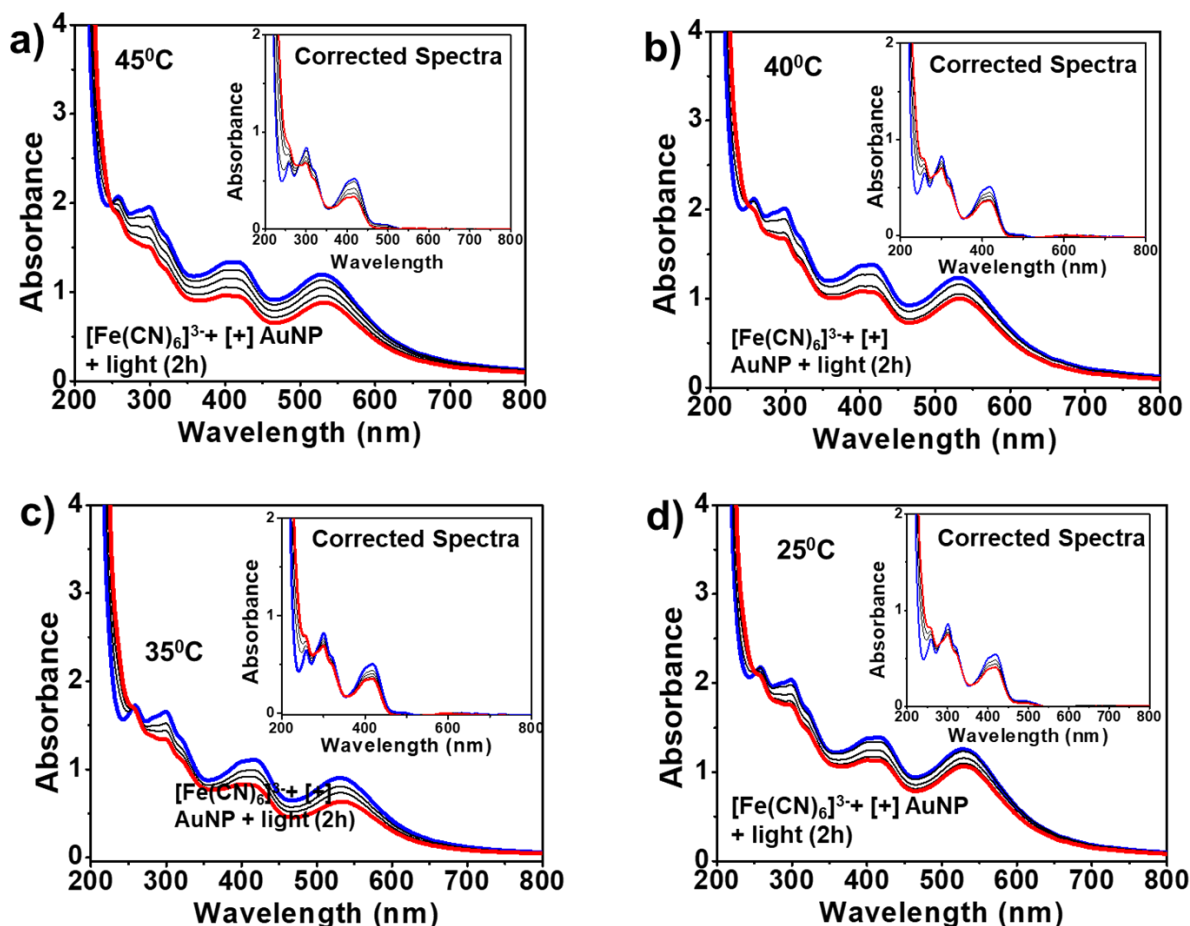


Figure 3.25. Temperature dependent catalytic reduction of ferricyanide with [+] AuNP. The progress of ferricyanide reduction by tracking the absorbance changes at 420 nm in the presence of [+] AuNPs at a) 45 °C, b) 40 °C, c) 35 °C and d) 25 °C. Inset shows the corresponding corrected spectra.

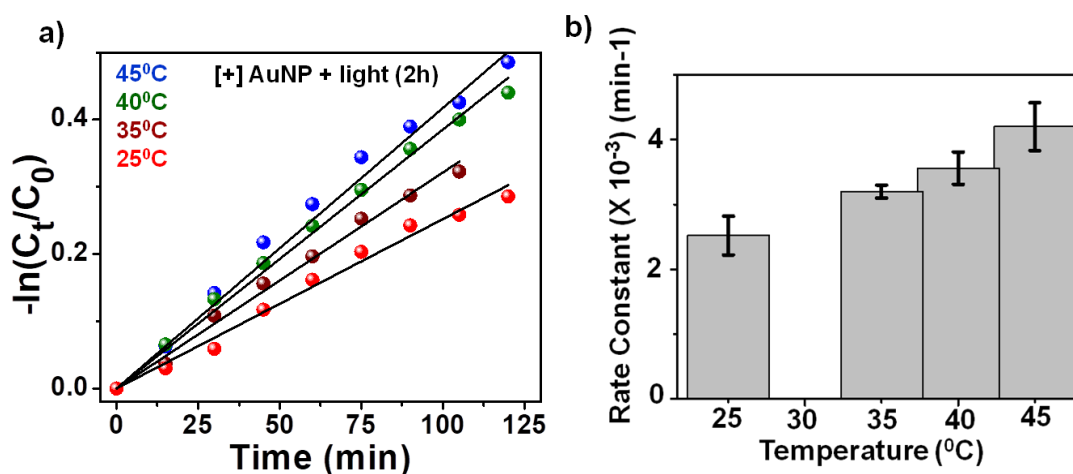


Figure 3.26. Effect of temperature on the rate constant of photocatalytic reduction of ferricyanide with [+] AuNP. a) Linearized fit for the first order analysis by tracking the absorbance at 420 nm at four different temperatures. b) Comparison of the rate constants calculated from the

corresponding linearized fits at four different temperatures. The error bars correspond to standard deviations based on three independent sets of experiments.

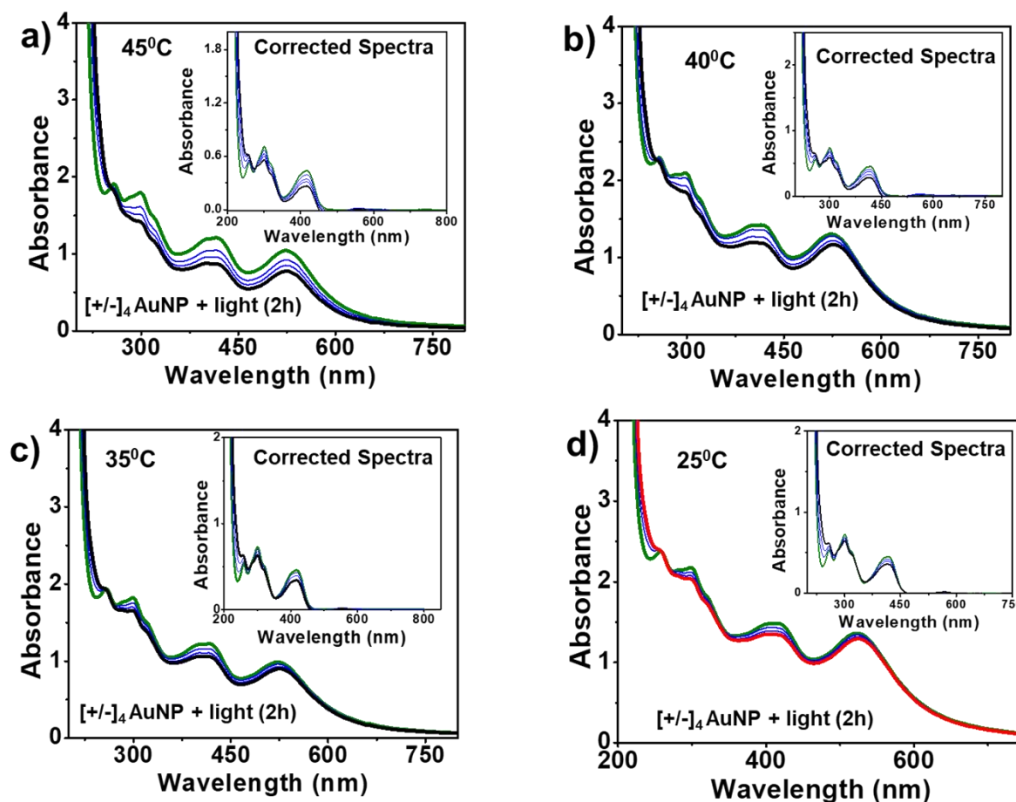


Figure 3.27. Temperature dependent catalytic reduction of ferricyanide with $[\pm]_4$ AuNPs. The progress of ferricyanide reduction by tracking the absorbance changes of ferricyanide peak at 420 nm in the presence of $[\pm]_4$ AuNP at a) 45 °C, b) 40 °C, c) 35 °C and d) 25 °C. Inset shows the corresponding corrected spectra.

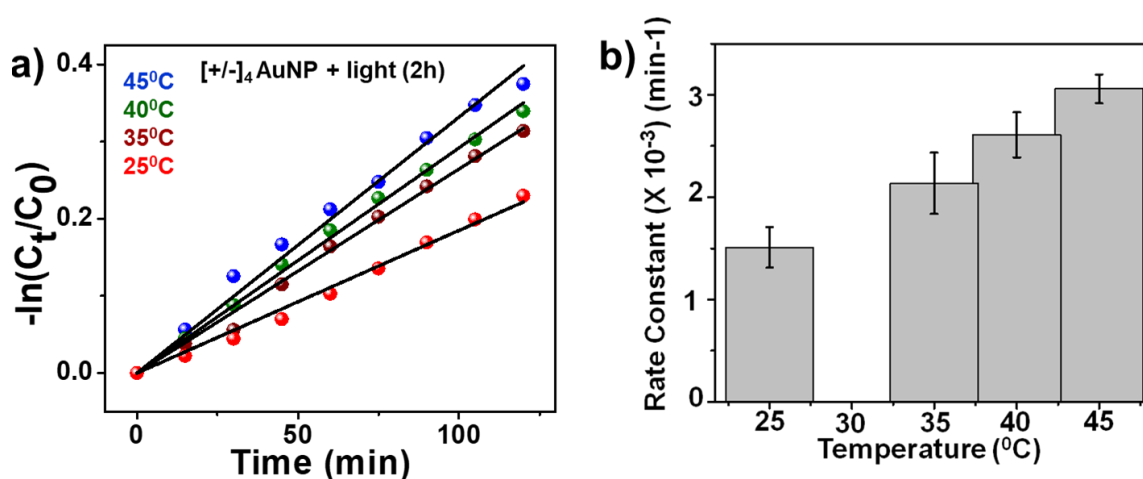


Figure 3.28. Effect of temperature on the rate constant of photocatalytic reduction of ferricyanide with $[\pm]_4$ AuNPs. a) Linearized fit for the first order analysis by tracking the absorbance at 420 nm at four different temperatures. b) Comparison of the rate constants calculated from the

corresponding linearized fits at four different temperatures. The error bars correspond to standard deviations based on three independent sets of experiments.

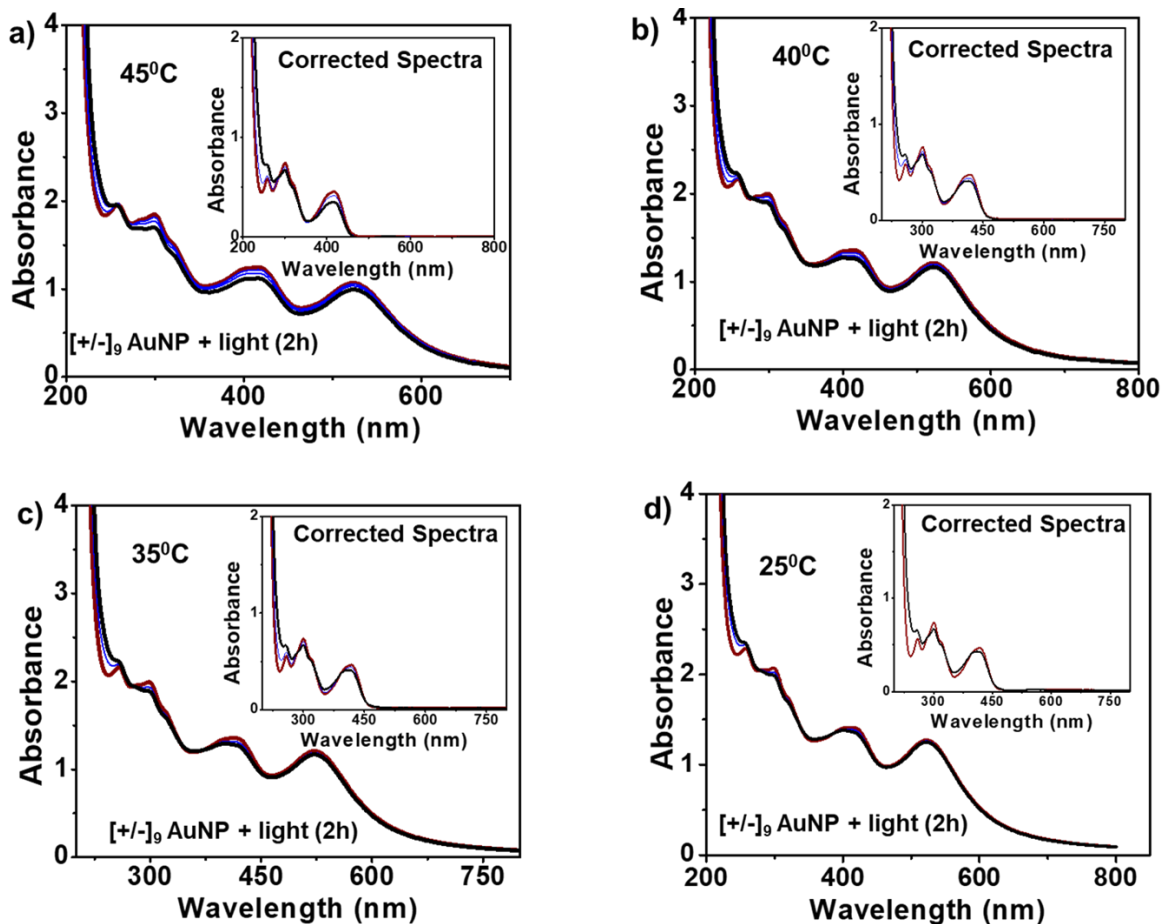


Figure 3.29. Temperature dependent catalytic reduction of ferricyanide with $[\pm]_9$ AuNPs. The progress of ferricyanide reduction by tracking the absorption changes of ferricyanide peak at 420 nm in the presence of $[\pm]_9$ AuNPs at a) 45 °C, b) 40 °C, c) 35 °C and d) 25 °C. Inset shows the corresponding corrected spectra.

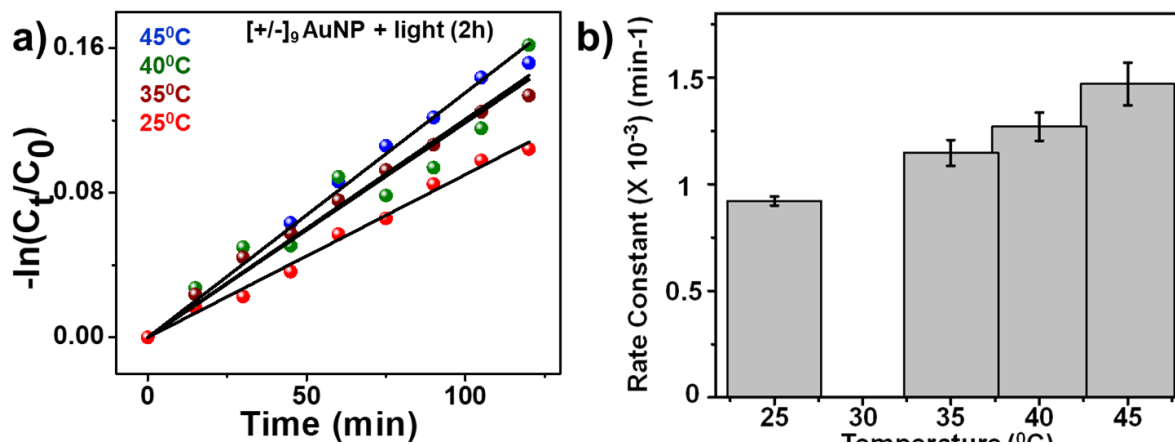


Figure 3.30. Effect of temperature on the rate constant of photocatalytic reduction of ferricyanide with $[+/-]_9$ AuNPs. a) Linearized fit for the first order analysis by tracking the absorbance at 420 nm at four different temperatures. b) Comparison of the rate constants calculated from the corresponding linearized fits at four different temperatures. The error bars correspond to standard deviations based on three independent sets of experiments.

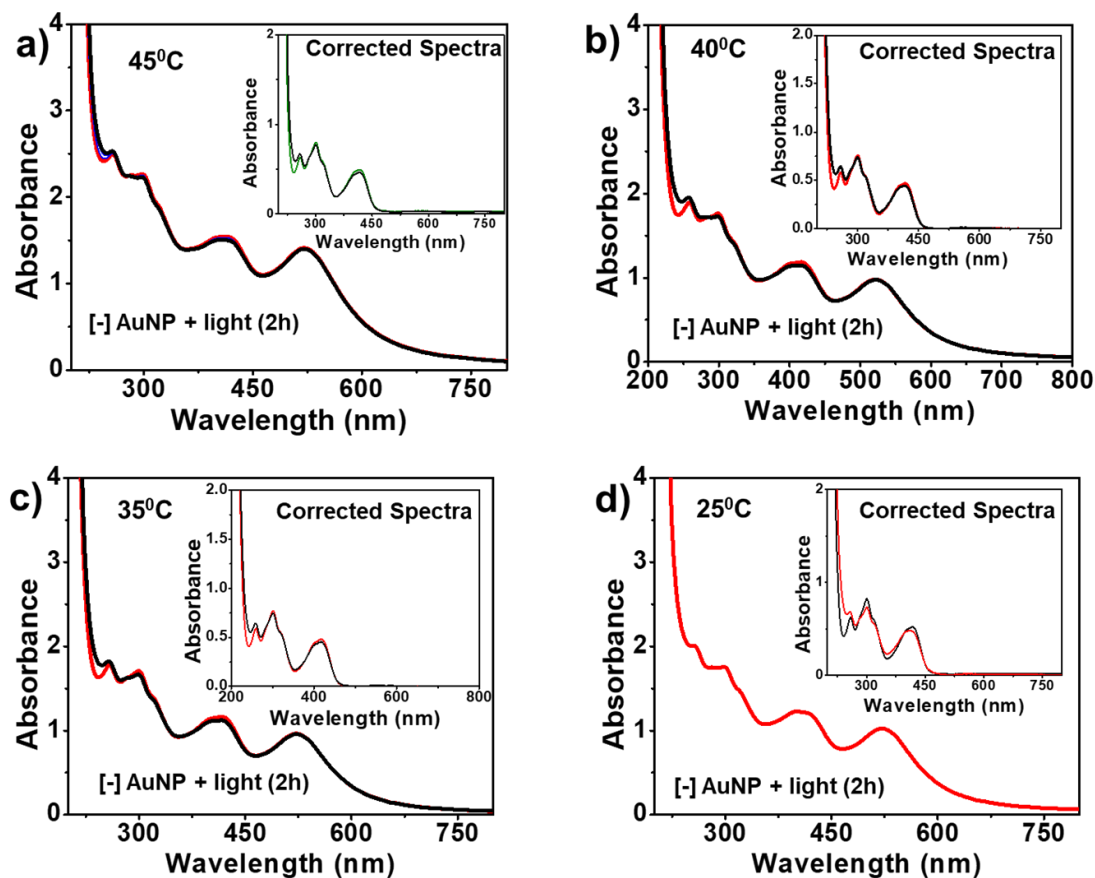


Figure 3.31. Temperature dependent catalytic reduction of ferricyanide with $[-]$ AuNPs. The progress of ferricyanide reduction by tracking the absorption changes of ferricyanide peak at 420 nm in the presence of $[-]$ AuNPs at a) 45 °C, b) 40 °C, c) 35 °C and d) 25 °C. Inset shows the corresponding corrected spectra.

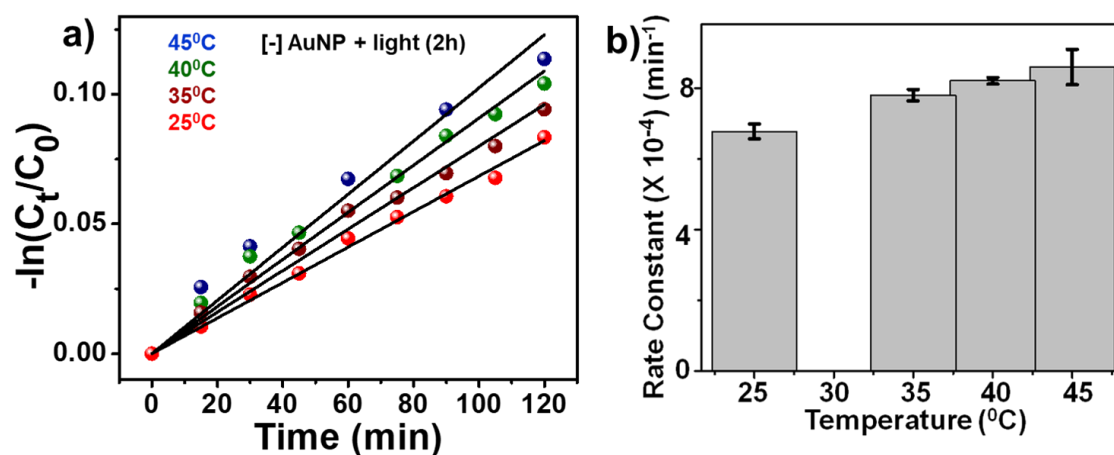


Figure 3.32. Effect of temperature on the rate constant of photocatalytic reduction of ferricyanide with [-] AuNPs. a) Linearized fit for the first order analysis by tracking the absorbance at ~ 420 nm at four different temperatures. b) Comparison of the rate constants calculated from the corresponding linearized fits at four different temperatures. The error bars correspond to standard deviations based on three independent sets of experiments.

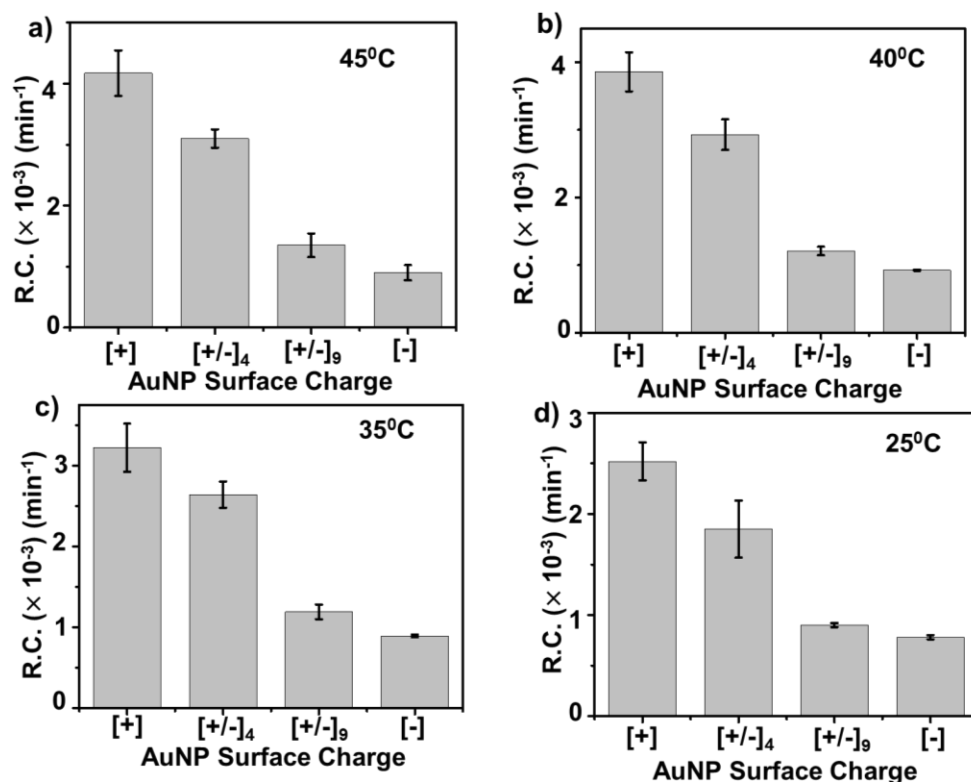
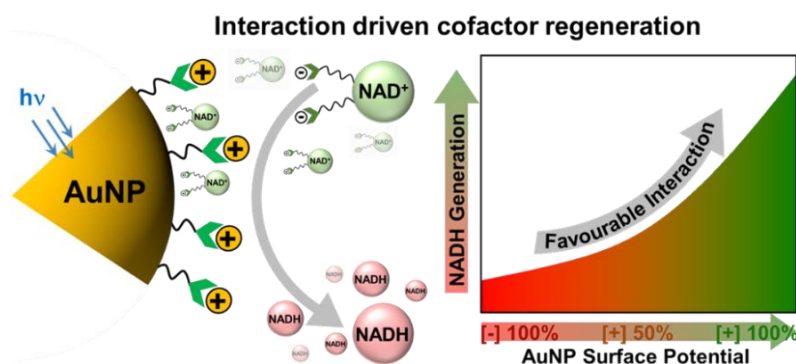


Figure 3.33. Variation in the hot electron transfer rate constant for the photocatalytic reduction of ferricyanide with AuNPs of varying surface charges at different temperatures. Bar diagrams showing the variation in rate constant values (calculated from the corresponding linearized fits) as a function of AuNP surface potential at a) 45 °C, b) 40 °C, c) 35 °C and d) 25 °C.

Chapter 4

Electrostatically Driven Multielectron Transfer for the Photocatalytic Regeneration of Nicotinamide Cofactor



This Chapter is adapted with permission from the following paper. Copyright 2020, American Chemical Society.

Roy, S.; Jain, V.; Kashyap, R. K.; Rao, A.; Pillai, P. P.* Electrostatically Driven Multielectron Transfer for the Photocatalytic Regeneration of Nicotinamide Cofactor. *ACS Catal.* **2020**, *10*, 5522-5528.

4.1. Abstract

Developing generic strategies, capable of driving multielectron processes, are essential to realize important photocatalytic conversions. Existing strategies often rely on complex catalytic systems, containing electron mediators and co-catalysts, for performing important multielectron photocatalytic transformations. We present here the idea of introducing favorable catalyst-reactant interaction in achieving efficient photocatalytic regeneration of Nicotinamide (NADH) cofactor, by gold nanoparticles (AuNPs). The electrostatic attraction emanating from the ligands on the surface of NP increases the channeling and local concentration of NAD^+ reactants around AuNP photocatalysts, thereby enhancing the probability of electron transfer process. Detailed kinetic and intensity dependent studies confirm the involvement of multiple electron transfer from AuNP photocatalyst to NAD^+ reactant. A ~ 10 times increase in the NADH formation, while switching from unfavorable to favorable interaction, proves the necessity of catalyst-reactant interaction in driving challenging photocatalytic multielectron reactions. The most interesting feature of the present idea of interaction is its flexibility to be coupled with other existing strategies, to boost the overall catalytic performances. The photocatalytic performances of AuNP presented here are in comparable or greater than most of the catalytic systems reported based on plasmonic NP, with the added advantage of being structurally less complex. The idea of electrostatically assisted photocatalysis can act as a generic approach for other important multielectron photocatalytic conversions as well.

4.2. Introduction

Driving multielectron redox reactions with visible light is one of the holy grails in the area of artificial photosynthesis. Improving the kinetics of multielectron processes is necessary to realize most of the important photocatalytic conversions like CO_2 to CH_4 , N_2 to NH_3 , H_2O to O_2 and so on.¹⁻³ This requires (i) high rate of electron excitation with accumulation of multiple charge carriers,⁴⁻⁷ and (ii) a fast funneling of charge carriers from the photocatalyst to the reactant molecules.⁴⁻⁷ The high molar extinction coefficient and photostability of metal and semiconductor nanoparticles have rendered its use as efficient photocatalysts in generating and storing multiple charge carriers.⁸⁻¹⁸ However, the subsequent transfer of the multiple charge carriers to reactants is still challenging due to its short lifetime and ligand poisoning effect in nanomaterials.¹⁸⁻²¹ As a result, charge mediators or co-catalysts are oftentimes used to facilitate the charge transfer process, thereby increasing the complexity of the photocatalytic system.²²⁻²⁴ For instance, in z-scheme

water splitting, electron mediators or co-catalysts are commonly used to facilitate the rate of forward electron transfer and improve the photocatalytic efficiency of the reaction (**Figure 4.1**).²⁴ These electron mediators oftentimes involve in several undesirable backward reactions, which affect the overall photocatalytic efficiency.

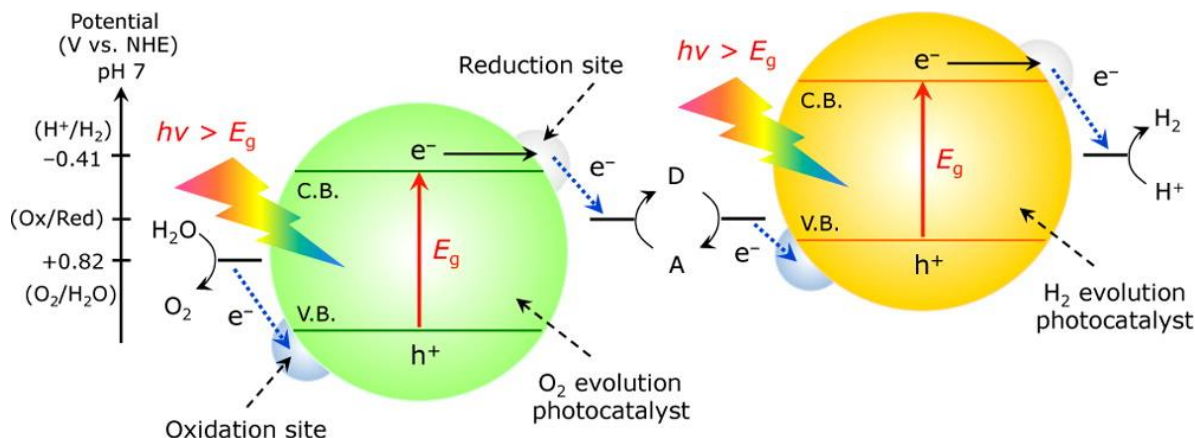


Figure 4.1. Schematics of photocatalytic water splitting in a Z-scheme water splitting system. Adapted with permission from reference 24. Copyright 2013, American Chemical Society.

Therefore, strategies to develop sole photocatalysts for multielectron reactions are highly desirable but yet not widely achieved. The idea of introducing favourable catalyst-reactant interaction is emerging as a promising strategy not only to improve the funnelling of charge carriers, but also to dictate the product selectivity.^{18,25-34} The exclusivity of such favorable catalyst-reactant interactions in multielectron photochemical reactions has been scarcely studied, which forms the basis of this Chapter. In this direction, we have chosen the task of photocatalytic regeneration of nicotinamide cofactor (NADH) by plasmonic gold nanoparticles (AuNPs), without the aid of any electron mediators or co-catalysts. NADH is a key cofactor molecule consumed by different oxidoreductase enzymes in various biocatalytic reactions, and hence the regeneration of NADH from NAD^+ is an active area in photo-redox biocatalysis.³⁵⁻³⁶ Most of the previous photocatalytic studies involves electron mediators or co-catalysts for the efficient regeneration of NADH cofactor.³⁷⁻⁴⁹ For instance, Baeg and co-workers developed a graphene based visible light active photocatalytic system for the regeneration of NADH (**Figure 4.2 a,b**). A porphyrin chromophore was covalently attached with the chemically converted graphene for efficient light harvesting, and an Rh based electron mediator complex was used for an efficient electron transfer from the photocatalyst to the NAD^+ molecules.⁴¹ A ~ 45 % yield of NADH regeneration was achieved under visible light irradiation of ~ 2 h. In another study, Park and co-workers synthesized a polydopamine

/ AuNP / Eosin Y (PDA-Au-EY) based nanohybrid system for the photocatalytic regeneration of NADH (**Figure 4.2 c,d**).³⁸ The LSPR of AuNPs was utilized to enhance the light absorbing property of the photosensitizer, and a similar Rh based electron mediator complex was used to facilitate the electron transfer from the photocatalyst to the NAD^+ molecules. A $\sim 15\%$ NADH regeneration yield was achieved under 3 h of visible light irradiation. Thus, majority of the previous photocatalytic studies used an electron mediators or co-catalysts for an efficient multielectron transfer. Dedicated synthesis procedures or advanced fabrication protocols are oftentimes required to integrate such electron mediators/co-catalysts into the catalytic systems.³⁷⁻⁴⁹ On the contrary, the present study aims to develop an interaction based strategy for direct multielectron transfer from the photoexcited AuNPs to the NAD^+ molecule without the aid of any electron mediators or co-catalysts.

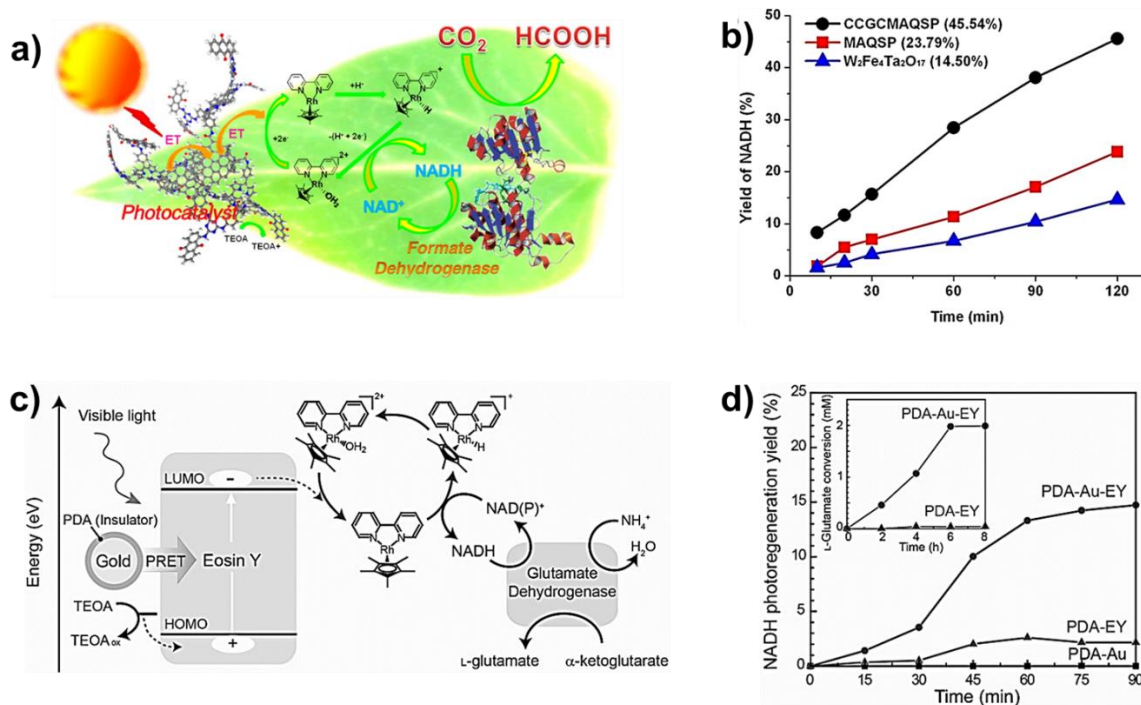


Figure 4.2. a) Schematic representation of the photocatalytic regeneration of NADH coupled with enzymatic reduction of CO_2 to formic acid with graphene based photocatalyst. b) Activity of graphene based photocatalysts in the photocatalytic regeneration of NADH. Adapted with permission from reference 41. Copyright 2012, American Chemical Society. c) Energy level diagram and the electron transfer pathway for the plasmon enhanced photocatalytic regeneration of NADH with PDA-Au-EY based core-shell photocatalyst. d) Photoregeneration of NADH with PDA-Au, PDA-EY and PDA-Au-EY photocatalysts. The inset shows the generation of L-glutamate in an enzymatic reduction of α -ketoglutarate coupled with the generation of NADH. Adapted with permission from reference 38. Copyright 2014, John Wiley and Sons.

The net negative charges on NAD^+ , due to two phosphate groups, allowed us to use electrostatic forces as the tool to impart favorable catalyst-reactant interaction (**Figure 4.3**). The ligands on the surface of AuNP regulates the channeling and local concentration of negatively charged NAD^+ , thereby controlling the charge transfer distance between the photocatalyst and reactant.

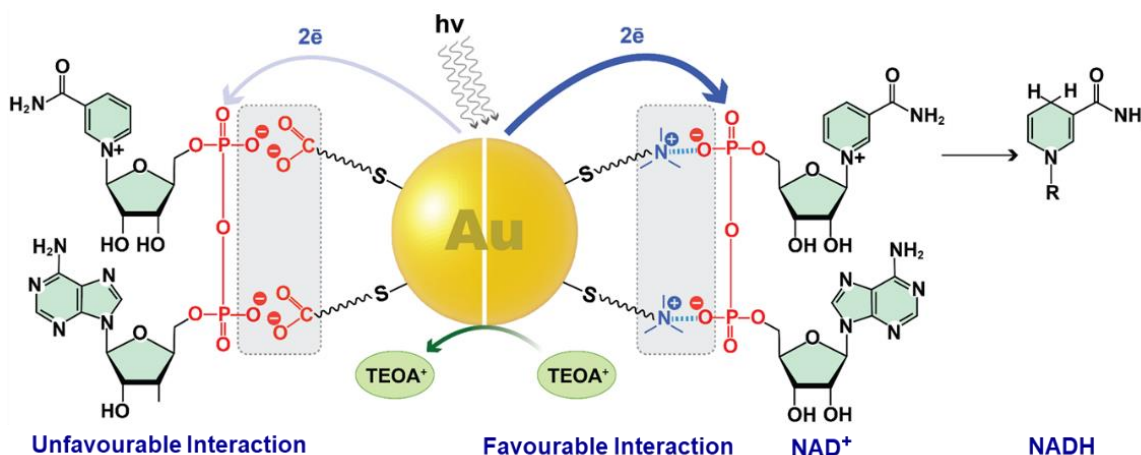


Figure 4.3. Schematics of electrostatically assisted photocatalytic multielectron reduction of NAD^+ to NADH by AuNP, without the aid of charge mediators or co-catalysts.

Accordingly, an efficient photocatalytic regeneration of NADH ($60 \mu\text{M}$; $\text{TON} \sim 12 \times 10^3 / \text{NP}$) was achieved using $[+]$ AuNP as the sole photocatalyst, without the aid of any electron mediator or co-catalyst. Interestingly, $[-]$ AuNP exhibited negligible catalytic activity even in the presence of an electron mediator, reemphasizing the necessity of favorable catalyst-reactant interaction to drive challenging multielectron photocatalytic transformations. Systematic studies by varying the surface potential of AuNPs proved the exclusivity of electrostatic interactions in the photocatalytic regeneration of NADH . Further, electrostatics was used to bind $[+]$ AuNP with a negatively charged electron mediator, to show the flexibility in coupling the present idea of interaction driven photocatalysis with existing strategies to boost the regeneration of NADH . Strikingly, only ~ 1 h of irradiation was sufficient to produce twice the amount of NADH cofactor, as compared to that in the absence of an electron mediator. Thus, the present study demonstrates the prodigious role of favorable catalyst-reactant interaction in dictating multi-electron photocatalytic reactions, which can serve as a generic approach for other important reactions as well.

4.3. Experimental Details:

4.3.1. Materials and Reagents:

Tetrachloroaurate trihydrate ($\text{HAuCl}_4 \cdot 3\text{H}_2\text{O}$), tetramethylammonium hydroxide (TMAOH) 25 % wt. in water, 11-mercaptoundecanoic acid (MUA), hydrazine monohydrate ($\text{N}_2\text{H}_4 \cdot \text{H}_2\text{O}$ 50-60%), tetrabutylammonium borohydride (TBAB), potassium ferricyanide, polyvinylpyrrolidone, β -nicotinamide adenine dinucleotide sodium salt (NAD^+), β -nicotinamide adenine dinucleotide reduced disodium salt (NADH), albumine from bovine serum (BSA), ethylenediaminetetraacetic acid tetrasodium salt hydrate (EDTA), and diaphorase from *Clostridium kluyveri* (100-UN) were purchased from Sigma-Aldrich. (Di-n-dodecyl) dimethyl ammonium bromide (DDAB) and dodecylamine (DDA) were purchased from Alfa Aesar. DL-6,8-thioctic acid amide (DL-lipoamide) was purchased from Maaspharmachemicals. Triethanolamine (TEOA) was purchased from Avra Chemicals. All the reagents were used as received without any further purification. The positively charged N,N,N-trimethyl (11- mercaptoundecyl) ammonium ion (TMA) was synthesized according to the reported procedure.⁵⁰

4.3.2. Synthesis of AuNPs:

All the nanoparticles were synthesized following a modified literature procedure.^{51,52} Hydrazine monohydrate ($\text{N}_2\text{H}_4 \cdot \text{H}_2\text{O}$) was used as the reducing agent. In a typical experiment, $\text{HAuCl}_4 \cdot 3\text{H}_2\text{O}$ (12 mg), DDA (140 mg), and DDAB (140 mg) were mixed together in toluene (4 mL) and sonicated for ~10 min for complete stabilization of Gold (III) ions. This was followed by a rapid injection of another toluene solution containing 30 mg of TBAB and 45 mg of DDAB. The resulting solution was left stirring overnight to ensure the complete reduction of gold (III). The seed particles were then grown to 5.5 ± 0.7 nm DDA-Au NPs. A growth solution was prepared by adding 460 mg of DDAB, 1.4 g of DDA, 120 mg of $\text{HAuCl}_4 \cdot 3\text{H}_2\text{O}$ and seed solution in 30 mL toluene. The growth solution was further reduced with a dropwise addition of another toluene solution containing 160 μL of $\text{N}_2\text{H}_4 \cdot \text{H}_2\text{O}$ and 560 mg of DDAB. The solution was stirred overnight for complete growth of the particles yielding monodisperse 5.5 ± 0.7 nm of DDA-Au NPs. The particles were further grown to ~11 nm DDA-Au NPs. A growth solution was prepared by adding 8 g of DDAB, 13.0 g of DDA, and 1.1 g of $\text{HAuCl}_4 \cdot 3\text{H}_2\text{O}$ and seed solution in 200 mL toluene. The growth solution was further reduced with a dropwise addition of another toluene solution containing 650 μL of $\text{N}_2\text{H}_4 \cdot \text{H}_2\text{O}$ and 4.4 g of DDAB. The solution was stirred overnight for

complete growth of the particles yielding monodisperse 11 ± 1.3 nm of DDA-Au NPs as confirmed through TEM analysis. The detail procedure for the place exchange of DDA-AuNP with different charged ligands (as per **Figure 4.4**) is described below.

4.3.3. Place Exchange of AuNPs:

In a typical synthesis of [+] AuNPs, DDA-Au NPs (15 mL) were first precipitated by adding 50 mL of methanol which yielded a black precipitate. The supernatant was carefully removed and the precipitate was then re-dispersed in 20 mL toluene. [+] TMA ligand (equal to the moles of Au(III) in solution) dissolved in 10 mL dichloromethane (DCM)) was added. The solution was left overnight to ensure a complete ligand exchange. Next, the supernatant was decanted and the precipitate was washed with DCM (3×50 mL) and acetone (50 mL) respectively. The precipitate was then dried and redispersed in miliQ water for further studies. The [-] AuNPs were redispersed in miliQ water by adding ~ 20 μ L of TMAOH (25 % wt. in water) base to deprotonate the carboxylic acid group. [+/-]₄, [+/-]₁ and [-/+]₄ AuNPs were synthesized by adding TMA and MUA ligands in a molar ratio of 4:1, 1:1 and 1:4 respectively. The on-NP ratio was estimated to be [+/-]_{4.8} [+/-]_{1.2} and [-/+]_{3.3}, using NMR studies as reported in the previous works.^{53,54}

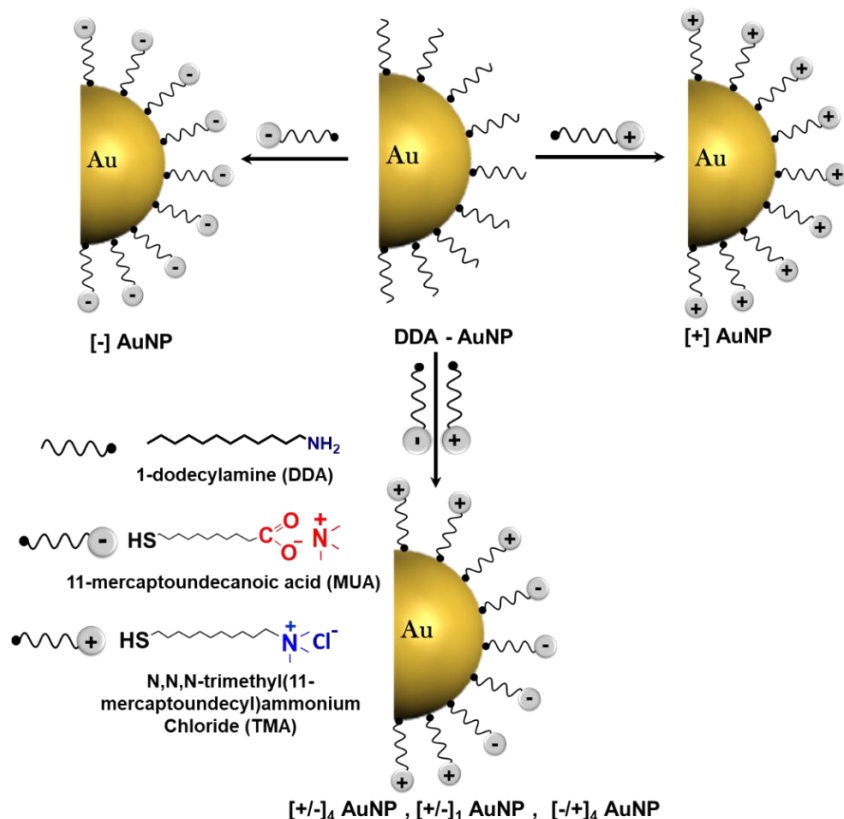


Figure 4.4. Schematic illustration of place exchange of DDA capped AuNP. DDA capped AuNPs were place exchanged with either [+], [-] or a mixture of [+] and [-] to synthesize positively, negatively or heterogeneously charged AuNPs, respectively.

4.3.4. Synthesis of Polyvinylpyrrolidone (PVP) AuNPs:

PVP AuNPs were synthesized following a citrate reduction method.⁵⁵ In a typical synthesis, 10 mg of HAuCl₄ · 3H₂O was dissolved in 100 mL water and the solution was heated to boiling. Next 0.6 mL of trisodium citrate solution (100 mg in 2 mL of water) was rapidly injected to the preheated gold solution under vigorous stirring. The solution was kept at the same temperature for ~30 min till a wine-red color was persistent. Subsequently, the solution was cooled to room temperature and 250 mg of PVP (Mw = 40000) was added to 15 mL of citrate AuNPs. The solution was then sonicated for 45 min followed by two cycles of centrifugation at 10000 rpm for 10 min. The supernatant was carefully removed and the NPs were finally redispersed in water.

4.3.5. Transmission Electron Microscopy (TEM) Study:

TEM studies were performed to characterize the AuNPs. The TEM sample for the nanoparticles was prepared by drop casting AuNP solution on a 400 mesh carbon coated copper grid (Tedpella Inc.) and dried under vacuum. The High-Resolution Transmission Electron Microscopic (HRTEM) imaging was performed on Jeol JEM2200FS (200 kV) HRTEM instrument.

4.3.6. Zeta Potential:

The zeta potential (ζ) of charged AuNPs were measured in Nano ZS90 (Malvern) Zetasizer instrument. The optical density of the nanoparticle solution was maintained ~0.2 during all the measurements. The error bar was calculated from three different experiments. ζ was determined by measuring the electrophoretic mobility and using Henry's equation.

$$U_E = \frac{2\varepsilon\zeta f(k_a)}{3\eta}$$

U_E : Electrophoretic mobility

ζ : Zeta potential

ε : Dielectric constant

η : Viscosity

$f(K_a)$: Henry's Function

4.3.7. Photocatalytic Reduction of Ferricyanide to Ferrocyanide:

All the photocatalytic reduction experiments were performed in a 3 mL quartz cuvette under continuous irradiation from a power tunable 532 nm continuous wave (CW) diode laser. The beam diameter was set to be 1.1 cm and the light intensity on the cuvette wall was measured by using an optical power meter from Newport (Model 842.PE). All the kinetic measurements were performed using SHIMADZU UV-3600 plus UV-Vis-NIR spectrophotometer and the temperature of the reaction mixture was maintained using a temperature controller equipped with the UV-Vis-NIR spectrophotometer. In a typical experiment, AuNP (absorbance was set to ~ 1 for all the NP systems), EtOH (1.5 M) and potassium ferricyanide (500 μM) were mixed in a 3 mL quartz cuvette and purged with Ar for 15 min. The cuvette was then sealed with Teflon and kept at for 15 min for temperature equilibration, prior to the irradiation. Photoreduction of ferricyanide was monitored by measuring the absorbance of the solution at a fast scan mode, at 15 min interval for 2 h.

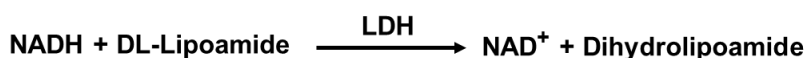
4.3.8. Photocatalytic Reduction of NAD^+ to NADH:

The photocatalytic reduction of NAD^+ was performed in a 3 mL quartz cuvette under continuous irradiation from a power tunable 450 nm continuous wave (CW) diode laser. The beam diameter was set to be 1.1 cm and the light intensity on the cuvette wall was measured by using an optical power meter from Newport (Model 842.PE). In a typical experiment, AuNP (absorbance was set to ~ 1.3 for all the NP systems), triethanolamine (TEOA) (1 M) and NAD^+ (1 mM) were mixed in phosphate buffer (50 mM) and the pH of the solution was maintained at ~ 8 . TEOA acts as a hole scavenger, as well as a source of proton in the presence of appropriate photocatalysts.⁵⁶ Next the solution was purged with Ar for 30 min under continuous stirring. The cuvette was then sealed with Teflon and subjected to the irradiation for 13 h. After 13 h of irradiation, the AuNPs were first separated by centrifuging the solution with a 100000 MWCO centrifuge filters and finally the quantitative analysis of NADH was performed through Lipoamide Dehydrogenase Assay (LDH). For the photocatalytic reduction in presence of Eosin Y, the AuNP and Eosin Y were first stirred for 30 min to ensure the complexation followed by the similar procedure as mentioned above.

4.3.9. Lipoamide Dehydrogenase (LDH) Assay

Lipoamide dehydrogenase assay was performed based on Sigma Quality Control Test Procedure (EC 1.8.1.4).^{57,58} The assay was performed at 25 $^{\circ}\text{C}$ and all the reagents were prepared fresh before the assay. Phosphate buffer (PB) (50 mM, pH = 7) was prepared by mixing Na_2HPO_4 and NaH_2PO_4

in miliQ water. Lipoamide solution (28 mM) was prepared by adding 20 mg of lipoamide in 2 mL of ethanol and 1.5 mL of PB, and sonicating the solution for 3 min. EDTA (600 mM) with 2% (w/v) BSA was prepared by dissolving 605 mg of EDTA and 100 mg of BSA in 5 mL water and the pH of the solution was maintained at 7. An enzyme (diaphorase from *Clostridium kluyveri*) stock solution was prepared by adding 2 mg of enzyme (5.2 units / mg of protein) in 2 mL of cold PB solution. In a typical enzymatic assay, 100 μ L of lipoamide solution, 100 μ L of EDTA solution and 100 μ L of enzyme were added to the reaction mixture (after separating the catalyst) and the decrease in absorption at 340 nm was monitored till the absorption decrease got saturated. In presence of enzyme, NADH will be consumed by the enzyme as per the following reaction resulting in a decrease in the absorbance at 340 nm.



A positive control experiment with the addition of equal amount of NADH (by making the absorption at 340 nm same to that of the reaction mixture) was always performed during analyzing the sample from the reaction mixture.

4.3.10. Calculation of Turnover Number (TON) & Turnover Frequency (TOF):

TON for the reaction was defined as the total number of NADH molecules generated per AuNP for a given time of irradiation. The total number of AuNPs was calculated using the Beers-Lambert's law. The absorbance of the AuNPs was set to be ~ 1.3 for all the experiments and the extinction coefficient of the NPs was considered to be $2.7 \times 10^8 \text{ M}^{-1} \text{ cm}^{-1}$ for $\sim 12 \text{ nm}$ particles.⁹³ Thus, the total no. of AuNPs in 3 mL of reaction volume was calculated to be 8.03×10^{12} . The Turnover Frequency (TOF) for the photocatalytic reaction is defined as the number of NADH molecules formed per AuNP per unit illumination time. Thus, the TOF value was calculated from the slope of a linear fit to the TON vs time plot.

4.3.11. Kinetic Analysis for the Photocatalytic Reduction of Ferricyanide:

Construction of Corrected Spectra:

All the rate constant analysis were performed after constructing a corrected spectra to subtract the contribution from the AuNP absorption. The corrected spectra were constructed as follow.⁶

$$\text{Spectrum}_{\text{corrected}} = \text{spectrum}_{\text{sample}} - \left(\frac{\text{peak absorbance}_{\text{sample}}}{\text{peak absorbance}_{\text{AuNP}}} \right) \times \text{spectrum}_{\text{AuNP}}$$

Peak absorbance *sample* is the difference between the absorbance at $\lambda_{\max} AuNP$ and at 800 nm in sample spectra. Peak absorbance *AuNP* is the difference between the absorbance at $\lambda_{\max} AuNP$ and at 800 nm for only AuNP (without ferricyanide) with the same NP concentration as in the reaction mixture.

Determination of Reaction Rate:

The reaction rate was calculated by plotting photoconversion (in units of M) as a function of time (min). The photoconversion was calculated from the corrected spectra as per the following equations.

$$\text{Conversion (t)} = - (A_{420\text{nm}} (t) - A_{420\text{nm}} (t=0)) / 1050$$

$$\text{Conversion (t)} = (A_{240\text{nm}} (t) - A_{240\text{nm}} (t=0)) / 6250$$

The extinction coefficient of ferricyanide and ferrocyanide are $1050 \text{ M}^{-1} \text{ cm}^{-1}$ and $6250 \text{ M}^{-1} \text{ cm}^{-1}$, respectively.⁶ The final conversion was calculated by taking an average of the two conversions. The photoconversion vs time plot was fitted with a straight line and the slope of which is the reaction rate in units of M min^{-1} .

Determination of Number of Photons Absorbed / NP /s (N_p):

The number of photons absorbed by each NPs at a particular intensity was calculated as per the following equation⁶

$$N_p = \frac{\text{laser power} \times (1 - 10^{-A})}{\text{energy of each photon} \times \text{number of NPs}}$$

Where A is the absorbance of AuNPs at the irradiation wavelength. The number of AuNPs was calculated from the absorption maxima (at 525nm) using the extinction co-efficient of $2.7 \times 10^8 \text{ M}^{-1} \text{ cm}^{-1}$ ⁶ for 12 nm AuNPs.

Quantum Yield (QY) calculation:

The quantum yield for the photocatalytic reduction of NAD^+ was calculated by using the following equation⁶

$$QY = \frac{6.023 \times 10^{23} \times \text{total conversion (moles of NADH formed after 13 h irradiation)}}{\text{No. of photons incident per second (photon flux)} \times (1 - 10^{-A}) \times 60 \times 60 \times 13}$$

Where, A is the absorbance of the nanoparticle solution, at the irradiation wavelength.

The photon flux or the no. of photons incident per second was calculated using the following equation:

$$\text{Photon flux} = \frac{\text{Excitation energy}}{\text{Energy per photon}}$$

The excitation energy for the photocatalytic reactions was 800 mW

Energy of each photon at $\lambda = 450$ nm would be 4.41×10^{-19} J.

So the photon flux will be

$$\text{photon flux} = \frac{0.8 \text{ J/s}}{4.41 \times 10^{-19} \text{ J}} = 1.81 \times 10^{18} / \text{s}$$

4.4. Results and Discussion

4.4.1. Design and Characterization of Plasmonic AuNP Catalysts:

The hypothesis of the present work was to investigate the role of interaction between AuNP catalyst and the reactant molecules to drive a multielectron reduction of NAD^+ to NADH. The presence of two negative charges (due to two phosphate groups) allowed the use of electrostatic forces as a handle to tune the catalyst-reactant interactions. The electrostatic field experienced by [-] NAD^+ molecule can be controlled by precise tuning of the surface ligands on AuNPs. Accordingly, N,N,N-trimethyl(11-mercaptopundecyl)ammonium chloride (TMA, [+]) and 11-mercaptopundecanoic acid (MUA, [-]) ligands were functionalized to render positive and negative surface potential around AuNPs, respectively (**Figure 4.5 a,b**).⁵² Further fine tuning in the surface potential was achieved by functionalizing a mixture of [+] and [-] ligands on the AuNP surface through a place exchange reaction (**Figure 4.5 a,b**. Details on the synthesis are provided in the **Experimental Section 4.3.2**).^{52,53} A decrease in the positive zeta potential from $+32.1 \pm 1.6$ mV to $+27.0 \pm 0.5$ mV was observed upon dilution of [+] ligands with ~ 20 % of [-] ligands, which further decreased to $+10.0 \pm 0.4$ mV with ~ 50 % of [-] ligands (**Figure 4.5 d,e**). Similarly, a decrease in the negative zeta potential from -35 ± 1.02 to -25 ± 1.3 was observed upon dilution of [-] ligands with ~ 20 % of [+] ligands on the surface. The spectroscopic (UV-Vis absorption) and Microscopy (Transmission Electron Microscopy, TEM) studies confirm negligible changes in the stability and average size of AuNPs upon various surface functionalizations (**Figure 4.5**). Thus,

similar sized AuNPs (12.0 ± 0.5 nm from TEM) with varying surface potentials were successfully prepared, which is crucial for comparing their photocatalytic performances.

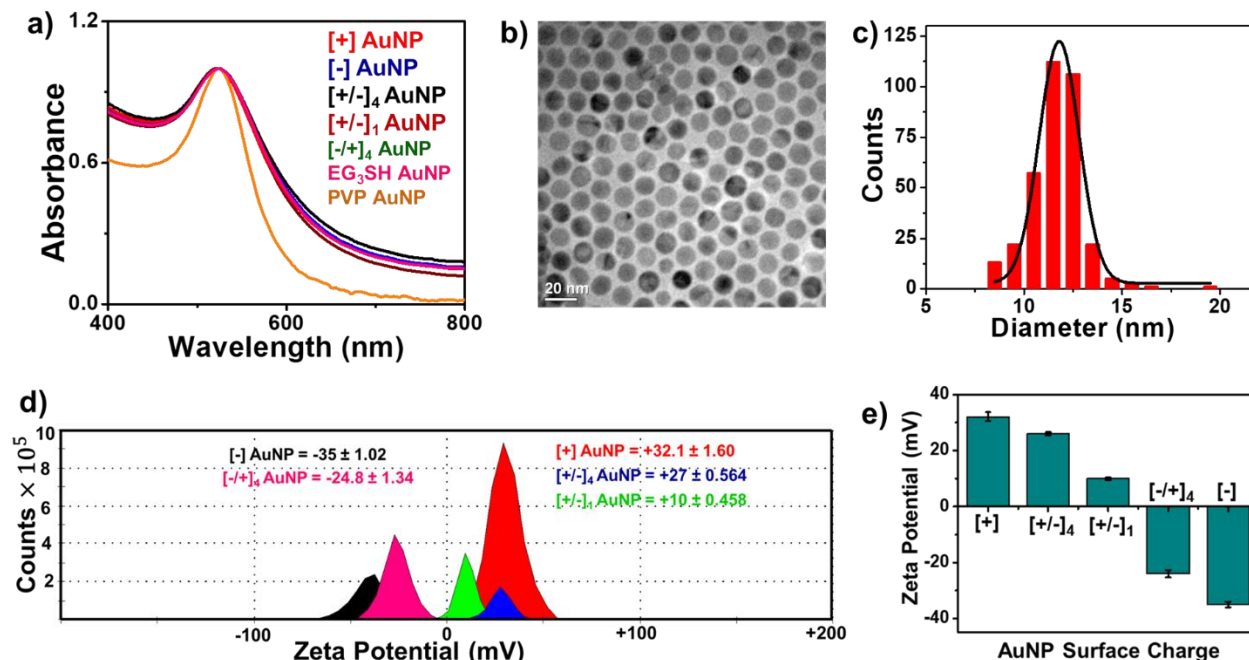


Figure 4.5. Spectroscopic, microscopic and surface characterization of AuNPs. a) UV-Vis absorption spectra of all AuNP systems under study. b) Representative TEM image of [+] AuNP and c) size distribution histogram generated from ~ 300 particle analysis (d) Typical zeta potential plots for different sets of AuNPs with varying surface charges. e) A bar diagram showing the variation of zeta potential as a function of ligands on the surface of AuNPs. The error bars correspond to standard deviations based on three different sets of experiment.

4.4.2. Photocatalytic Reduction of Ferricyanide to Ferrocyanide:

A model intensity dependent study was developed by Jain and coworkers to test the ability of AuNPs to participate in multielectron photocatalytic reactions.⁶ Specifically, a superlinear increase in the rate of ferricyanide reduction as a function of irradiation intensity (or photon flux) is a typical signature for a multielectron transfer process.⁶ A similar intensity dependent photocatalytic studies on ferricyanide reduction by AuNPs was first performed to test the power of NP-reactant interaction in driving multielectron reactions. Our group has previously shown the potency of NP catalyst-reactant interaction in the photocatalytic reduction of ferrocyanide;¹⁸ whereas its exclusivity in driving multielectron photocatalytic reactions is still unexplored. The electrostatic forces were used as the means for controlling the interaction between AuNP photocatalyst and negatively charged ferricyanide reactant. The NP-ferricyanide interaction was made favorable or unfavorable by introducing positive ([+]) and negative ([-]) surface potentials on AuNP

photocatalysts, respectively. No noticeable reduction of ferricyanide was achieved with [-] AuNP even at higher light intensity, which is attributed to the dominant ligand poisoning effect (**Figure 4.6 c and Figure 4.19 in Appendix**).¹⁸ As anticipated, [+] AuNPs not only photocatalyzed the reduction of ferricyanide but also showed an increase in the rate of reduction as a function of irradiation intensity. A strong favorable electrostatic attraction between [+] AuNP and [-] ferricyanide revealed a superlinear increase in the rate of reduction as a function of photon flux, which is a typical signature for multielectron transfer process ((**Figure 4.6 a,c,d and Figure 4.17 in Appendix Section**)).⁶ The linear regime at lower photon flux is dominated by $1e^-$ transfer process, whereas the non-linear regime at higher photon flux is characteristics of a $2e^-$ transfer process.⁶ The ability of [+] AuNP to transfer multielectrons was compared with standard polyvinylpyrrolidone (PVP) functionalized AuNPs, where a precise NP catalyst-reactant interaction was absent. To our delight, the rate constant for [+] AuNP was estimated to be $\sim 9 \times 10^{-7} \text{ M min}^{-1}$, which is at least two times higher than for the standard PVP- AuNPs ($\sim 4 \times 10^{-7} \text{ M min}^{-1}$) (**Figure 4.6 b-d, Figures 4.16 & 4.18 in Appendix**). A clear dominance of [+] AuNP confirms that the idea of NP-reactant interaction can play a decisive role in driving photocatalytic multielectron transfer reactions by plasmonic NPs.

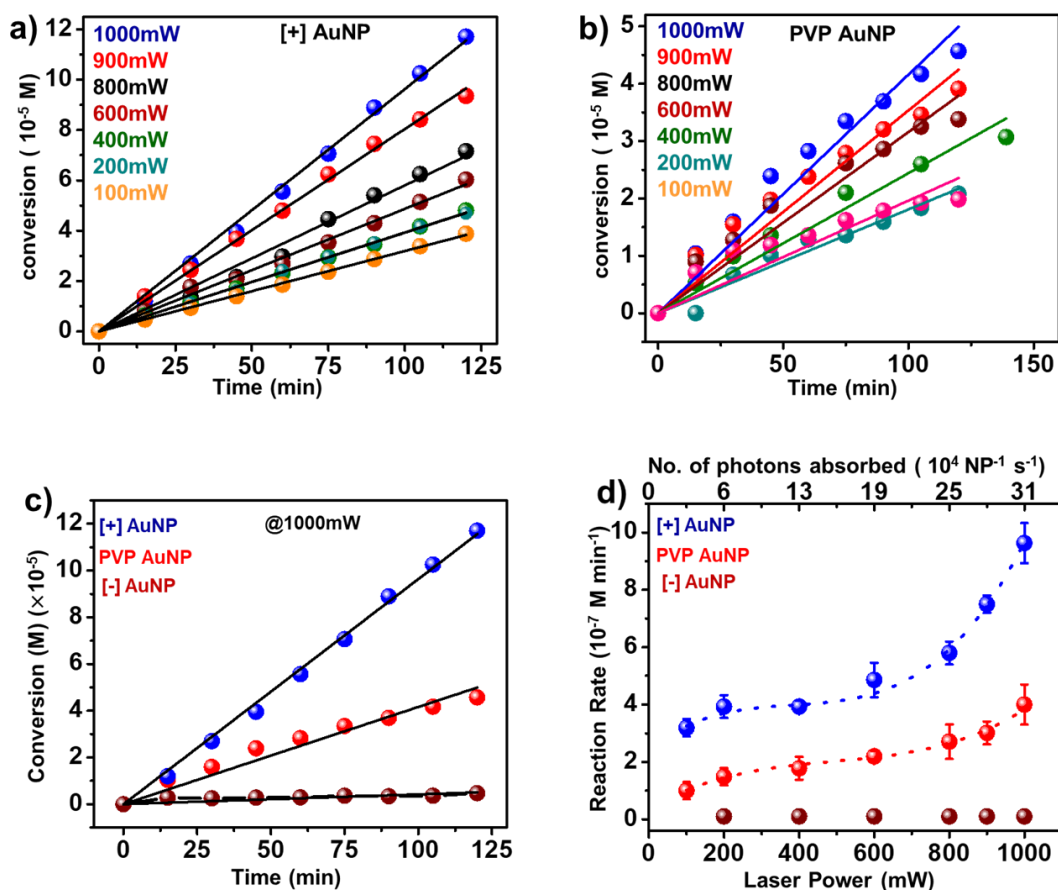


Figure 4.6. Intensity dependent photocatalytic reduction of ferricyanide with different sets of AuNPs. Linearized fit for the first order analysis by tracking the absorbance at 420 nm at seven different intensities with a) [+] and b) PVP AuNPs as the photocatalysts. c) Linearized first-order fits following the spectral changes at 420 nm during the photocatalytic reduction of ferricyanide by various AuNP systems at 40 °C, under CW 532 nm laser irradiation for ~ 2 h (intensity 1000 mW). d) The corresponding variation in the rate constant values as a function of light intensity (or photon flux), in the presence of different AuNP photocatalysts. The dashed lines are for guiding the eye to show the superlinear increase in the rate constant.

4.4.3. Photocatalytic Reduction of NAD^+ to NADH :

Our next focus was to check whether the idea of electrostatics assisted catalysis was potent enough to drive an important and challenging photocatalytic multielectron reaction. For this, the two electrons – 1 proton ($2e^- - 1H^+$) photocatalytic reduction of NAD^+ to NADH was selected, which has gained recent attention due to its significance in the area of redox biocatalysis.^{35,36} NADH is an important co-factor molecule which acts as a hydride ion currency for numerous biological transformations catalyzed by different oxidoreductase enzymes like dehydrogenases, peroxidases, oxidases etc (**Figure 4.7**).^{35,36}

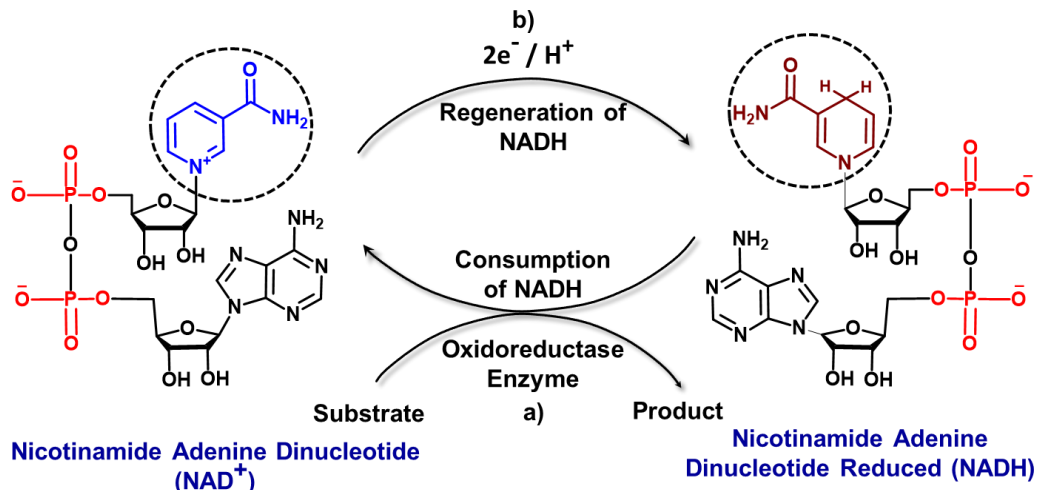
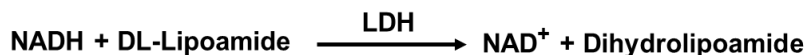


Figure 4.7. Schematic representation of an oxidoreductive enzymatic cycle using NADH as a cofactor. a) NADH is consumed in the oxidoreductase biotransformation. b) Regeneration pathway of NADH from NAD⁺

Most of the previously reported photocatalysts require additional co-catalyst (Pt), photosensitizer (Eosin Y) or an electron mediator (Rh or Ir based metal chelating agents) for the efficient transfer of multiple electrons to NAD⁺.³⁵⁻⁴⁹ Therefore, performing efficient photocatalytic regeneration of NADH by AuNPs, without the aid of any co-catalyst or electron mediator, will prove the exclusivity of NP catalyst-reactant interaction in facilitating multielectron reactions.

The reduction of NAD⁺ to NADH essentially involves the transfer of a hydride ion ($2e^- - 1H^+$), and the progress of the reaction can be monitored using UV-Vis spectroscopy (**Figure 4.8**).^{35,36} NAD⁺ exhibits a characteristic absorption maxima at ~ 260 nm due to $\pi-\pi^*$ transitions in nicotinamide and adenine moieties; whereas the absorption of NADH is centered at ~ 340 nm (**Figure 4.8**).³⁵ The reduction of NAD⁺ to the desired product 1,4-NADH is oftentimes contaminated with by-products like NAD₂ dimer and 1,6-NADH, both of which have absorption peaks at ~ 340 nm (**Figure 4.20 in the Appendix**).³⁵ Interestingly, only 1,4-NADH is enzymatically active among other by-products for further bio-transformations.³⁵ Accordingly, an enzymatic assay with lipoamide dehydrogenase (LDH) based on Sigma Quality Control Test Procedure (EC 1.8.1.4) has been conventionally used for the identification and quantification of NADH (see **experimental section 4.3.8 for more details**).^{56,57} During the assay, only the enzymatically active NADH will be converted to NAD⁺, as per the following reaction.^{56,57}



Thus, the subsequent decrease in the absorbance at ~ 340 nm can be used to estimate the amount of 1,4 NADH formed through the photocatalytic reduction of NAD^+ ($\epsilon \text{ NADH} = 6220 \text{ M}^{-1}\text{cm}^{-1}$) (Figures 4.8 and 4.21 in Appendix).

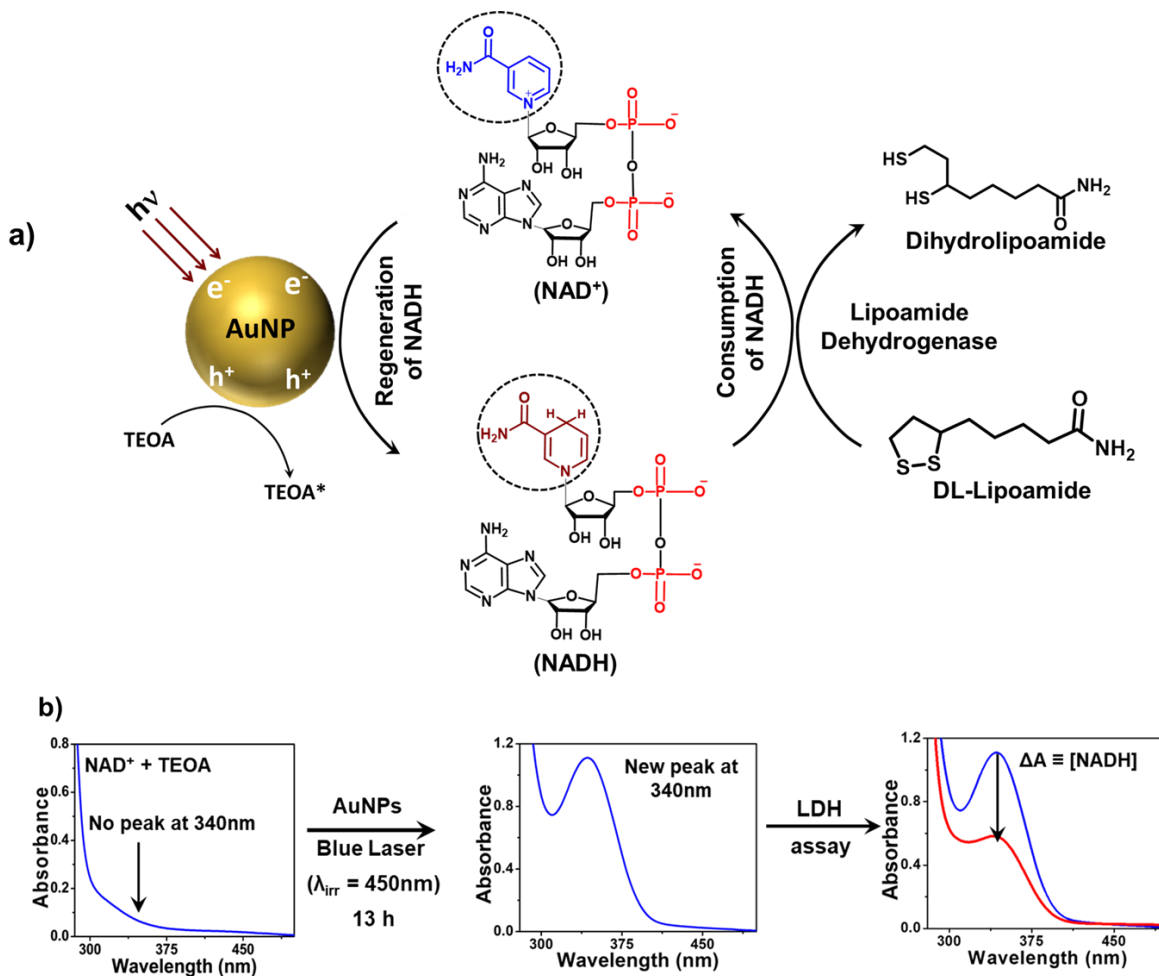


Figure 4.8: a) Schematic representation of AuNP photocatalyzed regeneration of NADH, and the lipoamide dehydrogenase assay adopted for quantifying the formation of NADH. b) Protocol for monitoring the reduction process with UV-Vis spectroscopy, and the quantitative detection of the NADH through lipoamide dehydrogenase assay.

The photocatalytic reduction of NAD^+ with AuNPs was performed in the presence of triethanolamine (TEOA) as a hole scavenger, under the continuous irradiation with a 450 nm laser (800 mw cm^{-2}). The photoexcitation of AuNP leads to the generation of e^- - h^+ pairs, and the electrons will participate in the reduction of NAD^+ , whereas the holes will be scavenged by TEOA to regenerate the photocatalyst.³⁵ In a typical photocatalytic experiment, a mixture of NAD^+ (1mM), TEOA (1 M) and AuNP (absorbance ~ 1.3) in phosphate buffer (50 mM, pH ~ 8) was

continuously irradiated for 13 h (see **Experimental Section 4.3.7** for more details). The AuNP photocatalyst was separated before performing the LDH assay for the quantification of the desired product NADH. Irradiation experiments in the absence of a photocatalyst, and the presence of [-] AuNP photocatalyst showed a noticeable increase in the absorbance peak at ~ 340 nm (**Figures 4.9 a and 4.22 a,b in the Appendix**). Whereas, a strong and prominent peak was observed at ~ 340 nm when [+] AuNP was used as the photocatalyst, indicating the formation of NADH in a decent yield (**Figures 4.9 a, and 4.23 in the Appendix**). Remarkably, the enzymatic LDH assay revealed that the amount of NADH formed with [+] AuNP photocatalyst was at least ~ 10 times higher than with [-] AuNPs ($\sim 60 \mu\text{M}$ vs $\sim 5 \mu\text{M}$, respectively) (**Figures 4.9 b, 4.22 c,d, and 4.23 b in the Appendix**). The formation of NADH with [+] AuNPs was further corroborated with detailed NMR analysis (**Figure 4.24 in the Appendix**). The higher catalytic activity of [+] AuNPs is attributed to a strong electrostatic attraction between [+] AuNP catalyst and NAD^+ reactant. As a result, the channelling and local concertation of NAD^+ increases around [+] AuNP, thereby enhancing the probability of photocatalytic multielectron transfer.

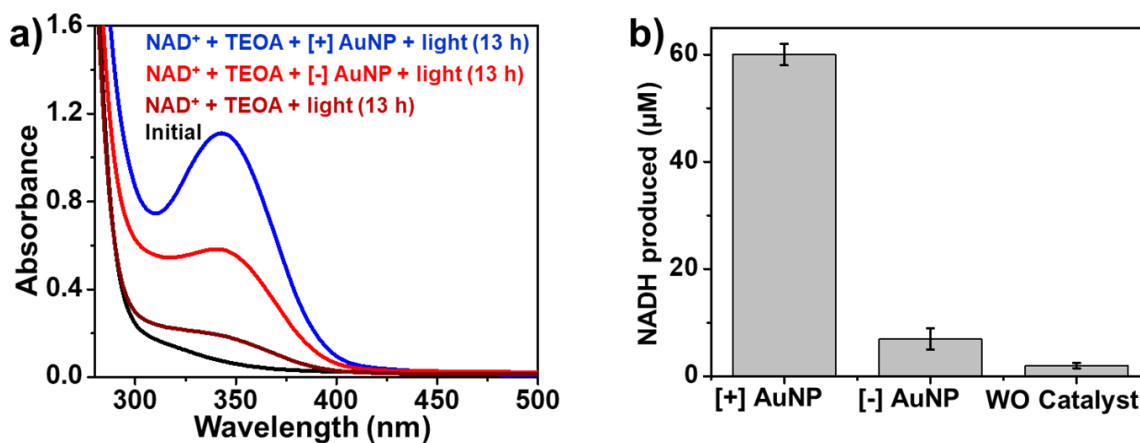


Figure 4.9. a) UV-Vis spectral change of the reaction mixture (NAD^+ and TEOA) before and after irradiation (~ 13 h) in the presence and absence of different AuNPs (~ 5 nM). b) Bar diagram showing the difference in concentration of NADH (as calculated from the LDH assay) produced during the photocatalytic reaction in presence and absence of different AuNP catalysts.

4.4.4. Role of Electrostatic Interaction:

The exclusivity of favorable electrostatic interaction was confirmed by controlling the positive surface potential around the AuNP photocatalyst. For this, the [+] TMA ligand on AuNP surface was systematically diluted with 20 %, 50 % and 80 % [-] MUA ligands to yield heterogeneously charged $[+/-]_4$, $[+/-]_1$ and $[-/+]_4$ AuNPs, respectively (**Figures 4.10 a and 4.5 d,e**).^{52,53} The on-NP

ratio was estimated to be $[+/-]_{4.8}$, $[+/-]_{1.2}$ and $[-/+]_{3.3}$, using NMR studies as reported in the previous works.^{52,53} A steady rise in the NADH formation was obtained as the percentage of positive charges increased on the surface of AuNP photocatalysts (**Figures 4.10 b and 4.25, 4.26 in Appendix**). Similarly, the catalytic performance of $[+]$ AuNP was superior to AuNP functionalized with neutral EG₃SH ligand. Thus, a clear dominance of $[+]$ AuNP, without any co-catalyst or electron mediator, demonstrates the decisive role of favorable NP-reactant interaction in driving the direct multielectron transfer from photocatalyst to NAD⁺ reactant.

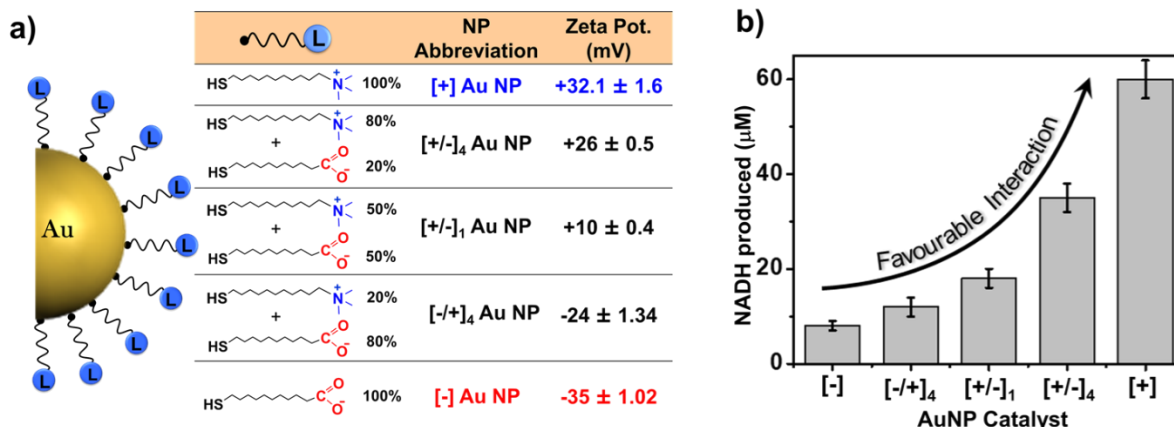


Figure 4.10. Proof for electrostatically assisted multielectron transfer in the photocatalytic regeneration of NADH. a) Different AuNP catalysts with varying surface potential have been used in the photocatalytic regeneration of NADH. b) Bar diagram showing the variation in NADH formation as a function of AuNP surface charge.

4.4.5. Determination of NAD⁺ to NADH Reduction Pathway:

As per recent literature, there is a possibility for this reaction to undergo either through a light dependent or through a light independent pathway (**Figure 4.11 a,b**). In the light dependent pathway the hot electrons are involved in the reduction of NAD⁺, whereas the hot holes are scavenged by TEOA to complete the other half of the redox cycle (**Figure 4.11 a**). However, in light independent pathway, the hot holes first oxidize the TEOA to glycoaldehyde followed by the reduction of NAD⁺ by the as formed glycoaldehyde (**Figure 4.11 b**).⁵⁸ Here the reduction step of NAD⁺ with glycoaldehyde is independent of light irradiation and can proceed under dark condition. To test this hypothesis, mixture of TEOA (1M) and $[+]$ AuNPs were irradiated for 13 h under our experimental condition, and then NAD⁺ (1mM) was added to the solution and kept under dark for another 13 h. The rationale is, if the reduction follows the light independent pathway then

there should be a reduction of NAD^+ under dark condition by glycoaldehyde formed in the light reaction. No reduction of NAD^+ under dark condition (**Figure 4.11 c**) clearly confirmed that, under our experimental condition, the reduction of NAD^+ follows a light dependent pathway where the hot electrons are responsible for the reduction process and the hot holes are scavenged by TEOA to complete the full redox cycle.

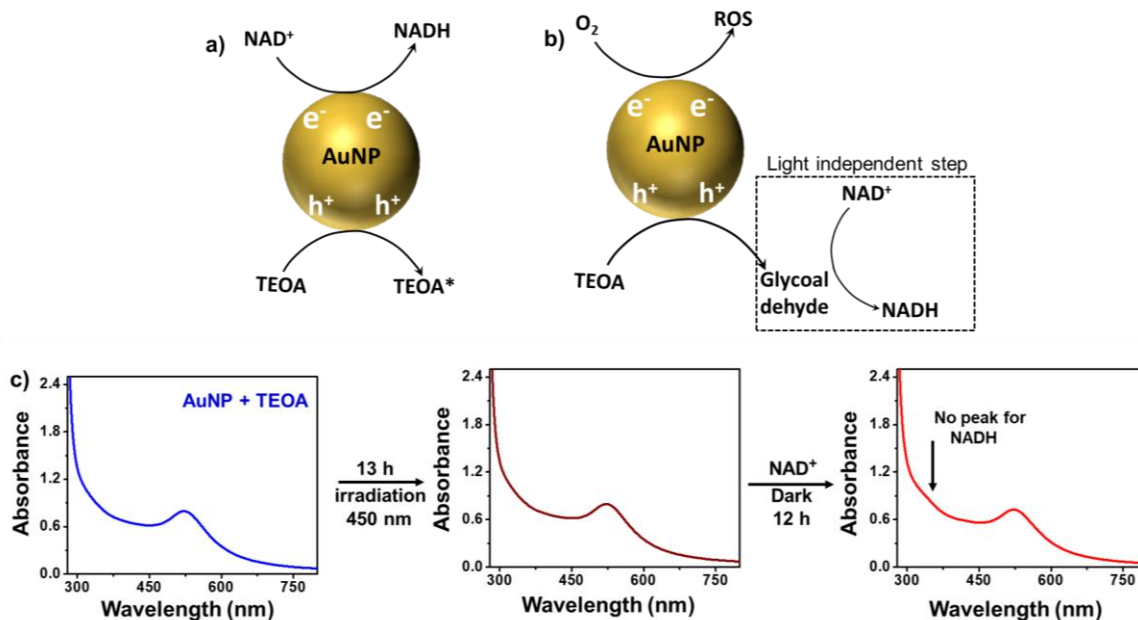


Figure 4.11. Reaction mechanism for the photogeneration of NADH using TEOA. a) Schematic illustration of light dependent pathway with a simultaneous TEOA oxidation and NAD^+ reduction. b) Schematic illustration of light independent pathway which involves the oxidation of TEOA to glycoaldehyde, followed by reduction of NAD^+ with glycoaldehyde in absence of light. c) Progress of NADH generation under dark by adding NAD^+ to pre-irradiated solution of $[+]$ AuNP and TEOA. Appearance of no peak at 340 nm under dark confirms the light dependent pathway to be the dominant mechanism under the present experimental condition.

4.4.6. Intensity Dependent Study:

Next, we discuss on the active participation of hot electrons, and the kinetics of multielectron transfer process. A detailed intensity dependent kinetic analysis was performed to confirm the involvement of multielectron transfer in the photocatalytic reduction of NAD^+ . As shown in **Figure 4.12 a**, the formation of NADH product increased superlinearly with increase in the photon flux, which is a characteristic feature of a multielectron transfer process (see **Figures 4.27 and 4.28 in the Appendix for more detail**). Recently, Jain and co-workers have proposed a heuristic model to explain super-linearity in photocatalytic reduction of CO_2 with plasmonic AuNPs.⁵⁹ As

per this model, the plasmon excitation is considered as a reagent, and hence the free energy contribution from this reagent should be included in the kinetic analysis of a photochemical reaction.⁵⁹ Accordingly, the following rate equation has been derived to include the free energy contribution from plasmonic excitation:⁵⁹

$$RT \ln \frac{R_f}{R_b} = -\Delta G_{dark} + \frac{z E_{ib} \sigma \eta_{ib} I}{h\nu k_{nr}}$$

Where, R_f and R_b is the forward and backward reaction rates respectively. z is the no. of e^-h^+ pairs involved in the reaction, E_{ib} is the interband energy gap, σ is the absorption cross section of NP, η_{ib} is the efficiency of conversion of plasmon excitation, I is the intensity of light and k_r is the rate of recombination. The equation essentially shows that the rate (or product formation) of a photochemical reaction is exponentially dependent on the intensity of light. Specifically, the higher the intensity of light, the higher will be the free energy contribution of $e^- - h^+$ pair, and larger will be the product formation. This model has been proposed to be universal, and hence was validated in the present Chapter by extracting the data from our intensity dependent photocatalytic experiments. A linear dependence of $RT \ln C_{NADH}$ on the intensity of light confirmed the indispensable contribution of the photoexcited $e^- - h^+$ pairs in driving the multielectron reduction of NAD^+ (Figure 4.12 b).

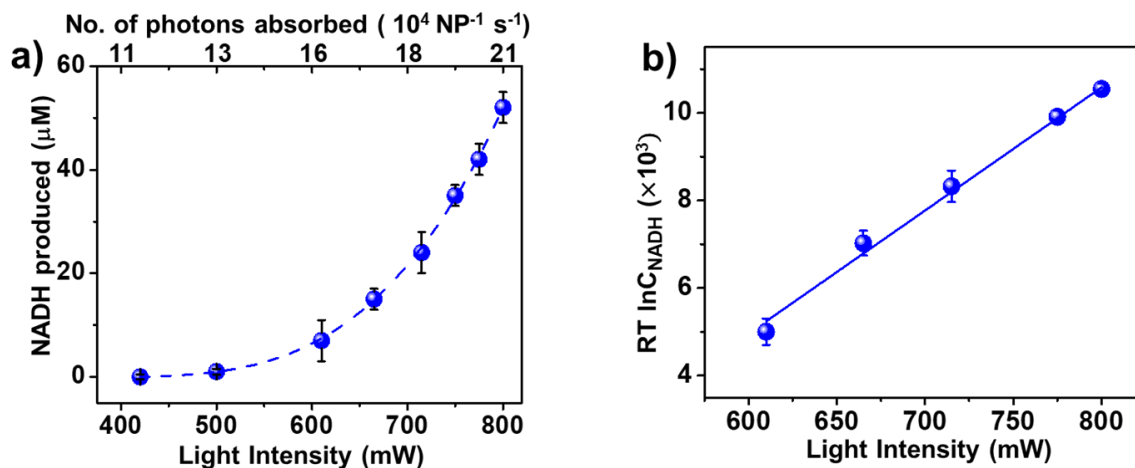


Figure 4.12. Intensity dependent photocatalytic NADH generation with [+] AuNP as the catalyst. a) Variation in the formation of NADH as a function of light intensity (or photon flux), for the photocatalytic reduction of NAD^+ by [+] AuNP photocatalyst. The dashed lines are the guide to the eye to show the superlinear increase in the photocatalytic regeneration of NADH cofactor. b) The linearized first-order fit for the variation in $RT \ln C_{NADH}$ as a function of light intensity. All the

photocatalytic experiments were performed using a 450 nm laser for ~ 13 h. The concentration of NADH regenerated was estimated using LDH assay in all the photocatalytic studies.

4.4.7. Hot Electron vs Photothermal Heating:

To consider the effect of plasmonic heating, we performed a reaction under dark condition at an elevated temperature of 50⁰C, which was measured to be the bulk temperature during the irradiation process. Considering the higher thermal conductivity of water, and our present experimental condition which consists of well dispersed colloidal NP catalyst and a CW light irradiation, the difference between bulk temperature and that on the surface of NP (ΔT) will be negligible and can be expressed as⁵⁹⁻⁶⁰

$$\Delta T = T_s - T_{bulk} = \frac{\sigma I}{4\pi k r}$$

Where, 'r' is the radius of the AuNP which is ~ 6 nm in the present study, ' σ ' is the absorption cross section at the maxima of LSPR and reported to be 50 nm² for 12 nm AuNPs, 'I' is the intensity of light and 'k' is the thermal conductivity of water (0.6 w m⁻¹ K⁻¹). With all these values, the temperature difference at an intensity as high as 1kW/cm² would be in the order of 10⁻² K.^{59,60} So under our experimental condition the bulk temperature (50⁰C) can be considered as a proxy for the surface temperature of AuNPs.

A negligible generation of NADH under dark condition at 50⁰C (**Figure 4.13**) eliminates the effect of plasmonic heating. Although the above experiments confirm the contribution of hot electrons, the effect of photothermal heating cannot be completely ruled out. Separate detailed studies will be required to disentangle the relative contribution of hot electrons and the photothermal heating, which is beyond the scope of the present interest.

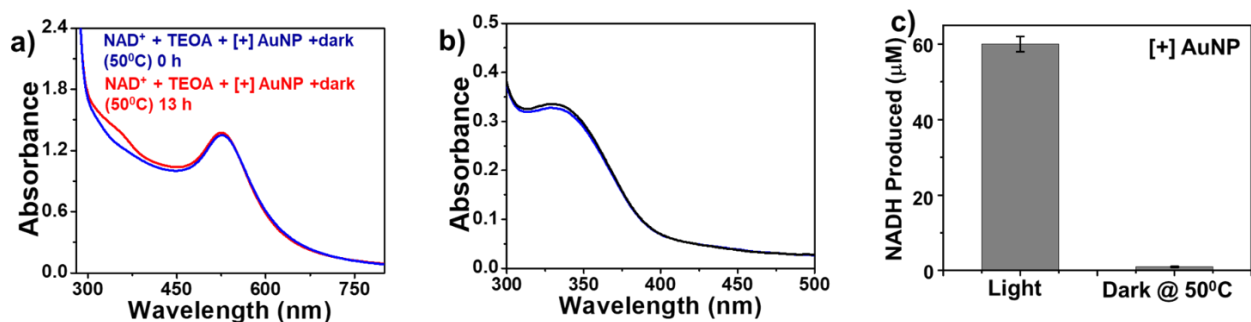


Figure 4.13. Effect of photothermal heating on the reduction of NAD⁺. a) Progress of the reduction of NAD⁺ by tracking the absorbance change with [+] AuNP, under dark at 50⁰C. b) Lipoamide

dehydrogenase assay with the reaction mixture. c) Comparison between the concentrations of NADH produced during the reaction with [+] AuNP, under light and dark conditions.

4.4.8. Wavelength dependent photocatalytic reduction of NAD⁺ (intraband vs interband transition):

Wavelength dependent photocatalytic experiments were performed to ascertain the role of hot electrons in driving the photocatalytic reduction of NAD⁺. **Figure 4.14** shows a comparison of photocatalytic NADH generation at two different excitation wavelengths (450 nm and 532 nm) keeping the irradiation intensity constant at 800 mW/cm² (measured by using an optical power meter from Newport. Model: 842.PE). A higher generation of NADH at 450 nm excitation compared to that of 532 nm can be explained in terms of interband vs intraband transition. In plasmonic metal NPs, the nonradiative decay of surface plasmon resonance leads to the generation of hot charge carriers either through intraband ('s' to 'sp') or through interband ('d' to 'sp') transition^{6,8,60,61}

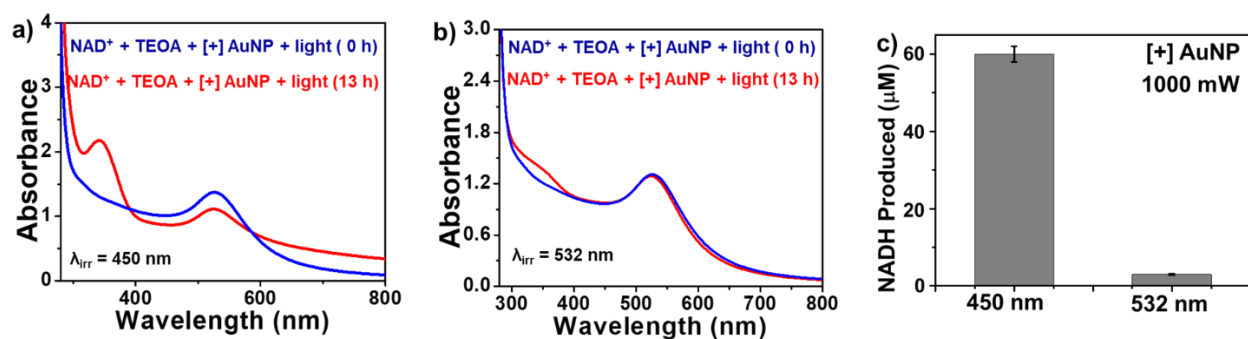


Figure 4.14. Effect of irradiation wavelength on photocatalytic NADH generation. Progress of the photocatalytic reduction of NAD⁺ with [+] AuNPs under a) 450 nm and b) 532 nm CW laser irradiation for 13 h. c) Bar diagram comparing the formation of NADH with [+] AuNP under 450 nm and 532 nm of laser irradiation. The irradiation intensity was kept constant at 800 mW/cm² for both the laser excitations.

For plasmonic AuNPs, there is a strong overlap between the LSPR and the higher energy interband transition.^{6,62} This makes the interband d-sp excitation as the dominant plasmon decay pathway at energies where it's energetically accessible.⁶¹ Thus, the higher energy 450 nm excitation generates hot charge carriers predominantly via interband 'd' – 'sp' transition, compared to the 's' to 'sp' transition for 532 nm excitation. Now, the 'd' band hole created through interband transition is typically 1.9 eV more energetic than a 'sp' band hole created through intraband transition.⁶² The more oxidizing power of the 'd' band hole is beneficial to complete the oxidation half cycle for a

multielectron reduction process.⁶² Moreover, the hot electrons and holes generated through the interband transitions reside in two different bands ('d' and 'sp') and hence exhibits a higher lifetime (~1 ps) compared to that in intraband transition.^{6,62} Therefore, the 450 nm excitation in the region of strong interband absorption exhibited a higher generation of NADH compared to that at 532 nm excitation. Thus the wavelength dependent experiments prove that the photocatalytic reduction of NAD⁺ is driven by the hot electrons generated predominantly via 'd' – 'sp' transition.

4.4.9. Flexibility of the Strategy:

One of the main flexibilities of the present idea of electrostatically assisted catalysis is the ease with which it can be coupled with other existing strategies, to improve the overall catalytic performances. As a proof of concept, the catalytic properties of AuNPs were tested by incorporating a commonly used electron mediator Eosin Y. It is worth mentioning that, dedicated synthesis procedures or advanced fabrication protocols are commonly used to integrate such electron mediators/co-catalysts in the plasmonic catalytic system.^{37,38} In the present work, the negative charges on Eosin Y ([−] EY) paved the way for the strong complexation with [+] AuNPs through electrostatic attraction (**Figure 4.15 a**). The mixture of [+] AuNP and [−] EY was stirred for ~ 30 min prior to the reaction, to ensure complete complexation. A dramatic increase in the photocatalytic activity of [+] AuNP was witnessed in the presence of [−] EY. For instance, the amount of NADH produced by [+] AuNP increased from ~ 60 μM to ~ 110 μM, in the presence of [−] EY (**Figure 4.15 b,c and Figure 4.29 a,c in Appendix section**). The conversion yield of ~ 10 % obtained with [+] AuNP::[−] EY nanohybrid catalyst is comparable or greater than most of the catalytic systems reported based on plasmonic NP, with the added advantage of being structurally less complex. More strikingly, the time required for the NADH production reduced drastically from ~ 13 h to ~ 1 h, in the presence of [−] EY. Control experiment shows that [−] EY fail to photocatalyze the reduction of NAD⁺ by itself, thereby overruling the direct involvement of EY in the observed catalytic properties of [+] AuNP::[−] EY nanohybrid catalyst (**Figure 4.15 b and Figure 4.30 in Appendix section**). Interestingly, the presence of [−] EY failed to improve the photocatalytic activity of [−] AuNP, due to the unfavorable electrostatic repulsion (**Figure 4.15 b and Figure 4.29 b,d in Appendix**). The turn-over-number (TON) for the [+] AuNP::[−] EY nanohybrid catalyst was ~ 12 folds higher than that of [−] AuNP::[−] EY, which further confirms the potent role of electrostatic interaction in photocatalytic formation of NADH cofactor (**Figure 4.15 b**). Detailed procedure for the TON calculation is given in Experimental section 4.3.8). A

detailed time-dependent analysis further revealed a turn-over-frequency (TOF) of $\sim 400 \text{ NP}^{-1} \text{ min}^{-1}$ for [+] AuNP:::[-] EY nanohybrid photocatalyst (**Figures 4.15 c and 4.31 in the Appendix**. Detailed procedure for the TOF calculation is given in Experimental section 4.3.8), which proves the importance of electrostatic interactions in completing the reduction process in a short time (1 h).

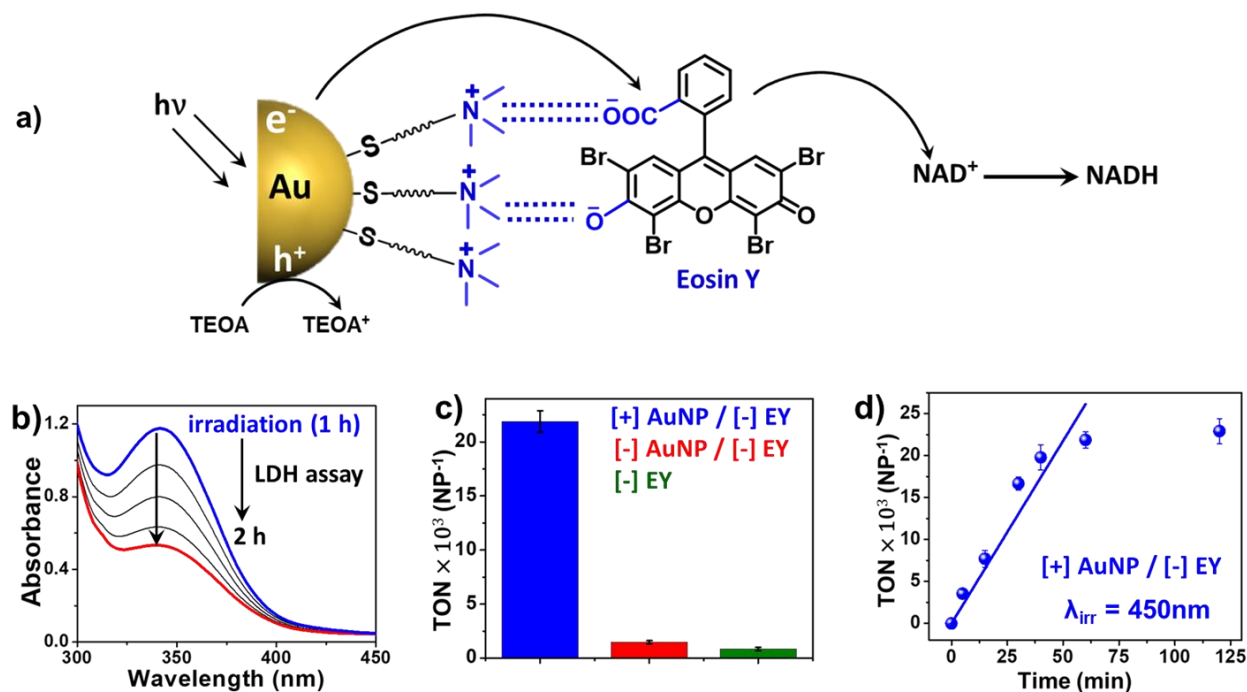


Figure 4.15. Flexibility in coupling the idea of interaction driven photocatalysis with electron mediator. a) Schematic representation of electrostatics assisted complexation between [+] AuNP and [-] EY molecule, leading to the fast funneling of hot electrons from AuNP photocatalyst to NAD⁺ reactant, via EY. b) Time dependent spectral changes in the absorbance of photocatalytically generated NADH, during the LDH assay. c) Bar diagram showing the Turnover Number (TON) for different photocatalysts. (d) Estimation of Turnover Frequency (TOF) by studying the time dependent variation in the TON of NADH during the photocatalytic reduction of NAD⁺ with [+] AuNP:::[-] EY hybrid catalyst, under ~ 1 h irradiation with 450 nm laser (800 mW).

4.5. Conclusion

In conclusion, establishing a favorable catalyst-reactant interaction paved the way for the photocatalytic regeneration of NADH by AuNPs, without the aid of any electron-mediator or co-catalyst. The electrostatic forces emanating from ligands on the surface of plasmonic NPs was used a tool to control the catalyst-reactant interaction. A strong electrostatic attraction between [+] AuNP photocatalyst and [-] NAD⁺ reactant increased the channeling and local concentration of the reactants around the photocatalyst, thereby enhancing the probability of multielectron transfer.

Systematic studies by varying the surface potential of AuNPs proved the exclusivity of electrostatic interactions in the photocatalytic regeneration of NADH. A superlinear increase in the rate of NADH formation as a function of intensity of light proved the involvement of multiple charge carriers from AuNPs photocatalyst. Further, the potency of electrostatics was used to bind [+] AuNP with a [-] electron mediator, to show the flexibility in coupling the present idea of interaction driven photocatalysis with existing strategies to boost the regeneration of NADH. Strikingly, only ~ 1 h of irradiation was sufficient to produce twice the amount of NADH cofactor, as compared to that in the absence of an electron mediator. The photocatalytic performances of [+] AuNP were in comparable or greater than most of the catalytic systems reported based on plasmonic NP, with the added advantage of being structurally less complex. The exclusive role of electrostatics in the photocatalytic regeneration of NADH presented here can serve as a generic approach for other useful photocatalytic multielectron reactions as well.

Thus, the first part of the thesis reveals the prudent role of NP-reactant interaction (emanated from the surface ligands) in dictating the catalytic property of metal NPs. The *idea of interaction* developed in the first part was further utilized in the next Chapter to circumvent the “*ligand poisoning*” effect in metal NP photocatalysis. Finally, the knowledge gained from these two Chapters was employed to perform a challenging multielectron reaction without the aid of any electron mediators or co-catalysts. Thus, the present thesis introduces a new strategy of “*ligand directed catalysis*” for addressing the long standing challenge of “*ligand poisoning*” in the area of NP catalysis. In future, *the idea of interaction* can be replicated in more challenging multielectron reactions like CO₂ reduction or N₂ reduction, where the interaction between the reactant molecules (CO₂ or N₂) and the catalyst, can even play an important role in dictating the product selectivity.

4.6. References

1. Yu, S.; Wilson, A. J.; Kumari, G.; Zhang, X.; Jain, P. K. Opportunities and Challenges of Solar-Energy-Driven Carbon Dioxide to Fuel Conversion with Plasmonic Catalysts. *ACS Energy Lett.* **2017**, *2*, 2058–2070.
2. Medford, A. J.; Hatzell, M. C. Photon-Driven Nitrogen Fixation: Current Progress, Thermodynamic Considerations, and Future Outlook. *ACS Catal.* **2017**, *7*, 2624–2643.
3. Wang, Q.; Domen, K. Particulate Photocatalysts for Light-Driven Water Splitting: Mechanisms, Challenges, and Design Strategies *Chem. Rev.* **2020**, *120*, 919–985.

4. Shaik, F.; Peer, I.; Jain, P. K.; Amirav, L. Plasmon-Enhanced Multicarrier Photocatalysis. *Nano Lett.* **2018**, *18*, 4370–4376.
5. Cate, S. T.; Sandeep, C. S. S.; Liu, Y.; Law, M.; Kinge, S.; Houtepen, A. J.; Schins, J. M.; Siebbeles, L. D. A. Generating Free Charges by Carrier Multiplication in Quantum Dots for Highly Efficient Photovoltaics. *Acc. Chem. Res.* **2015**, *48*, 74–181.
6. Kim, Y.; Smith, J. G.; Jain, P. K. Harvesting Multiple Electron–Hole Pairs Generated through Plasmonic Excitation of Au Nanoparticles. *Nat. Chem.* **2018**, *10*, 763–769.
7. Jensen, S. C.; Homan, S. B.; Weiss, E. A. Photocatalytic Conversion of Nitrobenzene to Aniline through Sequential Proton-Coupled One-Electron Transfers from a Cadmium Sulfide Quantum Dot. *J. Am. Chem. Soc.* **2016**, *138*, 1591–1600.
8. Aslam, U.; Rao, V. G.; Chavez, S.; Linic, S. Catalytic Conversion of Solar to Chemical Energy on Plasmonic Metal Nanostructures. *Nat. Catal.* **2018**, *1*, 656–665.
9. Rao, V. G.; Aslam, U.; Linic, S. Chemical Requirement for Extracting Energetic Charge Carriers from Plasmonic Metal Nanoparticles to Perform Electron-Transfer Reactions. *J. Am. Chem. Soc.* **2019**, *141*, 643–647.
10. Seemala, B.; Therrien, A. J.; Lou, M.; Li, K.; Finzel, J. P.; Qi, Ji.; Nordlander, P.; Christopher, P. Plasmon-Mediated Catalytic O₂ Dissociation on Ag Nanostructures: Hot Electrons or Near Fields? *ACS Energy Lett.* **2019**, *4*, 8, 1803–1809.
11. Zhang, Y.; He, S.; Guo, W.; Hu, Y.; Huang, J.; Mulcahy, J. R.; Wei, W. D. Surface-Plasmon-Driven Hot Electron Photochemistry. *Chem. Rev.* **2018**, *118*, 2927–2954.
12. Chakraborty, I. N.; Roy, S.; Devatha, G.; Rao, A.; Pillai, P. P. InP/ZnS Quantum Dots as Efficient Visible-Light Photocatalysts for Redox and Carbon–Carbon Coupling Reactions. *Chem. Mater.* **2019**, *31*, 2258–2262.
13. Kamat, P. V. Semiconductor Surface Chemistry as Holy Grail in Photocatalysis and Photovoltaics. *Acc. Chem. Res.* **2017**, *50*, 527–531.
14. Xie, W.; Schlücker, S. Hot Electron-Induced Reduction of Small Molecules on Photorecycling Metal Surfaces. *Nat. Commun.* **2015**, *6*, 7570.
15. Zhao, L-M.; Meng, Q-Y.; Fan, X-B.; Ye, C.; Li, X-B.; Chen, B.; Ramamurthy, V.; Tung, C-H.; Wu, L-Z. Photocatalysis with Quantum Dots and Visible Light: Selective and Efficient Oxidation of Alcohols to Carbonyl Compounds through a Radical Relay Process in Water. *Angew. Chem. Int. Ed.* **2017**, *56*, 3020–3024.

16. Taniguchi, Y.; Takishita, T.; Kawai, T.; Nakashima, T. End-to-End Self-Assembly of Semiconductor Nanorods in Water by Using an Amphiphilic Surface Design. *Angew. Chem. Int. Ed.* **2016**, *55*, 2083–2086.
17. Kale, M. J.; Avanesian, T.; Christopher, P. Direct Photocatalysis by Plasmonic Nanostructures. *ACS Catal.* **2014**, *4*, 116–128.
18. Roy, S.; Roy, S.; Rao, A.; Devatha, G.; Pillai, P. P. Precise Nanoparticle–Reactant Interaction Outplays Ligand Poisoning in Visible-Light Photocatalysis. *Chem. Mater.* **2018**, *30*, 8415–8419.
19. Smith, J. G.; Jain, P. K. The Ligand Shell as an Energy Barrier in Surface Reactions on Transition Metal Nanoparticles. *J. Am. Chem. Soc.* **2016**, *138*, 6765–6773.
20. Dolzhnikov, D. S.; Zhang, H.; Jang, J.; Son, J. S.; Panthani, M. G.; Shibata, T.; Chattopadhyay, S.; Talapin, D. V. Composition-Matched Molecular “Solders” for Semiconductors. *Science* **2015**, *347*, 425–428.
21. Wilker, M. B.; Utterback, J. K.; Greene, S.; Brown, K. A.; Mulder, D. W.; King, P. W.; Dukovic, G. Role of Surface-Capping Ligands in Photoexcited Electron Transfer between CdS Nanorods and [FeFe] Hydrogenase and the Subsequent H₂ Generation. *J. Phys. Chem. C* **2018**, *122*, 741–750.
22. Mubeen, S.; Lee, J.; Singh, N.; Krämer, S.; Stucky, G. D.; Moskovits, M. An Autonomous Photosynthetic Device in Which All Charge Carriers Derive from Surface Plasmons. *Nat. Nanotechnol.* **2013**, *8*, 247–251.
23. Wolff, C. M.; Frischmann, P. D.; Schulze, M.; Bohn, B. J.; Wein, R.; Livadas, P.; Carlson, M. T.; Jäckel, F.; Feldmann, J.; Würthner, F.; et al. All-in-One Visible-Light-Driven Water Splitting by Combining Nanoparticulate and Molecular Co-Catalysts on CdS Nanorods. *Nat. Energy* **2018**, *3*, 862–869.
24. Maeda, K. Z-Scheme Water Splitting Using Two Different Semiconductor Photocatalysts. *ACS Catal.* **2013**, *3*, 1486–1503.
25. Marshall, S. T.; O’Brien, M.; Oetter, B.; Corpuz, A.; Richards, R. M.; Schwartz, D. K.; Medlin, J. W. Controlled Selectivity for Palladium Catalysts Using Self-Assembled Monolayers. *Nat. Mater.* **2010**, *9*, 853–858.
26. Roy, S.; Rao, A.; Devatha, G.; Pillai, P. P. Revealing the Role of Electrostatics in Gold-Nanoparticle-Catalyzed Reduction of Charged Substrates. *ACS Catal.* **2017**, *7*, 7141–7145.

27. Cui, X.; Wang, J.; Liu, B.; Ling, S.; Long, R.; Xiong, Y. Turning Au Nanoclusters Catalytically Active for Visible-Light-Driven CO₂ Reduction through Bridging Ligands. *J. Am. Chem. Soc.* **2018**, *140*, 16514–16520.
28. Lian, S.; Kodaimati, M. S.; Weiss, E. A. Photocatalytically Active Superstructures of Quantum Dots and Iron Porphyrins for Reduction of CO₂ to CO in Water. *ACS Nano* **2018**, *12*, 568–575.
29. Yu, S.; Fan, X-B.; Wang, X.; Li, J.; Zhang, Q.; Xia, A.; Wei, S.; Wu, L-Z.; Zhou, Y.; Patzke, G. R. Efficient Photocatalytic Hydrogen Evolution with Ligand Engineered All-Inorganic InP and InP/ZnS Colloidal Quantum Dots. *Nat. Commun.* **2018**, *9*, 4009.
30. Chen, G.; Xu, C.; Huang, X.; Ye, J.; Gu, L.; Li, G.; Tang, Z.; Wu, B.; Yang, H.; Zhao, Z.; et al. Interfacial Electronic Effects Control the Reaction Selectivity of Platinum Catalysts. *Nat. Mater.* **2016**, *15*, 564–569.
31. Hutton, G. A. M.; Reuillard, B.; Martindale, B. C. M.; Caputo, C. A.; Lockwood, C. W. J.; Butt, J. N.; Reisner, E. Carbon Dots as Versatile Photosensitizers for Solar-Driven Catalysis with Redox Enzymes. *J. Am. Chem. Soc.* **2016**, *138*, 16722–16730.
32. Brown, K. A.; Dayal, S.; Ai, X.; Rumbles, G.; and King, P. W. Controlled Assembly of Hydrogenase-CdTe Nanocrystal Hybrids for Solar Hydrogen Production. *J. Am. Chem. Soc.* **2010**, *132*, 9672–9680.
33. Brown, K. A.; Wilker, M. B.; Boehm, M.; Dukovic, G.; King, P. W. Characterization of Photochemical Processes for H₂ Production by CdS Nanorod–[FeFe] Hydrogenase Complexes. *J. Am. Chem. Soc.* **2012**, *134*, 5627–5636.
34. Smith, C. A.; Narouz, M. R.; Lummis, P. A.; Singh, I.; Nazemi, A.; Li, C-H.; Crudden, C. M. N-Heterocyclic Carbenes in Materials Chemistry. *Chem. Rev.* **2019**, *119*, 4986–5056.
35. Wang, X.; Saba, T.; Yiu, H. H. P.; Howe, R. F.; Anderson, J. A.; Shi, J. Cofactor NAD(P)H Regeneration Inspired by Heterogeneous Pathways. *Chem* **2017**, *2*, 621–654.
36. Lee, S. H.; Choi, D. S.; Kuk, S. K.; Park, C. B. Photobiocatalysis: Activating Redox Enzymes by Direct or Indirect Transfer of Photoinduced Electrons. *Angew. Chem. Int. Ed.* **2018**, *57*, 7958–7985.
37. Lee, M.; Kim, J. U.; Lee, K. J.; Ahn, S.; Shin, Y.-B.; Shin, J.; Park, C. B. Aluminum Nanoarrays for Plasmon-Enhanced Light Harvesting. *ACS Nano* **2015**, *9*, 6206–6213.

38. Lee, M.; Kim, J. U.; Lee, J. S.; Lee, B. I.; Shin, J.; Park, C. B. Mussel-Inspired Plasmonic Nanohybrids for Light Harvesting. *Adv. Mater.* **2014**, *26*, 4463–4468.
39. Sánchez-Iglesias, A.; Barroso, J.; Solis, D. M.; Taboada, J. M.; Obelleiro, F.; Pavlov, V.; Chuvilin, A.; Grzelczak, M. Plasmonic Substrates Comprising Gold Nanostars Efficiently Regenerate Cofactor Molecules. *J. Mater. Chem. A*, **2016**, *4*, 7045–7052.
40. Sanchez-Iglesias, A.; Chuvilin, A.; Grzelczak, M. Plasmon-Driven Photoregeneration of Cofactor Molecules. *Chem. Commun.* **2015**, *51*, 5330–5333.
41. Yadav, R. K.; Oh, G. H.; Park, N.-J.; Kumar, A.; Kong, K.; Baeg, J.-O. A Photocatalyst–Enzyme Coupled Artificial Photosynthesis System for Solar Energy in Production of Formic Acid from CO₂. *J. Am. Chem. Soc.* **2012**, *134*, 11455–11461.
42. Brown, K. A.; Wilker, M. B.; Boehm, M.; Hamby, H.; Dukovic, G.; King, P. W. Photocatalytic Regeneration of Nicotinamide Cofactors by Quantum Dot–Enzyme Biohybrid Complexes. *ACS Catal.* **2016**, *6*, 2201–2204.
43. Nam, D. H.; Lee, S. H.; Park, C. B. CdTe, CdSe, and CdS Nanocrystals for Highly Efficient Regeneration of Nicotinamide Cofactor Under Visible Light. *Small* **2010**, *6*, 922–926.
44. Zhang, S.; Shi, J.; Sun, Y.; Wu, Y.; Zhang, Y.; Cai, Z.; Chen, Y.; You, C.; Han, P.; Jiang, Z. Artificial Thylakoid for the Coordinated Photoenzymatic Reduction of Carbon Dioxide. *ACS Catal.* **2019**, *9*, 3913–3925.
45. Liu, J.; Antonietti, M. Bio-Inspired NADH Regeneration by Carbon Nitride Photocatalysis Using Diatom Templates. *Energy Environ. Sci.* **2013**, *6*, 1486.
46. Kim, J.; Lee, S. H.; Tieves, F.; Choi, D. S.; Hollmann, F.; Paul, C. E.; Park, C. B. Biocatalytic C=C Bond Reduction through Carbon Nanodot-Sensitized Regeneration of NADH Analogues. *Angew. Chem. Int. Ed.* **2018**, *57*, 13825–13828.
47. Kim, J. H.; Lee, M.; Lee, J. S.; Park, C. B. Self-Assembled Light-Harvesting Peptide Nanotubes for Mimicking Natural Photosynthesis. *Angew. Chem. Int. Ed.* **2012**, *51*, 517–520.
48. Zhang, L.; Can, M.; Ragsdale, S. W.; Armstrong, F. A. Fast and Selective Photoreduction of CO₂ to CO Catalyzed by a Complex of Carbon Monoxide Dehydrogenase, TiO₂, and Ag Nanoclusters. *ACS Catal.* **2018**, *8*, 2789–2795.
49. Wang, X.; Yiu, H. H. P. Heterogeneous Catalysis Mediated Cofactor NADH Regeneration for Enzymatic Reduction. *ACS Catal.* **2016**, *6*, 1880–1886.

50. Tien, J.; Terfort, A.; Whitesides, G. M. Microfabrication through Electrostatic Self-Assembly. *Langmuir* **1997**, *13*, 5349–5355.
51. Jana, N. R.; Peng, X. Single-Phase and Gram-Scale Routes toward Nearly Monodisperse Au and Other Noble Metal Nanocrystals. *J. Am. Chem. Soc.* **2003**, *125*, 14280–14281.
52. Rao, A.; Roy, S.; Unnikrishnan, M.; Bhosale, S. S.; Devatha, G.; Pillai, P. P. Regulation of Interparticle Forces Reveals Controlled Aggregation in Charged Nanoparticles. *Chem. Mater.* **2016**, *28*, 2348–2355.
53. Pillai, P. P.; Kowalczyk, B.; Pudlo, W. J.; Grzybowski, B. A. Electrostatic Titrations Reveal Surface Compositions of Mixed, On-Nanoparticle Monolayers Comprising Positively and Negatively Charged Ligands. *J. Phys. Chem. C* **2016**, *120*, 4139–4144.
54. Kim, Y.; Dumett Torres, D.; Jain, P. K. Activation Energies of Plasmonic Catalysts. *Nano Lett.* **2016**, *16*, 3399–3407.
55. Du, P.; Schneider, J.; Jarosz, P.; Eisenberg, R. Photocatalytic Generation of Hydrogen from Water Using a Platinum(II) Terpyridyl Acetylide Chromophore. *J. Am. Chem. Soc.* **2006**, *128*, 7726–7727.
56. Yuan, M.; Kummer, M. J.; Milton, R. D.; Quah, T.; Minter, S. D. Efficient NADH Regeneration by a Redox Polymer-Immobilized Enzymatic System. *ACS Catal.* **2019**, *9*, 5486–5495.
57. Wang, X.; Yiu, H. H. P. Heterogeneous Catalysis Mediated Cofactor NADH Regeneration for Enzymatic Reduction. *ACS Catal.* **2016**, *6*, 1880–1886.
58. Kinastowska, K.; Liu, J.; Tobin, J. M.; Rakovich, Y.; Vilela, F.; Xu, Z.; Bartkowiak, W.; Grzelczak, M. Photocatalytic Cofactor Regeneration Involving Triethanolamine Revisited: The Critical Role of Glycolaldehyde. *Appl. Catal. B Environ.* **2019**, *243*, 686–692.
59. Yu, S.; Jain, P. K. The Chemical Potential of Plasmonic Excitations. *Angew. Chem. Int. Ed.* **2020**, *59*, 2085–2088.
60. Jain, P. K. Taking the Heat Off of Plasmonic Chemistry. *J. Phys. Chem. C* **2019**, *123*, 24347–24351.
61. Brown, A. M.; Sundararaman, R.; Narang, P.; Goddard, W. A.; Atwater, H. A. Nonradiative Plasmon Decay and Hot Carrier Dynamics: Effects of Phonons, Surfaces, and Geometry. *ACS Nano* **2016**, *10*, 957–966.

62. Yu, S.; Mohan, V.; Jain, P. K. Using Plasmonically Generated Carriers as Redox Equivalents. *MRS Bull.* **2020**, *45*, 43–48.

4.7. Appendix

Photocatalytic reduction of ferricyanide with different AuNPs:

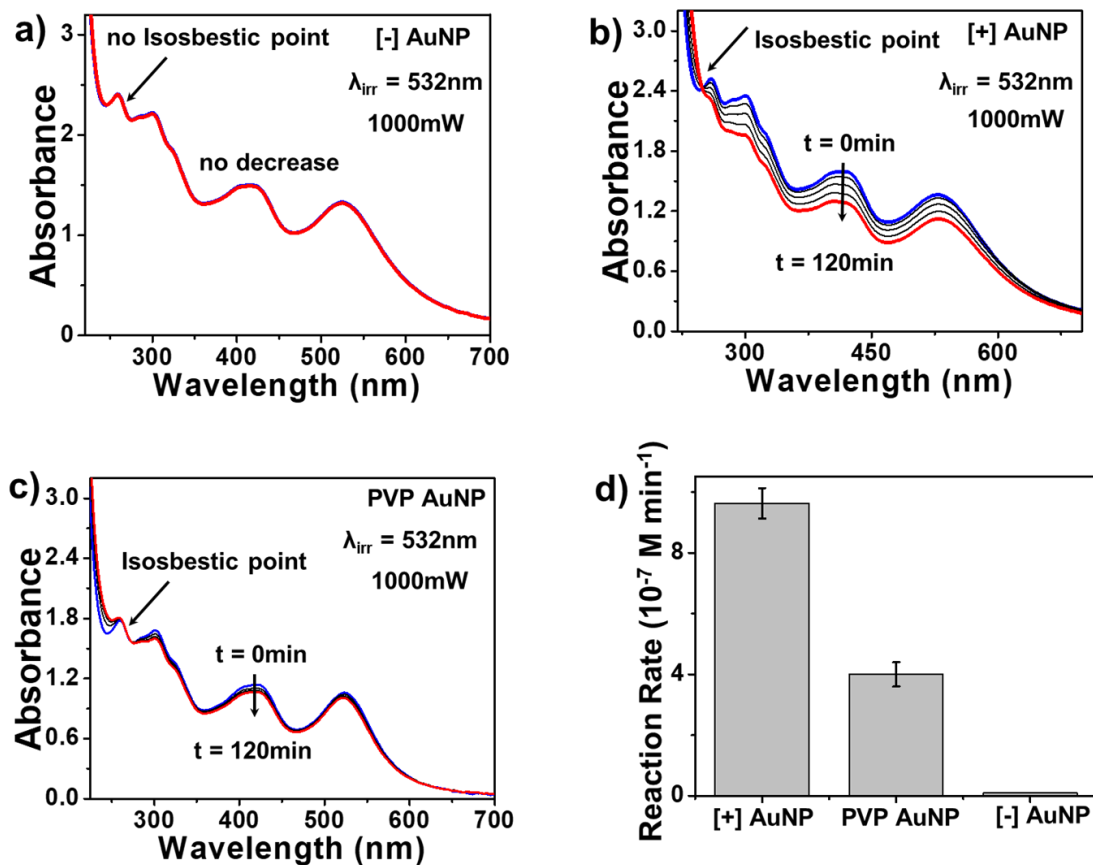


Figure 4.16. Photocatalytic reduction of ferricyanide with [+], [-] and PVP AuNPs. Progress of photocatalytic reduction of ferricyanide under CW 532nm laser irradiation at 40°C in the presence of a) [-] AuNP, b) [+] AuNP and c) PVP AuNPs by tracking the absorption changes at 15 min interval. (d) Comparison between the rate constants of ferricyanide reduction with [+], [-] and PVP AuNPs. The [-] AuNPs were completely non-catalytic whereas the rate constant for the [+] AuNPs was ~ 2 times higher than that of PVP NPs.

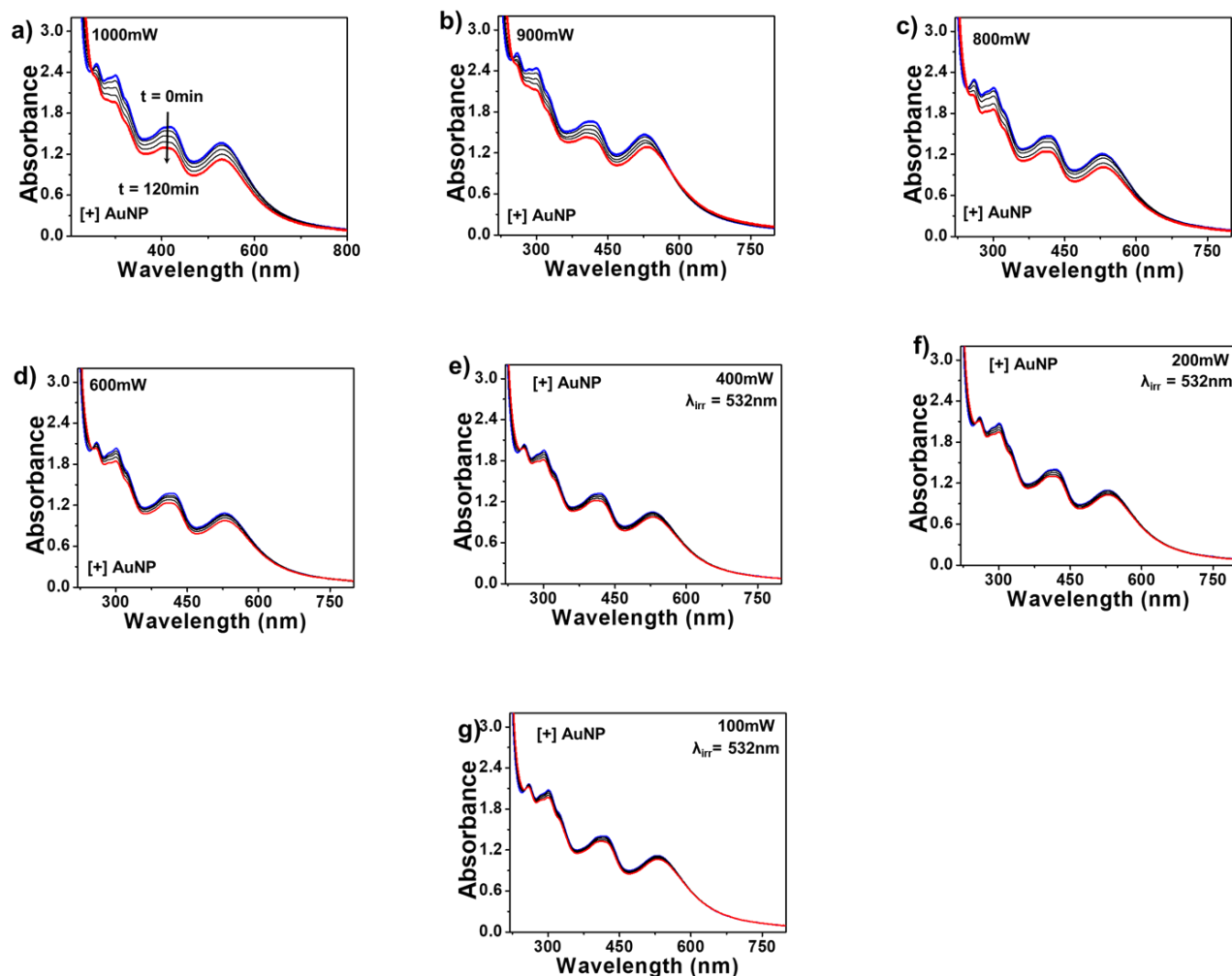


Figure 4.17. Intensity dependent catalytic reduction of ferricyanide with [+] AuNP. Progress of photocatalytic reduction of ferricyanide under CW 532 nm laser irradiation with [+] AuNPs at 40 °C by tracking the absorption changes at 15 min interval at an irradiation intensity of a) 1000 mW, b) 900 mW, c) 800 mW, d) 600 mW, e) 400 mW, f) 200 mW, and g) 100 mW.

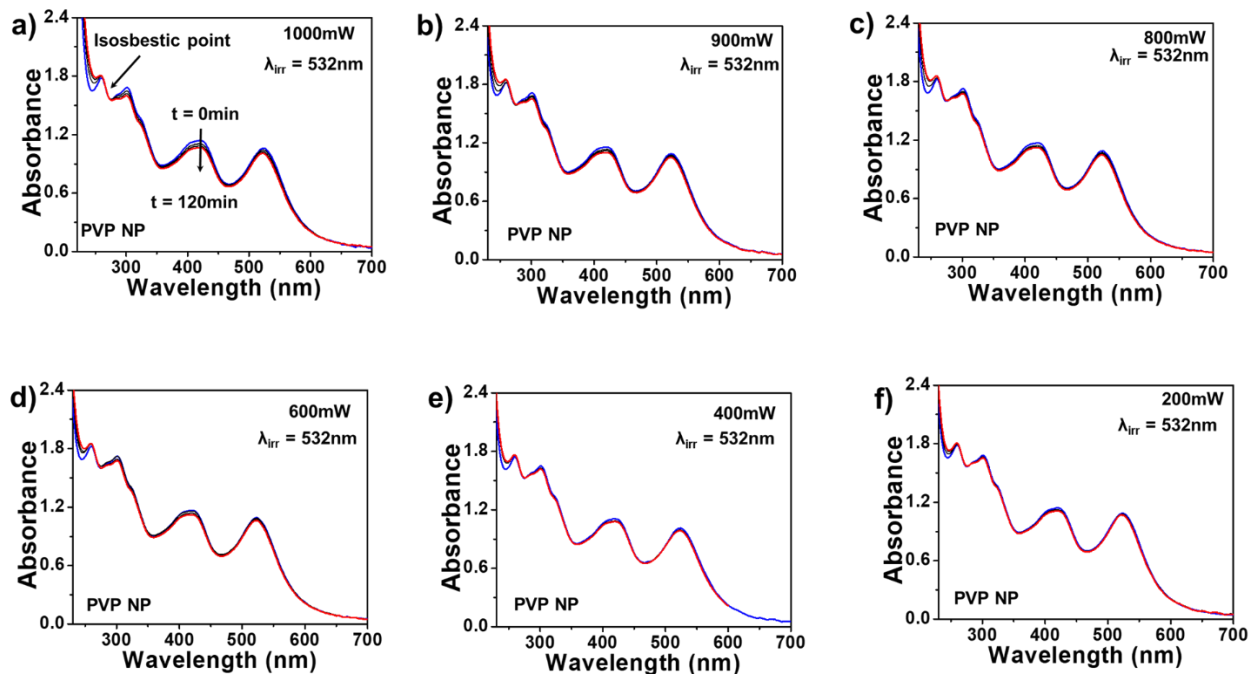


Figure 4.18. Intensity dependent catalytic reduction of ferricyanide with PVP AuNP. Progress of photocatalytic reduction of ferricyanide under CW 532 nm laser irradiation with PVP AuNPs at 40 °C by tracking the absorption changes at 15 min interval at an irradiation intensity of a) 1000 mW, b) 900 mW, c) 800 mW, d) 600 mW, e) 400 mW, and f) 200 mW.

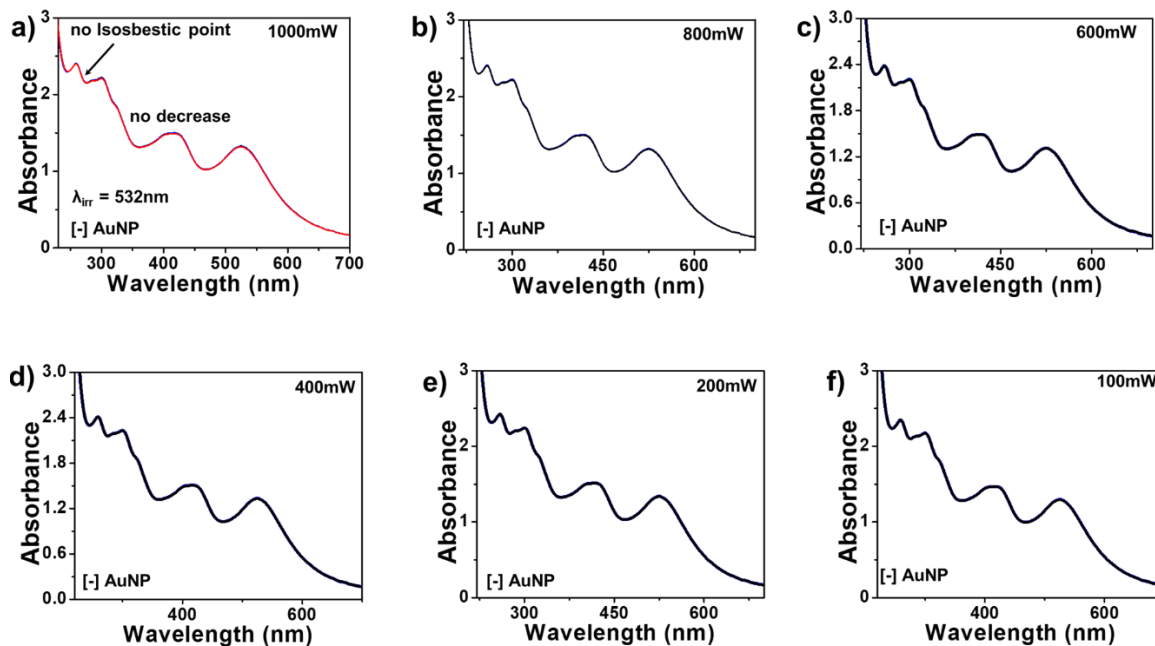


Figure 4.19. Intensity dependent catalytic reduction of ferricyanide with [-] AuNP. Progress of photocatalytic reduction of ferricyanide under CW 532 nm laser irradiation with [-] AuNPs at 40

$^{\circ}\text{C}$ by tracking the absorption changes at 15 min interval at an irradiation intensity of a) 1000 mW, b) 800 mW, c) 600 mW, d) 400mW, e) 200 mW, and f) 100 mW. The [-] AuNPs failed to photocatalyze the ferricyanide reduction irrespective of irradiation intensity.

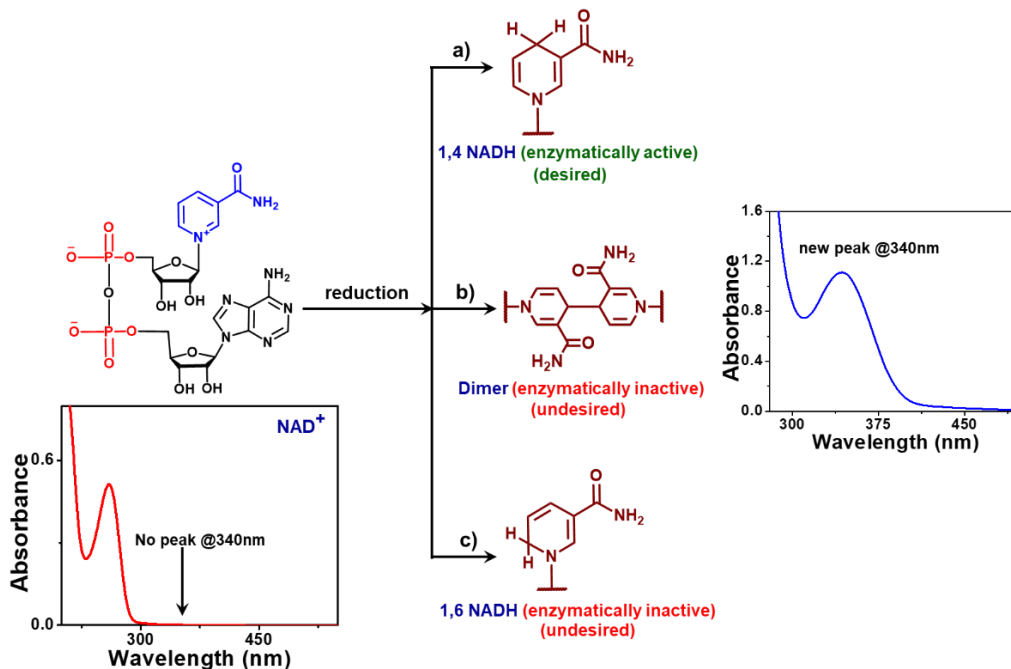


Figure 4.20. Schematic representation of NAD⁺ reduction routes, and possible product formation. a) Desired pathway producing enzymatically active 1,4-NADH. b) and c) Undesired pathways producing inactive dimer NAD₂ and isomer 1,6-NADH, respectively. The reduction process can be monitored with the appearance of a new peak at ~ 340 nm.

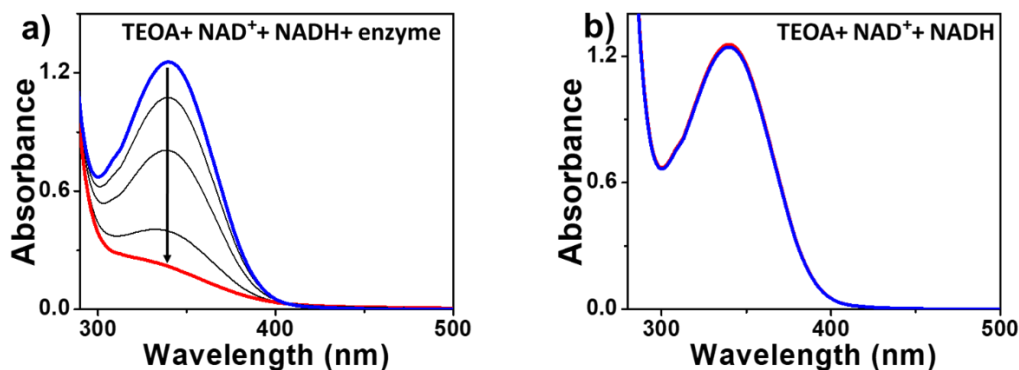


Figure 4.21. Control assay with lipoamide dehydrogenase enzyme. Variarion in the NADH absorbption at 340 nm for 2 h in a) presence and b) absence of enzyme.

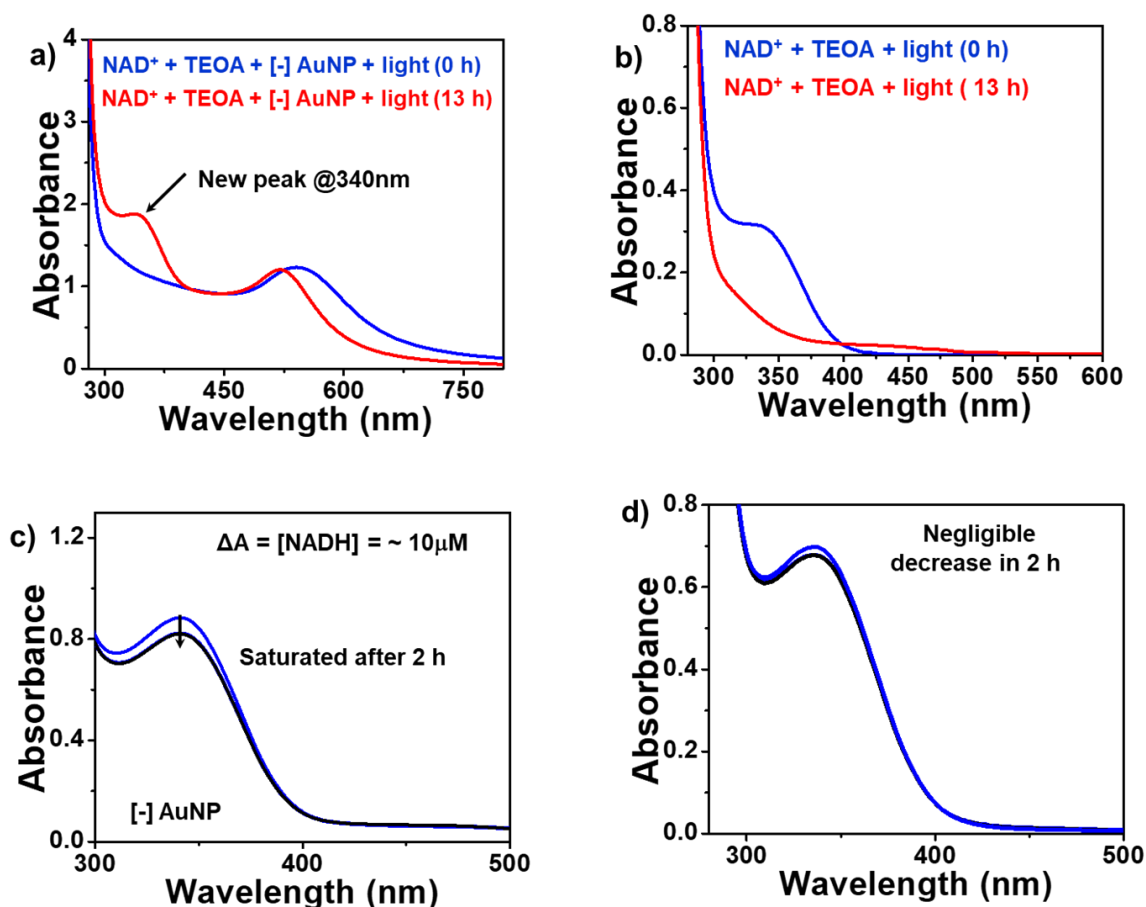


Figure 4.22. Photocatalytic reduction of NAD⁺ in absence of catalyst and in the presence of [-] AuNP catalyst. Progress of the photocatalytic reduction of NAD⁺ under 450 nm CW laser irradiation for 13 h a) with [-] AuNPs as the catalyst, and b) in absence of catalyst. Lipoamide dehydrogenase assay was performed with the reaction mixtures photoirradiated c) with [-] AuNPs as catalyst and d) in absence of catalyst. The amount of enzymatically active 1,4-NADH produced in the reaction was quantified from the decrease in absorbance at 340 nm.

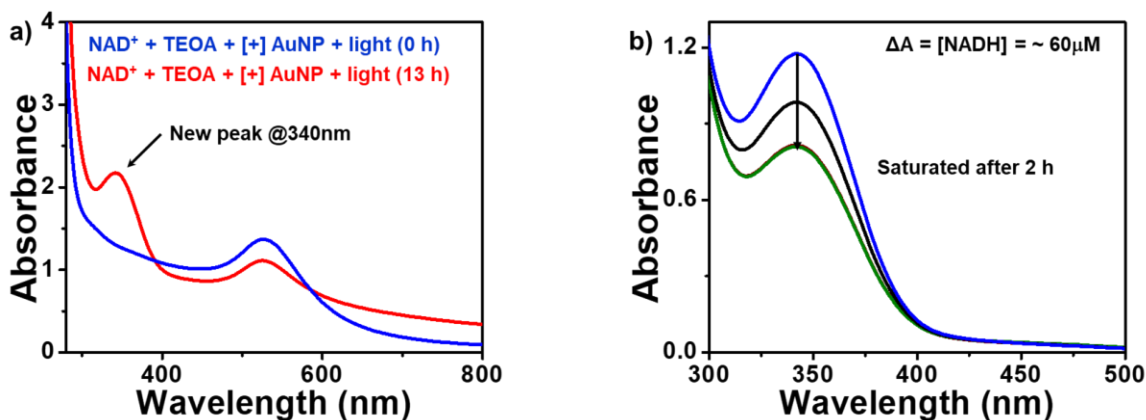


Figure 4.23. Photocatalytic reduction of NAD⁺ with [+] AuNPs. a) Progress of the photocatalytic reduction of NAD⁺ with 450 nm CW laser irradiation for 13 h using [+] AuNPs as the catalyst. b)

Lipoamide dehydrogenase assay with the reaction mixture after separating the catalyst. The amount of enzymatically active 1,4-NADH produced in the reaction was quantified from the decrease in absorbance at 340 nm.

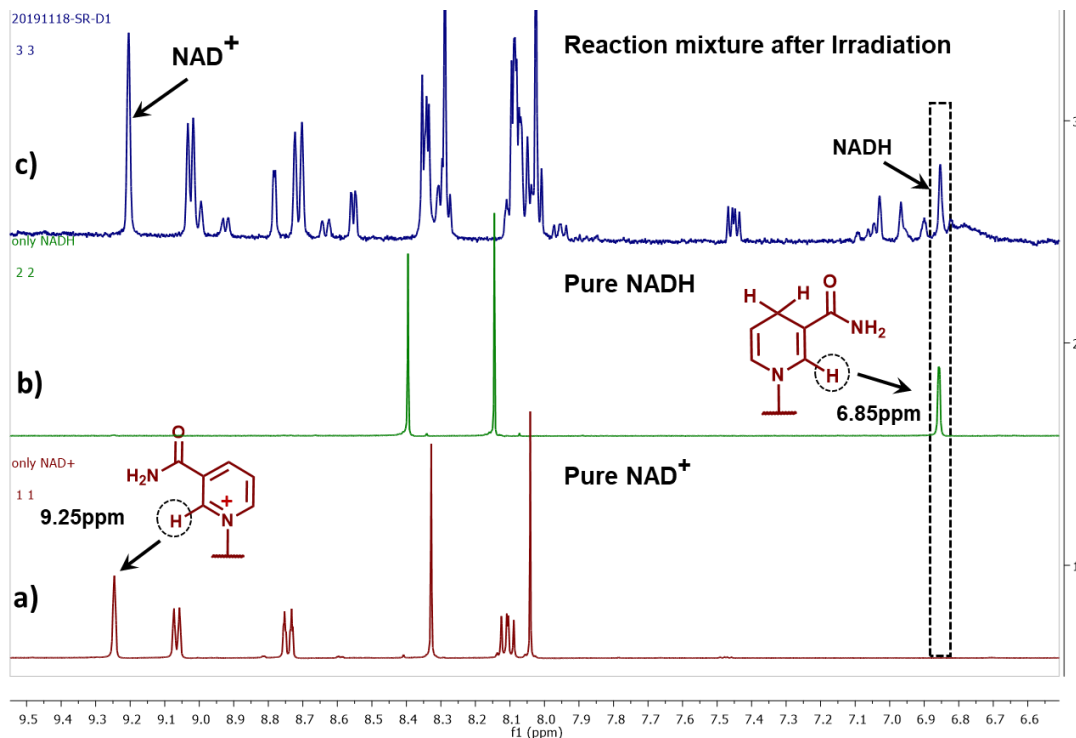


Figure 4.24. ^1H NMR spectra of a) pure NAD^+ , b) pure NADH , and c) reaction mixture after 13 h photoirradiation with $[+]$ AuNP.

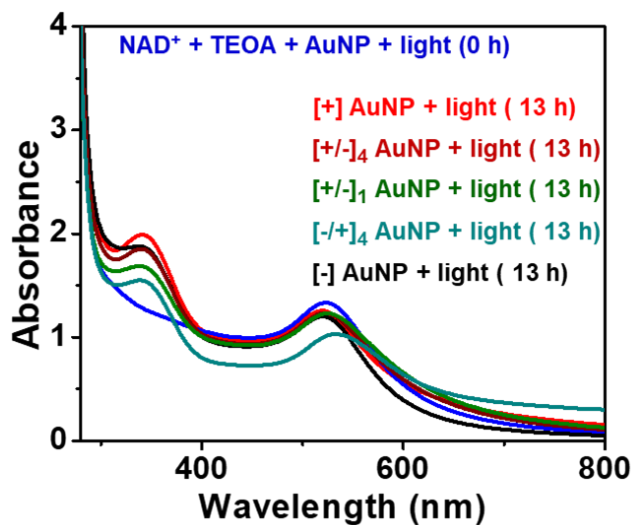


Figure 4.25. Effect of AuNP surface charge on NADH generation. Progress of photocatalytic reduction of NAD^+ with AuNPs of varying surface charges.

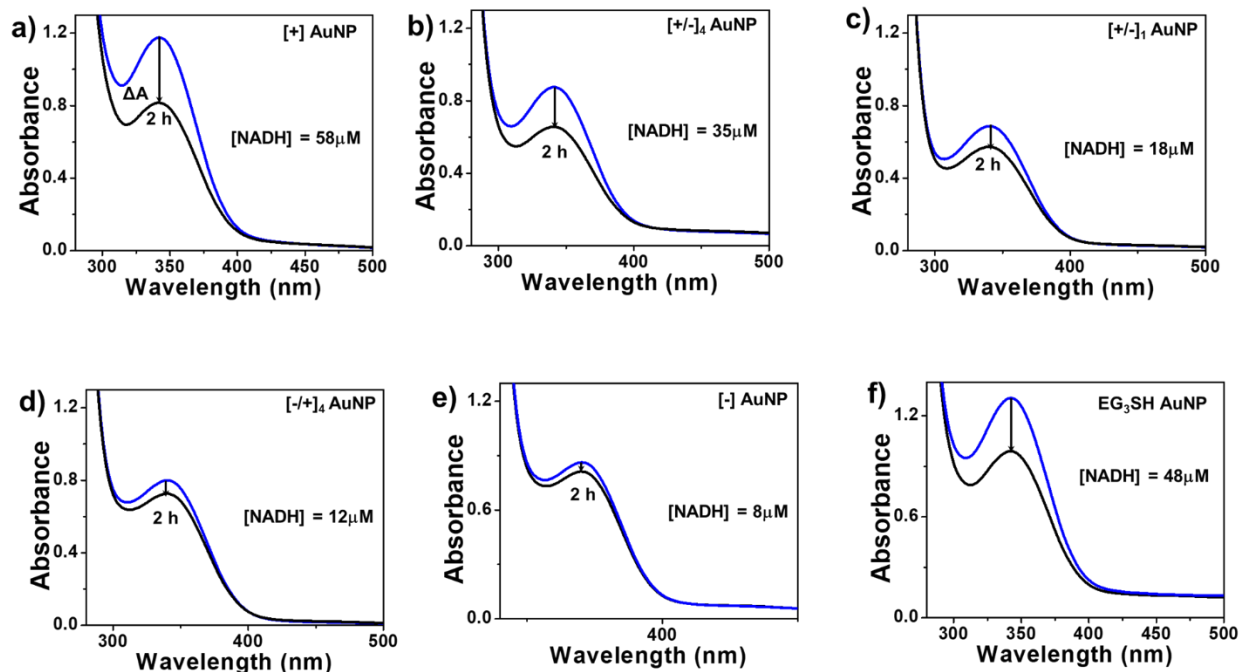


Figure 4.26. Lipoamide dehydrogenase assay with the reaction mixture photoirradiated with a) [+] AuNP, b) [+/-]₄ AuNP, c) [+/-]₁ AuNP, d) [-/+]₄ AuNP, e) [-] AuNP, and f) EG₃SH AuNP (neutral).

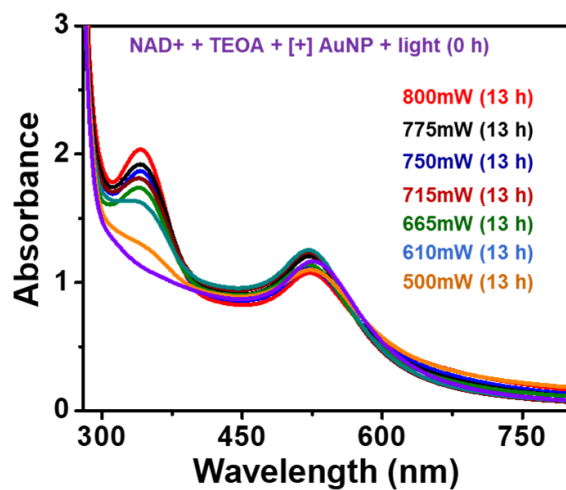


Figure 4.27. Intensity dependent catalytic reduction of NAD⁺ with [+] AuNP. Progress of photocatalytic reduction of NAD⁺ with [+] AuNP at seven different intensities.

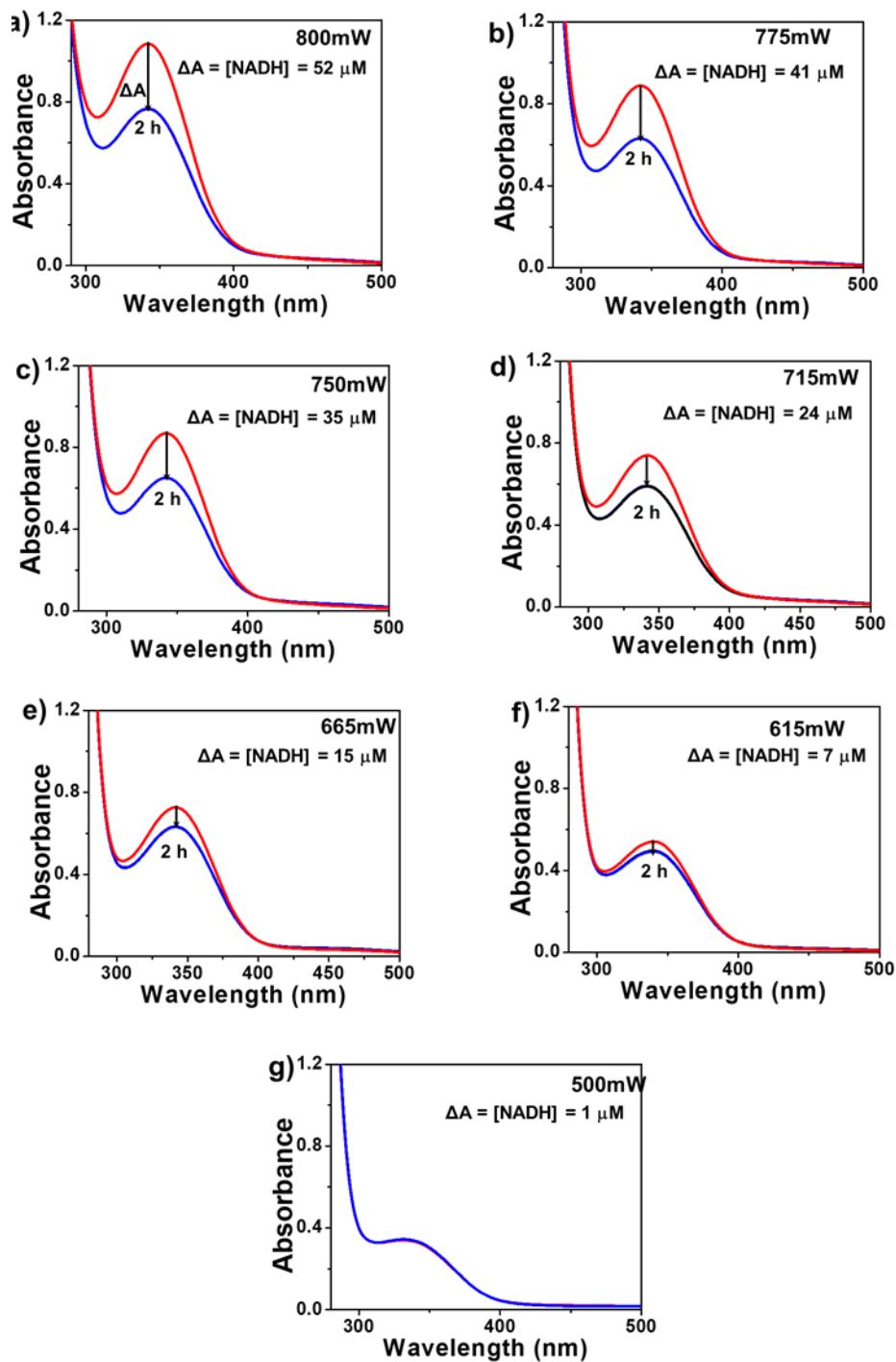


Figure 4.28. Lipoamide dehydrogenase assay with the reaction mixture photoirradiated with [+] AuNPs at a) 800 mW, b) 775 mW, c) 750 mW, d) 715 mW, e) 665 mW, f) 615mW, and g) 500 mW.

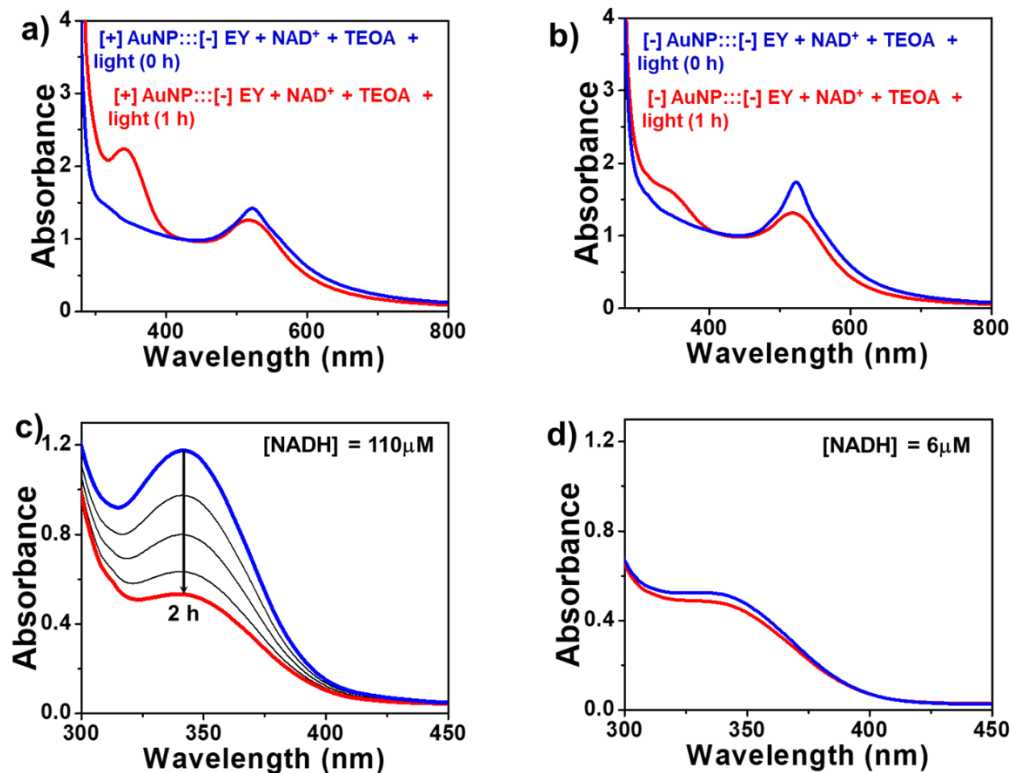


Figure 4.29. Photocatalytic reduction of NAD⁺ with [+]*AuNPs*::[-]*EY* and [-]*AuNPs*::[-]*EY* photocatalytic systems. Progress of the photocatalytic reduction of NAD⁺ under 450 nm CW laser irradiation for 1 h with a) [+]*AuNPs*::[-]*EY* and b) [-]*AuNPs*::[-]*EY* photocatalysts. Lipoamide dehydrogenase assay with the reaction mixtures photoirradiated with c) [+]*AuNPs*::[-]*EY* and d) [-]*AuNPs*::[-]*EY* photocatalysts.

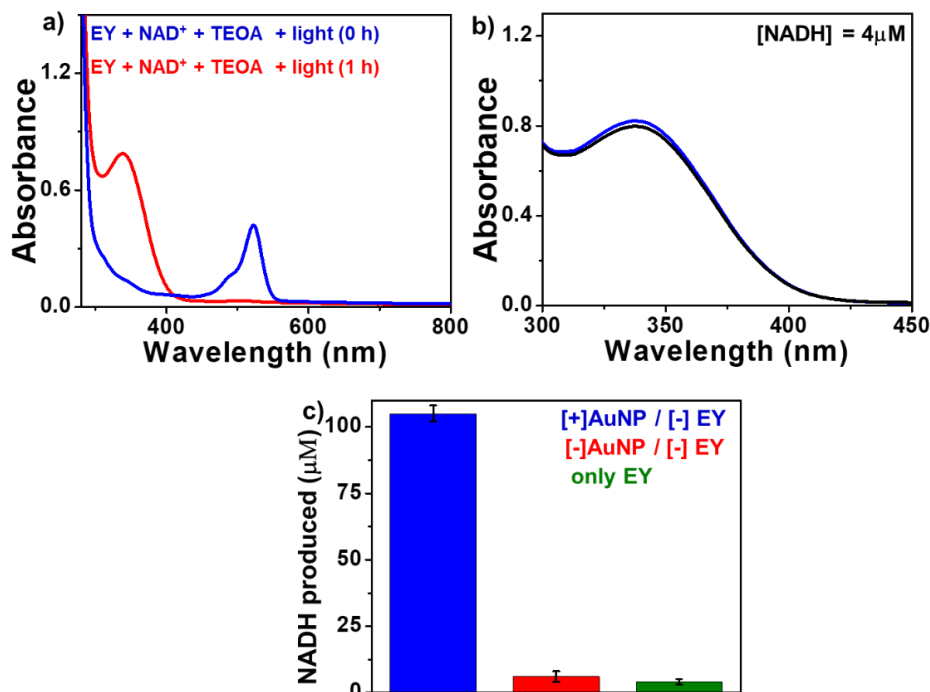


Figure 4.30. Photocatalytic reduction of NAD^+ with only EY. Photocatalytic reduction of NAD^+ with only EY. a) Progress of the photocatalytic reduction of NAD^+ under 450 nm CW laser irradiation for 1 h with only EY. b) Lipoamide dehydrogenase assay with the reaction mixture photoirradiated with EY. c) Bar diagram showing the concentrations of NADH produced during the photocatalytic reactions with [+]
AuNPs::[-] EY, [-]
AuNPs::[-] EY and only EY.

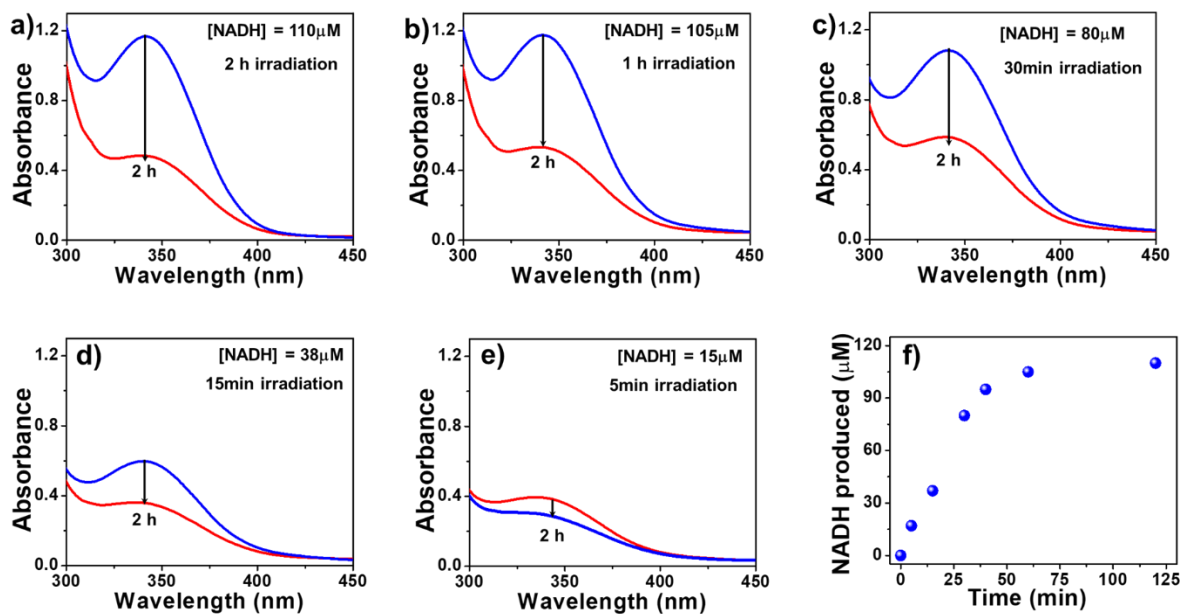


Figure 4.31. Time dependent photocatalytic reduction of NAD^+ with [+]
AuNP::EY photocatalyst. Lipoamide dehydrogenase assay with the reaction mixtures photoirradiated with [+]
AuNP::EY for a) 120 min, b) 60 min, c) 30 min, d) 15 min, and e) 5 min, under 450nm CW laser irradiation. f) Variation in NADH formation as a function of irradiation time.

Included in the thesis

1. **Soumendu Roy**, Anish Rao, Gayathri Devatha and Pramod P. Pillai.* Revealing the Role of Electrostatics in Gold-Nanoparticle-Catalyzed Reduction of Charged Substrates. *ACS Catal.* **2017**, 7, 7141-7145.
2. **Soumendu Roy**, Sumit Roy, Anish Rao, Gayathri Devatha and Pramod P. Pillai.* Precise Nanoparticle-Reactant Interaction Outplays Ligand Poisoning in Visible-Light Photocatalysis. *Chem. Mater.* **2018**, 30, 8415-8419.
3. **Soumendu Roy**, Vanshika Jain, Radha Krishna Kashyap, Anish Rao and Pramod P. Pillai.* Electrostatically Driven Multielectron Transfer for the Photocatalytic Regeneration of Nicotinamide Cofactor. *ACS Catal.* **2020**, 10, 5522-5528.

Not included in the thesis

4. Anish Rao, **Soumendu Roy**, Mahima Unnikrishnan, Sumit S. Bhosale, Gayathri Devatha and Pramod P. Pillai.* Regulation of Interparticle Forces Reveals Controlled Aggregation in Charged Nanoparticles. *Chem. Mater.* **2016**, 28, 2348–2355.
5. Gayathri Devatha, **Soumendu Roy**, Anish Rao, Abhik Mallick, Sudipta Basu and Pramod P. Pillai.* Electrostatically Driven Resonance Energy Transfer in “Cationic” Biocompatible Indium Phosphide Quantum Dots. *Chem. Sci.*, **2017**, 8, 3879–3884.
6. Jewel Ann Maria Xavier, Gayathri Devatha, **Soumendu Roy**, Anish Rao and Pramod P. Pillai.* *J. Mater. Chem. A*, **2018**, 6, 22248–22255.
7. Gayathri Devatha, Anish Rao, **Soumendu Roy**, and Pramod P. Pillai.* Förster Resonance Energy Transfer Regulated Multicolor Photopatterning from Single Quantum Dot Nanohybrid Films. *ACS Energy Lett.* **2019**, 4, 1710–1716.
8. Anish Rao, Govind Sasi Kumar, **Soumendu Roy**, Ajesh T. Rajesh, Gayathri Devatha and Pramod P. Pillai.* Turn-On Selectivity in Inherently Nonselective Gold Nanoparticles for Pb^{2+} Detection by Preferential Breaking of Interparticle Interactions. *ACS Appl. Nano Mater.* **2019**, 2, 5625–5633.
9. Indra Narayan Chakraborty, **Soumendu Roy**, Gayathri Devatha, Anish Rao and Pramod P. Pillai.* InP/ZnS Quantum Dots as Efficient Visible-Light Photocatalysts for Redox and Carbon–Carbon Coupling Reactions. *Chem. Mater.* **2019**, 31, 2258-2262.

- 10.** *Gayathri Devatha, Pradyut Roy, Anish Rao, Soumendu Roy, and Pramod P. Pillai.**
Multicolor Luminescent Patterning via Photoregulation of Electron and Energy Transfer
Processes in Quantum Dots *J. Phys. Chem. Lett.* **2020**, *11*, 4099-4106.

1. Presented a poster titled “ *Precise Nanoparticle – Reactant Interaction Outplays Ligand Poisoning in Visible Light Photocatalysis*” in **Gordon Research Conference (GRC) on Plasmonically Powered Processes** held at **The Hong Kong University of Science and Technology, Hong Kong** in July 2019
2. Presented a poster as well as short 90 second talk titled “ *Precise Catalyst – Reactant Interaction Outplays Ligand Poisoning in Nanoparticle – Catalysis*” at **Alexander von Humboldt (AvH) Kolleg on Innovation Entrepreneurship: Role of Science and Technology** held at **Kashid, Pune** in January 2019
3. Presented a poster titled “*Revealing the Role of Electrostatics in Gold Nanoparticle Catalyzed Reductions*” in **Gordon Research Conference (GRC) and Gordon Research Seminar (GRS) on Noble Metal Nanoparticles** held at **Boston, U. S. A.** in June 2018
4. Presented a poster titled “*Revealing the Role of Electrostatics in Gold Nanoparticle Catalyzed Reductions*” in **Conference on Advances in Catalysis for Energy and Environment (CACEE)** held at **TIFR Mumbai** in January 2018
5. Presented a poster titled “*Electrostatically Driven Energy Transfer in Bio-compatible InP Quantum Dots Towards Live Cell Imaging*” in **International Conference on Nanoscience and Technology (ICONSAT)** held at **IISER Pune** in February 2016



RightsLink®



Home



Help



Email Support



Sign in



Create Account

Single-Atom Catalysts: A New Frontier in Heterogeneous Catalysis



Author: Xiao-Feng Yang, Aiqin Wang, Botao Qiao, et al

Publication: Accounts of Chemical Research

Publisher: American Chemical Society

Date: Aug 1, 2013

Copyright © 2013, American Chemical Society

PERMISSION/LICENSE IS GRANTED FOR YOUR ORDER AT NO CHARGE

This type of permission/license, instead of the standard Terms & Conditions, is sent to you because no fee is being charged for your order. Please note the following:

- Permission is granted for your request in both print and electronic formats, and translations.
 - If figures and/or tables were requested, they may be adapted or used in part.
 - Please print this page for your records and send a copy of it to your publisher/graduate school.
 - Appropriate credit for the requested material should be given as follows: "Reprinted (adapted) with permission from (COMPLETE REFERENCE CITATION). Copyright (YEAR) American Chemical Society." Insert appropriate information in place of the capitalized words.
 - One-time permission is granted only for the use specified in your request. No additional uses are granted (such as derivative works or other editions). For any other uses, please submit a new request.
- If credit is given to another source for the material you requested, permission must be obtained from that source.

[BACK](#)

[CLOSE WINDOW](#)



Insights into the reactivity of supported Au nanoparticles: combining theory and experiments

SPRINGER NATURE

Author: Ton V. W. Janssens et al

Publication: Topics in Catalysis

Publisher: Springer Nature

Date: Jan 1, 2007

Copyright © 2007, Springer Nature

Order Completed

Thank you for your order.

This Agreement between Indian Institute of Science Education and Research pune -- soumendu roy ("You") and Springer Nature ("Springer Nature") consists of your license details and the terms and conditions provided by Springer Nature and Copyright Clearance Center.

Your confirmation email will contain your order number for future reference.

License Number 4773060708528

[Printable Details](#)

License date Feb 20, 2020

✓ Licensed Content

Licensed Content Publisher	Springer Nature
Licensed Content Publication	Topics in Catalysis
Licensed Content Title	Insights into the reactivity of supported Au nanoparticles: combining theory and experiments
Licensed Content Author	Ton V. W. Janssens et al
Licensed Content Date	Jan 1, 2007

📄 Order Details

Type of Use	Thesis/Dissertation academic/university or research institute
Requestor type	print and electronic
Format	figures/tables/illustrations
Portion	1
Number of figures/tables/illustrations	no
Will you be translating?	1 - 29
Circulation/distribution	no
Author of this Springer Nature content	

📄 About Your Work

Title	PhD student
Institution name	Indian Institute of Science Education and Research
Expected presentation date	Apr 2020

📄 Additional Data

Order reference number	10
Portions	Figure 2 in the main article

📍 Requestor Location	📄 Tax Details
Indian Institute of Science Education and Research pune iiser pune, pune 411008	
Requestor Location	Pune, Maharashtra 411008 India Attn: Indian Institute of Science Education and Research pune
\$ Price	
Total	0.00 USD
Total: 0.00 USD	
CLOSE WINDOW	ORDER MORE

© 2020 Copyright - All Rights Reserved | [Copyright Clearance Center, Inc.](#) | [Privacy statement](#) | [Terms and Conditions](#)
Comments? We would like to hear from you. E-mail us at customer@copyright.com

**ELSEVIER LICENSE
TERMS AND CONDITIONS**

Feb 20, 2020

This Agreement between Indian Institute of Science Education and Research pune -- soumendu roy ("You") and Elsevier ("Elsevier") consists of your license details and the terms and conditions provided by Elsevier and Copyright Clearance Center.

License Number	4773081048757
License date	Feb 20, 2020
Licensed Content Publisher	Elsevier
Licensed Content Publication	Journal of Catalysis
Licensed Content Title	Size-dependent catalytic activity over carbon-supported palladium nanoparticles in dehydrogenation of formic acid
Licensed Content Author	Junjie Li,Wei Chen,Han Zhao,Xusheng Zheng,Lihui Wu,Haibin Pan,Junfa Zhu,Yanxia Chen,Junling Lu
Licensed Content Date	Aug 1, 2017
Licensed Content Volume	352
Licensed Content Issue	n/a
Licensed Content Pages	11
Start Page	371
End Page	381
Type of Use	reuse in a thesis/dissertation

Portion	figures/tables/illustrations
Number of figures/tables/illustrations	1
Format	both print and electronic
Are you the author of this Elsevier article?	No
Will you be translating?	No
Title	PhD student
Institution name	Indian Institute of Science Education and Research
Expected presentation date	Apr 2020
Order reference number	13
Portions	Graphical abstract of the article
	Indian Institute of Science Education and Research pune iiser pune, pune 411008
Requestor Location	Pune, Maharashtra 411008 India Attn: Indian Institute of Science Education and Research pune
Publisher Tax ID	GB 494 6272 12
Total	0.00 USD
Terms and Conditions	

INTRODUCTION

1. The publisher for this copyrighted material is Elsevier. By clicking "accept" in connection with completing this licensing transaction, you agree that the following terms and conditions apply to this transaction (along with the Billing and Payment terms and conditions established by Copyright Clearance Center, Inc. ("CCC"), at the time that you opened your Rightslink account and that are available at any time at <http://myaccount.copyright.com>).

GENERAL TERMS

2. Elsevier hereby grants you permission to reproduce the aforementioned material subject to the terms and conditions indicated.
3. Acknowledgement: If any part of the material to be used (for example, figures) has appeared in our publication with credit or acknowledgement to another source, permission must also be sought from that source. If such permission is not obtained then that material may not be included in your publication/copies. Suitable acknowledgement to the source must be made, either as a footnote or in a reference list at the end of your publication, as follows:

"Reprinted from Publication title, Vol /edition number, Author(s), Title of article / title of chapter, Pages No., Copyright (Year), with permission from Elsevier [OR APPLICABLE SOCIETY COPYRIGHT OWNER]." Also Lancet special credit - "Reprinted from The Lancet, Vol. number, Author(s), Title of article, Pages No., Copyright (Year), with permission from Elsevier."
4. Reproduction of this material is confined to the purpose and/or media for which permission is hereby given.
5. Altering/Modifying Material: Not Permitted. However figures and illustrations may be altered/adapted minimally to serve your work. Any other abbreviations, additions, deletions and/or any other alterations shall be made only with prior written authorization of Elsevier Ltd. (Please contact Elsevier at permissions@elsevier.com). No modifications can be made to any Lancet figures/tables and they must be reproduced in full.
6. If the permission fee for the requested use of our material is waived in this instance, please be advised that your future requests for Elsevier materials may attract a fee.
7. Reservation of Rights: Publisher reserves all rights not specifically granted in the combination of (i) the license details provided by you and accepted in the course of this licensing transaction, (ii) these terms and conditions and (iii) CCC's Billing and Payment terms and conditions.
8. License Contingent Upon Payment: While you may exercise the rights licensed immediately upon issuance of the license at the end of the licensing process for the transaction, provided that you have disclosed complete and accurate details of your proposed use, no license is finally effective unless and until full payment is received from you (either by publisher or by CCC) as provided in CCC's Billing and Payment terms and conditions. If full payment is not received on a timely basis, then any license preliminarily granted shall be deemed automatically revoked and shall be void as if never granted. Further, in the event that you breach any of these terms and conditions or any of CCC's Billing and Payment terms and conditions, the license is automatically revoked and shall be void as if never granted. Use of materials as described in a revoked license, as well as any use of the materials beyond the scope of an unrevoked license, may constitute copyright infringement and publisher reserves the right to take any and all action to protect its copyright in the materials.
9. Warranties: Publisher makes no representations or warranties with respect to the licensed material.
10. Indemnity: You hereby indemnify and agree to hold harmless publisher and CCC, and their respective officers, directors, employees and agents, from and against any and all claims arising out of your use of the licensed material other than as specifically authorized pursuant to this license.
11. No Transfer of License: This license is personal to you and may not be sublicensed, assigned, or transferred by you to any other person without publisher's written permission.

12. **No Amendment Except in Writing:** This license may not be amended except in a writing signed by both parties (or, in the case of publisher, by CCC on publisher's behalf).

13. **Objection to Contrary Terms:** Publisher hereby objects to any terms contained in any purchase order, acknowledgment, check endorsement or other writing prepared by you, which terms are inconsistent with these terms and conditions or CCC's Billing and Payment terms and conditions. These terms and conditions, together with CCC's Billing and Payment terms and conditions (which are incorporated herein), comprise the entire agreement between you and publisher (and CCC) concerning this licensing transaction. In the event of any conflict between your obligations established by these terms and conditions and those established by CCC's Billing and Payment terms and conditions, these terms and conditions shall control.

14. **Revocation:** Elsevier or Copyright Clearance Center may deny the permissions described in this License at their sole discretion, for any reason or no reason, with a full refund payable to you. Notice of such denial will be made using the contact information provided by you. Failure to receive such notice will not alter or invalidate the denial. In no event will Elsevier or Copyright Clearance Center be responsible or liable for any costs, expenses or damage incurred by you as a result of a denial of your permission request, other than a refund of the amount(s) paid by you to Elsevier and/or Copyright Clearance Center for denied permissions.

LIMITED LICENSE

The following terms and conditions apply only to specific license types:

15. **Translation:** This permission is granted for non-exclusive world **English** rights only unless your license was granted for translation rights. If you licensed translation rights you may only translate this content into the languages you requested. A professional translator must perform all translations and reproduce the content word for word preserving the integrity of the article.

16. **Posting licensed content on any Website:** The following terms and conditions apply as follows: Licensing material from an Elsevier journal: All content posted to the web site must maintain the copyright information line on the bottom of each image; A hyper-text must be included to the Homepage of the journal from which you are licensing at <http://www.sciencedirect.com/science/journal/xxxxx> or the Elsevier homepage for books at <http://www.elsevier.com>; Central Storage: This license does not include permission for a scanned version of the material to be stored in a central repository such as that provided by Heron/XanEdu.

Licensing material from an Elsevier book: A hyper-text link must be included to the Elsevier homepage at <http://www.elsevier.com> . All content posted to the web site must maintain the copyright information line on the bottom of each image.

Posting licensed content on Electronic reserve: In addition to the above the following clauses are applicable: The web site must be password-protected and made available only to bona fide students registered on a relevant course. This permission is granted for 1 year only. You may obtain a new license for future website posting.

17. **For journal authors:** the following clauses are applicable in addition to the above:

Preprints:

A preprint is an author's own write-up of research results and analysis, it has not been peer-reviewed, nor has it had any other value added to it by a publisher (such as formatting, copyright, technical enhancement etc.).

Authors can share their preprints anywhere at any time. Preprints should not be added to or enhanced in any way in order to appear more like, or to substitute for, the final versions of articles however authors can update their preprints on arXiv or RePEc with their Accepted Author Manuscript (see below).

If accepted for publication, we encourage authors to link from the preprint to their formal publication via its DOI. Millions of researchers have access to the formal publications on ScienceDirect, and so links will help users to find, access, cite and use the best available version. Please note that Cell Press, The Lancet and some society-owned have different preprint policies. Information on these policies is available on the journal homepage.

Accepted Author Manuscripts: An accepted author manuscript is the manuscript of an article that has been accepted for publication and which typically includes author-incorporated changes suggested during submission, peer review and editor-author communications.

Authors can share their accepted author manuscript:

- immediately
 - via their non-commercial person homepage or blog
 - by updating a preprint in arXiv or RePEc with the accepted manuscript
 - via their research institute or institutional repository for internal institutional uses or as part of an invitation-only research collaboration work-group
 - directly by providing copies to their students or to research collaborators for their personal use
 - for private scholarly sharing as part of an invitation-only work group on commercial sites with which Elsevier has an agreement
- After the embargo period
 - via non-commercial hosting platforms such as their institutional repository
 - via commercial sites with which Elsevier has an agreement

In all cases accepted manuscripts should:

- link to the formal publication via its DOI
- bear a CC-BY-NC-ND license - this is easy to do
- if aggregated with other manuscripts, for example in a repository or other site, be shared in alignment with our hosting policy not be added to or enhanced in any way to appear more like, or to substitute for, the published journal article.

Published journal article (JPA): A published journal article (PJA) is the definitive final record of published research that appears or will appear in the journal and embodies all value-adding publishing activities including peer review co-ordination, copy-editing, formatting, (if relevant) pagination and online enrichment.

Policies for sharing publishing journal articles differ for subscription and gold open access articles:

Subscription Articles: If you are an author, please share a link to your article rather than the full-text. Millions of researchers have access to the formal publications on ScienceDirect, and so links will help your users to find, access, cite, and use the best available version.

Theses and dissertations which contain embedded PJAs as part of the formal submission can be posted publicly by the awarding institution with DOI links back to the formal publications on ScienceDirect.

If you are affiliated with a library that subscribes to ScienceDirect you have additional private sharing rights for others' research accessed under that agreement. This includes use for classroom teaching and internal training at the institution (including use in course packs and courseware programs), and inclusion of the article for grant funding purposes.

Gold Open Access Articles: May be shared according to the author-selected end-user license and should contain a [CrossMark logo](#), the end user license, and a DOI link to the formal publication on ScienceDirect.

Please refer to Elsevier's [posting policy](#) for further information.

18. For book authors the following clauses are applicable in addition to the above: Authors are permitted to place a brief summary of their work online only. You are not allowed to download and post the published electronic version of your chapter, nor may you scan the printed edition to create an electronic version. **Posting to a repository:** Authors are permitted to post a summary of their chapter only in their institution's repository.

19. Thesis/Dissertation: If your license is for use in a thesis/dissertation your thesis may be submitted to your institution in either print or electronic form. Should your thesis be published commercially, please reapply for permission. These requirements include permission for the Library and Archives of Canada to supply single copies, on demand, of the complete thesis and include permission for Proquest/UMI to supply single copies, on demand, of the complete thesis. Should your thesis be published commercially, please reapply for permission. Theses and dissertations which contain embedded PJAs as part of the formal submission can be posted publicly by the awarding institution with DOI links back to the formal publications on ScienceDirect.

Elsevier Open Access Terms and Conditions

You can publish open access with Elsevier in hundreds of open access journals or in nearly 2000 established subscription journals that support open access publishing. Permitted third party re-use of these open access articles is defined by the author's choice of Creative Commons user license. See our [open access license policy](#) for more information.

Terms & Conditions applicable to all Open Access articles published with Elsevier:

Any reuse of the article must not represent the author as endorsing the adaptation of the article nor should the article be modified in such a way as to damage the author's honour or reputation. If any changes have been made, such changes must be clearly indicated.

The author(s) must be appropriately credited and we ask that you include the end user license and a DOI link to the formal publication on ScienceDirect.

If any part of the material to be used (for example, figures) has appeared in our publication with credit or acknowledgement to another source it is the responsibility of the user to ensure their reuse complies with the terms and conditions determined by the rights holder.

Additional Terms & Conditions applicable to each Creative Commons user license:

CC BY: The CC-BY license allows users to copy, to create extracts, abstracts and new works from the Article, to alter and revise the Article and to make commercial use of the Article (including reuse and/or resale of the Article by commercial entities), provided the user gives appropriate credit (with a link to the formal publication through the relevant DOI), provides a link to the license, indicates if changes were made and the licensor is not represented as endorsing the use made of the work. The full details of the license are available at <http://creativecommons.org/licenses/by/4.0>.

CC BY NC SA: The CC BY-NC-SA license allows users to copy, to create extracts, abstracts and new works from the Article, to alter and revise the Article, provided this is not done for commercial purposes, and that the user gives appropriate credit (with a link to the formal publication through the relevant DOI), provides a link to the license, indicates if changes were made and the licensor is not represented as endorsing the use made of the

work. Further, any new works must be made available on the same conditions. The full details of the license are available at <http://creativecommons.org/licenses/by-nc-sa/4.0>.

CC BY NC ND: The CC BY-NC-ND license allows users to copy and distribute the Article, provided this is not done for commercial purposes and further does not permit distribution of the Article if it is changed or edited in any way, and provided the user gives appropriate credit (with a link to the formal publication through the relevant DOI), provides a link to the license, and that the licensor is not represented as endorsing the use made of the work. The full details of the license are available at <http://creativecommons.org/licenses/by-nc-nd/4.0>. Any commercial reuse of Open Access articles published with a CC BY NC SA or CC BY NC ND license requires permission from Elsevier and will be subject to a fee.

Commercial reuse includes:

- Associating advertising with the full text of the Article
- Charging fees for document delivery or access
- Article aggregation
- Systematic distribution via e-mail lists or share buttons

Posting or linking by commercial companies for use by customers of those companies.

20. Other Conditions:

v1.9

Questions? customercare@copyright.com or +1-855-239-3415 (toll free in the US) or +1-978-646-2777.

様式 2

COPYRIGHT PERMISSION REQUEST FORM

Date: 20/02/2020

To: The Chemical Society of Japan
1-5, Kanda-Surugadai, Chiyoda-ku,
Tokyo 101-8307, Japan

Fax: +81-3-3292-6318
E-mail: info@chemistry.or.jp

From: Soumendu Roy
IISER Pune, India

Phone: 8551963352
Fax: _____

E-mail: Soumendu.roy@students.iiserpune.ac.in

I am preparing my thesis entitled:

Regulation of Nanoparticle – Reactant Interaction Outplays Ligand Poisoning in Metal Nanoparticle Catalyzed Reactions

to appear in

My thesis _____

which is published by

Indian Institute of Science Education and Research

Expected publication date: 30th April, 2020

I request your permission to include the following material in this and in all subsequent editions of this work to be published by Indian Institute of Science Education and Research or its licensees for distribution throughout the world, in all media including electronic/online and microfilm.

Title of Thesis: Regulation of Nanoparticle – Reactant Interaction Outplays Ligand Poisoning in Metal Nanoparticle Catalyzed Reactions


Author(s)/Editor(s): Soumendu Roy

Title of Selection: Facile synthesis of size-controlled Rh nanoparticles via microwave-assisted alcohol reduction and their catalysis of CO oxidation

Year: 2017 Vol.: 46 No.: 8

Figure(s)/Table(s): Figure 4 Page(s): 1254-1257

We hereby grant permission for the use of the material requested above.


Shin-ichi Suzuki
Secretary-general
The Chemical Society of Japan

Date: February 25, 2020

Our Ref. No. CY-RT-20-184

**SPRINGER NATURE LICENSE
TERMS AND CONDITIONS**

Feb 20, 2020

This Agreement between Indian Institute of Science Education and Research pune -- soumendu roy ("You") and Springer Nature ("Springer Nature") consists of your license details and the terms and conditions provided by Springer Nature and Copyright Clearance Center.

License Number	4773091253957
License date	Feb 20, 2020
Licensed Content Publisher	Springer Nature
Licensed Content Publication	Nature Catalysis
Licensed Content Title	Catalytic conversion of solar to chemical energy on plasmonic metal nanostructures
Licensed Content Author	Umar Aslam et al
Licensed Content Date	Sep 12, 2018
Type of Use	Thesis/Dissertation
Requestor type	academic/university or research institute
Format	print and electronic
Portion	figures/tables/illustrations
Number of figures/tables/illustrations	1
High-res required	no

Will you be translating?	no
Circulation/distribution	1 - 29
Author of this Springer Nature content	no
Title	PhD student
Institution name	Indian Institute of Science Education and Research
Expected presentation date	Apr 2020
Order reference number	14
Portions	Figure 1
Requestor Location	Indian Institute of Science Education and Research pune iiser pune, pune 411008
Total	0.00 USD

Terms and Conditions

Springer Nature Customer Service Centre GmbH Terms and Conditions

This agreement sets out the terms and conditions of the licence (the **Licence**) between you and **Springer Nature Customer Service Centre GmbH** (the **Licensor**). By clicking 'accept' and completing the transaction for the material (**Licensed Material**), you also confirm your acceptance of these terms and conditions.

1. Grant of License

1. 1. The Licensor grants you a personal, non-exclusive, non-transferable, world-wide licence to reproduce the Licensed Material for the purpose specified in your order only. Licences are granted for the specific use requested in the order and for no other use, subject to the conditions below.

1. 2. The Licensor warrants that it has, to the best of its knowledge, the rights to license reuse of the Licensed Material. However, you should ensure that the material you are requesting is original to the Licensor and does not carry the copyright of

another entity (as credited in the published version).

1. 3. If the credit line on any part of the material you have requested indicates that it was reprinted or adapted with permission from another source, then you should also seek permission from that source to reuse the material.

2. Scope of Licence

2. 1. You may only use the Licensed Content in the manner and to the extent permitted by these Ts&Cs and any applicable laws.

2. 2. A separate licence may be required for any additional use of the Licensed Material, e.g. where a licence has been purchased for print only use, separate permission must be obtained for electronic re-use. Similarly, a licence is only valid in the language selected and does not apply for editions in other languages unless additional translation rights have been granted separately in the licence. Any content owned by third parties are expressly excluded from the licence.

2. 3. Similarly, rights for additional components such as custom editions and derivatives require additional permission and may be subject to an additional fee.

Please apply to

Journalpermissions@springernature.com/bookpermissions@springernature.com for these rights.

2. 4. Where permission has been granted **free of charge** for material in print, permission may also be granted for any electronic version of that work, provided that the material is incidental to your work as a whole and that the electronic version is essentially equivalent to, or substitutes for, the print version.

2. 5. An alternative scope of licence may apply to signatories of the [STM Permissions Guidelines](#), as amended from time to time.

3. Duration of Licence

3. 1. A licence for is valid from the date of purchase ('Licence Date') at the end of the relevant period in the below table:

Scope of Licence	Duration of Licence
Post on a website	12 months
Presentations	12 months
Books and journals	Lifetime of the edition in the language purchased

4. Acknowledgement

4. 1. The Licensor's permission must be acknowledged next to the Licenced Material in print. In electronic form, this acknowledgement must be visible at the same time as the figures/tables/illustrations or abstract, and must be hyperlinked to the journal/book's homepage. Our required acknowledgement format is in the Appendix below.

5. Restrictions on use

5. 1. Use of the Licensed Material may be permitted for incidental promotional use and minor editing privileges e.g. minor adaptations of single figures, changes of format, colour and/or style where the adaptation is credited as set out in Appendix 1 below. Any other changes including but not limited to, cropping, adapting, omitting material that affect the meaning, intention or moral rights of the author are strictly prohibited.

5. 2. You must not use any Licensed Material as part of any design or trademark.

5. 3. Licensed Material may be used in Open Access Publications (OAP) before publication by Springer Nature, but any Licensed Material must be removed from OAP sites prior to final publication.

6. Ownership of Rights

6. 1. Licensed Material remains the property of either Licensor or the relevant third party and any rights not explicitly granted herein are expressly reserved.

7. Warranty

IN NO EVENT SHALL LICENSOR BE LIABLE TO YOU OR ANY OTHER PARTY OR ANY OTHER PERSON OR FOR ANY SPECIAL, CONSEQUENTIAL, INCIDENTAL OR INDIRECT DAMAGES, HOWEVER CAUSED, ARISING OUT OF OR IN CONNECTION WITH THE DOWNLOADING, VIEWING OR USE OF THE MATERIALS REGARDLESS OF THE FORM OF ACTION, WHETHER FOR BREACH OF CONTRACT, BREACH OF WARRANTY, TORT, NEGLIGENCE, INFRINGEMENT OR OTHERWISE (INCLUDING, WITHOUT LIMITATION, DAMAGES BASED ON LOSS OF PROFITS, DATA, FILES, USE, BUSINESS OPPORTUNITY OR CLAIMS OF THIRD PARTIES), AND WHETHER OR NOT THE PARTY HAS BEEN ADVISED OF THE POSSIBILITY OF SUCH DAMAGES. THIS LIMITATION SHALL APPLY NOTWITHSTANDING ANY FAILURE OF ESSENTIAL PURPOSE OF ANY LIMITED REMEDY PROVIDED HEREIN.

8. Limitations

8. 1. BOOKS ONLY: Where '**reuse in a dissertation/thesis**' has been selected the following terms apply: Print rights of the final author's accepted manuscript (for clarity, NOT the published version) for up to 100 copies, electronic rights for use only on a personal website or institutional repository as defined by the Sherpa guideline (www.sherpa.ac.uk/romeo/).

9. Termination and Cancellation

9. 1. Licences will expire after the period shown in Clause 3 (above).

9. 2. Licensee reserves the right to terminate the Licence in the event that payment is not received in full or if there has been a breach of this agreement by you.

Appendix 1 — Acknowledgements:**For Journal Content:**

Reprinted by permission from [the Licensor]: [Journal Publisher (e.g. Nature/Springer/Palgrave)] [JOURNAL NAME] [REFERENCE CITATION (Article name, Author(s) Name), [COPYRIGHT] (year of publication)

For Advance Online Publication papers:

Reprinted by permission from [the Licensor]: [Journal Publisher (e.g. Nature/Springer/Palgrave)] [JOURNAL NAME] [REFERENCE CITATION (Article name, Author(s) Name), [COPYRIGHT] (year of publication), advance online publication, day month year (doi: 10.1038/sj.[JOURNAL ACRONYM].)

For Adaptations/Translations:

Adapted/Translated by permission from [the Licensor]: [Journal Publisher (e.g. Nature/Springer/Palgrave)] [JOURNAL NAME] [REFERENCE CITATION (Article name, Author(s) Name), [COPYRIGHT] (year of publication)

Note: For any republication from the British Journal of Cancer, the following credit line style applies:

Reprinted/adapted/translated by permission from [the Licensor]: on behalf of Cancer Research UK: : [Journal Publisher (e.g. Nature/Springer/Palgrave)] [JOURNAL NAME] [REFERENCE CITATION (Article name, Author(s) Name), [COPYRIGHT] (year of publication)

For Advance Online Publication papers:

Reprinted by permission from The [the Licensor]: on behalf of Cancer Research UK: [Journal Publisher (e.g. Nature/Springer/Palgrave)] [JOURNAL NAME] [REFERENCE CITATION (Article name, Author(s) Name), [COPYRIGHT] (year of publication), advance online publication, day month year (doi: 10.1038/sj.[JOURNAL ACRONYM])

For Book content:

Reprinted/adapted by permission from [the Licensor]: [Book Publisher (e.g. Palgrave Macmillan, Springer etc)] [Book Title] by [Book author(s)] [COPYRIGHT] (year of publication)

Other Conditions:

Version 1.2

Questions? customercare@copyright.com or +1-855-239-3415 (toll free in the US) or +1-978-646-2777.



Home



Help



Email Support



soumendu roy ▾

Nonradiative Plasmon Decay and Hot Carrier Dynamics: Effects of Phonons, Surfaces, and Geometry



Author: Ana M. Brown, Ravishankar Sundararaman, Prineha Narang, et al

Publication: ACS Nano

Publisher: American Chemical Society

Date: Jan 1, 2016

Copyright © 2016, American Chemical Society

PERMISSION/LICENSE IS GRANTED FOR YOUR ORDER AT NO CHARGE

This type of permission/license, instead of the standard Terms & Conditions, is sent to you because no fee is being charged for your order. Please note the following:

- Permission is granted for your request in both print and electronic formats, and translations.
 - If figures and/or tables were requested, they may be adapted or used in part.
 - Please print this page for your records and send a copy of it to your publisher/graduate school.
 - Appropriate credit for the requested material should be given as follows: "Reprinted (adapted) with permission from (COMPLETE REFERENCE CITATION). Copyright (YEAR) American Chemical Society." Insert appropriate information in place of the capitalized words.
 - One-time permission is granted only for the use specified in your request. No additional uses are granted (such as derivative works or other editions). For any other uses, please submit a new request.
- If credit is given to another source for the material you requested, permission must be obtained from that source.

[BACK](#)[CLOSE WINDOW](#)



RightsLink®



Home



Help



Email Support



soumendu roy ▾

Charge Separation and Catalytic Activity of Ag@TiO₂ Core-Shell Composite Clusters under UV-Irradiation



Author: Tsutomu Hirakawa, Prashant V. Kamat

Publication: Journal of the American Chemical Society

Publisher: American Chemical Society

Date: Mar 1, 2005

Copyright © 2005, American Chemical Society

PERMISSION/LICENSE IS GRANTED FOR YOUR ORDER AT NO CHARGE

This type of permission/license, instead of the standard Terms & Conditions, is sent to you because no fee is being charged for your order. Please note the following:

- Permission is granted for your request in both print and electronic formats, and translations.
 - If figures and/or tables were requested, they may be adapted or used in part.
 - Please print this page for your records and send a copy of it to your publisher/graduate school.
 - Appropriate credit for the requested material should be given as follows: "Reprinted (adapted) with permission from (COMPLETE REFERENCE CITATION). Copyright (YEAR) American Chemical Society." Insert appropriate information in place of the capitalized words.
 - One-time permission is granted only for the use specified in your request. No additional uses are granted (such as derivative works or other editions). For any other uses, please submit a new request.
- If credit is given to another source for the material you requested, permission must be obtained from that source.

[BACK](#)[CLOSE WINDOW](#)



Home



Help



Email Support



soumendu roy ▾

Mechanisms and Applications of Plasmon-Induced Charge Separation at TiO₂ Films Loaded with Gold Nanoparticles



Author: Yang Tian, Tetsu Tatsuma

Publication: Journal of the American Chemical Society

Publisher: American Chemical Society

Date: May 1, 2005

Copyright © 2005, American Chemical Society

PERMISSION/LICENSE IS GRANTED FOR YOUR ORDER AT NO CHARGE

This type of permission/license, instead of the standard Terms & Conditions, is sent to you because no fee is being charged for your order. Please note the following:

- Permission is granted for your request in both print and electronic formats, and translations.
 - If figures and/or tables were requested, they may be adapted or used in part.
 - Please print this page for your records and send a copy of it to your publisher/graduate school.
 - Appropriate credit for the requested material should be given as follows: "Reprinted (adapted) with permission from (COMPLETE REFERENCE CITATION). Copyright (YEAR) American Chemical Society." Insert appropriate information in place of the capitalized words.
 - One-time permission is granted only for the use specified in your request. No additional uses are granted (such as derivative works or other editions). For any other uses, please submit a new request.
- If credit is given to another source for the material you requested, permission must be obtained from that source.

[BACK](#)[CLOSE WINDOW](#)



IOP Publishing, Ltd - License Terms and Conditions

Order Date	21-Feb-2020
Order license ID	1019270-1
ISSN	0034-4885
Type of Use	Republish in a thesis/dissertation
Publisher	IOP Publishing
Portion	Chart/graph/table/figure

LICENSED CONTENT

Publication Title	Reports on Progress in Physics	Country	United Kingdom of Great Britain and Northern Ireland
Author/Editor	Institute of Physics (Great Britain), Physical Society (Great Britain), Institute of Physics and the Physical Society., Institute of Physics Publishing.	Rightsholder	IOP Publishing, Ltd
		Publication Type	Journal
Date	01/01/1934		
Language	English		

REQUEST DETAILS

Portion Type	Chart/graph/table/figure	Distribution	Worldwide
Number of charts / graphs / tables / figures requested	1	Translation	Other translation needs
Format (select all that apply)	Electronic	Enter languages	English
Who will republish the content?	Academic institution	Copies for the disabled?	No
		Minor editing privileges?	No
Duration of Use	Life of current edition	Incidental promotional use?	No
Lifetime Unit Quantity	Up to 499	Currency	USD
Rights Requested	Main product		

NEW WORK DETAILS

Title	Precise Nanoparticle reactant interaction outplays ligand poisoning in metal nanoparticle catalyzed reactions	Institution name	Indian Institute of Science Education and Research Pune
Instructor name	Soumendu Roy	Expected presentation date	2020-04-30

ADDITIONAL DETAILS

Order reference number	15	The requesting person / organization to appear on the license	Soumendu Roy
------------------------	----	---	--------------

REUSE CONTENT DETAILS

Title, description or numeric reference of the portion(s)	Plasmonic photocatalysis	Title of the article/chapter the portion is from	Plasmonic photocatalysis
Editor of portion(s)	NA	Author of portion(s)	Institute of Physics (Great Britain); Physical Society (Great Britain); Institute of Physics and the Physical Society.; Institute of Physics Publishing.
Volume of serial or monograph	76	Issue, if republishing an article from a serial	N/A
Page or page range of portion	14	Publication date of portion	1934-01-01

PUBLISHER TERMS AND CONDITIONS

These special terms and conditions are in addition to the standard terms and conditions for CCC's Republication Service and, together with those standard terms and conditions, govern the use of the Works. As the User you will make all reasonable efforts to contact the author(s) of the article which the Work is to be reused from, to seek consent for your intended use. Contacting one author who is acting expressly as authorised agent for their co-author(s) is acceptable. User will reproduce the following wording prominently alongside the Work: the source of the Work, including author, article title, title of journal, volume number, issue number (if relevant), page range (or first page if this is the only information available) and date of first publication. This information can be contained in a footnote or reference note; and a link back to the article (via DOI); and if practicable, and IN ALL CASES for new works published under any of the Creative Commons licences, the words "© IOP Publishing. Reproduced with permission. All rights reserved" Without the express permission of the author(s) and the Rightsholder of the article from which the Work is to be reused, User shall not use it in any way which, in the opinion of the Rightsholder, could: (i) distort or alter the author(s)' original intention(s) and meaning; (ii) be prejudicial to the honour or reputation of the author(s); and/or (iii) imply endorsement by the author(s) and/or the Rightsholder. This licence does not apply to any article which is credited to another source and which does not have the copyright line '© IOP Publishing Ltd'. User must check the copyright line of the article from which the Work is to be reused to check that IOP Publishing Ltd has all the necessary rights to be able to grant permission. User is solely responsible for identifying and obtaining separate licences and permissions from the copyright owner for reuse of any such third party material/figures which the Rightsholder is not the copyright owner of. The Rightsholder shall not reimburse any fees which User pays for a republication license for such third party content. This licence does not apply to any material/figure which is credited to another source in the Rightsholder's publication or has been obtained from a third party. User must check the Version of Record of the article from which the Work is to be reused, to check whether any of the material in the Work is third party material. Third party citations and/or copyright notices and/or permissions statements may not be included in any other version of the article from which the Work is to be reused and so cannot be relied upon by the User. User is solely responsible for identifying and obtaining separate licences and permissions from the copyright owner for reuse of any such third party material/figures where the Rightsholder is not the copyright owner. The Rightsholder shall not reimburse any fees which User pays for a republication license for such third party content. User and CCC acknowledge that the Rightsholder may, from time to time, make changes or additions to these special terms and conditions without express notification, provided that these shall not apply to permissions already secured and paid for by User prior to such change or addition. User acknowledges that the Rightsholder (which includes companies within its group and third parties for whom it publishes its titles) may make use of personal data collected through the service in the course of their business. If User is the author of the Work, User may automatically have the right to reuse it under the rights granted back when User transferred the copyright in the article to the Rightsholder. User should check the copyright form and the relevant author rights policy to check whether permission is required. If User is the author of the Work and does require permission for proposed reuse of the Work, User should select 'Author of requested content' as the Requestor Type. The Rightsholder shall not reimburse any fees which User pays for a republication license. If User is the author of the article which User wishes to reuse in User's thesis or dissertation, the republication licence covers the right to include the Accepted Manuscript version (not the Version of Record) of the article. User must include citation details and, for online use, a link to the Version of Record of the article on the Rightsholder's website. User may need to obtain separate permission for any third party content included within the article. User must check this with the copyright owner of such third party content. User may not include the article in a thesis or dissertation which is published by ProQuest. Any other commercial use of User's thesis or dissertation containing the article would also need to be expressly notified in writing to the Rightsholder at the time of request and would require separate written permission from the Rightsholder. User does not need to request permission for Work which has been published under a CC BY licence. User must check the Version of Record of the CC BY article from which the Work is to be reused, to check whether any of the material in the Work is third party material and so not published under the CC BY licence. User is solely responsible for identifying and obtaining separate licences and permissions from the copyright owner for reuse of any such third party material/figures. The Rightsholder shall not reimburse any fees which User pays for such licences and permissions. As well as CCC, the Rightsholder shall have the right to bring any legal action that it deems necessary to enforce its rights should it consider that the Work infringes those rights in any way. For STM Signatories ONLY (as agreed as part of the STM

Guidelines) Any licence granted for a particular edition of a Work will apply also to subsequent editions of it and for editions in other languages, provided such editions are for the Work as a whole in situ and do not involve the separate exploitation of the permitted illustrations or excerpts.

CCC Republication Terms and Conditions

1. Description of Service; Defined Terms. This Republication License enables the User to obtain licenses for republication of one or more copyrighted works as described in detail on the relevant Order Confirmation (the "Work(s)"). Copyright Clearance Center, Inc. ("CCC") grants licenses through the Service on behalf of the rightsholder identified on the Order Confirmation (the "Rightsholder"). "Republication", as used herein, generally means the inclusion of a Work, in whole or in part, in a new work or works, also as described on the Order Confirmation. "User", as used herein, means the person or entity making such republication.
2. The terms set forth in the relevant Order Confirmation, and any terms set by the Rightsholder with respect to a particular Work, govern the terms of use of Works in connection with the Service. By using the Service, the person transacting for a republication license on behalf of the User represents and warrants that he/she/it (a) has been duly authorized by the User to accept, and hereby does accept, all such terms and conditions on behalf of User, and (b) shall inform User of all such terms and conditions. In the event such person is a "freelancer" or other third party independent of User and CCC, such party shall be deemed jointly a "User" for purposes of these terms and conditions. In any event, User shall be deemed to have accepted and agreed to all such terms and conditions if User republishes the Work in any fashion.
3. Scope of License; Limitations and Obligations.
 - 3.1. All Works and all rights therein, including copyright rights, remain the sole and exclusive property of the Rightsholder. The license created by the exchange of an Order Confirmation (and/or any invoice) and payment by User of the full amount set forth on that document includes only those rights expressly set forth in the Order Confirmation and in these terms and conditions, and conveys no other rights in the Work(s) to User. All rights not expressly granted are hereby reserved.
 - 3.2. General Payment Terms: You may pay by credit card or through an account with us payable at the end of the month. If you and we agree that you may establish a standing account with CCC, then the following terms apply: Remit Payment to: Copyright Clearance Center, 29118 Network Place, Chicago, IL 60673-1291. Payments Due: Invoices are payable upon their delivery to you (or upon our notice to you that they are available to you for downloading). After 30 days, outstanding amounts will be subject to a service charge of 1-1/2% per month or, if less, the maximum rate allowed by applicable law. Unless otherwise specifically set forth in the Order Confirmation or in a separate written agreement signed by CCC, invoices are due and payable on "net 30" terms. While User may exercise the rights licensed immediately upon issuance of the Order Confirmation, the license is automatically revoked and is null and void, as if it had never been issued, if complete payment for the license is not received on a timely basis either from User directly or through a payment agent, such as a credit card company.
 - 3.3. Unless otherwise provided in the Order Confirmation, any grant of rights to User (i) is "one-time" (including the editions and product family specified in the license), (ii) is non-exclusive and non-transferable and (iii) is subject to any and all limitations and restrictions (such as, but not limited to, limitations on duration of use or circulation) included in the Order Confirmation or invoice and/or in these terms and conditions. Upon completion of the licensed use, User shall either secure a new permission for further use of the Work(s) or immediately cease any new use of the Work(s) and shall render inaccessible (such as by deleting or by removing or severing links or other locators) any further copies of the Work (except for copies printed on paper in accordance with this license and still in User's stock at the end of such period).
 - 3.4. In the event that the material for which a republication license is sought includes third party materials (such as photographs, illustrations, graphs, inserts and similar materials) which are identified in such material as having been used by permission, User is responsible for identifying, and seeking separate licenses (under this Service or otherwise) for, any of such third party materials; without a separate license, such third party materials may not be used.
 - 3.5. Use of proper copyright notice for a Work is required as a condition of any license granted under the Service. Unless otherwise provided in the Order Confirmation, a proper copyright notice will read substantially as follows: "Republished with permission of [Rightsholder's name], from [Work's title, author, volume, edition number and year of copyright]; permission conveyed through Copyright Clearance Center, Inc. " Such notice must be provided in a reasonably legible font size and must be placed either

immediately adjacent to the Work as used (for example, as part of a by-line or footnote but not as a separate electronic link) or in the place where substantially all other credits or notices for the new work containing the republished Work are located. Failure to include the required notice results in loss to the Rightsholder and CCC, and the User shall be liable to pay liquidated damages for each such failure equal to twice the use fee specified in the Order Confirmation, in addition to the use fee itself and any other fees and charges specified.

- 3.6. User may only make alterations to the Work if and as expressly set forth in the Order Confirmation. No Work may be used in any way that is defamatory, violates the rights of third parties (including such third parties' rights of copyright, privacy, publicity, or other tangible or intangible property), or is otherwise illegal, sexually explicit or obscene. In addition, User may not conjoin a Work with any other material that may result in damage to the reputation of the Rightsholder. User agrees to inform CCC if it becomes aware of any infringement of any rights in a Work and to cooperate with any reasonable request of CCC or the Rightsholder in connection therewith.
4. Indemnity. User hereby indemnifies and agrees to defend the Rightsholder and CCC, and their respective employees and directors, against all claims, liability, damages, costs and expenses, including legal fees and expenses, arising out of any use of a Work beyond the scope of the rights granted herein, or any use of a Work which has been altered in any unauthorized way by User, including claims of defamation or infringement of rights of copyright, publicity, privacy or other tangible or intangible property.
5. Limitation of Liability. UNDER NO CIRCUMSTANCES WILL CCC OR THE RIGHTSHOLDER BE LIABLE FOR ANY DIRECT, INDIRECT, CONSEQUENTIAL OR INCIDENTAL DAMAGES (INCLUDING WITHOUT LIMITATION DAMAGES FOR LOSS OF BUSINESS PROFITS OR INFORMATION, OR FOR BUSINESS INTERRUPTION) ARISING OUT OF THE USE OR INABILITY TO USE A WORK, EVEN IF ONE OF THEM HAS BEEN ADVISED OF THE POSSIBILITY OF SUCH DAMAGES. In any event, the total liability of the Rightsholder and CCC (including their respective employees and directors) shall not exceed the total amount actually paid by User for this license. User assumes full liability for the actions and omissions of its principals, employees, agents, affiliates, successors and assigns.
6. Limited Warranties. THE WORK(S) AND RIGHT(S) ARE PROVIDED "AS IS". CCC HAS THE RIGHT TO GRANT TO USER THE RIGHTS GRANTED IN THE ORDER CONFIRMATION DOCUMENT. CCC AND THE RIGHTSHOLDER DISCLAIM ALL OTHER WARRANTIES RELATING TO THE WORK(S) AND RIGHT(S), EITHER EXPRESS OR IMPLIED, INCLUDING WITHOUT LIMITATION IMPLIED WARRANTIES OF MERCHANTABILITY OR FITNESS FOR A PARTICULAR PURPOSE. ADDITIONAL RIGHTS MAY BE REQUIRED TO USE ILLUSTRATIONS, GRAPHS, PHOTOGRAPHS, ABSTRACTS, INSERTS OR OTHER PORTIONS OF THE WORK (AS OPPOSED TO THE ENTIRE WORK) IN A MANNER CONTEMPLATED BY USER; USER UNDERSTANDS AND AGREES THAT NEITHER CCC NOR THE RIGHTSHOLDER MAY HAVE SUCH ADDITIONAL RIGHTS TO GRANT.
7. Effect of Breach. Any failure by User to pay any amount when due, or any use by User of a Work beyond the scope of the license set forth in the Order Confirmation and/or these terms and conditions, shall be a material breach of the license created by the Order Confirmation and these terms and conditions. Any breach not cured within 30 days of written notice thereof shall result in immediate termination of such license without further notice. Any unauthorized (but licensable) use of a Work that is terminated immediately upon notice thereof may be liquidated by payment of the Rightsholder's ordinary license price therefor; any unauthorized (and unlicensable) use that is not terminated immediately for any reason (including, for example, because materials containing the Work cannot reasonably be recalled) will be subject to all remedies available at law or in equity, but in no event to a payment of less than three times the Rightsholder's ordinary license price for the most closely analogous licensable use plus Rightsholder's and/or CCC's costs and expenses incurred in collecting such payment.
8. Miscellaneous.
 - 8.1. User acknowledges that CCC may, from time to time, make changes or additions to the Service or to these terms and conditions, and CCC reserves the right to send notice to the User by electronic mail or otherwise for the purposes of notifying User of such changes or additions; provided that any such changes or additions shall not apply to permissions already secured and paid for.
 - 8.2. Use of User-related information collected through the Service is governed by CCC's privacy policy, available online here: <https://marketplace.copyright.com/rs-ui-web/mp/privacy-policy>
 - 8.3. The licensing transaction described in the Order Confirmation is personal to User. Therefore, User may not assign or transfer to any other person (whether a natural person or an organization of any kind) the

license created by the Order Confirmation and these terms and conditions or any rights granted hereunder; provided, however, that User may assign such license in its entirety on written notice to CCC in the event of a transfer of all or substantially all of User's rights in the new material which includes the Work(s) licensed under this Service.

- 8.4. No amendment or waiver of any terms is binding unless set forth in writing and signed by the parties. The Rightsholder and CCC hereby object to any terms contained in any writing prepared by the User or its principals, employees, agents or affiliates and purporting to govern or otherwise relate to the licensing transaction described in the Order Confirmation, which terms are in any way inconsistent with any terms set forth in the Order Confirmation and/or in these terms and conditions or CCC's standard operating procedures, whether such writing is prepared prior to, simultaneously with or subsequent to the Order Confirmation, and whether such writing appears on a copy of the Order Confirmation or in a separate instrument.
- 8.5. The licensing transaction described in the Order Confirmation document shall be governed by and construed under the law of the State of New York, USA, without regard to the principles thereof of conflicts of law. Any case, controversy, suit, action, or proceeding arising out of, in connection with, or related to such licensing transaction shall be brought, at CCC's sole discretion, in any federal or state court located in the County of New York, State of New York, USA, or in any federal or state court whose geographical jurisdiction covers the location of the Rightsholder set forth in the Order Confirmation. The parties expressly submit to the personal jurisdiction and venue of each such federal or state court. If you have any comments or questions about the Service or Copyright Clearance Center, please contact us at 978-750-8400 or send an e-mail to support@copyright.com.

v 1.1

**SPRINGER NATURE LICENSE
TERMS AND CONDITIONS**

Feb 20, 2020

This Agreement between Indian Institute of Science Education and Research pune -- soumendu roy ("You") and Springer Nature ("Springer Nature") consists of your license details and the terms and conditions provided by Springer Nature and Copyright Clearance Center.

License Number 4773120421724

License date Feb 20, 2020

Licensed Content Publisher Springer Nature

Licensed Content Publication Nature Chemistry

Licensed Content Title Visible-light-enhanced catalytic oxidation reactions on plasmonic silver nanostructures

Licensed Content Author Phillip Christopher et al

Licensed Content Date May 1, 2011

Type of Use Thesis/Dissertation

Requestor type academic/university or research institute

Format print and electronic

Portion figures/tables/illustrations

Number of figures/tables/illustrations 3

High-res required no

Will you be translating? no

Circulation/distribution 1 - 29

Author of this Springer Nature content no

Title PhD student

Institution name Indian Institute of Science Education and Research

Expected presentation date Apr 2020

Order reference number 16

Portions Figure 1 a,b, Figure 3b

Indian Institute of Science Education and Research pune
iiser pune, pune 411008

Requestor Location

Pune, Maharashtra 411008

India

Attn: Indian Institute of Science Education and Research pune

Total 0.00 USD

Terms and Conditions

Springer Nature Customer Service Centre GmbH Terms and Conditions

This agreement sets out the terms and conditions of the licence (the **Licence**) between you and **Springer Nature Customer Service Centre GmbH** (the **Licensor**). By clicking 'accept' and completing the transaction for the material (**Licensed Material**), you also confirm your acceptance of these terms and conditions.

1. Grant of License

1. 1. The Licensor grants you a personal, non-exclusive, non-transferable, world-wide licence to reproduce the Licensed Material for the purpose specified in your order only. Licences are granted for the specific use requested in the order and for no other use, subject to the conditions below.

1. 2. The Licensor warrants that it has, to the best of its knowledge, the rights to license reuse of the Licensed Material. However, you should ensure that the material you are requesting is original to the Licensor and does not carry the copyright of

another entity (as credited in the published version).

1. 3. If the credit line on any part of the material you have requested indicates that it was reprinted or adapted with permission from another source, then you should also seek permission from that source to reuse the material.

2. Scope of Licence

2. 1. You may only use the Licensed Content in the manner and to the extent permitted by these Ts&Cs and any applicable laws.

2. 2. A separate licence may be required for any additional use of the Licensed Material, e.g. where a licence has been purchased for print only use, separate permission must be obtained for electronic re-use. Similarly, a licence is only valid in the language selected and does not apply for editions in other languages unless additional translation rights have been granted separately in the licence. Any content owned by third parties are expressly excluded from the licence.

2. 3. Similarly, rights for additional components such as custom editions and derivatives require additional permission and may be subject to an additional fee.

Please apply to

Journalpermissions@springernature.com/bookpermissions@springernature.com for these rights.

2. 4. Where permission has been granted **free of charge** for material in print, permission may also be granted for any electronic version of that work, provided that the material is incidental to your work as a whole and that the electronic version is essentially equivalent to, or substitutes for, the print version.

2. 5. An alternative scope of licence may apply to signatories of the [STM Permissions Guidelines](#), as amended from time to time.

3. Duration of Licence

3. 1. A licence for is valid from the date of purchase ('Licence Date') at the end of the relevant period in the below table:

Scope of Licence	Duration of Licence
Post on a website	12 months
Presentations	12 months
Books and journals	Lifetime of the edition in the language purchased

4. Acknowledgement

4. 1. The Licensor's permission must be acknowledged next to the Licenced Material in print. In electronic form, this acknowledgement must be visible at the same time as the figures/tables/illustrations or abstract, and must be hyperlinked to the journal/book's homepage. Our required acknowledgement format is in the Appendix below.

5. Restrictions on use

5. 1. Use of the Licensed Material may be permitted for incidental promotional use and minor editing privileges e.g. minor adaptations of single figures, changes of format, colour and/or style where the adaptation is credited as set out in Appendix 1 below. Any other changes including but not limited to, cropping, adapting, omitting material that affect the meaning, intention or moral rights of the author are strictly prohibited.

5. 2. You must not use any Licensed Material as part of any design or trademark.

5. 3. Licensed Material may be used in Open Access Publications (OAP) before publication by Springer Nature, but any Licensed Material must be removed from OAP sites prior to final publication.

6. Ownership of Rights

6. 1. Licensed Material remains the property of either Licensor or the relevant third party and any rights not explicitly granted herein are expressly reserved.

7. Warranty

IN NO EVENT SHALL LICENSOR BE LIABLE TO YOU OR ANY OTHER PARTY OR ANY OTHER PERSON OR FOR ANY SPECIAL, CONSEQUENTIAL, INCIDENTAL OR INDIRECT DAMAGES, HOWEVER CAUSED, ARISING OUT OF OR IN CONNECTION WITH THE DOWNLOADING, VIEWING OR USE OF THE MATERIALS REGARDLESS OF THE FORM OF ACTION, WHETHER FOR BREACH OF CONTRACT, BREACH OF WARRANTY, TORT, NEGLIGENCE, INFRINGEMENT OR OTHERWISE (INCLUDING, WITHOUT LIMITATION, DAMAGES BASED ON LOSS OF PROFITS, DATA, FILES, USE, BUSINESS OPPORTUNITY OR CLAIMS OF THIRD PARTIES), AND WHETHER OR NOT THE PARTY HAS BEEN ADVISED OF THE POSSIBILITY OF SUCH DAMAGES. THIS LIMITATION SHALL APPLY NOTWITHSTANDING ANY FAILURE OF ESSENTIAL PURPOSE OF ANY LIMITED REMEDY PROVIDED HEREIN.

8. Limitations

8. 1. BOOKS ONLY: Where '**reuse in a dissertation/thesis**' has been selected the following terms apply: Print rights of the final author's accepted manuscript (for clarity, NOT the published version) for up to 100 copies, electronic rights for use only on a personal website or institutional repository as defined by the Sherpa guideline (www.sherpa.ac.uk/romeo/).

9. Termination and Cancellation

9. 1. Licences will expire after the period shown in Clause 3 (above).

9. 2. Licensee reserves the right to terminate the Licence in the event that payment is not received in full or if there has been a breach of this agreement by you.

Appendix 1 — Acknowledgements:**For Journal Content:**

Reprinted by permission from [the Licensor]: [Journal Publisher (e.g. Nature/Springer/Palgrave)] [JOURNAL NAME] [REFERENCE CITATION (Article name, Author(s) Name), [COPYRIGHT] (year of publication)

For Advance Online Publication papers:

Reprinted by permission from [the Licensor]: [Journal Publisher (e.g. Nature/Springer/Palgrave)] [JOURNAL NAME] [REFERENCE CITATION (Article name, Author(s) Name), [COPYRIGHT] (year of publication), advance online publication, day month year (doi: 10.1038/sj.[JOURNAL ACRONYM].)

For Adaptations/Translations:

Adapted/Translated by permission from [the Licensor]: [Journal Publisher (e.g. Nature/Springer/Palgrave)] [JOURNAL NAME] [REFERENCE CITATION (Article name, Author(s) Name), [COPYRIGHT] (year of publication)

Note: For any republication from the British Journal of Cancer, the following credit line style applies:

Reprinted/adapted/translated by permission from [the Licensor]: on behalf of Cancer Research UK: : [Journal Publisher (e.g. Nature/Springer/Palgrave)] [JOURNAL NAME] [REFERENCE CITATION (Article name, Author(s) Name), [COPYRIGHT] (year of publication)

For Advance Online Publication papers:

Reprinted by permission from The [the Licensor]: on behalf of Cancer Research UK: [Journal Publisher (e.g. Nature/Springer/Palgrave)] [JOURNAL NAME] [REFERENCE CITATION (Article name, Author(s) Name), [COPYRIGHT] (year of publication), advance online publication, day month year (doi: 10.1038/sj.[JOURNAL ACRONYM])

For Book content:

Reprinted/adapted by permission from [the Licensor]: [Book Publisher (e.g. Palgrave Macmillan, Springer etc)] [Book Title] by [Book author(s)] [COPYRIGHT] (year of publication)

Other Conditions:

Version 1.2

Questions? customercare@copyright.com or +1-855-239-3415 (toll free in the US) or +1-978-646-2777.



RightsLink®



Home



Help



Email Support



soumendu roy ▾

Hot Electrons Do the Impossible: Plasmon-Induced Dissociation of H₂ on Au



Author: Shaunak Mukherjee, Florian Libisch, Nicolas Large, et al

Publication: Nano Letters

Publisher: American Chemical Society

Date: Jan 1, 2013

Copyright © 2013, American Chemical Society

PERMISSION/LICENSE IS GRANTED FOR YOUR ORDER AT NO CHARGE

This type of permission/license, instead of the standard Terms & Conditions, is sent to you because no fee is being charged for your order. Please note the following:

- Permission is granted for your request in both print and electronic formats, and translations.
 - If figures and/or tables were requested, they may be adapted or used in part.
 - Please print this page for your records and send a copy of it to your publisher/graduate school.
 - Appropriate credit for the requested material should be given as follows: "Reprinted (adapted) with permission from (COMPLETE REFERENCE CITATION). Copyright (YEAR) American Chemical Society." Insert appropriate information in place of the capitalized words.
 - One-time permission is granted only for the use specified in your request. No additional uses are granted (such as derivative works or other editions). For any other uses, please submit a new request.
- If credit is given to another source for the material you requested, permission must be obtained from that source.

[BACK](#)[CLOSE WINDOW](#)



RightsLink®



Home



Help



Email Support



soumendu roy ▾

Plasmonic Control of Multi-Electron Transfer and C–C Coupling in Visible-Light-Driven CO₂ Reduction on Au Nanoparticles



Author: Sungju Yu, Andrew J. Wilson, Jaeyoung Heo, et al

Publication: Nano Letters

Publisher: American Chemical Society

Date: Apr 1, 2018

Copyright © 2018, American Chemical Society

PERMISSION/LICENSE IS GRANTED FOR YOUR ORDER AT NO CHARGE

This type of permission/license, instead of the standard Terms & Conditions, is sent to you because no fee is being charged for your order. Please note the following:

- Permission is granted for your request in both print and electronic formats, and translations.
 - If figures and/or tables were requested, they may be adapted or used in part.
 - Please print this page for your records and send a copy of it to your publisher/graduate school.
 - Appropriate credit for the requested material should be given as follows: "Reprinted (adapted) with permission from (COMPLETE REFERENCE CITATION). Copyright (YEAR) American Chemical Society." Insert appropriate information in place of the capitalized words.
 - One-time permission is granted only for the use specified in your request. No additional uses are granted (such as derivative works or other editions). For any other uses, please submit a new request.
- If credit is given to another source for the material you requested, permission must be obtained from that source.

[BACK](#)[CLOSE WINDOW](#)



Soumendu Roy <soumendu.roy@students.iiserpune.ac.in>

Regarding Incident 3335394 Request for rights and permission

1 message

support@services.acs.org <support@services.acs.org>
To: soumendu.roy@students.iiserpune.ac.in

Thu, Feb 20, 2020 at 11:09 PM



Dear Soumendu,

Your permission requested is granted and there is no fee for this reuse.

In your planned reuse, you must cite the ACS article as the source, add this direct link: <<https://pubs.acs.org/doi/abs/10.1021/jacs.6b00179>>, and include a notice to readers that further permissions related to the material excerpted should be directed to the ACS.

Please do not hesitate to contact me if you need any further assistance.

Regards,

Jawwad Saeed

ACS Customer Services & Information

<https://help.acs.org>

Incident Information:

Incident #: 3335394

Date Created: 2020-02-20T11:36:20

Priority: 3

Customer: Soumendu Roy

Title: Request for rights and permission

Description: Hi...

This is Soumendu Roy, a Graduate Student in the Department of Chemistry, Indian Institute of Science Education and Research Pune, India. I am writing this, asking for your permission for reusing some figures from the following ACS article in my thesis. My thesis is focused on investigating the role of surface ligands on the catalytic property of metal NPs. The figures will be used to explain the inadvertent role of surface ligands in metal NP catalysis.

The details of my request are mentioned below. I would appreciate it if you kindly allow me to use the following content.

Article link: <https://pubs.acs.org/doi/abs/10.1021/jacs.6b00179>

2/21/2020

IISER, Pune Mail - Regarding Incident 3335394 Request for rights and permission
no.of figures to be reused: 3, Figures 1J, 3 A, D

Best Regards

Soumendu

--

Soumendu Roy

PhD student

Dr. Pramod P.Pillai's Group

Chemistry Department

IISER Pune

{CMI: MCID867820}



RightsLink®



Home



Help



Email Support



soumendu roy ▾

Impact of Gold Nanoparticle Stabilizing Ligands on the Colloidal Catalytic Reduction of 4-Nitrophenol

**Author:** Siyam M. Ansar, Christopher L. Kitchens**Publication:** ACS Catalysis**Publisher:** American Chemical Society**Date:** Aug 1, 2016*Copyright © 2016, American Chemical Society*

PERMISSION/LICENSE IS GRANTED FOR YOUR ORDER AT NO CHARGE

This type of permission/license, instead of the standard Terms & Conditions, is sent to you because no fee is being charged for your order. Please note the following:

- Permission is granted for your request in both print and electronic formats, and translations.
 - If figures and/or tables were requested, they may be adapted or used in part.
 - Please print this page for your records and send a copy of it to your publisher/graduate school.
 - Appropriate credit for the requested material should be given as follows: "Reprinted (adapted) with permission from (COMPLETE REFERENCE CITATION). Copyright (YEAR) American Chemical Society." Insert appropriate information in place of the capitalized words.
 - One-time permission is granted only for the use specified in your request. No additional uses are granted (such as derivative works or other editions). For any other uses, please submit a new request.
- If credit is given to another source for the material you requested, permission must be obtained from that source.

[BACK](#)[CLOSE WINDOW](#)



RightsLink®



Home



Help



Email Support



soumendu roy ▾

Ligands Affect Hydrogen Absorption and Desorption by Palladium Nanoparticles



Author: Noah J. J. Johnson, Brian Lam, Rebecca S. Sherbo, et al

Publication: Chemistry of Materials

Publisher: American Chemical Society

Date: Nov 1, 2019

Copyright © 2019, American Chemical Society

PERMISSION/LICENSE IS GRANTED FOR YOUR ORDER AT NO CHARGE

This type of permission/license, instead of the standard Terms & Conditions, is sent to you because no fee is being charged for your order. Please note the following:

- Permission is granted for your request in both print and electronic formats, and translations.
 - If figures and/or tables were requested, they may be adapted or used in part.
 - Please print this page for your records and send a copy of it to your publisher/graduate school.
 - Appropriate credit for the requested material should be given as follows: "Reprinted (adapted) with permission from (COMPLETE REFERENCE CITATION). Copyright (YEAR) American Chemical Society." Insert appropriate information in place of the capitalized words.
 - One-time permission is granted only for the use specified in your request. No additional uses are granted (such as derivative works or other editions). For any other uses, please submit a new request.
- If credit is given to another source for the material you requested, permission must be obtained from that source.

[BACK](#)[CLOSE WINDOW](#)

**SPRINGER NATURE LICENSE
TERMS AND CONDITIONS**

Feb 21, 2020

This Agreement between Indian Institute of Science Education and Research pune --
soumendu roy ("You") and Springer Nature ("Springer Nature") consists of your license
details and the terms and conditions provided by Springer Nature and Copyright Clearance
Center.

License Number 4773670986301

License date Feb 21, 2020

Licensed Content Publisher Springer Nature

Licensed Content Publication Nature Materials

Licensed Content Title Controlled selectivity for palladium catalysts using self-
assembled monolayers

Licensed Content Author Stephen T. Marshall et al

Licensed Content Date Sep 12, 2010

Type of Use Thesis/Dissertation

Requestor type academic/university or research institute

Format print and electronic

Portion figures/tables/illustrations

Number of
figures/tables/illustrations 2

High-res required no

Will you be translating?	no
Circulation/distribution	1 - 29
Author of this Springer Nature content	no
Title	PhD student
Institution name	Indian Institute of Science Education and Research
Expected presentation date	Apr 2020
Order reference number	21
Portions	Figures 1 and 3
Requestor Location	Indian Institute of Science Education and Research pune iiser pune, pune 411008
Total	0.00 USD

Terms and Conditions

Springer Nature Customer Service Centre GmbH Terms and Conditions

This agreement sets out the terms and conditions of the licence (the **Licence**) between you and **Springer Nature Customer Service Centre GmbH** (the **Licensor**). By clicking 'accept' and completing the transaction for the material (**Licensed Material**), you also confirm your acceptance of these terms and conditions.

1. Grant of License

1. 1. The Licensor grants you a personal, non-exclusive, non-transferable, world-wide licence to reproduce the Licensed Material for the purpose specified in your order only. Licences are granted for the specific use requested in the order and for no other use, subject to the conditions below.

1. 2. The Licensor warrants that it has, to the best of its knowledge, the rights to license reuse of the Licensed Material. However, you should ensure that the material

you are requesting is original to the Licensor and does not carry the copyright of another entity (as credited in the published version).

1. 3. If the credit line on any part of the material you have requested indicates that it was reprinted or adapted with permission from another source, then you should also seek permission from that source to reuse the material.

2. Scope of Licence

2. 1. You may only use the Licensed Content in the manner and to the extent permitted by these Ts&Cs and any applicable laws.

2. 2. A separate licence may be required for any additional use of the Licensed Material, e.g. where a licence has been purchased for print only use, separate permission must be obtained for electronic re-use. Similarly, a licence is only valid in the language selected and does not apply for editions in other languages unless additional translation rights have been granted separately in the licence. Any content owned by third parties are expressly excluded from the licence.

2. 3. Similarly, rights for additional components such as custom editions and derivatives require additional permission and may be subject to an additional fee.

Please apply to

Journalpermissions@springernature.com/bookpermissions@springernature.com for these rights.

2. 4. Where permission has been granted **free of charge** for material in print, permission may also be granted for any electronic version of that work, provided that the material is incidental to your work as a whole and that the electronic version is essentially equivalent to, or substitutes for, the print version.

2. 5. An alternative scope of licence may apply to signatories of the [STM Permissions Guidelines](#), as amended from time to time.

3. Duration of Licence

3. 1. A licence for is valid from the date of purchase ('Licence Date') at the end of the relevant period in the below table:

Scope of Licence	Duration of Licence
Post on a website	12 months
Presentations	12 months
Books and journals	Lifetime of the edition in the language purchased

4. Acknowledgement

4. 1. The Licensor's permission must be acknowledged next to the Licenced Material in print. In electronic form, this acknowledgement must be visible at the same time as the figures/tables/illustrations or abstract, and must be hyperlinked to the journal/book's homepage. Our required acknowledgement format is in the Appendix below.

5. Restrictions on use

5. 1. Use of the Licensed Material may be permitted for incidental promotional use and minor editing privileges e.g. minor adaptations of single figures, changes of format, colour and/or style where the adaptation is credited as set out in Appendix 1 below. Any other changes including but not limited to, cropping, adapting, omitting material that affect the meaning, intention or moral rights of the author are strictly prohibited.

5. 2. You must not use any Licensed Material as part of any design or trademark.

5. 3. Licensed Material may be used in Open Access Publications (OAP) before publication by Springer Nature, but any Licensed Material must be removed from OAP sites prior to final publication.

6. Ownership of Rights

6. 1. Licensed Material remains the property of either Licensor or the relevant third party and any rights not explicitly granted herein are expressly reserved.

7. Warranty

IN NO EVENT SHALL LICENSOR BE LIABLE TO YOU OR ANY OTHER PARTY OR ANY OTHER PERSON OR FOR ANY SPECIAL, CONSEQUENTIAL, INCIDENTAL OR INDIRECT DAMAGES, HOWEVER CAUSED, ARISING OUT OF OR IN CONNECTION WITH THE DOWNLOADING, VIEWING OR USE OF THE MATERIALS REGARDLESS OF THE FORM OF ACTION, WHETHER FOR BREACH OF CONTRACT, BREACH OF WARRANTY, TORT, NEGLIGENCE, INFRINGEMENT OR OTHERWISE (INCLUDING, WITHOUT LIMITATION, DAMAGES BASED ON LOSS OF PROFITS, DATA, FILES, USE, BUSINESS OPPORTUNITY OR CLAIMS OF THIRD PARTIES), AND WHETHER OR NOT THE PARTY HAS BEEN ADVISED OF THE POSSIBILITY OF SUCH DAMAGES. THIS LIMITATION SHALL APPLY NOTWITHSTANDING ANY FAILURE OF ESSENTIAL PURPOSE OF ANY LIMITED REMEDY PROVIDED HEREIN.

8. Limitations

8. 1. BOOKS ONLY: Where 'reuse in a dissertation/thesis' has been selected the following terms apply: Print rights of the final author's accepted manuscript (for clarity, NOT the published version) for up to 100 copies, electronic rights for use only on a personal website or institutional repository as defined by the Sherpa guideline (www.sherpa.ac.uk/romeo/).

9. Termination and Cancellation

9. 1. Licences will expire after the period shown in Clause 3 (above).

9. 2. Licensee reserves the right to terminate the Licence in the event that payment is not received in full or if there has been a breach of this agreement by you.

Appendix 1 — Acknowledgements:**For Journal Content:**

Reprinted by permission from [the Licensor]: [Journal Publisher (e.g. Nature/Springer/Palgrave)] [JOURNAL NAME] [REFERENCE CITATION (Article name, Author(s) Name), [COPYRIGHT] (year of publication)

For Advance Online Publication papers:

Reprinted by permission from [the Licensor]: [Journal Publisher (e.g. Nature/Springer/Palgrave)] [JOURNAL NAME] [REFERENCE CITATION (Article name, Author(s) Name), [COPYRIGHT] (year of publication), advance online publication, day month year (doi: 10.1038/sj.[JOURNAL ACRONYM].)

For Adaptations/Translations:

Adapted/Translated by permission from [the Licensor]: [Journal Publisher (e.g. Nature/Springer/Palgrave)] [JOURNAL NAME] [REFERENCE CITATION (Article name, Author(s) Name), [COPYRIGHT] (year of publication)

Note: For any republication from the British Journal of Cancer, the following credit line style applies:

Reprinted/adapted/translated by permission from [the Licensor]: on behalf of Cancer Research UK: : [Journal Publisher (e.g. Nature/Springer/Palgrave)] [JOURNAL NAME] [REFERENCE CITATION (Article name, Author(s) Name), [COPYRIGHT] (year of publication)

For Advance Online Publication papers:

Reprinted by permission from The [the Licensor]: on behalf of Cancer Research UK: [Journal Publisher (e.g. Nature/Springer/Palgrave)] [JOURNAL NAME] [REFERENCE CITATION (Article name, Author(s) Name), [COPYRIGHT] (year of publication), advance online publication, day month year (doi: 10.1038/sj.[JOURNAL ACRONYM])

For Book content:

Reprinted/adapted by permission from [the Licensor]: [Book Publisher (e.g. Palgrave Macmillan, Springer etc)] [Book Title] by [Book author(s)] [COPYRIGHT] (year of publication)

Other Conditions:

Version 1.2

Questions? customercare@copyright.com or +1-855-239-3415 (toll free in the US) or +1-978-646-2777.

SPRINGER NATURE LICENSE TERMS AND CONDITIONS

Feb 21, 2020

This Agreement between Indian Institute of Science Education and Research pune -- soumendu roy ("You") and Springer Nature ("Springer Nature") consists of your license details and the terms and conditions provided by Springer Nature and Copyright Clearance Center.

License Number 4773670098032

License date Feb 21, 2020

Licensed Content Publisher Springer Nature

Licensed Content Publication Nature Materials

Licensed Content Title Interfacial electronic effects control the reaction selectivity of platinum catalysts

Licensed Content Author Guangxu Chen et al

Licensed Content Date Jan 25, 2016

Type of Use Thesis/Dissertation

Requestor type academic/university or research institute

Format print and electronic

Portion figures/tables/illustrations

Number of figures/tables/illustrations 2

High-res required no

Will you be translating?	no
Circulation/distribution	1 - 29
Author of this Springer Nature content	no
Title	PhD student
Institution name	Indian Institute of Science Education and Research
Expected presentation date	Apr 2020
Order reference number	20
Portions	Figures 2b and 3a
Requestor Location	Indian Institute of Science Education and Research pune iiser pune, pune 411008
	Pune, Maharashtra 411008 India Attn: Indian Institute of Science Education and Research pune
Total	0.00 USD

Terms and Conditions

Springer Nature Customer Service Centre GmbH Terms and Conditions

This agreement sets out the terms and conditions of the licence (the **Licence**) between you and **Springer Nature Customer Service Centre GmbH** (the **Licensor**). By clicking 'accept' and completing the transaction for the material (**Licensed Material**), you also confirm your acceptance of these terms and conditions.

1. Grant of License

1. 1. The Licensor grants you a personal, non-exclusive, non-transferable, world-wide licence to reproduce the Licensed Material for the purpose specified in your order only. Licences are granted for the specific use requested in the order and for no other use, subject to the conditions below.

1. 2. The Licensor warrants that it has, to the best of its knowledge, the rights to license reuse of the Licensed Material. However, you should ensure that the material you are requesting is original to the Licensor and does not carry the copyright of

another entity (as credited in the published version).

1. 3. If the credit line on any part of the material you have requested indicates that it was reprinted or adapted with permission from another source, then you should also seek permission from that source to reuse the material.

2. Scope of Licence

2. 1. You may only use the Licensed Content in the manner and to the extent permitted by these Ts&Cs and any applicable laws.

2. 2. A separate licence may be required for any additional use of the Licensed Material, e.g. where a licence has been purchased for print only use, separate permission must be obtained for electronic re-use. Similarly, a licence is only valid in the language selected and does not apply for editions in other languages unless additional translation rights have been granted separately in the licence. Any content owned by third parties are expressly excluded from the licence.

2. 3. Similarly, rights for additional components such as custom editions and derivatives require additional permission and may be subject to an additional fee.

Please apply to

Journalpermissions@springernature.com/bookpermissions@springernature.com for these rights.

2. 4. Where permission has been granted **free of charge** for material in print, permission may also be granted for any electronic version of that work, provided that the material is incidental to your work as a whole and that the electronic version is essentially equivalent to, or substitutes for, the print version.

2. 5. An alternative scope of licence may apply to signatories of the [STM Permissions Guidelines](#), as amended from time to time.

3. Duration of Licence

3. 1. A licence for is valid from the date of purchase ('Licence Date') at the end of the relevant period in the below table:

Scope of Licence	Duration of Licence
Post on a website	12 months
Presentations	12 months
Books and journals	Lifetime of the edition in the language purchased

4. Acknowledgement

4. 1. The Licensor's permission must be acknowledged next to the Licenced Material in print. In electronic form, this acknowledgement must be visible at the same time as the figures/tables/illustrations or abstract, and must be hyperlinked to the journal/book's homepage. Our required acknowledgement format is in the Appendix below.

5. Restrictions on use

5. 1. Use of the Licensed Material may be permitted for incidental promotional use and minor editing privileges e.g. minor adaptations of single figures, changes of format, colour and/or style where the adaptation is credited as set out in Appendix 1 below. Any other changes including but not limited to, cropping, adapting, omitting material that affect the meaning, intention or moral rights of the author are strictly prohibited.

5. 2. You must not use any Licensed Material as part of any design or trademark.

5. 3. Licensed Material may be used in Open Access Publications (OAP) before publication by Springer Nature, but any Licensed Material must be removed from OAP sites prior to final publication.

6. Ownership of Rights

6. 1. Licensed Material remains the property of either Licensor or the relevant third party and any rights not explicitly granted herein are expressly reserved.

7. Warranty

IN NO EVENT SHALL LICENSOR BE LIABLE TO YOU OR ANY OTHER PARTY OR ANY OTHER PERSON OR FOR ANY SPECIAL, CONSEQUENTIAL, INCIDENTAL OR INDIRECT DAMAGES, HOWEVER CAUSED, ARISING OUT OF OR IN CONNECTION WITH THE DOWNLOADING, VIEWING OR USE OF THE MATERIALS REGARDLESS OF THE FORM OF ACTION, WHETHER FOR BREACH OF CONTRACT, BREACH OF WARRANTY, TORT, NEGLIGENCE, INFRINGEMENT OR OTHERWISE (INCLUDING, WITHOUT LIMITATION, DAMAGES BASED ON LOSS OF PROFITS, DATA, FILES, USE, BUSINESS OPPORTUNITY OR CLAIMS OF THIRD PARTIES), AND WHETHER OR NOT THE PARTY HAS BEEN ADVISED OF THE POSSIBILITY OF SUCH DAMAGES. THIS LIMITATION SHALL APPLY NOTWITHSTANDING ANY FAILURE OF ESSENTIAL PURPOSE OF ANY LIMITED REMEDY PROVIDED HEREIN.

8. Limitations

8. 1. BOOKS ONLY: Where 'reuse in a dissertation/thesis' has been selected the following terms apply: Print rights of the final author's accepted manuscript (for clarity, NOT the published version) for up to 100 copies, electronic rights for use only on a personal website or institutional repository as defined by the Sherpa guideline (www.sherpa.ac.uk/romeo/).

9. Termination and Cancellation

9. 1. Licences will expire after the period shown in Clause 3 (above).

9. 2. Licensee reserves the right to terminate the Licence in the event that payment is not received in full or if there has been a breach of this agreement by you.

Appendix 1 — Acknowledgements:**For Journal Content:**

Reprinted by permission from [the Licensor]: [Journal Publisher (e.g. Nature/Springer/Palgrave)] [JOURNAL NAME] [REFERENCE CITATION (Article name, Author(s) Name), [COPYRIGHT] (year of publication)

For Advance Online Publication papers:

Reprinted by permission from [the Licensor]: [Journal Publisher (e.g. Nature/Springer/Palgrave)] [JOURNAL NAME] [REFERENCE CITATION (Article name, Author(s) Name), [COPYRIGHT] (year of publication), advance online publication, day month year (doi: 10.1038/sj.[JOURNAL ACRONYM].)

For Adaptations/Translations:

Adapted/Translated by permission from [the Licensor]: [Journal Publisher (e.g. Nature/Springer/Palgrave)] [JOURNAL NAME] [REFERENCE CITATION (Article name, Author(s) Name), [COPYRIGHT] (year of publication)

Note: For any republication from the British Journal of Cancer, the following credit line style applies:

Reprinted/adapted/translated by permission from [the Licensor]: on behalf of Cancer Research UK: : [Journal Publisher (e.g. Nature/Springer/Palgrave)] [JOURNAL NAME] [REFERENCE CITATION (Article name, Author(s) Name), [COPYRIGHT] (year of publication)

For Advance Online Publication papers:

Reprinted by permission from The [the Licensor]: on behalf of Cancer Research UK: [Journal Publisher (e.g. Nature/Springer/Palgrave)] [JOURNAL NAME] [REFERENCE CITATION (Article name, Author(s) Name), [COPYRIGHT] (year of publication), advance online publication, day month year (doi: 10.1038/sj.[JOURNAL ACRONYM])

For Book content:

Reprinted/adapted by permission from [the Licensor]: [Book Publisher (e.g. Palgrave Macmillan, Springer etc)] [Book Title] by [Book author(s)] [COPYRIGHT] (year of publication)

Other Conditions:

Version 1.2

Questions? customercare@copyright.com or +1-855-239-3415 (toll free in the US) or +1-978-646-2777.



RightsLink®



Home



Help



Email Support



Sign in



Create Account

Complementary Structure Sensitive and Insensitive Catalytic Relationships



Author: Rutger A. Van Santen

Publication: Accounts of Chemical Research

Publisher: American Chemical Society

Date: Jan 1, 2009

Copyright © 2009, American Chemical Society

PERMISSION/LICENSE IS GRANTED FOR YOUR ORDER AT NO CHARGE

This type of permission/license, instead of the standard Terms & Conditions, is sent to you because no fee is being charged for your order. Please note the following:

- Permission is granted for your request in both print and electronic formats, and translations.
 - If figures and/or tables were requested, they may be adapted or used in part.
 - Please print this page for your records and send a copy of it to your publisher/graduate school.
 - Appropriate credit for the requested material should be given as follows: "Reprinted (adapted) with permission from (COMPLETE REFERENCE CITATION). Copyright (YEAR) American Chemical Society." Insert appropriate information in place of the capitalized words.
 - One-time permission is granted only for the use specified in your request. No additional uses are granted (such as derivative works or other editions). For any other uses, please submit a new request.
- If credit is given to another source for the material you requested, permission must be obtained from that source.

[BACK](#)

[CLOSE WINDOW](#)



Marketplace™

Order Confirmation

Thank you, your order has been placed. An email confirmation has been sent to you. Your order license details and printable licenses will be available within 24 hours. Please access Manage Account for final order details.

This is not an invoice. Please go to manage account to access your order history and invoices.

CUSTOMER INFORMATION

Payment by invoice: You can cancel your order until the invoice is generated by contacting customer service.

☰ Billing Address

Mr. soumendu roy
Indian Institute of Science Education and Research
pune
iiser pune, pune 411008
Pune, Maharashtra 411008
India

+91 8551963352
soumendu.roy@students.iiserpune.ac.in

☰ PO Number (optional)

N/A

📍 Customer Location

Mr. soumendu roy
Indian Institute of Science Education and Research
pune
iiser pune, pune 411008
Pune, Maharashtra 411008
India

☰ Payment options

Invoice

PENDING ORDER CONFIRMATION

Total Due: 0.00 USD

Confirmation Number: Pending

Order Date: 24-Feb-2020

1. Chemical communications

0.00 USD

Order license ID
ISSN
Type of Use
Publisher
Portion

Pending
1364-548X
Republish in a thesis/dissertation
ROYAL SOCIETY OF CHEMISTRY
Chart/graph/table/figure

LICENSED CONTENT

Publication Title

Chemical
communications

Author/Editor	Royal Society of Chemistry (Great Britain)	Country	United Kingdom of Great Britain and Northern Ireland
Date	01/01/1996	Rightsholder	Royal Society of Chemistry
Language	English	Publication Type	e-Journal

REQUEST DETAILS

Portion Type	Chart/graph/table/figure	Distribution	Worldwide
Number of charts / graphs / tables / figures requested	1	Translation	Original language of publication
Format (select all that apply)	Print, Electronic	Copies for the disabled?	No
Who will republish the content?	Academic institution	Minor editing privileges?	No
Duration of Use	Life of current edition	Incidental promotional use?	No
Lifetime Unit Quantity	Up to 499	Currency	USD
Rights Requested	Main product		

NEW WORK DETAILS

Title	Regulation of Nanoparticle-reactant interaction outplays ligand poisoning in metal nanoparticle catalyzed reactions	Institution name	Indian Institute of Science Education and Research Pune
Instructor name	Dr.Pramod Pillai	Expected presentation date	2020-04-30

ADDITIONAL DETAILS

Order reference number	25	The requesting person / organization to appear on the license	Soumendu Roy
------------------------	----	---	--------------

REUSE CONTENT DETAILS

Title, description or numeric reference of the portion(s)	Nitroarene reduction: a trusted model reaction to test nanoparticle catalysts	Title of the article/chapter the portion is from	Nitroarene reduction: a trusted model reaction to test nanoparticle catalysts
Editor of portion(s)	NA	Author of portion(s)	Royal Society of Chemistry (Great Britain)
Volume of serial or monograph	51	Issue, if republishing an article from a serial	N/A
Page or page range of portion	9415,9416	Publication date of portion	2015-03-20

Order Total: 0.00 USD

Total Items: 1

Total Due: 0.00 USD

Accepted: All Publisher and CCC Terms and Conditions



Home



Help



Email Support



Sign in



Create Account

Redox Catalytic Properties of Palladium Nanoparticles: Surfactant and Electron Donor–Acceptor Effects



Author: Nikhil R. Jana, Z. L. Wang, Tarasankar Pal

Publication: Langmuir

Publisher: American Chemical Society

Date: Mar 1, 2000

Copyright © 2000, American Chemical Society

PERMISSION/LICENSE IS GRANTED FOR YOUR ORDER AT NO CHARGE

This type of permission/license, instead of the standard Terms & Conditions, is sent to you because no fee is being charged for your order. Please note the following:

- Permission is granted for your request in both print and electronic formats, and translations.
 - If figures and/or tables were requested, they may be adapted or used in part.
 - Please print this page for your records and send a copy of it to your publisher/graduate school.
 - Appropriate credit for the requested material should be given as follows: "Reprinted (adapted) with permission from (COMPLETE REFERENCE CITATION). Copyright (YEAR) American Chemical Society." Insert appropriate information in place of the capitalized words.
 - One-time permission is granted only for the use specified in your request. No additional uses are granted (such as derivative works or other editions). For any other uses, please submit a new request.
- If credit is given to another source for the material you requested, permission must be obtained from that source.

[BACK](#)

[CLOSE WINDOW](#)



Marketplace™

Order Confirmation

Thank you, your order has been placed. An email confirmation has been sent to you. Your order license details and printable licenses will be available within 24 hours. Please access Manage Account for final order details.

This is not an invoice. Please go to manage account to access your order history and invoices.

CUSTOMER INFORMATION

Payment by invoice: You can cancel your order until the invoice is generated by contacting customer service.

☰ Billing Address

Mr. soumendu roy
Indian Institute of Science Education and Research
pune
iiser pune, pune 411008
Pune, Maharashtra 411008
India

+91 8551963352
soumendu.roy@students.iiserpune.ac.in

☰ PO Number (optional)

N/A

📍 Customer Location

Mr. soumendu roy
Indian Institute of Science Education and Research
pune
iiser pune, pune 411008
Pune, Maharashtra 411008
India

☰ Payment options

Invoice

PENDING ORDER CONFIRMATION

Total Due: 0.00 USD

Confirmation Number: Pending

Order Date: 25-Feb-2020

1. Chemical communications

0.00 USD

Order license ID
ISSN
Type of Use
Publisher
Portion

Pending
1364-548X
Republish in a thesis/dissertation
ROYAL SOCIETY OF CHEMISTRY
Chart/graph/table/figure

LICENSED CONTENT

Publication Title

Chemical
communications

Author/Editor	Royal Society of Chemistry (Great Britain)	Country	United Kingdom of Great Britain and Northern Ireland
Date	01/01/1996	Rightsholder	Royal Society of Chemistry
Language	English	Publication Type	e-Journal

REQUEST DETAILS

Portion Type	Chart/graph/table/figure	Distribution	Worldwide
Number of charts / graphs / tables / figures requested	1	Translation	Original language of publication
Format (select all that apply)	Print, Electronic	Copies for the disabled?	No
Who will republish the content?	Academic institution	Minor editing privileges?	No
Duration of Use	Life of current edition	Incidental promotional use?	No
Lifetime Unit Quantity	Up to 499	Currency	USD
Rights Requested	Main product		

NEW WORK DETAILS

Title	Regulation of Nanoparticle-reactant interaction outplays ligand poisoning in metal nanoparticle catalyzed reactions	Institution name	Indian Institute of Science Education and Research Pune
Instructor name	Dr.Pramod Pillai	Expected presentation date	2020-04-30

ADDITIONAL DETAILS

Order reference number	25	The requesting person / organization to appear on the license	Soumendu Roy
------------------------	----	---	--------------

REUSE CONTENT DETAILS

Title, description or numeric reference of the portion(s)	Nitroarene reduction: a trusted model reaction to test nanoparticle catalysts	Title of the article/chapter the portion is from	Nitroarene reduction: a trusted model reaction to test nanoparticle catalysts
Editor of portion(s)	NA	Author of portion(s)	Royal Society of Chemistry (Great Britain)
Volume of serial or monograph	51	Issue, if republishing an article from a serial	N/A
Page or page range of portion	9415,9416	Publication date of portion	2015-03-20

2. Chemical communications

0.00 USD

Order license ID	Pending
ISSN	1364-548X

Type of Use	Republish in a thesis/dissertation
Publisher	ROYAL SOCIETY OF CHEMISTRY
Portion	Chart/graph/table/figure

LICENSED CONTENT

Publication Title	Chemical communications	Country	United Kingdom of Great Britain and Northern Ireland
Author/Editor	Royal Society of Chemistry (Great Britain)	Rights holder	Royal Society of Chemistry
Date	01/01/1996	Publication Type	e-Journal
Language	English		

REQUEST DETAILS

Portion Type	Chart/graph/table/figure	Distribution	Worldwide
Number of charts / graphs / tables / figures requested	3	Translation	Original language of publication
Format (select all that apply)	Print, Electronic	Copies for the disabled?	No
Who will republish the content?	Academic institution	Minor editing privileges?	No
Duration of Use	Life of current edition	Incidental promotional use?	No
Lifetime Unit Quantity	Up to 499	Currency	USD
Rights Requested	Main product		

NEW WORK DETAILS

Title	Regulation of Nanoparticle reactant interaction outplays ligand poisoning in metal nanoparticle catalyzed reduction of charged substrates	Institution name	Indian Institute of Science Education and Research Pune
Instructor name	Dr.Pramod Pillai	Expected presentation date	2020-04-30

ADDITIONAL DETAILS

Order reference number	26	The requesting person / organization to appear on the license	Soumendu Roy
------------------------	----	---	--------------

REUSE CONTENT DETAILS

Title, description or numeric reference of the portion(s)	The significant impact of polydopamine on the catalytic performance of the carried Au nanoparticles	Title of the article/chapter the portion is from	The significant impact of polydopamine on the catalytic performance of the carried Au nanoparticles
Editor of portion(s)	NA	Author of portion(s)	Royal Society of Chemistry (Great Britain)
Volume of serial or monograph	51	Issue, if republishing an article from a serial	N/A

Page or page range of
portion

1469-1471

Publication date of
portion

1996-01-01

Order Total: 0.00 USD

Total Items: 2

Total Due: 0.00 USD

Accepted: All Publisher and CCC Terms and Conditions



RightsLink®



Home



Help



Email Support



Sign in



Create Account

Opportunities and Challenges of Solar-Energy-Driven Carbon Dioxide to Fuel Conversion with Plasmonic Catalysts



Author: Sungju Yu, Andrew J. Wilson, Gayatri Kumari, et al

Publication: ACS Energy Letters

Publisher: American Chemical Society

Date: Sep 1, 2017

Copyright © 2017, American Chemical Society

PERMISSION/LICENSE IS GRANTED FOR YOUR ORDER AT NO CHARGE

This type of permission/license, instead of the standard Terms & Conditions, is sent to you because no fee is being charged for your order. Please note the following:

- Permission is granted for your request in both print and electronic formats, and translations.
 - If figures and/or tables were requested, they may be adapted or used in part.
 - Please print this page for your records and send a copy of it to your publisher/graduate school.
 - Appropriate credit for the requested material should be given as follows: "Reprinted (adapted) with permission from (COMPLETE REFERENCE CITATION). Copyright (YEAR) American Chemical Society." Insert appropriate information in place of the capitalized words.
 - One-time permission is granted only for the use specified in your request. No additional uses are granted (such as derivative works or other editions). For any other uses, please submit a new request.
- If credit is given to another source for the material you requested, permission must be obtained from that source.

[BACK](#)

[CLOSE WINDOW](#)



Home



Help



Email Support



soumendu roy ▾

Z-Scheme Water Splitting Using Two Different Semiconductor Photocatalysts



Author: Kazuhiko Maeda

Publication: ACS Catalysis

Publisher: American Chemical Society

Date: Jul 1, 2013

Copyright © 2013, American Chemical Society

PERMISSION/LICENSE IS GRANTED FOR YOUR ORDER AT NO CHARGE

This type of permission/license, instead of the standard Terms & Conditions, is sent to you because no fee is being charged for your order. Please note the following:

- Permission is granted for your request in both print and electronic formats, and translations.
 - If figures and/or tables were requested, they may be adapted or used in part.
 - Please print this page for your records and send a copy of it to your publisher/graduate school.
 - Appropriate credit for the requested material should be given as follows: "Reprinted (adapted) with permission from (COMPLETE REFERENCE CITATION). Copyright (YEAR) American Chemical Society." Insert appropriate information in place of the capitalized words.
 - One-time permission is granted only for the use specified in your request. No additional uses are granted (such as derivative works or other editions). For any other uses, please submit a new request.
- If credit is given to another source for the material you requested, permission must be obtained from that source.

[BACK](#)[CLOSE WINDOW](#)



RightsLink®



Home



Help



Email Support



soumendu roy ▾

A Photocatalyst-Enzyme Coupled Artificial Photosynthesis System for Solar Energy in Production of Formic Acid from CO₂



Author: Rajesh K. Yadav, Jin-Ook Baeg, Gyu Hwan Oh, et al

Publication: Journal of the American Chemical Society

Publisher: American Chemical Society

Date: Jul 1, 2012

Copyright © 2012, American Chemical Society

PERMISSION/LICENSE IS GRANTED FOR YOUR ORDER AT NO CHARGE

This type of permission/license, instead of the standard Terms & Conditions, is sent to you because no fee is being charged for your order. Please note the following:

- Permission is granted for your request in both print and electronic formats, and translations.
 - If figures and/or tables were requested, they may be adapted or used in part.
 - Please print this page for your records and send a copy of it to your publisher/graduate school.
 - Appropriate credit for the requested material should be given as follows: "Reprinted (adapted) with permission from (COMPLETE REFERENCE CITATION). Copyright (YEAR) American Chemical Society." Insert appropriate information in place of the capitalized words.
 - One-time permission is granted only for the use specified in your request. No additional uses are granted (such as derivative works or other editions). For any other uses, please submit a new request.
- If credit is given to another source for the material you requested, permission must be obtained from that source.

[BACK](#)[CLOSE WINDOW](#)

JOHN WILEY AND SONS LICENSE TERMS AND CONDITIONS

Feb 22, 2020

This Agreement between Indian Institute of Science Education and Research pune -- soumendu roy ("You") and John Wiley and Sons ("John Wiley and Sons") consists of your license details and the terms and conditions provided by John Wiley and Sons and Copyright Clearance Center.

License Number	4774240346201
License date	Feb 22, 2020
Licensed Content Publisher	John Wiley and Sons
Licensed Content Publication	Advanced Materials
Licensed Content Title	Mussel-Inspired Plasmonic Nanohybrids for Light Harvesting
Licensed Content Author	Chan Beum Park, Jonghwa Shin, Byung Il Lee, et al
Licensed Content Date	Mar 13, 2014
Licensed Content Volume	26
Licensed Content Issue	26
Licensed Content Pages	6
Type of use	Dissertation/Thesis
Requestor type	University/Academic
Format	Print and electronic
Portion	Figure/table

Number of figures/tables	2
Original Wiley figure/table number(s)	Figure 4a and 4b
Will you be translating?	
Order reference number	25
Title of your thesis / dissertation	PhD student
Expected completion date	Apr 2020
Expected size (number of pages)	1
Requestor Location	Indian Institute of Science Education and Research pune iiser pune, pune 411008
Publisher Tax ID	Pune, Maharashtra 411008 India Attn: Indian Institute of Science Education and Research pune
Total	EU826007151
	0.00 USD

Terms and Conditions

TERMS AND CONDITIONS

This copyrighted material is owned by or exclusively licensed to John Wiley & Sons, Inc. or one of its group companies (each a "Wiley Company") or handled on behalf of a society with which a Wiley Company has exclusive publishing rights in relation to a particular work (collectively "WILEY"). By clicking "accept" in connection with completing this licensing transaction, you agree that the following terms and conditions apply to this transaction (along with the billing and payment terms and conditions established by the Copyright Clearance Center Inc., ("CCC's Billing and Payment terms and conditions"), at the time that you opened your RightsLink account (these are available at any time at <http://myaccount.copyright.com>).

Terms and Conditions

- The materials you have requested permission to reproduce or reuse (the "Wiley Materials") are protected by copyright.
- You are hereby granted a personal, non-exclusive, non-sub licensable (on a stand-alone basis), non-transferable, worldwide, limited license to reproduce the Wiley Materials for the purpose specified in the licensing process. This license, **and any CONTENT (PDF or image file) purchased as part of your order**, is for a one-time use only and limited to any maximum distribution number specified in the license. The first instance of republication or reuse granted by this license must be completed within two years of the date of the grant of this license (although copies prepared before the end date may be distributed thereafter). The Wiley Materials shall not be used in any other manner or for any other purpose, beyond what is granted in the license. Permission is granted subject to an appropriate acknowledgement given to the author, title of the material/book/journal and the publisher. You shall also duplicate the copyright notice that appears in the Wiley publication in your use of the Wiley Material. Permission is also granted on the understanding that nowhere in the text is a previously published source acknowledged for all or part of this Wiley Material. Any third party content is expressly excluded from this permission.
- With respect to the Wiley Materials, all rights are reserved. Except as expressly granted by the terms of the license, no part of the Wiley Materials may be copied, modified, adapted (except for minor reformatting required by the new Publication), translated, reproduced, transferred or distributed, in any form or by any means, and no derivative works may be made based on the Wiley Materials without the prior permission of the respective copyright owner.**For STM Signatory Publishers clearing permission under the terms of the [STM Permissions Guidelines](#) only, the terms of the license are extended to include subsequent editions and for editions in other languages, provided such editions are for the work as a whole in situ and does not involve the separate exploitation of the permitted figures or extracts,** You may not alter, remove or suppress in any manner any copyright, trademark or other notices displayed by the Wiley Materials. You may not license, rent, sell, loan, lease, pledge, offer as security, transfer or assign the Wiley Materials on a stand-alone basis, or any of the rights granted to you hereunder to any other person.
- The Wiley Materials and all of the intellectual property rights therein shall at all times remain the exclusive property of John Wiley & Sons Inc, the Wiley Companies, or their respective licensors, and your interest therein is only that of having possession of and the right to reproduce the Wiley Materials pursuant to Section 2 herein during the continuance of this Agreement. You agree that you own no right, title or interest in or to the Wiley Materials or any of the intellectual property rights therein. You shall have no rights hereunder other than the license as provided for above in Section 2. No right, license or interest to any trademark, trade name, service mark or other branding ("Marks") of WILEY or its licensors is granted hereunder, and you agree that you shall not assert any such right, license or interest with respect thereto
- NEITHER WILEY NOR ITS LICENSORS MAKES ANY WARRANTY OR REPRESENTATION OF ANY KIND TO YOU OR ANY THIRD PARTY, EXPRESS, IMPLIED OR STATUTORY, WITH RESPECT TO THE MATERIALS OR THE ACCURACY OF ANY INFORMATION CONTAINED IN THE MATERIALS, INCLUDING, WITHOUT LIMITATION, ANY IMPLIED WARRANTY OF MERCHANTABILITY, ACCURACY, SATISFACTORY QUALITY, FITNESS FOR A PARTICULAR PURPOSE, USABILITY, INTEGRATION OR NON-INFRINGEMENT AND ALL SUCH WARRANTIES ARE HEREBY EXCLUDED BY WILEY AND ITS LICENSORS AND WAIVED BY YOU.
- WILEY shall have the right to terminate this Agreement immediately upon breach of this Agreement by you.

- You shall indemnify, defend and hold harmless WILEY, its Licensors and their respective directors, officers, agents and employees, from and against any actual or threatened claims, demands, causes of action or proceedings arising from any breach of this Agreement by you.
- IN NO EVENT SHALL WILEY OR ITS LICENSORS BE LIABLE TO YOU OR ANY OTHER PARTY OR ANY OTHER PERSON OR ENTITY FOR ANY SPECIAL, CONSEQUENTIAL, INCIDENTAL, INDIRECT, EXEMPLARY OR PUNITIVE DAMAGES, HOWEVER CAUSED, ARISING OUT OF OR IN CONNECTION WITH THE DOWNLOADING, PROVISIONING, VIEWING OR USE OF THE MATERIALS REGARDLESS OF THE FORM OF ACTION, WHETHER FOR BREACH OF CONTRACT, BREACH OF WARRANTY, TORT, NEGLIGENCE, INFRINGEMENT OR OTHERWISE (INCLUDING, WITHOUT LIMITATION, DAMAGES BASED ON LOSS OF PROFITS, DATA, FILES, USE, BUSINESS OPPORTUNITY OR CLAIMS OF THIRD PARTIES), AND WHETHER OR NOT THE PARTY HAS BEEN ADVISED OF THE POSSIBILITY OF SUCH DAMAGES. THIS LIMITATION SHALL APPLY NOTWITHSTANDING ANY FAILURE OF ESSENTIAL PURPOSE OF ANY LIMITED REMEDY PROVIDED HEREIN.
- Should any provision of this Agreement be held by a court of competent jurisdiction to be illegal, invalid, or unenforceable, that provision shall be deemed amended to achieve as nearly as possible the same economic effect as the original provision, and the legality, validity and enforceability of the remaining provisions of this Agreement shall not be affected or impaired thereby.
- The failure of either party to enforce any term or condition of this Agreement shall not constitute a waiver of either party's right to enforce each and every term and condition of this Agreement. No breach under this agreement shall be deemed waived or excused by either party unless such waiver or consent is in writing signed by the party granting such waiver or consent. The waiver by or consent of a party to a breach of any provision of this Agreement shall not operate or be construed as a waiver of or consent to any other or subsequent breach by such other party.
- This Agreement may not be assigned (including by operation of law or otherwise) by you without WILEY's prior written consent.
- Any fee required for this permission shall be non-refundable after thirty (30) days from receipt by the CCC.
- These terms and conditions together with CCC's Billing and Payment terms and conditions (which are incorporated herein) form the entire agreement between you and WILEY concerning this licensing transaction and (in the absence of fraud) supersedes all prior agreements and representations of the parties, oral or written. This Agreement may not be amended except in writing signed by both parties. This Agreement shall be binding upon and inure to the benefit of the parties' successors, legal representatives, and authorized assigns.
- In the event of any conflict between your obligations established by these terms and conditions and those established by CCC's Billing and Payment terms and conditions, these terms and conditions shall prevail.
- WILEY expressly reserves all rights not specifically granted in the combination of (i) the license details provided by you and accepted in the course of this licensing transaction, (ii) these terms and conditions and (iii) CCC's Billing and Payment terms and conditions.

- This Agreement will be void if the Type of Use, Format, Circulation, or Requestor Type was misrepresented during the licensing process.
- This Agreement shall be governed by and construed in accordance with the laws of the State of New York, USA, without regards to such state's conflict of law rules. Any legal action, suit or proceeding arising out of or relating to these Terms and Conditions or the breach thereof shall be instituted in a court of competent jurisdiction in New York County in the State of New York in the United States of America and each party hereby consents and submits to the personal jurisdiction of such court, waives any objection to venue in such court and consents to service of process by registered or certified mail, return receipt requested, at the last known address of such party.

WILEY OPEN ACCESS TERMS AND CONDITIONS

Wiley Publishes Open Access Articles in fully Open Access Journals and in Subscription journals offering Online Open. Although most of the fully Open Access journals publish open access articles under the terms of the Creative Commons Attribution (CC BY) License only, the subscription journals and a few of the Open Access Journals offer a choice of Creative Commons Licenses. The license type is clearly identified on the article.

The Creative Commons Attribution License

The [Creative Commons Attribution License \(CC-BY\)](#) allows users to copy, distribute and transmit an article, adapt the article and make commercial use of the article. The CC-BY license permits commercial and non-

Creative Commons Attribution Non-Commercial License

The [Creative Commons Attribution Non-Commercial \(CC-BY-NC\) License](#) permits use, distribution and reproduction in any medium, provided the original work is properly cited and is not used for commercial purposes.(see below)

Creative Commons Attribution-Non-Commercial-NoDerivs License

The [Creative Commons Attribution Non-Commercial-NoDerivs License](#) (CC-BY-NC-ND) permits use, distribution and reproduction in any medium, provided the original work is properly cited, is not used for commercial purposes and no modifications or adaptations are made. (see below)

Use by commercial "for-profit" organizations

Use of Wiley Open Access articles for commercial, promotional, or marketing purposes requires further explicit permission from Wiley and will be subject to a fee.

Further details can be found on Wiley Online Library
<http://olabout.wiley.com/WileyCDA/Section/id-410895.html>

Other Terms and Conditions:

v1.10 Last updated September 2015

Questions? customercare@copyright.com or +1-855-239-3415 (toll free in the US) or

+1-978-646-2777.



Home



Help



Email Support



Sign in



Create Account

Electrostatically Driven Multielectron Transfer for the Photocatalytic Regeneration of Nicotinamide Cofactor



Author: Soumendu Roy, Vanshika Jain, Radha Krishna Kashyap, et al

Publication: ACS Catalysis

Publisher: American Chemical Society

Date: Apr 1, 2020

Copyright © 2020, American Chemical Society

PERMISSION/LICENSE IS GRANTED FOR YOUR ORDER AT NO CHARGE

This type of permission/license, instead of the standard Terms & Conditions, is sent to you because no fee is being charged for your order. Please note the following:

- Permission is granted for your request in both print and electronic formats, and translations.
- If figures and/or tables were requested, they may be adapted or used in part.
- Please print this page for your records and send a copy of it to your publisher/graduate school.
- Appropriate credit for the requested material should be given as follows: "Reprinted (adapted) with permission from (COMPLETE REFERENCE CITATION). Copyright (YEAR) American Chemical Society." Insert appropriate information in place of the capitalized words.
- One-time permission is granted only for the use specified in your request. No additional uses are granted (such as derivative works or other editions). For any other uses, please submit a new request.

[BACK](#)[CLOSE WINDOW](#)



Home



Help



Email Support



Sign in



Create Account

Revealing the Role of Electrostatics in Gold-Nanoparticle-Catalyzed Reduction of Charged Substrates



Author: Soumendu Roy, Anish Rao, Gayathri Devatha, et al

Publication: ACS Catalysis

Publisher: American Chemical Society

Date: Oct 1, 2017

Copyright © 2017, American Chemical Society

PERMISSION/LICENSE IS GRANTED FOR YOUR ORDER AT NO CHARGE

This type of permission/license, instead of the standard Terms & Conditions, is sent to you because no fee is being charged for your order. Please note the following:

- Permission is granted for your request in both print and electronic formats, and translations.
- If figures and/or tables were requested, they may be adapted or used in part.
- Please print this page for your records and send a copy of it to your publisher/graduate school.
- Appropriate credit for the requested material should be given as follows: "Reprinted (adapted) with permission from (COMPLETE REFERENCE CITATION). Copyright (YEAR) American Chemical Society." Insert appropriate information in place of the capitalized words.
- One-time permission is granted only for the use specified in your request. No additional uses are granted (such as derivative works or other editions). For any other uses, please submit a new request.

[BACK](#)[CLOSE WINDOW](#)



Precise Nanoparticle–Reactant Interaction Outplays Ligand Poisoning in Visible-Light Photocatalysis



Author: Soumendu Roy, Sumit Roy, Anish Rao, et al

Publication: Chemistry of Materials

Publisher: American Chemical Society

Date: Dec 1, 2018

Copyright © 2018, American Chemical Society

PERMISSION/LICENSE IS GRANTED FOR YOUR ORDER AT NO CHARGE

This type of permission/license, instead of the standard Terms & Conditions, is sent to you because no fee is being charged for your order. Please note the following:

- Permission is granted for your request in both print and electronic formats, and translations.
- If figures and/or tables were requested, they may be adapted or used in part.
- Please print this page for your records and send a copy of it to your publisher/graduate school.
- Appropriate credit for the requested material should be given as follows: "Reprinted (adapted) with permission from (COMPLETE REFERENCE CITATION). Copyright (YEAR) American Chemical Society." Insert appropriate information in place of the capitalized words.
- One-time permission is granted only for the use specified in your request. No additional uses are granted (such as derivative works or other editions). For any other uses, please submit a new request.

[BACK](#)

[CLOSE WINDOW](#)